

CONFIDENTIAL



FP7-ICT Future Networks
SPECIFIC TARGETTED RESEARCH PROJECT
Project Deliverable

PHYDYAS Doc. Number	PHYDYAS_ 014
Project Number	ICT - 211887
Project Acronym+Title	PHYDYAS – PHYsical layer for DYnamic AccesS and cognitive radio
Deliverable Nature	Report
Deliverable Number	D8.1
Contractual Delivery Date	July 1, 2009
Actual Delivery Date	July 29, 2009
Title of Deliverable	Application of the FBMC physical layer in a cognitive radio scenario
Contributing Workpackage	WP8: Radio scene spectrum analysis and cognitive radio
Project starting date; Duration	01/01/2008; 30 months
Dissemination Level	CO
Author(s)	Haijian Zhang, Didier Le Ruyet, Michel Terré, Daniel Roviras (CNAM), Markku Renfors, Tero Ihalainen (TUT), Carlos Bader, Musbah Shaat (CTTC), Andreas Merentitis, Dionysia Triantafyllopoulou (RA-CTI), Mathieu Huchard (LETI), Alexandr Kuzminskiy (ALUK – WP8 leader)

Abstract: The FBMC PHY has been studied and compared with OFDM as a potential physical layer for CR networks. Spectral efficiency, impact of the RF impairments, and resource allocation techniques have been investigated. It has been shown that FBMC can be considered as a perspective PHY for future CR network.

Contents

1	Introduction	7
2	Cognitive radio overview	11
2.1	Spectrum sensing	11
2.1.1	Noise floor, dynamic range, and interference rejection	12
2.1.2	Frequency resolution and sensing window	12
2.1.3	Sensing latency	13
2.1.4	Simultaneous spectrum monitoring and communication	13
2.2	Spectrum decision.....	14
2.3	Spectrum sharing	15
2.4	Spectrum mobility.....	17
2.5	Conclusions.....	18
3	FBMC as cognitive radio physical layer	18
3.1	Spectral selectivity and dynamic range.....	18
3.2	Spectral efficiency	19
3.3	Spectrum monitoring in FBMC	20
3.4	Spectrum sensing methods	21
3.4.1	Energy detection.....	22
3.4.2	Cyclostationarity detection	27
3.4.3	Other sensing methods	30
3.5	Conclusions.....	31
4	FBMC and OFDM spectral efficiency comparison	32
4.1	Out-of-band radiation analysis	33
4.1.1	CP-OFDM based spectrum pooling systems.....	33
4.1.2	RC-OFDM based spectrum pooling systems	34
4.1.3	IOTA/OQAM based spectrum pooling systems	35
4.1.4	PHYDYAS/OQAM based spectrum pooling systems	37
4.2	Spectral efficiency analysis.....	39
4.3	Simulation results	41
4.3.1	Interference for licensed user	42
4.3.2	Throughput for rental user.....	43
4.3.3	Tradeoff between throughput and interference	44
4.4	Conclusions.....	45

5	RF impairments at the transmitter	45
5.1	Introduction	45
5.1.1	Cognitive radio background	46
5.1.2	State of the art of WIMAX OFDM transmitter	47
5.2	Test scenario for cognitive radio	48
5.3	Baseband simulation parameters	51
5.4	Non linearity of a power amplifier	53
5.4.1	Model amplifier used	53
5.4.2	Measurement and modeling of the power amplifier	53
5.4.3	Simulations	55
5.4.4	Power consumption	56
5.5	IQ imbalance	57
5.5.1	Model	57
5.5.2	Effect on the spectral selectivity	58
5.5.3	Simulations	59
5.6	Phase noise	60
5.6.1	Model	60
5.6.2	Simulations	61
5.7	Joint effect of the three imperfections	62
5.8	Other values for K and M	64
5.9	Summary of the requirements	66
5.10	Conclusions	66
6	Interference-aware power allocation algorithm in multicarrier based cognitive radio networks: OFDM and FBMC systems	67
6.1	System model	68
6.1.1	Interference induced to/from the PU's	69
6.1.2	OFDM system and its PSD model	70
6.1.3	FBMC system and its PSD model	71
6.2	Problem formulation	73
6.2.1	Optimization problem	73
6.2.2	Subcarriers to users allocation	73
6.2.3	Subcarriers power loading (optimal solution)	74
6.3	Proposed sub-optimal algorithm	76
6.4	Simulation results	80

6.4.1	Case 1: two active PU bands	81
6.4.2	Case 2: one active PU band	84
6.5	Conclusions.....	86
7	Resource allocation in cognitive radio networks with MAC layer cooperation	86
7.1	Problem definition and requirements.....	86
7.2	Algorithm outline	87
7.3	Results	91
7.4	Conclusions.....	98
8	Decentralized dynamic spectrum allocation in uncoordinated cognitive radio networks based on adaptive antenna array interference mitigation diversity	99
8.1	System model and problem formulation	101
8.2	Potential performance of IM-based DSA	104
8.2.1	SINR pdf for $K \geq N_0$	106
8.2.2	SINR pdf for $K < N_0$	107
8.3	IM-based DSA algorithms.....	110
8.3.1	"Selfish" IM-based DSA algorithm	110
8.3.2	"Good Neighbor" threshold-regulated IM-based DSA algorithm.....	112
8.4	Power control for IM-based DSA algorithms.....	113
8.5	Using absorbing Markov chains for analysis of the IM-based DSA algorithms	115
8.5.1	Markov chain model for IM-based DSA	115
8.5.2	Analysis of low-dimensional DSA networks	117
8.5.3	Possibilities to reduce non-convergence probability.....	121
8.6	Mixed "good neighbor"/"selfish" IM-based DSA networks	126
8.7	Simulation results	130
8.7.1	Stationary horizontal CR scenarios without pathloss and shadowing.....	131
8.7.2	Stationary horizontal CR scenarios with pathloss and shadowing	136
8.7.3	Nonstationary vertical CR scenarios	139
8.8	Conclusions.....	141
9	Summary	142
	References	146

List of Acronyms

ACM	Adaptive Coding and Modulation
ACPR	Adjacent Channel Power Ratio
ADC	Analog-to-Digital Converter
AMAM	Amplitude Modulation to Amplitude Modulation
AMPM	Amplitude Modulation to Phase Modulation
AWGN	Additive White Gaussian Noise
BER	Bit Error Rate
BS	Base Station
CBS	Cognitive Base Station
cdf	Cumulative Distribution Function
CNR	Channel Gain to Noise Ratio
COG	Center of Gravity
CP	Cyclic Prefix
CR	Cognitive Radio
CSMA/CA	Carrier Sense Multiple Access / Collision Avoidance
CWER	Codeword Error Rate
DAC	Digital-to-Analog Converter
DC (offset)	Direct Current (offset)
DSA	Dynamic Spectrum Access/Allocation
EVM	Error Vector Magnitude
FBMC	Filter Bank based Multicarrier
FCC	The Federal Communication Commission
FEC	Forward Error Correction
FFT	Fast Fourier Transform
GN	Good Neighbor
GN-MaxMin	Good Neighbor algorithm with MaxMin search
GN-MinSwitch	Good Neighbor algorithm with MinSwitch search
I	In-phase
IBO	Input power Back-Off
IDFT	Inverse Discrete Fourier Transform
ICI	Inter-Carrier Interference
IF	Intermediate Frequency
IFFT	Inverse Fast Fourier Transform
i.i.d	Independent and Identically Distributed
IM	Interference Mitigation
IM3	IM3 3 rd Order Intermodulation
IOTA	Isotropic Orthogonal Transform Algorithm
ISI	Intersymbol Interference
KKT	Karush-Kuhn-Tucker
LTE	Long Term Evolution
LU	Licensed User
MAC	Medium Access Control
MaxMin	Maximum of Minimum Search
MCM	Multicarrier
MIMO	Multiple Input Multiple Output

MinSwitch	Minimum Switch Search
NE	Nash Equilibrium
NF	Noise Factor
OIP3	Output 3 rd Order Intercept Point
OFDM	Orthogonal Frequency Division Multiplexing
OP1dB	Output 1dB compression Point
OQAM	Offset Quadrature Amplitude Modulation
PA	Power Amplifier
PAE	Power Added Efficiency
PC	Power Control
pdf	Probability Distribution Function
PHY	Physical Layer
PI-Algorithm	Power Interference constrained algorithm
PSD	Power Spectrum Density
PU	Primary Users
RBW	Resolution Bandwidth
RC	Raised Cosine
RCP-BLDPC	Rate Compatible Punctured Block-circulant Low Density Parity Check
RF	Radio Frequency
RU	Rental User
Q	Quadrature
QoS	Quality of Service
SCF	Spectral Correlation Function
SDR	Spectral Dynamic Range
SEA	Spectral Efficiency Analysis
SINR	Signal to Interference plus Noise Ratio
SNR	Signal to Noise Ratio
SS	Subscriber Station
SSPA	Solid State Power Amplifier
SU	Secondary Users
TWT	Traveling Wave Tube (amplifier)
VBW	Video Bandwidth
WIMAX	Worldwide Interoperability for Microwave Access
WLAN	Wireless Local Area Network

1 Introduction

Cognitive radio (CR) is a design approach for introducing new adaptive systems that enable higher and more efficient spectrum utilization. During recent years, CR has attracted significant attention of the research community and became a subject of numerous publications including books, e.g., [Mit06] and [Cog07]; special conferences, e.g., DySPAN and CrownCom; special issues, e.g., [Cog08] and [Cog09]; tutorials, e.g., [Mac09] and [Zha07], and research articles.

In conventional wire or wireless systems, the frequency bandwidth of the transmission channel is analyzed in real time to perform equalization or optimize the global performance. The CR concept goes one step further: the spectrum analysis is exploited to determine the transmission channel itself. This is a major change which confers to the physical layer an increased importance, because the whole system relies on the quality, the reliability and the robustness of the spectral estimation. Moreover, the system architecture itself is impacted, because the physical layer does not just adapt to instructions from upper layers, but it becomes tightly involved in the decisions and management of the network [Bel08-1].

The opportunistic nature of cognitive radio systems offers big promises in terms of spectrum usage, but generates a lot of constraints. Basically, such systems must act quickly to access the spectrum and to cease transmission, they must be reliable and robust and they must provide quality of service. Two different cases of applications can be distinguished, namely public spaces and white spaces in a licensed band. Public spaces are frequency bands which are specifically reserved for CR systems, for example in the spectrum which will be freed by analog television. In public spaces the CR users compete for the resource and the main issues for physical layer are density and protection of other users. In a licensed band, the main issue is the protection of the primary user, although the coexistence with other CR users has to be considered as well, for the sake of global efficiency. These two cases might lead to different specifications, but the architecture of the CR layer can be the same for both.

The generic architecture of the cognitive radio system is shown in Fig. 1.1. The physical layer has two distinct functionalities, associated with two distinct sections, namely spectral resource discovery and adaptive transmission. The information collected about the spectrum is forwarded to the policy generator which, taking into account the user instructions, sets the objectives of the transmission. A key component in the spectral resource estimation section is the real time spectrum sensing module, which delivers the raw information on which future decisions will be based. However, since the decisions will be ultimately implemented by the adaptive transceiver section, the two sections of the CR physical layer cannot run independently but, instead, a high level of coherence and compatibility must be maintained.

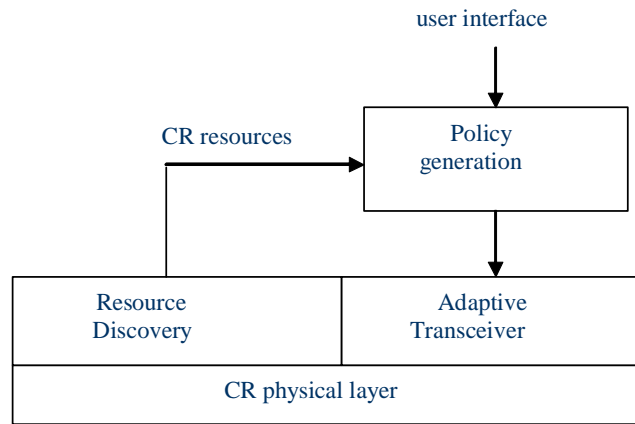


Figure 1.1. The physical layer in a cognitive radio system

The objective of this deliverable is to study the physical layer impact on the main blocks of a CR system shown on Fig. 1.1. To be more precise, let us consider a particular CR network illustrated in Fig. 1.2 with the following main assumptions:

- A number of frequency bands formed at some physical layer is available in some geographical area.
- Primary users dynamically occupy some of them.
- Secondary network consists of a number of independent subsystems that are allowed to use bands, which are not currently occupied by the primary users.
- Secondary subsystems include base stations (BS) and users (subscriber stations (SS)) transmitting data to their base stations.
- Each base station is sensing spectrum in all the available bands to detect presence of the active primary users.
- Secondary subsystems are not coordinated and synchronized.
- Secondary base stations have full information and control on their own users.
- Propagation conditions are typical for wireless indoor/outdoor low mobility scenarios [Mol09]

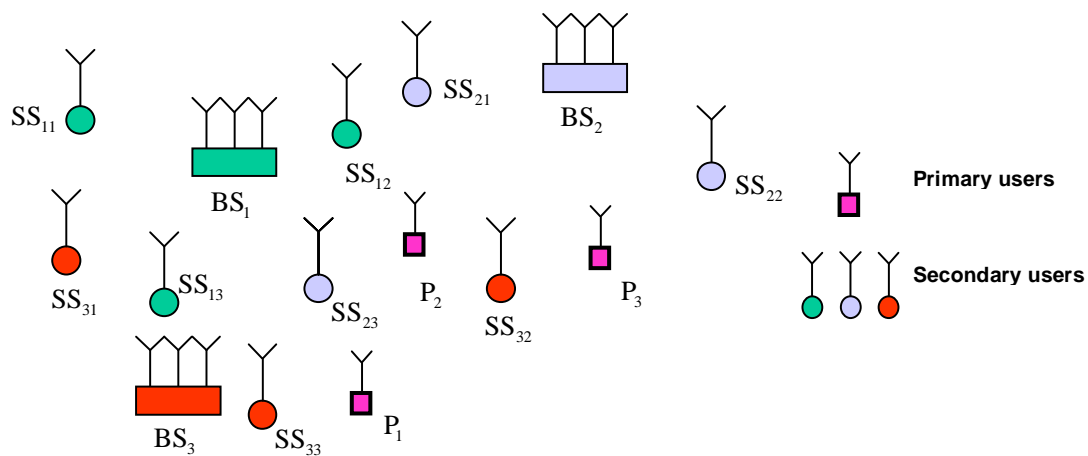


Figure 1.2. CR system model

One can see that all the elements of a general CR system shown in Fig. 1.1 are assumed in the scenario in Fig. 1.2. Indeed, a physical layer is responsible for forming frequency channels and data transmission/reception for each subsystem; resource discovery in terms of spectrum sensing for the primary users and interference environment analysis for the secondary CR system is required; policy generation and regulation is assumed for spectrum sharing; and adaptive transceivers are needed to react on the changing environment according to the discovered resources and spectrum sharing policy.

One example of such a scenario based on OFDM physical layer could be a number of fixed WIMAX [802.16-04] systems sharing a license exempt spectrum [Ash07]. The main feature of the OFDM physical layer in this case is that guard bands are required between frequency bands allocated to users from different unsynchronized subsystems to prevent energy leakage between them as illustrated in Fig. 1.3 in the 3-band case. Particularly, the fixed WIMAX standard [802.16-04] defines the OFDM physical layer with totally $F_{\text{total}} = 256$ sub-carriers, $F_{\text{guard}} = 27$ guard sub-carriers and minimum 10 sub-carriers in a frequency band. This means that maximum $F = 6$ bands for unsynchronized users can be formed [Ash07] and their spectrum efficiency in terms of spectrum utilization defined as

$$\rho = \frac{(1 + F)F_{\text{guard}}}{F_{\text{total}}}, \quad (1.1)$$

is shown in Fig. 1.4.

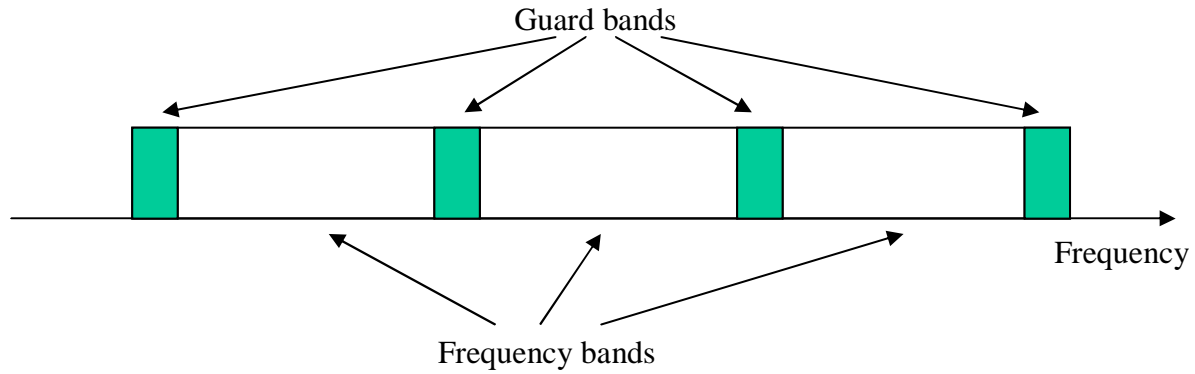


Figure 1.3. Frequency bands for unsynchronized users

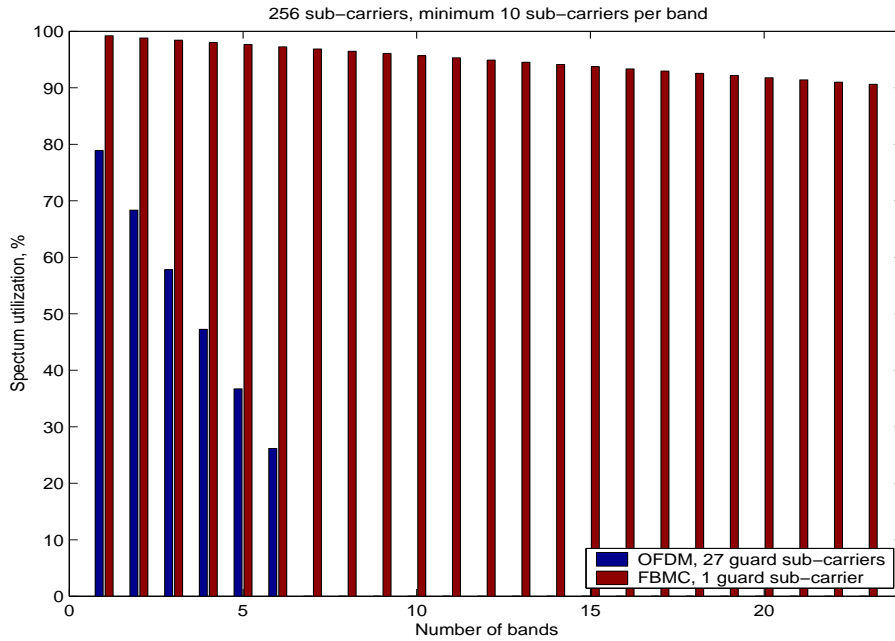


Figure 1.4. Spectrum utilization for unsynchronized systems sharing license exempt spectrum

One can see in Fig. 1.4 that only about 26% of spectrum can be used for data transmission in the 6 bands case. The rest of the spectrum is wasted for guard bands in this system. Obviously, OFDM physical layer is not a spectrally efficient solution in this situation.

Another physical layer with reduced F_{guard} could be more efficient in the asynchronous CR scenario. FBMC can be considered as such a candidate. Particularly, if FBMC could allow $F_{\text{guard}} = 1$, then up to 23 bands with spectrum efficiency above 90% could be formed in the same scenario as also illustrated in Fig. 1.4.

Obviously, this is just an illustration example to emphasize the physical layer importance in the CR scenario. In practice, guard bands for both OFDM and FBMC depend on particular power density spectrum, RF imperfections, system parameters, etc. Furthermore, physical layer features affect spectrum sensing and other basic CR modules specified in Fig. 1.1 and assumed in scenario in Fig. 1.2.

The objective of this deliverable is to study the physical layer impact on the main blocks of a CR system shown on Fig. 1.1 in the context of the particular CR network scenario in Fig. 1.2. Cognitive radio overview is given in Section 2. FBMC as cognitive radio physical layer is considered in Section 3. Section 4 compares FBMC and OFDM PHY in terms of spectrum efficiency. Section 5 is devoted to the RF impairments impact on both OFDM and FBMC PHY. Resource allocation in CR networks is addressed in Sections 6 - 8. Particularly, interference-aware power allocation algorithm in OFDM and FBMC based CR networks is proposed and analyzed in Section 6. Resource allocation in CR networks with MAC layer cooperation between secondary subsystems is addressed in Section 7. New “good neighbor” resource sharing strategy and algorithms are introduced and investigated in Section 8 in a decentralized rule-regulated asynchronous CR network. Summary of the main results and problems for further investigation in the next deliverables are given in Section 9.

2 Cognitive radio overview

Current wireless networks are characterized by a static spectrum allocation policy, where wireless spectrum is assigned on a long-term basis for large geographical regions. Due to the recent increase in spectrum demand, this policy has resulted in spectrum scarcity in particular spectrum bands. In contrast, a large portion of the assigned spectrum is used sporadically, leading to underutilization of a significant amount of spectrum. In order to solve this spectrum inefficiency problem, dynamic spectrum access techniques were recently proposed.

The key enabling technology of dynamic spectrum access techniques is cognitive radio (CR) technology, which aims to address the spectrum scarcity problem by opportunistically identifying the vacant or underutilized portions of the spectrum and transmitting in them, while ensuring that any licensed users of the spectrum are not affected. CR networks are envisioned to provide high bandwidth to mobile users via heterogeneous wireless architectures and dynamic spectrum access techniques. This goal can be realized only through dynamic and efficient spectrum management techniques. The time-varying nature of the wireless channel and the high fluctuation in the spectrum availability combined with the variety of characteristics and Quality of Service (QoS) requirements of various applications, however, impose unique challenges to CR networks.

In order to address these challenges, each CR user in the CR network must:

- i. Determine which portions of the spectrum are available (*spectrum sensing*)
- ii. Select the best available channel (*spectrum decision*)
- iii. Coordinate access to this channel with other users (*spectrum sharing*)
- iv. Vacate the channel when a licensed user is detected (*spectrum mobility*)

Obviously, in the case of cognitive systems in licensed areas, with primary users (PUs) and secondary users (SUs), all the above functionalities should be supported. On the other hand, for systems which operate in unlicensed spectrum bands where the notion of primary users is not defined, spectrum mobility is not necessary and the role of spectrum sensing is modified to the identification of areas that are underutilized and not necessarily empty.

2.1 Spectrum sensing

The primary goal of the spectrum sensing module is to detect the spectrum occupancy in the local area in which the system operates, and identify the spaces which are free of primary and other secondary users, the so-called spectrum holes. A secondary goal might be to analyze the frequency bands in which interferers are present in order to determine their profile and assess the limits of the perturbations they can tolerate. In fact, there are two sub-functionalities, namely occupancy sensing and identity sensing, as pointed out in [Wan08]. Here, the emphasis is on the primary goal and the following parameters are examined: noise floor, spectral dynamic range, interference rejection, frequency resolution, and sensing latency.

Spectrum holes are also referred to as white spaces and the target is to achieve pre-determined false alarm and missed detection probabilities, P_{FA} and P_{MD} , when identifying white spaces. We will make distinction between two modes of primary user sensing: (1) Spectrum hole acquisition is carried out before local secondary transmission has been started or in other situations where the particular frequency band is not used for secondary transmission. (2) Spectrum monitoring takes

place in parallel with secondary transmission and its main target is to detect reappearing primary users in the used frequency channel.

2.1.1 Noise floor, dynamic range, and interference rejection

The first parameter to be considered is the spectral dynamic range, which is crucial for the usefulness of the cognitive radio concept. The estimated noise floor determines the lower limit of the dynamic range. The noise floor can be observed in an unused frequency band, and it is a sum of thermal noise and various interferences. The interference may include co-channel interference from distant secondary users, as well as various interference sources from non-ideal implementation of the spectrum sensing receiver, such as intermodulation, ADC quantization noise, and leakage of the spectrum sensing filter. The thermal noise and possible co-channel interference cannot be controlled, but the measured interference level is determined partly by the rejection performance of the spectrum sensing filter and non-idealities of the analog front-end.

Fig. 2.1 illustrates the dynamic range in spectrum sensing. The targeted sensitivity level in spectrum sensing is often considered to be deep below the noise + co-channel interference level. In stand-alone spectrum sensing this is required, because significant margin has to be assumed for the shadowing effects in typical wireless communication scenarios. With co-operative spectrum sensing, the sensitivity level can be significantly raised, but typically the target is still somewhat (a few dB) below the noise level. Clearly the interferences due to the leakage of the spectrum sensing filter and other receiver imperfections should be clearly below the targeted sensitivity level.

Next, the receiver sensitivity level for secondary transmissions is some 0 ... 20 dB above the noise level, depending on the used modulation and coding, on one hand, and efficiency of power control on the other. The maximum level of primary and secondary users in other frequency channels within the analyzed frequency band determines the upper limit of the dynamic range.

In generic communication scenarios, the dynamic range of the active primary and secondary signals is 50 ... 80 dB, and the requirement for overall dynamic range, between RX interference level and maximum signal level, could be 80 dB or more.

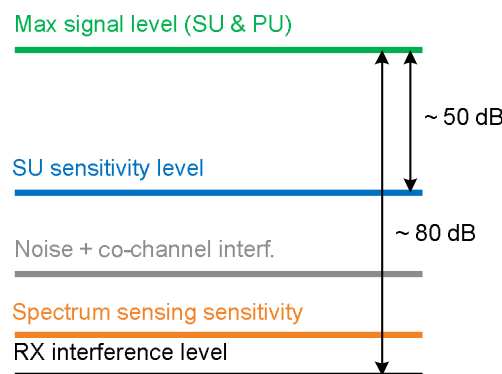


Figure 2.1. Dynamic range in spectrum sensing.

2.1.2 Frequency resolution and sensing window

The next parameter to be considered is the frequency resolution, which is determined by the smallest spectrum hole which must be detected. Then, since this bandwidth is to be used for data

transmission, the frequency granularity of the transmission system must be considered simultaneously. At this stage, it becomes obvious that the multicarrier modulation technique fits very well to the cognitive radio context. In multicarrier modulation, the smallest bandwidth is the subchannel spacing. Therefore, spectrum sensing and multicarrier modulation should have the same resolution. In such conditions, there is an inclination to use the same device to perform the two functions.

In general, if the sensing device is based on a multicarrier receiver, the sensing window can be configured to consist of a block of contiguous subchannel samples in time-frequency plane. The basic energy measurements are obtained for each subchannel sample, and the decision variable for sensing decisions is obtained by averaging the energy observations within the window. The benefit of such an approach is high flexibility in adjusting the window size and shape according to the radio scene and targeted sensing parameters. Also multiple dwell approaches can be easily realized: Appearing strong primary signals are rapidly detected with short integration window and potential spectral holes can then be identified. Then more detailed analysis of the remaining parts of the spectrum is carried out using longer integration window. The sensing time analysis (see Section 3.4.1.1) leads to a specific minimum window size, i.e., a specific minimum number of independent energy observations to reach the targeted P_{FA} and P_{MD} with the target primary signal SNR.

2.1.3 Sensing latency

A key aspect in the cognitive radio context is that high performance spectral estimation is carried out in real time. The efficiency of the system depends on its reactivity, which is the time it takes to reliably extract the information about the available resources, relay it to the policy generator, make decisions and implement them in the transceiver. The sensing latency is a significant part of this reactivity time and it must be minimized. The sensing latency is discussed in more details later in Section 3.4.1.1.

2.1.4 Simultaneous spectrum monitoring and communication

So far, it has been usually assumed that it is not possible to sense possible primary users from a frequency channel which is used simultaneously for local secondary communication. Therefore, spectrum monitoring type of sensing is usually assumed to be interleaved with data transmission [Gha08]. The secondary system periodically senses the transmission band to detect the start of primary transmission. In this process, a first parameter is the sensing period which sets the maximum time during which the secondary user is unaware of a reappearing primary user. Another parameter is the time during which secondary transmission must be interrupted in order to obtain an accurate and reliable measurement. Obviously, these two parameters have a great impact on the throughput of the CR network and on the confidence operators may have in the cognitive radio concept. On the contrary, with simultaneous communication and sensing in the spectrum monitoring sense, the problem of the coexistence between primary and secondary users and between secondary users themselves is greatly simplified. The idea here is not that the transmitting device itself does the sensing, but rather that receivers, or specific sensing devices [Sen08], which have means to communicate to the transmitter about possible collisions, do sensing for the frequency band that is used for on-going communication.

Now, the issue is how this desirable feature can be implemented. At first glance, two different approaches can be envisaged, namely spectrum reservation and residual interference based monitoring.

The spectrum reservation approach is basically an extension of the periodic sensing approach and it is highly facilitated by the multicarrier system model. It consists in leaving silent sensing windows, in the transmission band within the transmission burst, which the sensing device exploits to check the occupancy. If the sensing window consists of narrow frequency slot(s) over the whole transmission burst, then fast reaction to reappearing primary users can be achieved. With respect to the following technique, this one is less efficient, since it reduces the total bit rate. However, it can be more accurate and robust.

In a receiver, at the final stage, the data symbols are provided by a decision device. It is customary in digital transmission to exploit the residual signal which is the difference between the input of the decision device and the output. For example, it can serve a decision-directed adaptive equalizer, assuming that the decisions are correct and the error rate is very low. In the present context, this residual signal can be considered as representing the sum of the thermal noise and the various kinds of interferences, as well as the potential PU signal. If multicarrier modulation is employed, real time observations of the noise and signals behind the active SU waveform become available for the complete transmission frequency bandwidth and they can be exploited to detect the arrival of a new user in the spectrum.

Regarding the feasibility of the proposed residual interference based monitoring scheme, it is important to consider the dynamic range while performing simultaneous sensing and reception. While the dynamic range of different frequency channels is very wide in many dynamic spectrum access scenarios, the signal power level at the target SU receiver can be assumed to be much better under control, assuming that effective power control is implemented in the system. On the other hand, if the SU receiver would be operating at a high SNR (e.g., in case of a sensing device located closer to the transmitter than the actual target receiver), then also the cancellation of the secondary signal would operate well. Further, symbol decision errors, which would have significant impact on the residual interference, would not be expected to take place. In any case, it is expected that this scheme sets stringent requirements for the synchronization and channel equalization quality in high dynamic range scenarios, and further studies are needed to explore the feasibility of such schemes.

The role of the receiver in the spectrum monitoring function described above is worth emphasizing. Going one step further in that direction leads to employing the same device for sensing and reception. With this in mind, the filter bank technique is proposed to implement the CR physical layer.

2.2 Spectrum decision

The term spectrum decision refers to the CR network's capability to determine the most appropriate spectrum band according to the QoS requirements of the end users. Spectrum decision is highly affected by the channel characteristics and operations of primary users as well as the activities of other CR users in the network. Spectrum decision usually consists of two steps: first, each spectrum band is characterized, based on not only local observations of CR users but also statistical information of primary networks. Then, based on this characterization, the most appropriate spectrum band can be chosen (see e.g., [Zhe05],[Pen05],[Xu08],[Shi08],[Fu08] and [Sub08]).

Due to the time-varying characteristics of the wireless channel and the available spectrum holes, each spectrum hole should be characterized considering both the time-varying radio environment and spectrum parameters, such as operating frequency and bandwidth. The parameters that can represent a particular spectrum band are the following:

1. *Interference*
2. *Path loss*
3. *Wireless link errors*
4. *Link layer delay*

For example, in [Zhe05], a device-centric spectrum management scheme with low communication costs, where users observe local interference patterns and act independently according to preset spectrum rules is presented. The users' spectrum access is regulated by five rules that aim to tradeoff fairness and utilization with communication costs and algorithm complexity.

In [Pen05], a general framework for spectrum allocation in open spectrum systems is described. Centralized and distributed approaches to optimize spectrum allocation for utilization and fairness are presented. Efficient and fair access in open spectrum systems is described by a graph-theoretic model. Three policy-driven utility functions that combine efficient spectrum utilization and fairness are defined.

In [Xu08] the tradeoff of Secondary Users' throughput maximization by accessing larger bands and channel switching overhead and contention among multiple Secondary Users is considered. An optimal bandwidth allocation scheme is proposed, accounting for the effects of channel switching overhead.

In [Shi08] a multi-agent learning approach which allows the various nodes to optimize their transmission strategies autonomously, in a distributed manner, in multi-hop cognitive radio networks is proposed, taking into account the tradeoffs between the cost of the required information exchange and the learning efficiency of the multi-agent learning approach in terms of the utility impact.

In [Sub08], the dynamic spectrum access in a distributed network is modeled as a noncooperative game and the equilibrium solutions are obtained through a bimatrix game. In distributed cognitive radio networks, the secondary users are vulnerable to several unexpected events such as primary user arrival or a deep fade or sudden increase in interference which could potentially disrupt or disconnect the transmission link. In such cases, any strategic decision or information that could lead to uninterrupted channel access and facilitate maintaining links could be modeled as a Stackelberg game.

In the development of the spectrum decision function, several challenges still remain unsolved, such as the decision model, the issue of cooperation with reconfiguration as well as the spectrum decision over heterogeneous spectrum bands.

2.3 Spectrum sharing

Another important component of a Cognitive Radio network is the coordination of the CR users' transmission attempts over the shared wireless medium. In this respect, spectrum sharing should include much of the functionality of a MAC protocol. However, the unique characteristics of CRs, such as the coexistence of CR users with licensed users and the wide range of available spectrum, incur substantially different challenges for spectrum sharing in CR networks. The existing work in spectrum sharing aims to address these challenges and can be classified by four aspects: architecture, spectrum allocation behavior, spectrum access technique, and scope [Bri05],[Lee08],[Cao05],[Ma05],[Hua05],[Nie06],[Bak08],[Zha08-1],[Zho08],[Nie05],[Pen06] and [Zhe05].

The first classification is based on the architecture, which can be centralized or distributed:

1. *Centralized spectrum sharing:*

In centralized spectrum sharing, all the procedures considering spectrum allocation and access are controlled by a central entity. The sensing procedure can be performed in a distributed manner and where the measurements of the spectrum allocation are forwarded to the central entity, and a spectrum allocation map is constructed. Furthermore, the central entity can lease spectrum to users in a limited geographical region for a specific amount of time. In addition to competition for the spectrum, competition for users can also be considered through a central spectrum policy server [Bri05], [Lee08].

2. *Distributed spectrum sharing:*

In distributed spectrum sharing, the operations of spectrum allocation and access are based on local policies that are performed by each node distributively. Distributed solutions can also be used between different networks such that a base station competes with its interferer base stations according to the QoS requirements of its users to allocate a portion of the spectrum [Cao05],[Ma05],[Hua05],[Nie06].

For example, in [Cao05], a distributed approach to spectrum allocation that starts from the previous spectrum assignment and performs a limited number of computations to adapt to recent topology changes is considered. According to the proposed local bargaining approach, the users affected by the mobility event self-organize into bargaining groups and adapt their spectrum assignment to approximate a new optimal conflict-free assignment.

A dynamic open spectrum sharing MAC protocol that allows nodes to adaptively select an arbitrary spectrum for the incipient communication subject to spectrum availability is introduced in [Ma05]. It offers real-time dynamic spectrum allocation and high spectrum utilization without relying on any infrastructure. It also coexists with legacy wireless applications, while avoiding the hidden and exposed terminal problems.

In [Hua06], the problem of spectrum sharing is addressed by the introduction of the “Asynchronous Distributed Pricing” scheme according to which the users exchange “price” signals that indicate the negative effect of interference at the receivers. Given this set of prices, each transmitter chooses a channel and power level to maximize its utility.

In [Nie06] the radios can measure the local interference temperature on different frequencies and can adjust by optimizing the information transmission rate for a given channel quality (using adaptive channel coding) and by possibly switching to a different frequency channel. The cognitive radios’ decisions are based on their perceived utility associated with each possible action. The overall network performance is improved at the expense of an increased overhead required for information exchange.

In general, it is shown that distributed solutions generally closely follow the centralized solutions, but at the cost of message exchanges between nodes.

The second classification is based on the allocation behavior, where spectrum access can be cooperative or non-cooperative.

1. *Cooperative spectrum sharing:*

Cooperative solutions exploit the interference measurements of each node in order to consider the effect of the communication of one node on other nodes. A common technique used in these schemes is forming clusters to share interference information locally. This localized operation

provides an effective balance between a fully centralized and a distributed scheme [Bri05], [Cao05], [Ma05], [Hua05], [Nie06].

2. Non-cooperative spectrum sharing:

In non-cooperative (or non-collaborative, selfish) solutions only a single node is considered. Because interference in other CR nodes is not considered, non-cooperative solutions may result in reduced spectrum utilization. However, these solutions do not require frequent message exchanges between neighbors as in cooperative solutions [Zhe05].

The Cooperative approaches in general outperform the non-cooperative ones. Moreover, cooperative techniques result in a certain degree of fairness, as well as improved throughput. On the other hand, the performance degradation of non-cooperative approaches is generally offset by the significantly low information exchange and hence, energy consumption.

The third classification for spectrum sharing in CR networks concerns only CRs operating in licensed spectrum areas (with primary and secondary users) and is based on the access technology. According to the way the secondary users interact with the primary and access the spectrum we have:

1. Overlay spectrum sharing:

Nodes access the network using a portion of the spectrum that has not been used by licensed users. This minimizes interference to the primary network [Bri05], [Cao05], [Ma05], [Nie06].

2. Underlay spectrum sharing:

The spread spectrum techniques are exploited such that the transmission of a CR node is regarded as noise by licensed users [Hua05]. Underlay techniques can utilize higher bandwidth at the cost of a slight increase in complexity. Considering this trade-off, hybrid techniques can be considered for the spectrum access technology for CR networks.

Finally, spectrum sharing techniques are generally focused on two types of solutions: spectrum sharing inside a CR network (intranetwork spectrum sharing) and among multiple coexisting CR networks (internetwork spectrum sharing):

1. Intranetwork spectrum sharing:

These solutions focus on spectrum allocation between the entities of a CR network. Thus, the users of a CR network try to access the available spectrum without causing interference to the primary users.

2. Internetwork spectrum sharing:

The CR architecture enables multiple systems to be deployed in overlapping spectrum bands. A specific sub-class of internetwork spectrum sharing is the co-existence of multiple operators in license exempt spectrum bands. Usually, the internetwork spectrum sharing solutions provide a broader view of the spectrum sharing concept by including certain operator policies [Lee08].

2.4 Spectrum mobility

Spectrum mobility is necessary in cases of systems with primary and secondary users, if the primary user becomes active in a spectrum band that was previously used from the secondary user. CR users are regarded as visitors to the spectrum. Hence, if the specific portion of the spectrum in use is required by a primary user, the communication must be continued in another vacant portion of the

spectrum. Thus, the notion of spectrum handoff is introduced. Protocols for different layers of the network stack must adapt to the channel parameters of the operating frequency. Moreover, they should be transparent to spectrum handoff and the associated latency [Shi07].

2.5 Conclusions

DSA and Cognitive Radio constitute a challenging field with requirements that span across different technologies and vary according to the characteristics of the studied CR scenario. Specifically, for Cognitive Radio systems operating in licensed spectrum bands with primary and secondary users, the effect of the secondary users on the primary users QoS should be minimal and therefore mechanisms for supporting spectrum sensing and spectrum mobility are of key importance. At the same time, efficient mechanisms for spectrum decision and spectrum sharing are also required for achieving high QoS. On the other hand, CR systems operating in license exempt spectrum bands, as in the case of different operators in unlicensed spectrum bands, do not require explicit spectrum mobility functionalities with hard real-time requirements and the role of spectrum sensing is modified from the identification of primary user activity to the detection of underutilized spectrum areas (gray spaces). However, in these systems the requirement for effective spectrum decision and spectrum sharing mechanisms, including power control schemes for interference mitigation, is even more important for efficient system operation. Further work on many of the previous areas is required for the key enabler technologies to reach a high level of maturity before CR systems become the norm. In this context the role of the physical layer is in many ways the cornerstone for realizing efficient CR systems.

3 FBMC as cognitive radio physical layer

The benefits of multicarrier modulation in spectrum sensing context have already been emphasized:

- Flexible multiplexing of silent sensing windows within data symbols in secondary transmission for spectrum monitoring purposes.
- Flexible way of building decision statistics from basic observations within the sensing window.
- High spectral resolution.
- Commonality of sensing and communication functions.

Naturally, OFDM is usually the first choice when talking about multicarrier systems. However, the weaknesses of the OFDM technique, i.e., using plain FFT for spectral analysis [Far08-2] on one hand and as a multiplexing technique [Iha08], [Zha09] on the other hand, have been pointed out and the introduction of filter banks has been advocated by a number of authors. These issues are discussed in the following.

3.1 Spectral selectivity and dynamic range

The OFDM receiver processing has poor selectivity against spectral components which are not synchronized to the cyclic prefix (CP) structure of OFDM. This appears as spectral leakage in scenarios with high dynamic range of signals appearing in the frequency band under analysis. Fig. 3.1 illustrates this issue. FBMC-based spectrum analyzer, utilizing the PHYDYAS reference filter bank with $M = 1024$ subbands and overlapping factor $K = 4$, is not blinded by strong primary users,

and the spectral holes (SH) can be sharply identified. Clearly, FBMC has superior performance in comparison to OFDM.

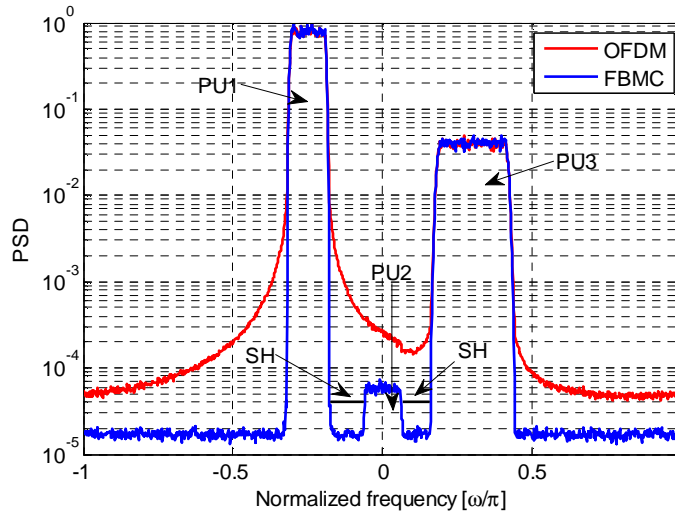


Figure 3.1. Power spectral density (PSD) estimates obtained with OFDM and FBMC receivers running energy detection in subband processing.

Fig. 3.1 basically demonstrates that with proper filter bank design, the challenging dynamic range requirements discussed in Section 2.1.1 can be achieved on the DSP side. However, it should be noted that when implementing such universal radio scene analysis covering a large bandwidth, there are great challenges for the analog RF side and the required high-speed, high dynamic range ADC is a major bottleneck. Various advanced ideas for solving these problems have been introduced in the literature, see e.g., [Cab05].

3.2 Spectral efficiency

From a transmission perspective, the FBMC technique has the potential to increase the bit rate, due to the reduced guardbands and the absence of the cyclic prefix needed in OFDM. FBMC gives also the possibility to allocate different subcarriers to different non-synchronized users in a spectrally efficient manner. It is enough to leave just one subband as guardband between different users, which may be operating asynchronously in the sense that only coarse carrier frequency synchronization is required [Bel08-3].

Another side is the spectral efficiency when multiplexing silent sensing windows with data symbols in the secondary transmission bursts. Again, leaving just one subband as guardband between spectrum monitoring blocks and transmission blocks is sufficient in FBMC. In contrast, with OFDM based secondary transmission, 5/24/92 subbands, respectively, are needed as guardband to achieve -20/-30/-40 dB interference level in reference to the subchannel power level.

In general, the overheads in spectrum reservation based monitoring depend on the guard intervals in time domain and guard bands in frequency domain around the silent spectrum sensing block (see Fig. 3.2). In time direction, the cyclic prefix of OFDM is sufficient to isolate the sensing window from previous/following data symbols and no additional overheads are introduced. In FBMC, time-domain guard intervals of length K samples are needed, where K is the overlapping factor in the filter bank design. In the PHYDYAS reference filter bank, $K = 4$.

Due to its obvious benefits, we will focus in the following on FBMC based spectrum sensing.

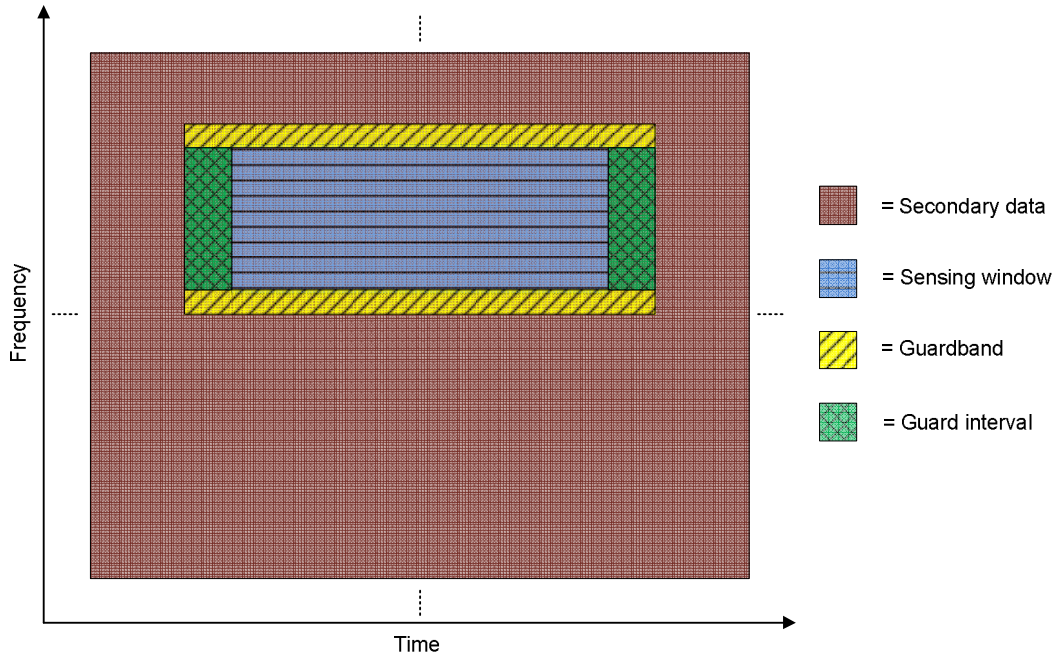


Figure 3.2. Silent window principle for spectrum monitoring.

3.3 Spectrum monitoring in FBMC

Here, we will discuss in some more details the introduced spectrum monitoring schemes. In general, assume that the time-domain guard interval is K_G OQAM symbol intervals ($2K_G$ samples in oversampled subband domain), the frequency-domain guardband is M_G subbands, and N_S independent energy observations of complex OQAM-rate samples are needed for sensing decision. Then the optimum rectangular shape of the sensing window, minimizing the overheads, can be solved as $\sqrt{N_S M_G / K_G}$ subbands and $\sqrt{N_S K_G / M_G}$ OQAM symbol intervals. The needed integer-valued solution is found close to this real valued solution. This result assumes that the spectrum sensing block is located in the middle of data symbols. If it is placed at the edge of the transmission band or in the beginning or end of the transmission burst, the additional guard space around the sensing block is reduced.

There are also other aspects which should be considered when choosing the sensing window shape (see Fig. 3.3). For rapid detection of reappearing PUs, continuous sensing subbands are very useful. On the other hand, in case of frequency selective channel, frequency diversity is useful also in spectrum sensing. In other words, it is advantageous to distribute the sensing observations over the whole transmission burst and PU frequency channel.

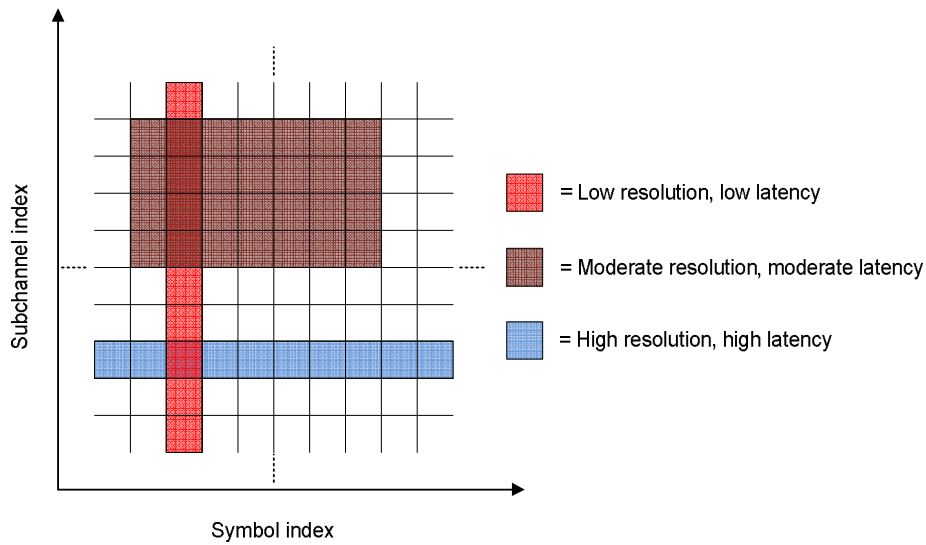


Figure 3.3. Time-frequency sensing windows: Tradeoff between spectral resolution and sensing latency.

In single-user scenarios, it is also possible to create scattered zero-symbols in the middle of data symbols, without overhead due to guard spaces. In OFDM, just 0-symbols could be utilized. In FBMC this is slightly more complicated, but still possible by utilizing the auxiliary pilot idea, which is utilized in PHYDYAS deliverables D2.1, D2.2, D3.1, and D4.1 for creating scattered pilot symbols for synchronization and channel estimation purposes. A prerequisite for the utilization of such zero-pilots in spectrum sensing is that the sensing device synchronizes itself to the active secondary user signal. Thus this approach is feasible for the simultaneous sensing and reception scheme. For specific sensing devices, additional complexity would be introduced.

It is clear that in the presence of significant multiuser interference, the sensing performance of zero-pilot based sensing would degrade. The interference could be due to the multiple access scheme of local SU system, or co-channel interference due to distant SU systems. In these cases also the residual interference based sensing (see Section 2.1.4) might not be feasible, either, so the scheme of silent sensing blocks would be preferred. This latter scheme requires only coarse time and frequency synchronization of secondary users operating in the same frequency band. Further, using continuous subband based monitoring, the time synchronization requirement is relaxed.

In summary, spectrum sensing methods based on continuous silent subchannels are the most robust approach, supporting also dynamic spectrum access schemes where different SU systems are not time synchronized and may introduce significant interference to each others. If the PU-to-SU channel is frequency selective, it is advantageous to have a sufficient number of spectrum sensing subbands (e.g., 4...16) within the PU bandwidth available for the spectrum sensing device. As already mentioned, the FBMC transmission scheme supports spectrum sensing subbands in a spectrally efficient manner, as well as wideband spectrum sensing over multiple PU frequency channels.

3.4 Spectrum sensing methods

In the literature, a number of spectrum sensing techniques have been discussed, which can coarsely be classified as cooperative or non-cooperative detection methods based on whether or not information from multiple CRs are incorporated for primary user detection. The different schemes

can further be categorized into matched filter detection, energy detection, cyclostationary feature detection techniques, and various others, each with their individual pros and cons [Höy07]. Approaches differ from each other in terms of implementation complexity, amount of prior knowledge required, processing gain obtained, and detection time required.

3.4.1 Energy detection

In a multicarrier receiver exploiting energy detection (radiometer) principle, the samples of the subband signals at output of the analysis filter bank are squared and averaged over a chosen observation interval to obtain estimates of the received energy on each subband. These estimates can be then compared to a pre-defined threshold level to make subband-wise decisions on whether the PU signal is present or not.

The main advantage of the energy detector is its simplicity. There is virtually no extra implementation cost, as the same analysis filter bank can be used for both data reception and spectrum sensing. However, an evident disadvantage is that the performance of energy detector is limited by the noise level and especially by its uncertainty, as discussed in the following section.

3.4.1.1 Sensing time in energy detection

The sensing decision is a binary hypothesis testing problem, which is characterized by two probability distributions as shown in Fig. 3.4. The distribution with lower mean value corresponds to the case where a PU signal is not present, and the observations are energies of Gaussian noise. The other distribution corresponds to the case where the PU signal is at the targeted minimum detectable level. The observations are still energies of Gaussian-distributed complex samples, but now the mean value and variance are higher. Both cases follow chi-squared probability distribution, but in practical cases they can be well approximated by Gaussian functions [Dur04]. A primary parameter of this setup is the primary signal SNR, i.e., the ratio of the signal variance to the noise variance. The SNR and the number of independent observations, N_s , determine how well the distributions are separated. The decision threshold γ then makes the tradeoff between the missed detection probability, P_{MD} , and the false alarm probability, P_{FA} .

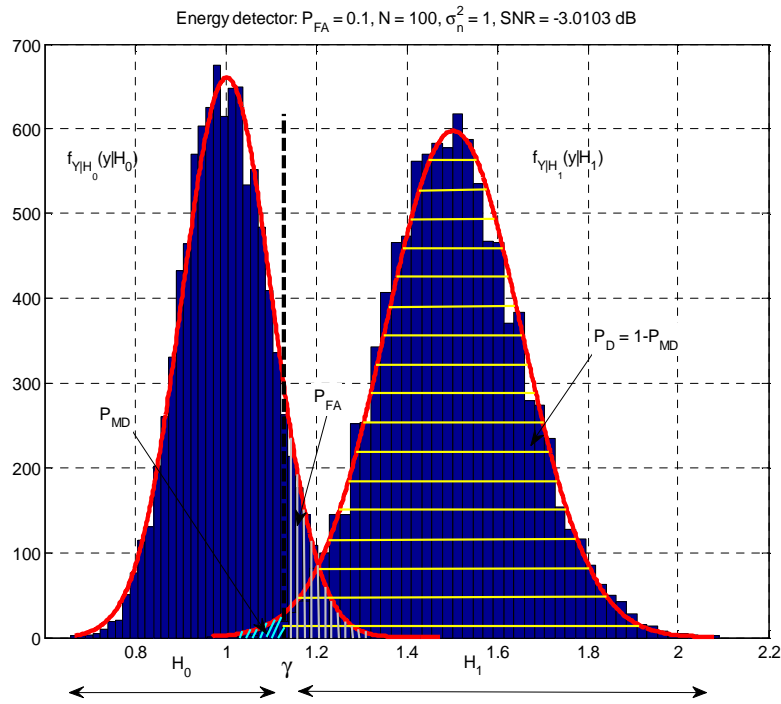


Figure 3.4. Binary hypothesis testing problem.

In FBMC, the subband signals at the analysis bank output are oversampled by a factor of two, and downsampling by two according to the OQAM subcarrier signal model is required to get independent energy observations. In the following, the sample complexity N_S refers to such OQAM rate complex samples. It should be noted that, e.g., [Tan08] uses energy observations of real samples as the basis, and the sample complexity values are double compared to what is given below. (It can be noted that the oversampled subband observations are not completely correlated at the edges of the spectrum sensing block, and some benefit can be obtained by using the oversampled observations. It is one topic of further studies to characterize this effect.)

In case there is no uncertainty and the noise variance is completely known, the required sample complexity to achieve target P_{FA} and P_{MD} can be approximated as

$$N_S = \frac{[\Phi^{-1}(P_{FA}) - \Phi^{-1}(1 - P_{MD})(1 + SNR)]^2}{SNR^2}, \quad (3.1)$$

where Φ denotes the standard Gaussian complementary CDF. On the other hand, when the energy detector is assumed to operate under a noise level uncertainty of $x = 10 \log_{10} \rho$ dB, the sample complexity can be approximated [Tan08] according to

$$N_S \approx \frac{[\Phi^{-1}(P_{FA}) - \Phi^{-1}(1 - P_{MD})]^2}{\left[SNR - \left(\rho - \frac{1}{\rho}\right)\right]^2}. \quad (3.2)$$

This introduces the so-called SNR wall [Tan08]: For example, with ± 0.1 dB uncertainty of the noise variance, the sensing sample complexity grows without limits when the SNR approaches -13.3 dB.

Fig. 3.5 shows the influence of the number of subbands on the required sensing time. We assume a sampling rate (bandwidth) of $f_s = 20.48$ MHz at the input of the analysis filter bank. The target false alarm and missed detection probabilities are set to $P_{FA} = 0.1$ and $P_{MD} = 0.01$, respectively. The effects of the sensing bandwidth and noise variance uncertainty are clearly visible. We can conclude that it is important to match the sensing bandwidth to signal bandwidth to minimize sensing time.

As mentioned, in multicarrier systems, the basic energy observations can be integrated both in time and frequency directions. This gives the possibility to utilize filter banks with subband spacing much smaller than the bandwidth of the signal to be detected. Furthermore, a filter bank with suitable subband spacing can be used flexibly in the detection of different types of primary signals and different SNR values by adjusting the integration range.

In the example of Fig. 3.6, the spectrum sensing is assumed to be carried out over bandwidths of $\Delta f = [80:80:640]$ kHz. In case the nominal subband spacing f_s/M is smaller than the sensing bandwidth Δf , the non-coherent integration will be extended over the $Q = \Delta f \cdot M / f_s$ adjacent subbands to shorten the sensing time. The effective sensing frequency resolution of Δf is therefore obtained with all considered choices of M . The required sensing times to achieve the target false alarm and missed detection probabilities of $P_{FA} = 0.1$ and $P_{MD} = 0.01$, respectively, at SNRs of -12 / -6 / -3 dB were evaluated.

In general, the sensing time (the length of the sensing window) in low rate samples after decimation can be expressed as $\lceil N_s / Q \rceil + K$. With small sample complexity N_s (i.e., at higher SNRs) and high sensing bandwidth, the use of high number of subbands unduly increases the sensing time. With high number of subbands and higher SNR, also the filter bank impulse response length has to be taken into consideration. When only few samples are needed in energy detection, the overheads due to the impulse response tails, corresponding to the time domain guard intervals in the sensing window of Fig. 3.2, become significant.

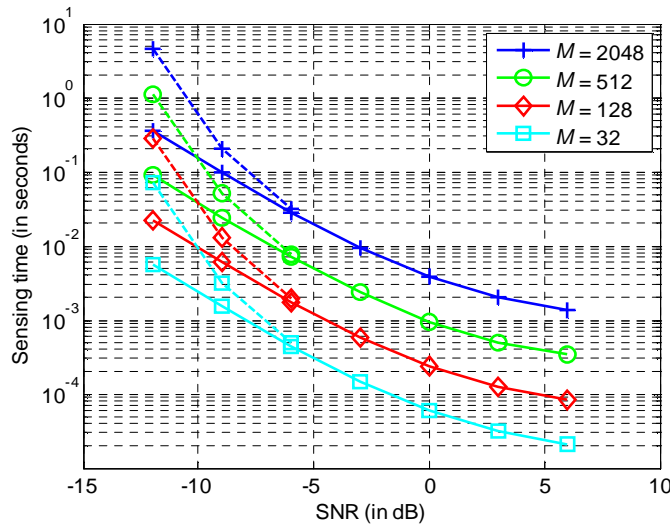


Figure 3.5. Sensing time dependence on the number of subbands in FBMC receiver running subband level energy detection with complete knowledge of the noise level (solid line) and with ± 0.1 dB uncertainty of the noise variance (dashed line).

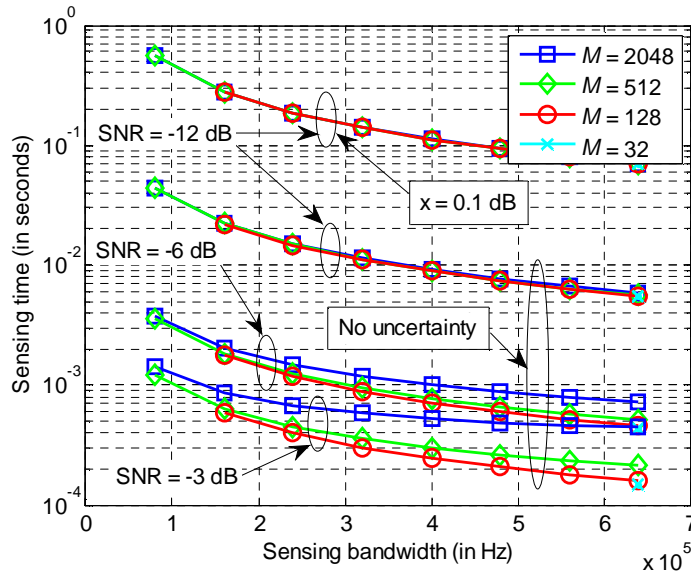


Figure 3.6. Sensing time dependence on the sensing bandwidth and number of subbands in FBMC receiver using energy detector with complete knowledge of the noise level and with ± 0.1 dB uncertainty of the noise variance.

Examples

Let us consider energy detection based spectrum sensing with target false alarm and missed detection probabilities of $P_{FA} = 0.1$ and $P_{MD} = 0.01$, respectively. The minimum primary signal SNR is assumed to be -3 dB or -6 dB. The required sample complexity is then 83 complex observations with -3 dB SNR and 268 complex observations with -6 dB SNR. Assuming overlapping factor $K = 4$ in the filter bank design, then $K_G = 2$ and $M_G = 1$. Then the optimum sensing window sizes are as follows:

For SNR = -3 dB:

Sensing window: 12 symbol intervals x 7 subbands = 84 OQAM symbols

Sensing window with guards: 16 symbol intervals x 9 subbands = 144 OQAM symbols

For SNR = -6 dB:

Sensing window: 23 symbol intervals x 12 subbands = 276 OQAM symbols

Sensing window with guards: 27 symbol intervals x 14 subbands = 378 OQAM symbols

Notice that these window sizes are independent of the parameters of the multicarrier system, as long as the PU signal bandwidth is wider than the sensing bandwidth.

Now let us assume that spectrum sensing with the above target values is applied in an FBMC system with the following parameters:

- Subcarrier spacing: 10 kHz
- Overall bandwidth: 10 MHz
- Each secondary transmission uses one or several groups of 18 contiguous subchannels.
- Sensing results are needed once in every 100 ms for each group of subchannels

- For example, if the PU bandwidth is 1 MHz, then 5 different sensing results are obtained in different frequency slots. This improves the performance essentially with frequency-selective PU-to-SU channel.

We consider two different structures for the sensing window, as shown in Fig. 3.7. In case (a), optimally shaped sensing windows are inserted in the beginning of each 100 ms frame at the edge of the subchannel group, in which case the overhead due to guards is reduced to half of the above values. One empty subchannel is inserted between the groups of subchannels in order to facilitate asynchronous transmission in different groups.

Case (b) uses continuous sensing subbands between the groups of subchannels. In this case, 3 empty subchannels are needed in each guard/sensing band.

In this simplified scenario, the overhead due to the sensing window and guardbands is

- About 5 % just due to guardbands, in the absence of sensing windows.
- About 6 % in scheme (a) with - 3 dB SNR and 7 % with - 6 dB SNR
- About 14 % in scheme (b)

In scheme (a), the above values assume that the sensing is done only in one direction (uplink or downlink) during the 100 ms interval. For example, using time division duplexing (TDD) principle the sensing could be implemented in both directions by dividing the 100 ms frame into uplink and downlink subframes, which should be of sufficient length to accommodate the sensing windows in both directions. In this case the overhead values become 6.5 % and 9 % for - 3 dB and - 6 dB SNR, respectively.

In scheme (b), use of the TDD principle doesn't affect the overheads but rather the P_{FA} and P_{MD} values.

In order to reach the target P_{FA} and P_{MD} in either direction, the sensing subbands should be available for spectrum monitoring for 8.4 ms in the - 3 dB SNR case and for 27.6 ms in the - 6 dB case.

Scheme (b) has somewhat higher overhead in this example scenario. On the other hand, it is a very robust scheme requiring only coarse frequency synchronization between different SU systems and sensing devices. Utilizing the FBMC concept, it is possible to arrange subbands which are free of interference from all SUs respecting the subchannel grouping structure. The sensing performance of scheme (a) is degraded, e.g., by distant non-synchronized SU systems utilizing the same group of subchannels.

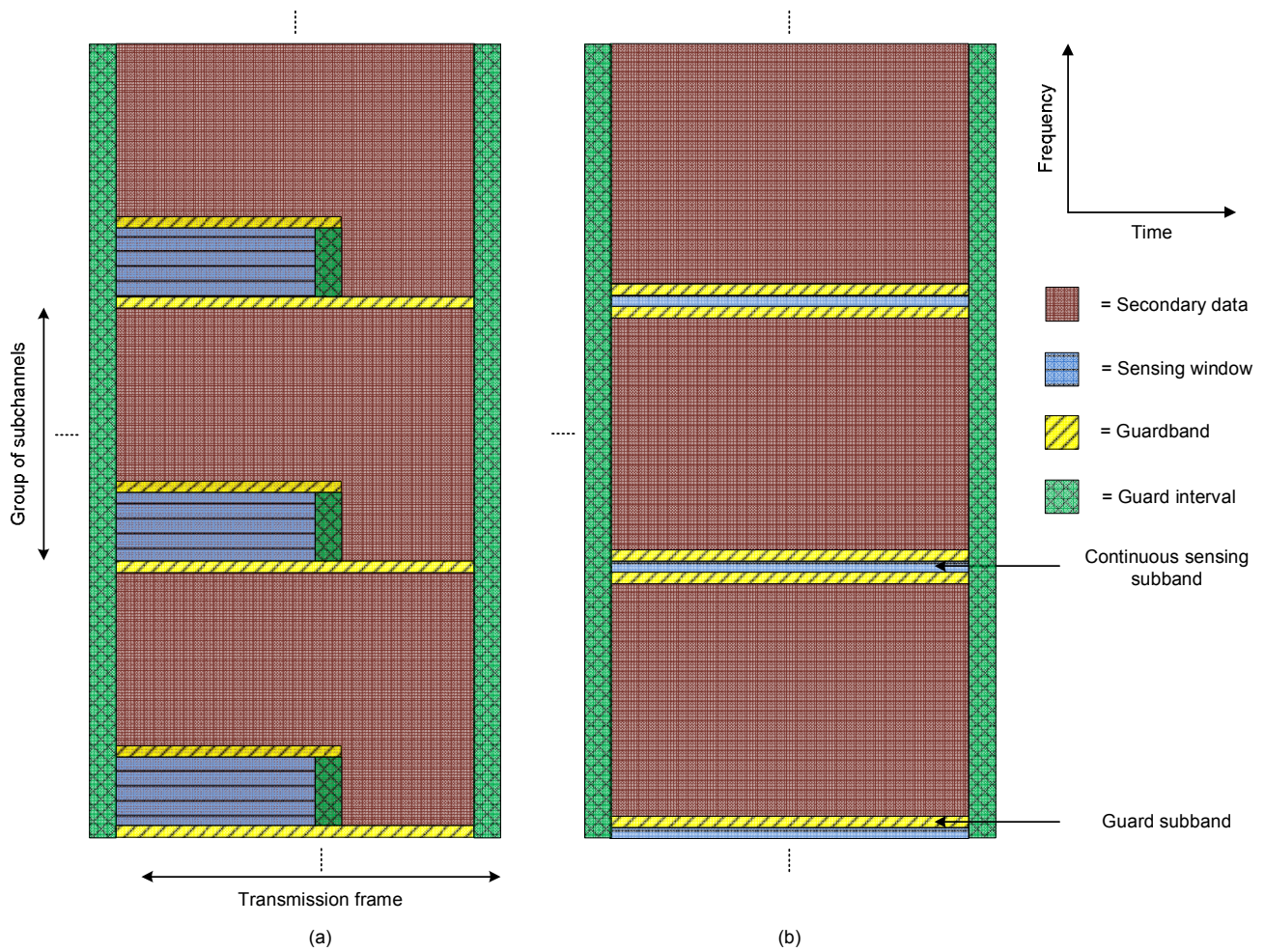


Figure 3.7. Two alternative sensing window structures.

3.4.2 Cyclostationarity detection

Spectrum sensing is challenged due to noise uncertainty when energy detection is used as the underlying sensing technique. More specifically, a very weak primary will not be distinguishable from noise if its SNR falls below a certain threshold (SNR wall) determined by the level the noise uncertainty. Cyclostationarity detector, however, is not susceptible to this limitation because of its ability to differentiate between signal and noise.

A cyclostationary process is an appropriate probabilistic model for the signals that have undergone periodic transformation, such as sampling, scanning, modulating, multiplexing, and coding operations, provided that the signal is appropriately modelled as a stationary process before undergoing the periodic transformation. Increasing demands on communication system performance show the importance of recognizing the cyclostationary character of multicarrier communicated (MCM) signals. The growing role of the concept of cyclostationarity is illustrated by past works in the detection area and other signal processing areas. Spectral correlation is an important characteristic property of wide sense cyclostationarity, and a spectral correlation function (SCF) is a generalization of the power spectral density function. Recently, the spectral correlation function has been largely exploited for signal detection, estimation, extraction and classification

mainly because different types of modulated signals have highly distinct spectral correlation functions and that stationary noise and interference exhibit no spectral correlation. Furthermore, the spectral correlation function contains phase and frequency information related to timing parameters in modulated signals. SCF is very helpful for blind signals detection and classification.

In [Gar87-1], [Gar87-2], explicit formulas of the SCF for various types of single carrier modulated signals are derived. The formula of the SCF of OFDM signal is derived by mathematic deduce in [One07]. The explicit theoretical formula of the SCF for OQAM signal is derived in [Zha08-2]. Some cyclostationary detection methods, by detecting the presence of cyclostationarity in some non-zero cyclic frequency, are proposed in [One07], [Zha08-2].

3.4.2.1 Definition of Spectral Correlation

A full understanding of the notion of spectral correlation is given in the tutorial paper [Gar86-1]. The probabilistic nonconjugate autocorrelation of a stochastic process $x(t)$ is:

$$R_x(t, \tau) = E[x(t + \tau/2)x^*(t - \tau/2)] \quad (3.3)$$

where the superscript asterisk denotes complex conjugation. $x(t)$ is defined to be second-order cyclostationary (in the wide sense) if $R_x(t, \tau)$ is the periodic function about t with period T_0 and can be represented as a Fourier series:

$$R_x(t, \tau) = \sum_{\alpha} R_x^{\alpha}(\tau) e^{j2\pi\alpha t} \quad (3.4)$$

which is called *periodic autocorrelation function*, where the sum is taken over integer multiples of the fundamental frequency " $1/T_0$ ". The Fourier coefficients can be calculated as:

$$R_x^{\alpha}(\tau) = \lim_{T \rightarrow \infty} \frac{1}{T} \int_{-\frac{T}{2}}^{\frac{T}{2}} R_x(t, \tau) e^{-j2\pi\alpha t} dt \quad (3.5)$$

where $\alpha = \text{integer}/T_0$, and $R_x^{\alpha}(\tau)$ is called the *cyclic autocorrelation function*. The idealized *cyclic spectrum function* can be characterized as the Fourier Transform:

$$S_x^{\alpha(*)}(f) = \int_{-\infty}^{\infty} R_x^{\alpha(*)}(\tau) e^{-j2\pi f \tau} d\tau \quad (3.6)$$

In the nonprobabilistic approach, for a time-series $x(t)$ that contains second-order periodicity, synchronized averaging applied to the lag product time-series " $y(t) = x(t + \tau/2)x^*(t - \tau/2)$ " yields:

$$\hat{R}_x(t, \tau) = \lim_{N \rightarrow \infty} \frac{1}{2N+1} \sum_{n=-N}^N x(t + nT_0 + \frac{\tau}{2}) x^*(t + nT_0 - \frac{\tau}{2}) \quad (3.7)$$

which is referred to as the *limit periodic autocorrelation function*. The nonprobabilistic counterpart of (3.5) is given by:

$$\hat{R}_x^\alpha(\tau) = \lim_{T \rightarrow \infty} \frac{1}{T} \int_{-\frac{T}{2}}^{\frac{T}{2}} x(t + \tau/2) x^*(t - \tau/2) e^{-j2\pi\alpha\tau} dt \quad (3.8)$$

which is recognized as the *limit cyclic autocorrelation function*. In summary, the limit cyclic autocorrelation can be interpreted as a Fourier coefficient in the Fourier series expansion of the limit periodic autocorrelation like (3.4). If $\hat{R}_x^\alpha(\tau) \equiv 0$ for all $\alpha \neq 0$ and $\hat{R}_x(\tau) \neq 0$, then $x(t)$ is said to be *purely stationary*. If $\hat{R}_x^\alpha(\tau) \neq 0$ only for $\alpha = \text{integer}/T_0$ for some period T_0 , then $x(t)$ is said to be *purely cyclostationary* with period T_0 . If $\hat{R}_x^\alpha(\tau) \neq 0$ for values of α that are not all integer multiples of some fundamental frequency $1/T_0$, then $x(t)$ is said to *exhibit cyclostationary* [Gar87-1]. For modulated signals, the periods of cyclostationarity correspond to carrier frequencies, pulse rates, spreading code repetition rates, time-division multiplexing rates, and so on.

Another interpretation of the limit cyclic autocorrelation can be obtained in [Gar86-1]. The generalized $\hat{R}_x^\alpha(\tau)$ defined by (3.8) is actually the conventional cross-correlation of the two complex-valued frequency-shifted versions:

$$\begin{aligned} u(t) &= x(t) e^{-j\pi\alpha\tau} \\ v(t) &= x(t) e^{j\pi\alpha\tau} \end{aligned} \quad (3.9)$$

of the time-series $x(t)$, that is:

$$\hat{R}_x^\alpha(\tau) \equiv \hat{R}_{uv}(\tau) = \lim_{T \rightarrow \infty} \frac{1}{T} \int_{-\frac{T}{2}}^{\frac{T}{2}} u(t + \tau/2) v^*(t - \tau/2) dt \quad (3.10)$$

Consequently, \hat{R}_x^α is the inverse Fourier transform of the cross-spectral density \hat{S}_{uv} :

$$\hat{R}_x^\alpha(\tau) = \int_{-\infty}^{\infty} \hat{S}_x^\alpha(f) e^{j2\pi f\tau} df \quad (3.11)$$

for which:

$$\hat{S}_x^\alpha(f) = \hat{S}_{uv}(f) \quad (3.12)$$

This special limit cross-spectral density is referred to as the *limit cyclic spectrum function*, and the Fourier transform relation (3.11) is called the *cyclic Wiener relation*. Following from the definition of the conventional cross-spectral density [Gar86-2], $\hat{S}_x^\alpha(f)$ is the limit temporal correlation of the two spectral components of $x(t)$ with frequencies $f + \alpha/2$ and $f - \alpha/2$:

$$\hat{S}_x^\alpha(f) = \lim_{T \rightarrow \infty} \lim_{\Delta t \rightarrow \infty} S_{uv}(f)_{\Delta t, T} \quad (3.13)$$

where $S_{uv}(f)_{\Delta t, T}$ is the temporal correlation normalized by \sqrt{T} and measured over an interval of length Δt :

$$\begin{aligned} S_{uv}(f)_{\Delta t, T} &= \frac{1}{\Delta t} \int_{-\frac{\Delta t}{2}}^{\frac{\Delta t}{2}} \frac{1}{\sqrt{T}} U_T(t, f) \cdot \frac{1}{\sqrt{T}} V_T^*(t, f) dt \\ U_T(t, f) &= X_T(t, f + \alpha/2) \\ V_T(t, f) &= X_T(t, f - \alpha/2) \end{aligned} \quad (3.14)$$

and $X_T(t, f)$ is the time-variant finite-time complex spectrum of $x(t)$ over the time interval $[t - T/2, t + T/2]$:

$$X_T(t, f) = \int_{t-T/2}^{t+T/2} x(u) e^{-j2\pi fu} du \quad (3.15)$$

Because of these spectral correlation characterizations, the limit cyclic spectrum function shall also be called *spectral correlation function*.

In paper [One07], a useful modification of the CAF called *conjugate cyclic autocorrelation function* is given as:

$$R_x^\alpha(\tau) = \lim_{T \rightarrow \infty} \frac{1}{T} \int_{-T/2}^{T/2} R_x^*(t, \tau) e^{-j2\pi\alpha t} dt \quad (3.16)$$

with $R_x^*(t, \tau) = E[x(t + \tau/2)x(t - \tau/2)]$, and the corresponding SCF called *conjugate spectral correlation function* is:

$$S_x^\alpha(f) = \int_{-\infty}^{\infty} R_x^\alpha(\tau) e^{-j2\pi f\tau} d\tau \quad (3.17)$$

For a non-cyclostationary signal, $R_x^\alpha(\tau) = R_x^*(\tau) = S_x^\alpha(f) = S_x^*(f) = 0 \quad \forall \alpha \neq 0$, and for a cyclostationary signal, any nonzero value of the frequency parameter α , for which the nonconjugate and conjugate SCFs differ from zero is called a *cycle frequency*. Both nonconjugate and conjugate SCFs are discrete functions of the cycle frequency α and are continuous in the frequency parameter f .

Because of its useful features, combining cyclostationary detection with FBMC will be one of the central topics in the spectrum sensing studies of PHYDYAS.

3.4.3 Other sensing methods

A number of more advanced spectrum sensing methods are briefly introduced here based on literature. The main goal is to identify potential techniques, in addition to energy detection, which could be operated in the frequency domain, utilizing the subband samples. Such methods could be efficiently combined with the FBMC receiver functionality.

(1) CP-correlation method

This method utilizes the CP structure of OFDM based on the autocorrelation of the received signal [Cha08]. Significant performance gain over energy detection has been demonstrated in the literature. This is a fairly generic method which can be easily configured for different OFDM systems. However, it cannot be utilized for other signal formats and it is operating in time domain. Thus it seems to be difficult to combine it efficiently with the multicarrier spectrum sensing concept.

(2) Methods based on information theoretic criteria

A method recently introduced in the literature utilizes Akaike information criterion to test whether the distribution of the received signal fits the noise distribution or not [Gho09]. Performance gain over energy detection was demonstrated also for this method. Also an entropy-based spectrum sensing method has been presented in the literature [Zay08]. This method utilizes experimental probability distribution of the observations for testing the fit. Further studies are needed to evaluate the feasibility of these methods in the FBMC context.

(3) Waveform-based sensing

This class of methods utilize special features of specific primary signals, like pilots or training patterns [Tan05]. The basic idea is to correlate the received signal with the specific signal pattern. Good performance can be achieved also with these methods, however with the loss of generality and requirement of some degree of synchronization of the sensing receiver with the PU signal.

3.5 Conclusions

In Section 3, the first steps in analyzing the FBMC technique in the context of energy detection based spectrum sensing were taken.

FBMC and OFDM receivers were compared in terms of spectral selectivity when signals with high dynamic range were assumed on the frequency band under investigation. The FBMC receiver was found to provide a clear advantage over OFDM due to its significantly enhanced spectral rejection properties.

As for the secondary data multiplexing, FBMC technique shows potential to facilitate flexible and spectrally efficient asynchronous multi-user access. Therefore, FBMC modulation is considered to be particularly well suited for the secondary transceivers.

A concept of a time-frequency sensing window, which allows for two-dimensional integration of the energy observations, was introduced and found to match well with the multicarrier receiver model. The basic tradeoff between the spectral resolution and the sensing latency, influenced by the dimensions of this window, was clarified. The sensing time can be shortened at the cost of the reduced spectral resolution and vice versa. Further, the presented concept is found to improve the flexibility of the system dimensioning and to provide adaptability to different primary signal scenarios and SNR conditions.

For spectrum monitoring during secondary transmission an idea of a silent sensing window (a spectrum sensing block within secondary data) was introduced. The overheads, resulting from multiplexing of these sensing blocks, were discussed both in case of OFDM and FBMC. Moreover, an optimal shape for the sensing window in FBMC case was presented.

Two different sensing window structures were proposed. They were found to provide different tradeoffs between the spectral efficiency of the secondary transmission (due to overheads in multiplexing silent sensing windows), the synchronization requirements, and the reaction time in case of a reappearing primary transmission. The optimally-shaped windows (located in the beginning or end of a frame at the edge of a subcarrier group) provide higher efficiency. On the other hand, the structure based on continuous sensing subbands both relaxes the time synchronization requirements among different SUs and sensing devices, and improves the ability to detect collisions due to reappearing PUs.

The future spectrum sensing studies are planned to focus on the following topics:

- More detailed studies of energy detection methods with FBMC, including the evaluation of the feasibility of residual interference and zero-pilot based methods.
- Combining cyclostationary detection with FBMC.
- Evaluation of the feasibility of the other mentioned sensing methods in the FBMC context
- Developing practical sensing methods for PHYDYAS dynamic spectrum access scheme.

4 FBMC and OFDM spectral efficiency comparison

Cognitive Radio is a context-aware intelligent radio potentially capable of autonomous reconfiguration by learning from and adapting to the communication environment, which has been proposed as a possible solution to improve spectrum utilization via dynamic spectrum access [Mit99]. A time-frequency illustration of CR network is displayed in Fig. 4.1, from which we can see that wide ranges of potential spectral resources (spectrum holes) are not used by primary users. Hence, secondary users can dynamically access by spectrum sensing that is responsible for accurately identifying and intelligently tracking idle spectrum holes that are dynamic in both time and frequency.

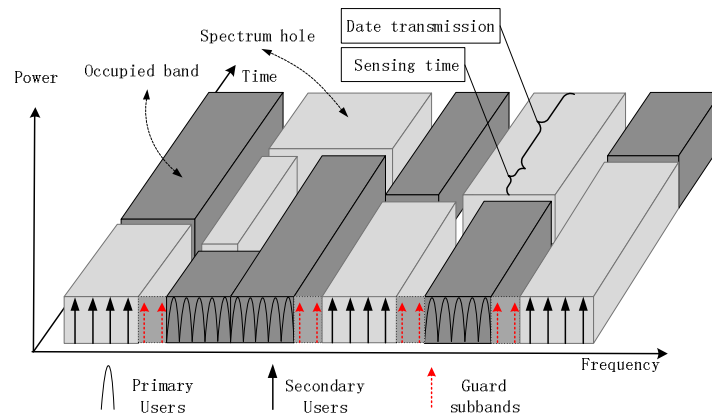


Figure 4.1. A time-frequency illustration of cognitive radio network

In a real OFDM based CR system problems arise from the IFFT/FFT operation resulting in additional interference from the CR system to the primary system and vice versa [Wei04-1][Wei04-2]. Using the IFFT transmitter implementation, the temporal pulse shape of one symbol is rectangular, resulting in a sinc-shaped frequency response on each subcarrier, thus OFDM systems suffer from high side-lobe radiation. Herein the spectral efficiency of OFDM/OQAM based multicarrier systems allowing for much lower out-of-band radiation are analyzed and compared with OFDM. In the literature of various parameters performance comparisons between OFDM and Filter bank can be found [Rhe98][Lac01][Lee04][Wal06][Du07]. However, there are few papers mentioning the spectral efficiency for CR application. Recently, the spectral efficiency analysis for OFDM and filter banks have been considered in [Iha08], where the trade-off between the level of interference caused by secondary transmission to primary user and the spectral efficiency of secondary user is studied in the CR context. Numerical results show that using filter bank approach, a low-interference secondary transmission can be obtained without sacrificing the bandwidth efficiency.

The objective of this section is to further focus on a complete spectral efficiency analysis (SEA) in the CR context. The SEA for a CR system contains two factors: time-frequency resource exploitation (or throughput) of CR users and interference level from CR user to licensed users. "Throughput" is a very important performance parameter for CR users, which refers to the amount of useful information that is transmitted over the free bandwidth in frequency and data transmission time. In practice, we usually balance these two factors to maximize the spectral efficiency under the premise to ensure compatibility between primary and secondary systems. The out-of-band radiation property is elaborated for various filter pulse shapes, the characteristics of which are confirmed by final simulated results. Two typical OFDM/OQAM pulseshapes are used in this section: The Isotropic Orthogonal Transform Algorithm (IOTA) [Flo95] (IOTA/OQAM) and the reference filter [Bel01] applied in the project PHYDYAS [PHY08] (PHYDYAS/OQAM).

4.1 Out-of-band radiation analysis

In this section, different multicarrier modulations used in cognitive radio systems are compared by quantifying the interferences of sidelobes radiation. We choose four multicarrier modulation systems: CP-OFDM, RC-OFDM, IOTA/OQAM and PHYDYAS/OQAM. We only consider the interference from rental user (RU) to licensed user (LU).

4.1.1 CP-OFDM based spectrum pooling systems

In real OFDM systems cyclic prefix is a cyclic extension of the transmitted signal in the time domain in order to overcome ISI in a multipath radio channel. This temporal extension of one OFDM symbol results in a narrower spectrum of the signals on each subcarrier. So the power spectral density (PSD) of each single carrier OFDM signal is represented in the form [Wei04-2]:

$$\Phi_{ofdm}(f) = A^2 T_s \left(\frac{\sin \pi f T_s}{\pi f T_s} \right)^2 \quad (4.1)$$

where A denotes signal amplitude and T_s in the symbol duration which consists of the sum of useful symbol duration T_u and guard interval. Assuming that the Licensed Users (LU) are co-located with this single subcarrier, as shown in Fig. 4.2. The bandwidth of one subcarrier spacing is $f_s = 1/T_u$. The mean relative interference power to one LU is defined as [Wei04-2]:

$$P_{ofdm}(n) = \frac{1}{P_{tot}} \int_{(n-1/2)f_s}^{(n+1/2)f_s} \Phi_{ofdm}(f) df \quad (4.2)$$

where P_{tot} is the total transmit power emitted on one subcarrier and n represents the distance between the considered subcarrier and the neighboring LU subband, which is illustrated in Fig. 4.2 for $n=1,2$ and 3 . In a pure OFDM system the power in (4.2) does not cause any interference to the adjacent subcarriers as their signals are orthogonal and can be separated in the OFDM receiver [Wei04-2]. In general, we cannot assume that a potential licensed system is OFDM-based. Even if it is, it would have to use the same subcarrier spacing and need to be synchronized with the rental system, which contradicts the assumptions in Cognitive Radio. So the signals of the licensed users are not orthogonal to the rental users (RU). Thus the sidelobes of the sinc-shaped spectra on each subcarrier (Fig. 4.2) fully interfere with the licensed users.

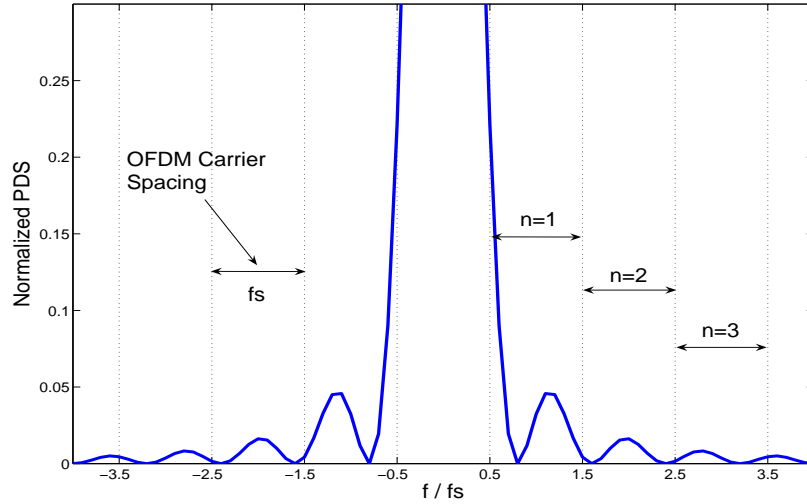


Figure 4. 2. PDS of a single CP-OFDM modulated carrier in CR system

Tabl. 4.1. interference power ratio from RU to LU

Different Systems	CP-OFDM	IOTA/OQAM	PHYDYAS/OQAM
$n = 1$	4.05%	11.83%	6.38%
$n = 2$	0.68%	2.78e-2%	3.14e-5%
$n = 3$	0.39%	5.56e-3%	9.33e-7%
$n = 4$	0.25%	3.04e-5%	1.20e-7%

Calculating (4.2), the values of interference for different n are displayed in the first column of Tabl. 4.1. In bad cases the mean interference power one LU encounters from the RU can be as large as 4 percent of the power transmitted on one subcarrier. One measure for the mitigation of this mutual interference is the introduction of adaptive guard bands in the rental system. It implies the additional deactivation of one or more subcarriers lying adjacent to allocated subbands of the licensed system. Unfortunately, this measure sacrifices bandwidth of the rental system.

4.1.2 RC-OFDM based spectrum pooling systems

Another interesting way to reduce the interference power to the licensed system is the use of time domain windowing techniques for the OFDM symbols of the rental system. Such as the root raised cosine windows can sharpen the spectral pulses on each subcarrier and lower the sidelobes. A common used raised cosine window is defined in [Wei04-2]:

$$p_{rc}(t) = \begin{cases} \frac{1}{2} + \frac{1}{2} \cos(\pi + \frac{\pi t}{\beta T_s}), & \text{for } 0 \leq t < \beta T_s \\ 1, & \text{for } \beta T_s \leq t < T_s \\ \frac{1}{2} + \frac{1}{2} \cos(\frac{\pi(t-T_s)}{\beta T_s}), & \text{for } T_s \leq t < (1+\beta)T_s \end{cases} \quad (4.3)$$

Where β denotes the rolloff factor. " $\beta = 0$ " corresponds the typical CP-OFDM, herein RC windows with " $\beta = 0.25, 0.5, 0.75, 1$ " are considered for performance comparison. Fig. 4.3 displays the PDSs of RC-OFDM modulated carriers for different rolloff factors. The side lobes are obviously attenuated as the increase of rolloff factor β . Using the same way as CP-OFDM, the values of interference for different n at each rolloff factor are displayed in Tabl. 4.2.

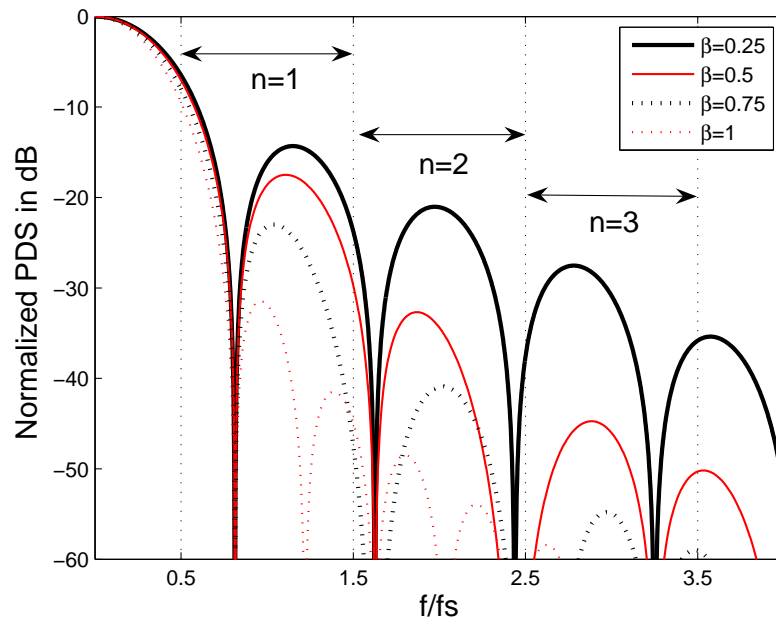


Figure 4.3. PDSs of RC-OFDM modulated carriers for different rolloff factor β in CR system

Tabl. 4.2. interference power ratio from RU to LU for RC-OFDM

Different rolloff factor	$\beta = 0.25$	$\beta = 0.5$	$\beta = 0.75$	$\beta = 1$
$n = 1$	3.70%	2.52%	1.52%	0.89%
$n = 2$	0.34%	2.16e-2%	2.78e-3%	5.07e-4%
$n = 3$	7.26e-2%	1.29e-3%	1.15e-4%	4.46e-5%
$n = 4$	8.84e-3%	2.41e-4%	3.48e-5%	5.83e-6%

We can see that RC-OFDM owns positive effect to reduce out-of-band radiation. Unfortunately, this method can only be carried out at the expense of a longer symbol duration, which reduces the throughput of CR system.

4.1.3 IOTA/OQAM based spectrum pooling systems

Le Floch [Flo95] gives an overview of the main features concerning IOTA. The closed-form expression z_{α, v_0, τ_0} can be found in [Sio00].

A orthogonalization method generates the function $z_{\alpha, \nu_0, \tau_0}$:

$$z_{\alpha, \nu_0, \tau_0}(t) = O_{\tau_0} F^{-1} O_{\nu_0} F g_{\alpha}(t) \quad (4.4)$$

where F is the Fourier transform operator, ν_0 and τ_0 are the frequency and time real parameters of the modulation system such that $\nu_0 \tau_0 = \frac{1}{2}$, O_a is an orthogonalization operator with a equal to ν_0 or τ_0 , which transforms a function x into a function y according to:

$$y(u) = \frac{x(u)}{\sqrt{a \sum_k |x(u-ka)|^2}} \quad (4.5)$$

and finally $g_{\alpha}(t) = (2\alpha)^{1/4} e^{-\pi\alpha^2 t^2}$ with α , which is the spreading parameter.

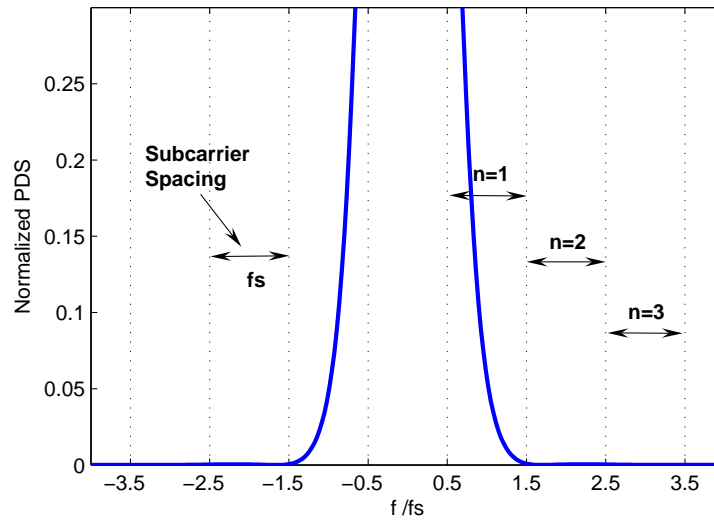


Figure 4.4. PDS of a single IOTA/OQAM modulated carrier in CR system

The function $z_{\alpha, \nu_0, \tau_0}$ satisfies: $Fz_{\alpha, \nu_0, \tau_0} = z_{1/\alpha, \tau_0, \nu_0}$, and in the special case where $\alpha = 1$ and $\nu_0 = \tau_0$, we get the function \mathfrak{Z} such that $F\mathfrak{Z} = \mathfrak{Z}$. Therefore the time and frequency properties of \mathfrak{Z} are nearly isotropic, which is called the Isotropic Orthogonal Transform Algorithm (IOTA) prototype function. In order to derive $z_{\alpha, \nu_0, \tau_0}$ from (4.4), one has to use the following closed-form expression:

$$z_{\alpha, \nu_0, \tau_0} = \frac{1}{2} \sum_{k=0}^{\infty} d_{k, \alpha, \nu_0} \left[g_{\alpha} \left(t + \frac{k}{\nu_0} \right) + g_{\alpha} \left(t - \frac{k}{\nu_0} \right) \right] \cdot \sum_{l=0}^{\infty} d_{l, 1/\alpha, \tau_0} \cos(2\pi l \frac{t}{\tau_0}) \quad (4.6)$$

where the d_{k,α,ν_0} are real coefficients, which can be computed according to a set of rational coefficients [Sio00]. So the Power Density Spectrum of IOTA signal on one single carrier band and the mean relative interference power can be similarly derived:

$$\begin{aligned}\Phi_{iota}(f) &= A^2(z_{1,\sqrt{2}/2,\sqrt{2}/2})^2 \\ P_{iota}(n) &= \frac{1}{P_{tot}} \int_{(n-1/2)f_s}^{(n+1/2)f_s} \Phi_{iota}(f) df\end{aligned}\quad (4.7)$$

where A is the signal amplitude and f_s is the subcarrier spacing. The PDS of one single IOTA modulated carrier is shown in Fig. 4.4. The second column in Tabl. 4.1 lists the interference values for different n . We can see that the sidelobes of IOTA function decline rapidly and cause very small interference to the neighboring users for $n > 1$.

4.1.4 PHYDYAS/OQAM based spectrum pooling systems

The PHYDYAS/OQAM prototype coefficients are defined as $h[n]$ [Bal07-1], with $n = 0, \dots, L-1$, where $L = KM + 1$, K is the length of each polyphase components and M is the number of subcarriers. We define the variable $\mathbb{L} = KM/2$ and assume that the prototype function is symmetry around \mathbb{L}^{th} coefficient, this means that $h[n] = h[KM - n]$. The individual amplitude of the ℓ^{th} subcarrier is then given by:

$$F_\ell(\omega) = [h[\mathbb{L}] + 2 \sum_{n=1}^{\mathbb{L}-1} h[\mathbb{L} - n] \cos(n(\omega - \frac{2\pi\ell}{M}))]\quad (4.8)$$

Similarly, the PDS of OQAM signal on one subcarrier and the mean relative interference power to LU subbands are calculated by:

$$\begin{aligned}\Phi_{phy_oqam}(f) &= A^2(F_0(f))^2 \\ P_{phy_oqam}(n) &= \frac{1}{P_{tot}} \int_{(n-1/2)f_s}^{(n+1/2)f_s} \Phi_{phy_oqam}(f) df\end{aligned}\quad (4.9)$$

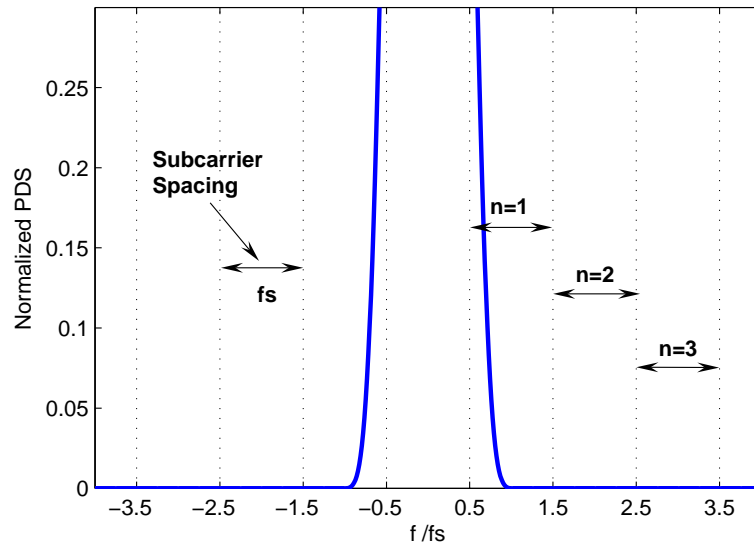


Figure 4.5. PDS of a single PHYDYAS/OQAM modulated carrier in CR system

The PDS of a single OQAM modulated carrier and the interference values for LUs are shown in Fig. 4.5 and the third column of Tabl. 4.1, respectively. We can see that almost perfect zero interference can be derived in this special OQAM-based system for $n > 1$.

According to a quantitative evaluation of the interference from RU to LU caused by the sidelobes for different multicarrier systems in Tabl. 4.1 and Tabl. 4.2, conclusions can be made that Filter Bank Based Multicarrier Systems (FBMCs) are more promising compared to OFDM system for spectrum pooling. In real applications the performance of OFDM system will be worse because:

- The practical interference from OFDM signal comes from accumulation of all the active subcarriers not just the neighboring one, so the interference caused by the big and long sidelobes will be higher. The relative interference power ratio considering all the active subcarriers is shown in Tabl. 4.3 and Tabl. 4.4, from which we can see that LU systems suffer from larger interferences from OFDM based CR system. On the contrary, FBMCs aren't sensitive to the accumulation effect because of their low and short sidelobes.
- The interference from the Licensed Signals occurs in the OFDM receivers of the Rental Signals due to the rectangular windows of the receive signal in the time domain, which originates from the FFT structure of the OFDM receiver. The received signal is windowed before it is fed to the Fourier transform. This multiplication with a rectangular window in the time domain corresponds to the convolution of the Fourier transforms of the original unwinded signal and the window function. Hence the original Fourier transform is smeared by a convolution with a sinc function [Wei04-1]. This impact will not occur for FBMC because of the filter-bank-based receiving structure.

Tabl. 4.3. interference power ratio from all the active subcarriers

Different Systems	CP-OFDM	IOTA/OQAM	PHYDYAS/OQAM
$n \geq 1$	5.76%	11.86%	6.38%
$n \geq 2$	1.71%	3.33e-2%	3.25e-5%
$n \geq 3$	1.03%	5.60e-3%	1.10e-6%
$n \geq 4$	0.64%	3.75e-5%	1.60e-7%

Tabl. 4.4. interference power ratio from all the active subcarriers for RC-OFDM

Different rolloff factor	$\beta = 0.25$	$\beta = 0.5$	$\beta = 0.75$	$\beta = 1$
$n \geq 1$	4.12%	2.55%	1.52%	0.89%
$n \geq 2$	0.42%	2.31e-2%	2.94e-3%	5.59e-4%
$n \geq 3$	8.22e-2%	1.63e-3%	1.66e-4%	5.28e-5%
$n \geq 4$	9.66e-3%	3.36e-4%	5.09e-5%	8.24e-6%

For different FBMCs, the PHYDYAS/OQAM prototype function is superior for spectrum pooling application than the IOTA/OQAM because of more concentrated frequency structure, but this superiority is obtained by compromising between the time and frequency localizations [Haa97]. In practice we always need to make a tradeoff between different parameters performance before making a decision.

4.2 Spectral efficiency analysis

SEA of one CR system includes two performance parameters: "interference" from CR user to LU user and "throughput" of CR user.

Considering the general situation, we assume that one LU band with l subcarriers is surrounded by RU band with subcarriers length n on both sides. The mean interference power density from CR users is normalized to the corresponding bandwidth l [Wei04-2]:

$$\overline{P}_{R \rightarrow L} = \frac{P_{R \rightarrow L}}{l} \quad (4.10)$$

where $P_{R \rightarrow L}$ is the interference accumulated over all the active secondary subcarriers. It is already proved in [Wei04-2] the wider the LU band, the less interference from CR users.

Throughput or bandwidth efficiency refers to the amount of information that can be transmitted over a given bandwidth in a specific communication system. It is a measure of how efficiently a limited frequency spectrum is utilized by the physical layer protocol. In digital wireless networks, the system bandwidth efficiency may for example be defined as the maximum throughput, summed over all users in the system, divided by the channel bandwidth and the transmission time. Generally, the throughput of a digital communication system is measured in bits/s/Hz.

Throughputs of a CR system over a wireless channel with coding are described as: when a return channel is available from receiver to transmitter, a more powerful feature than adaptive modulation without coding known as Adaptive Coding and Modulation (ACM) can be applied. With ACM it is possible to dynamically modify the coding rate and modulation scheme for every single frame, according to the measured channel conditions where the frame is received. This technique provides more exact channel protection and exploits the capacity of broadband frequency selective channels.

In order to reduce the signaling overhead, in different frameworks like 3GPP LTE Study Item [3GPP] and the IST Project WINNER [WINN], it has been recommended that the minimum unit (single frame) for link-adaptation and resource partitioning is a rectangular area in time and frequency denoted as "chunk". The size of one chunk should be chosen based on the coherence time

and bandwidth of the channel such that the fading within a chunk is essentially flat. The number of payload bits a chunk can offer depends on the modulation format and hence, on the channel quality. The payload bit capacity of a chunk is generally smaller than the codeword size required for the use of efficient Forward Error Correction (FEC) coding schemes. This means that the FEC coding has to be performed in the form of an "outer code", whose codewords span several chunks. In [Sti07], the authors present an adaptive coding and modulation scheme for bit-interleaved coded OFDM systems using Rate-Compatible Punctured Block-circulant Low-Density Parity-Check codes (RCP-BLDPC). This error correcting code is known to provide good performance together with efficient hardware implementation [Les06], and is considered as candidate for the FEC scheme within the WINNER project. This proposed algorithm consists of chunk-wise adaptation of the modulation and adaptive puncturing of the outer code. The throughput is maximized under a Codeword Error Rate (CWER) constraint. The number of bits per subsymbol is adapted per chunk depending on its short-term predicted Channel Gain to Noise Ratio (CNR) level. Finally, the puncturing rate of the outer code is adjusted to achieve the target CWER.

For target $CWER = 0.01$, paper [Sti07] generates the required SNR values for the code rate set $P = \{\frac{24}{48}, \frac{24}{44}, \frac{24}{40}, \frac{24}{36}, \frac{24}{32}, \frac{24}{30}, \frac{24}{28}, \frac{24}{26}\}$ and for information lengths $K = 288$ and $K = 1152$. We use the information size $K = 288$ as the chunk size of cognitive radio user as listed in Table 5. Each SNR entity of this table represents a mapping to a punctured code rate and modulation format combination.

Tabl. 4.5. Required SNR for a set of code rates for target $CWER=0.01$ and $K=288$

	Code rate R	24/48	24/44	24/40	24/36	24/32	24/30	24/28	24/26
SNR [dB] K=288	BPSK	-0.92	-0.27	0.50	1.34	2.47	3.25	4.37	6.41
	4QAM	2.09	2.74	3.51	4.35	5.48	6.26	7.38	9.42
	16QAM	7.56	8.36	9.27	10.40	11.06	12.70	13.90	16.18
	64QAM	12.08	13.13	14.26	15.59	17.21	18.38	19.71	22.07

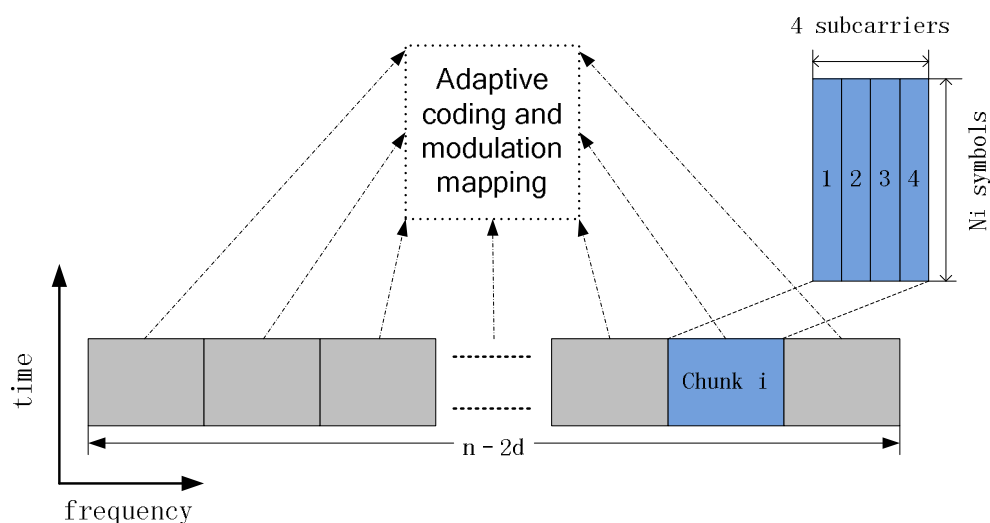


Figure 4.6. Adaptive coding and modulation scheme for chunks based CR subcarriers

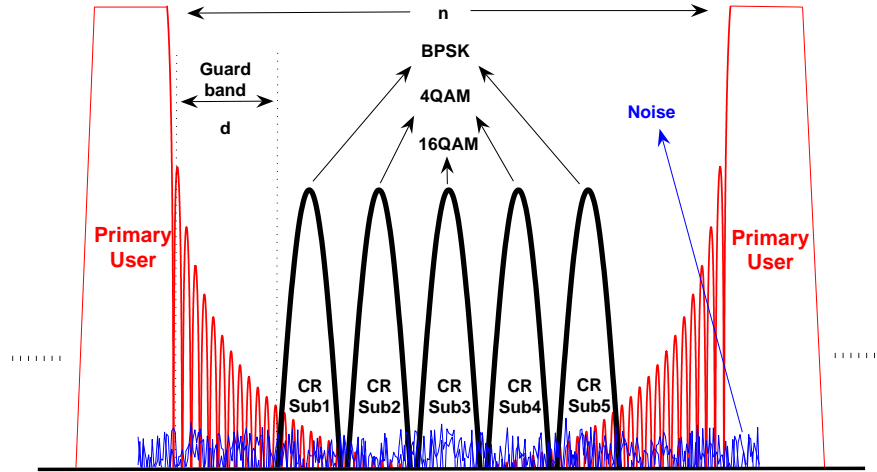


Figure 4.7. Different modulation scheme choices for each RU subcarrier

Fig. 4.6 shows the adaptive coding and modulation scheme for chunks based CR subcarriers, where "n" is the number of maximum subcarriers for one CR user and "d" is the number of guard band. The i^{th} chunk size " $4 \times N_i$ " is chosen based on the characteristic of CR network, where N_i is the number of symbols for i^{th} chunk. From Fig. 4.7 we can see that the SINR values of 4 subcarriers within one chunk closing to primary user are obviously different, in this case we consider the worst SINR value of the 4 subchannels as the mean SNR value of one chunk. The coding format and modulation scheme of each chunk for one CR user is decided by mapping its mean SNR to Tabl. 4.5.

Therefore, the "throughput" of one coded cognitive radio user during one reference transmission time is defined as:

$$T_{coded} = \frac{\lambda(T_h - T_d) \sum_{i=1}^{n-2d} P_i \log_2 M_i}{nT_h} \quad (bits/s/Hz) \quad (4.11)$$

Where " λ " is the useful data ratio, " T_h " is the reference transmission time length, " T_d " is the spectrum sensing time, " n " is the number of maximum available subcarriers for one CR user, " d " is the length of guard band, " P_i " is the code rate and " M_i " is the constellation size for i^{th} subcarrier decided by Tabl. 4.5.

4.3 Simulation results

In this section, we display numerical simulation results to evaluate the spectrum efficiency of OFDM/OQAM systems comparing with OFDM systems.

The simulations are performed under the analysis scenario as follows:

- CR context with 1024-subcarriers and a bandwidth of 5MHz , and signals are transmitted at 2.4GHz .
- Since the total number of subcarriers is 1024, we choose one LU and RU band width " $l = n = 32$ " for the following simulations.
- Four different multicarrier CR systems are investigated: CP-OFDM based multicarrier network with the CP length equal 1/4 time of one OFDM symbol, RC-OFDM based multicarrier network with the rolloff factor " $\beta = 0.25, 0.5, 0.75, 1$ ", IOTA/OQAM and PHYDYAS/OQAM based multicarrier systems.
- The licensed system is supposed to have the same physical layer modulation scheme with its corresponding CR system.

4.3.1 Interference for licensed user

Referring to Tabl. 4.3 and Tabl. 4.4, the normalized interference power as a function of guard band length is graphed in Fig. 4.8. Because of the improved spectral concentration as shown in Fig. 4.3, RC-OFDM achieves lower interference level than CP-OFDM. At the same time it can be observed that the filter bank based OQAM systems show a very fast and consistent attenuation of interference power. For a given interference power threshold (-80dB), PHYDYAS/OQAM and IOTA/OQAM can reach this threshold with only 2 and 5 widths of guard band, but bigger guard bandwidth is needed for CP-OFDM and RC-OFDM. Fig. 4.10 shows the guard bandwidth is directly relative to the throughput of CR user, so efficient performance for CR system can be achieved using OFDM/OQAM. On the contrary, considering a fixed guard band width ($d=5$), PHYDYAS/OQAM and IOTA/OQAM generate smaller interference power to neighboring LUs than OFDM, this property makes OFDM/OQAM more robust for cognitive radio application.

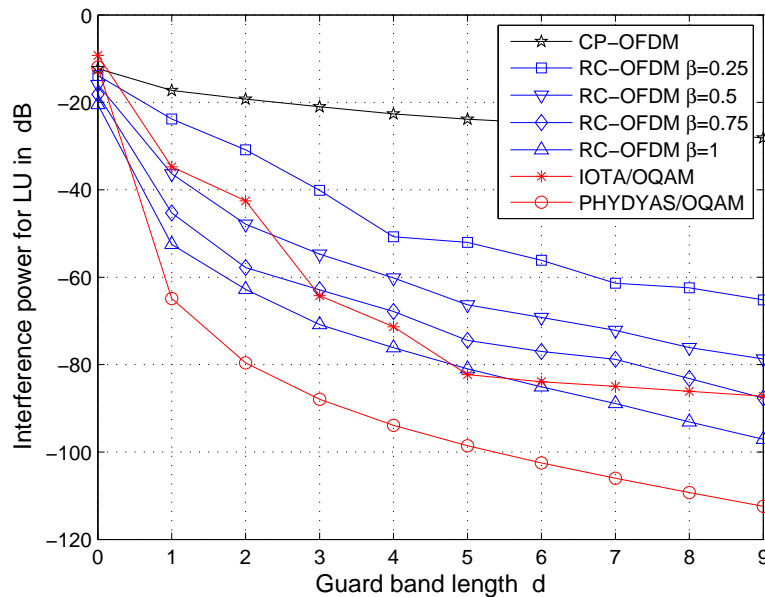


Figure 4.8. Interference power for different multicarrier modulation systems

4.3.2 Throughput for rental user

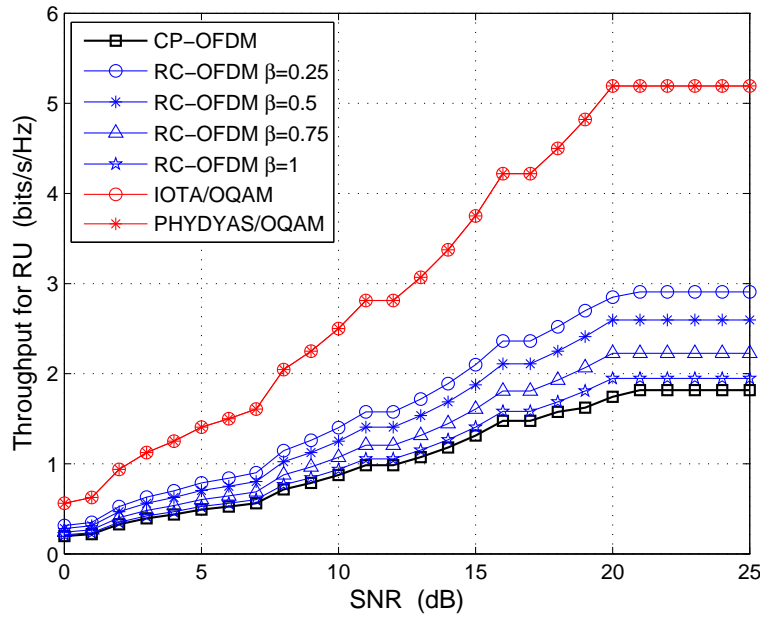


Figure 4.9. Throughputs of RU for different SNR values at a fixed interference level -30dB with RCP-BLDPC

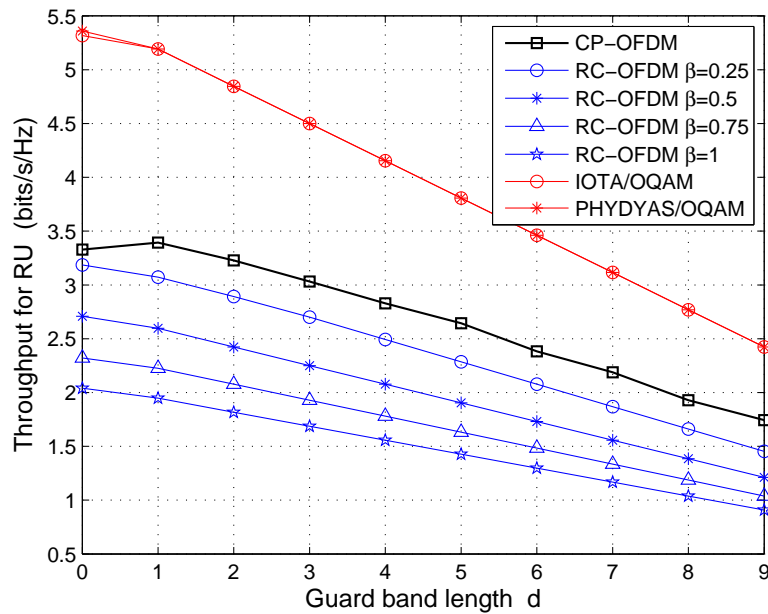


Figure 4.10. Throughputs for different guard band widths at a fixed SNR=20dB with RCP-BLDPC

We assume a required BER " $P_b = 10^{-3}$ ". Generally, the spectrum sensing time is negligible comparing to one duration of spectrum hole especially for TV channels [Cor05], that is " $T_h - T_d \approx T_h$ ". We define " $T_l = -30\text{dB}$ " as the limited interference level on a licensed system, below which the secondary user will not cause harmful impact to primary user and different guard band lengths are needed for corresponding systems (Fig. 4.8). Under this interference limitation,

throughputs (bits/s/Hz) of RU for various SNR with channel coding are shown in Fig. 4.9. Obviously, OFDM/OQAM systems without CP show higher throughput than OFDM systems. The low throughput for OFDM results mainly from repeated and overlapped transmission data and slightly from big side lobes. Besides, the raised cosine windowing with increasing β clearly pushes down the throughput due to increased symbol period, this overhead is not expected for CR system. SNR level impacts the throughput of RU at some extent. Throughputs at a fixed SNR level (20dB) for coded transmissions as a function of the normalized guard band width d are presented in Fig. 4.10, which again demonstrates that OFDM/OQAM systems generate higher throughput than OFDM at the same guard band length.

4.3.3 Tradeoff between throughput and interference

The ideal situation for CR network we expect is: maximum throughput for rental system and minimum interference for licensed system. Lots of literatures proposed to reach this "Two-Win" effect, but we always need to do some compromise between different performance parameters. Fig. 4.11 displays the mutual impact between throughput of RU and interference of LU of OFDM and OQAM based multicarrier systems. For CP-OFDM with large side-lobe, in order to ensure required throughput of RU, it is inevitable to cause heavy interference level to LU. So it is reasonable to overcome the interference by windowing the OFDM transmission signal, but the decreased interference gains are obtained by sacrificing the throughput of RU. As shown in Fig. 4.11, the performance curves of RC-OFDM with varying rolloff factors are like "Seesaw Game", the less interference you want, the more throughput you will lose. Furthermore, cyclic prefix is another important reason for the limitation performance of OFDM. Within the same conditions, OFDM/OQAM systems achieve higher performance comparing with OFDM. Although it also needs to make a tradeoff between interference and throughput, big improvements of system performance for both interference and throughput are observed from Fig. 4.11. The prototype filter of PHYDYAS/OQAM has a better spectral efficiency than IOTA/OQAM because of relative small out-of-band radiation. So quasi-perfect spectral efficiency of CR network is possible by designing small side-lobe prototype filter [Mar98].

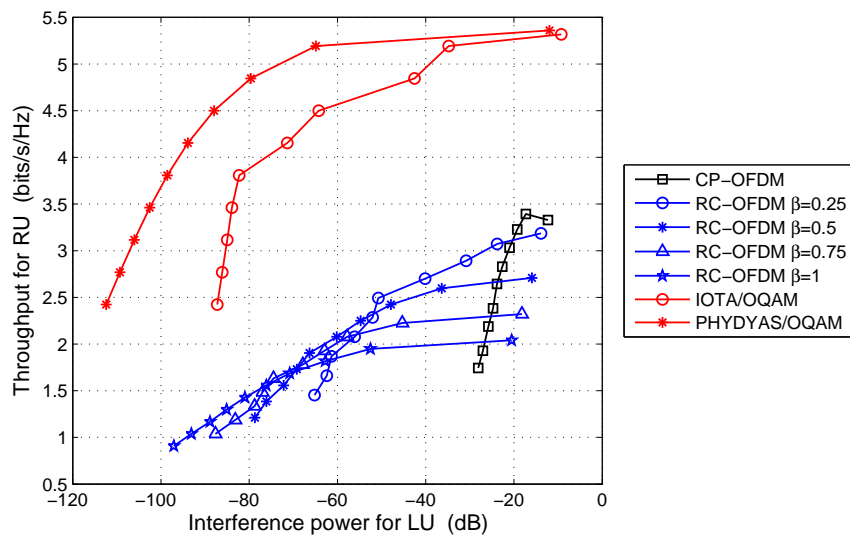


Figure 4.11. The relationship between throughput and interference at a fixed SNR=20dB with RCP-BLDPC

4.4 Conclusions

In this work, available time-frequency resource exploitation and corresponding interference power of OFDM/OQAM based systems were compared to OFDM in the Cognitive Radio context. According to the out-of-band radiation analysis of different multicarrier systems and the throughput definitions of RU, we demonstrated that when as a CR data communication technique, filter bank multicarrier modulation offers higher spectral efficiency than OFDM. As a result, OFDM/OQAM is a natural candidate for physical layer data communication in cognitive radio systems. Conventional OFDM and raised cosine windowed OFDM have to compromise between two important performance parameters: maximum throughput for secondary user and minimum interference on primary user. Although there is a little additional complexity for OFDM/OQAM system structure due to prototype pulse shaping, it is profitable for achieving better spectral efficiency.

5 RF impairments at the transmitter

5.1 Introduction

One of the main advantages of the filter bank multicarrier (FBMC) modulation scheme over OFDM is its increased spectral selectivity. This feature makes this modulation scheme attractive for cognitive radio applications where the spectrum is opportunistically reused. However, this intrinsic feature of the modulation scheme might be limited in a real application by the non idealities of the radio transmitter front-end.

The aim of this section is to evaluate how the RF impairments of the transmitter front-end impact the spectral selectivity of a filter bank multicarrier (FBMC) waveform. Three RF impairments occurring in a typical transmitter front-end are studied below because they degrade the spectral selectivity: non linearity of the power amplifier (PA), IQ mismatch and phase noise. Of these three, the most important one is the non linearity of the power amplifier which produces spectral regrowth due to the “leakage” of power from a subcarrier into adjacent ones. Typically, in order to optimize the power consumption, the PA is operated as closely as possible to its saturation region and therefore the impact of its non linearities is not negligible. In this study, the FBMC signal is compared to OFDM for a power amplifier model obtained by fitting to the measurements of a real amplifier designed for a WIMAX transmitter. The imbalance between I and Q branches, which produces interference of a subcarrier on its mirror subcarrier in a multicarrier spectrum, and phase noise, which produces ICI from a subcarrier into adjacent ones, can also degrade the spectral selectivity by limiting the dynamic range between signal and interference levels.

The first section of this study describes the test scenario, the simulation method and the parameters used to generate the waveform. The three next sections are respectively dedicated to PA non linearity, IQ imbalance and phase noise. Then the effects of the three imperfections are studied jointly. In the fifth one, the results are extended for other values of K and M. Finally, the results are summarized in a set of specifications that could be used for the design of a transmitter front-end.

The objectives are to:

- Relate the level of each RF imperfection to the level of spectral dynamic range (SDR) of the impaired FBMC waveform in a context of cognitive radio (CR) application.
 - Evaluate, in parallel, the effect of impairments on the transmission performance in terms of EVM per subcarrier.
-

- Compare the effect of the impairment to an equivalent system based on OFDM.
- Deduce the requirements that should be met by the RF front-end in order not to degrade excessively the spectral selectivity of the transmitted signal.

The latter point requires determining how much spectral regrowth or interference can be tolerated. This depends on each CR system and especially on the interference tolerance of the primary system. In this study, in order to remain as general as possible, we will provide such specifications for the following cases:

- The level at which the impaired FBMC signal is identical (in terms of SDR) to an equivalent OFDM-based signal without impairments.
- The level at which a minimum spectral dynamic range of 40dB can be preserved. This level was chosen arbitrarily because it is approximately twice as deep (in dB) than what can be expected of an OFDM system.
- The level at which the impairment becomes negligible and reaches the full spectral dynamic range inherent to the ideal FBMC waveform.

5.1.1 Cognitive radio background

The spectrum below 10 GHz is almost completely allocated to various licensed applications and it is known that there is a general shortage of free spectrum for the development of new applications at these frequencies. This is especially true for the high data rate applications which require large spectral resources but which are highly demanded. On the other hand, studies show that wide portions of this licensed spectrum are in reality only rarely used by the systems to which they are primarily allocated. The idea of cognitive radio (CR) is to reuse this available spectrum for other applications, providing that the licensed systems are not disturbed.

These already defined systems are called the primary users (PU), while the new cognitive radio systems are the secondary users (SU). An example of such a CR system which is currently under active development is the IEEE 802.22 standard which intends to reuse frequency channels left free by analog TV for a broadband access similar to WIMAX. Here, the PU is the analog TV system while the SUs are the broadband access subscribers.

Many other cognitive radio systems have been proposed either for use in dedicated licensed bands or in unlicensed bands. These are more or less complex, based on what are the PU and the SU requirements and how the PU is detected by the SU.

From the point of view of the PHY layer radio link, two underlying capabilities are always needed in order to fulfill the requirement of transmitting between SU without interfering with PU:

- Spectral selectivity of the transmitter: The SU should be able to transmit in a spectrum hole without interfering with PU in adjacent channels. Therefore, the SU must transmit with strict constraints of out-of-band radiation. In classical systems, such a constraint can be met using passive band-pass filters at the transmitter. However in a CR system which is dynamically and continuously reconfigured to use one or another portion of the spectrum among a wide range of frequencies, either adjustable filters have to be used or, alternatively, strict spectral selectivity should be a property of the adopted modulation scheme.
 - Spectral sensing at the receiver: The SU should be able to detect if primary users are or are not using the spectrum at a given time. If so, they do not start transmission or they stop to transmit. As a consequence, the SU should be equipped with spectrum sensing capabilities.
-

This contribution is related to the first requirement, that is to say the spectral selectivity of the transmitted signal and, within this scope, the present work focuses on the impact of the transmitter analog front-end non-idealities on the spectral selectivity.

5.1.2 State of the art of WIMAX OFDM transmitter

Zero-IF architecture presents several advantages compared to other classical radio transmitter architectures, such as super heterodyne or IF sampling, and is therefore the preferred choice in most WIMAX transceivers on the market. These advantages are as follows: the good performance of the IQ modulators at WIMAX frequency on current RF IC technologies; the fact that the WIMAX OFDM modulation scheme does not use the zero frequency and is therefore robust to DC offset; the mixer spurious are limited because no IF frequency stage is required; and specifications on filter are more relaxed because no band pass filters are needed, only low pass filters are used at DAC output. A typical direct conversion transmitter is depicted in Figure 5.1. As can be seen, the three main imperfections in this architecture are the phase noise, which has an important impact on OFDM signal especially as the subcarrier spacing becomes narrower, the IQ mismatch due to non identical I and Q branches and, most important for spectral regrowth, the non linearity of the power amplifier.

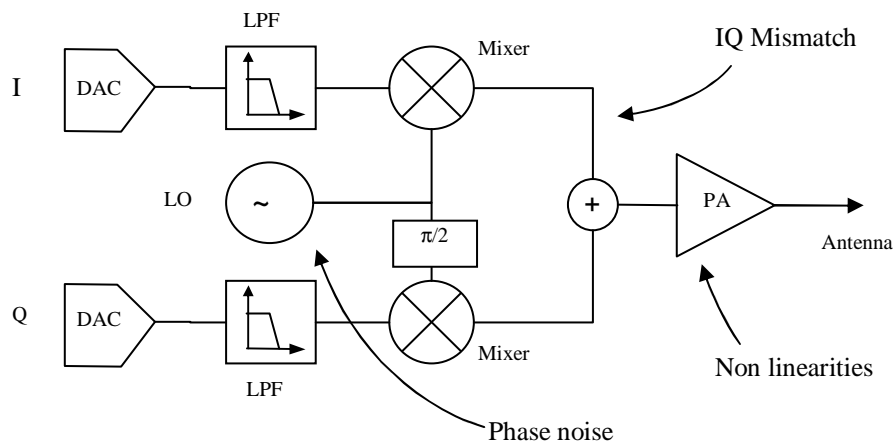


Figure 5.1. Zero-IF Direct Conversion architecture

The table below recaps typical values for each of these imperfections extracted from a state-of-the-art commercial WIMAX transmitter [Mas07]. Specifications for a typical power amplifier are given in Table 5.2. Table 5.3 presents EVM requirements at the transmitter output as a function of the constellation order given [802.16-04].

Table 5.1. Typical specifications of a commercial transmitter chipset (without PA) [Mas07]

Parameter	Value	Unit	Condition
EVM @ PA input	1.2	%	OFDM 64QAM
Max Power @ PA input	-3	dB	
OP1dB	12.4	dB	
OIP3	19	dB	
Adj. Channel Power	-55	dB	With 10 MHz signal, Measured at 10MHz Offset RBW = 100 kHz, VBW = 30 kHz
Noise Floor	-142.5	dBc/Hz	Measured at 20MHz offset
Phase Noise	-116	dBc/Hz @100 KHz	
	-138	dBc/Hz @1 MHz	
Amplitude IQ mismatch	Compensated by scaling appropriately the current driving the IQ modulator after a calibration measurement. This allows compensating interferences between subcarriers up to 60dB. However subsequent changes due to temperature variation cannot be compensated.		
Phase IQ mismatch	Phase imbalance is not specified and cannot be easily compensated.		

Table 5.2. Specifications of a WIMAX power amplifier (Sirenza SZP-3026Z)

Parameter	Value	Unit	Condition
F_0	2.7-3.8	MHz	
Pout	26	dBm	OFDM 64QAM
P1dB	33.5	dBm	
NF	5.9	dB	
IM3	-44	dB	For Pout=23dBm/tone
S_{21}	11.8	dB	

Table 5.3. EVM requirement for a WIMAX transmitter as a function of the constellation order (IEEE802.16-2004 standard, section 8.3.10.1.2)

Constellation order	EVM (dB)	EVM (%)
QPSK $\frac{3}{4}$	-18.5	12.58
16-QAM $\frac{3}{4}$	-25.0	5.62
64-QAM $\frac{3}{4}$	-31.0	2.81

5.2 Test scenario for cognitive radio

Spectral regrowth and intercarrier interferences due to non linear impairments in a communication system depends on the properties of the signal and cannot be simply studied without making assumptions on the transmitted signal [Gar99].

Therefore, a scenario is defined for the allocation of the subcarriers so that some groups of subcarriers of the test signals are modulated while others are set to zero as detailed below. Spectral Dynamic range (SDR) can be measured in these in-band spectrum holes relatively to the signal power of the modulated subcarriers.

The study is based on a system with $M = 256$ subcarriers and the test scenario is defined as follow:

- A 1st group of 32 subcarriers is modulated between subcarriers 65 and 96.
- A 2nd group of 96 subcarriers is modulated between subcarriers 129 and 224.

As a consequence, three groups of subcarriers are left to zero:

- The 64 first subcarriers.
- A hole of 32 subcarriers between subcarriers 97 and 128.
- The 32 last ones.

This could be for instance representative of a multi-user system where 256 subcarriers are divided between 8 user groups of 32 subcarriers each. Each of these two band groups accounts for the transmission of one or two primary users that shares the spectrum. An unused spectrum hole is present between users and can be used for a secondary opportunistic communication. However, interference and spectral regrowth due to the primary users will degrade the dynamic range in this portion of the spectrum.

From equation (9) of D2.1 page 13, it comes that a baseband multicarrier signal can be generally expressed as:

$$s(t) = \sum_{m=0}^{M-1} \sum_{n \in \mathbb{Z}} d_{m,n} \cdot p_m(t + n \cdot T) \cdot e^{j \cdot 2 \cdot \pi \cdot m \cdot \Delta f \cdot t} \quad (5.1)$$

With $d_{m,n}$, the constellation message, $p(t)$ the filter in time-domain, Δf the subcarrier interspacing, and T the duration of the MC symbol. For OFDM, $p(t)$ is a rectangular function of length T centered on 0. For FBMC, $p(t)$ is the filter at index m of the bank.

By applying Fourier transform, the power spectral density (PSD) of the signal can be expressed as:

$$PSD(f) = |S(f)|^2 = \left| \sum_{m=0}^{M-1} \sum_{n \in \mathbb{Z}} d_{m,n} \cdot \hat{P}_m(f + m \cdot \Delta f) \cdot e^{-j \cdot 2 \cdot \pi \cdot \Delta f \cdot n \cdot T} \right|^2 \quad (5.2)$$

With $\hat{P}_m(f)$ the frequency transfer function of the filter.

If we compute the PSD of a single MC symbol, we can assume $n=0$.

$$PSD_{1symbol}(f) = |S(f)|^2 = \left| \sum_{m=0}^{M-1} d_m \cdot \hat{P}_m(f + m \cdot \Delta f) \right|^2 \quad (5.3)$$

Figure 5.2 illustrates the PSD for the OFDM filter (Rectangular function) and for two FBMC prototype filters designed in PHYDYAS and computed with $d_{128}=1$ and $d_m=0$ otherwise.

Figure 5.3 illustrates the spectrum for the test scenario as defined above. The PSD is computed from (5.3) with $d_m=1$ for modulated subcarriers and $d_m=0$ for unmodulated ones.

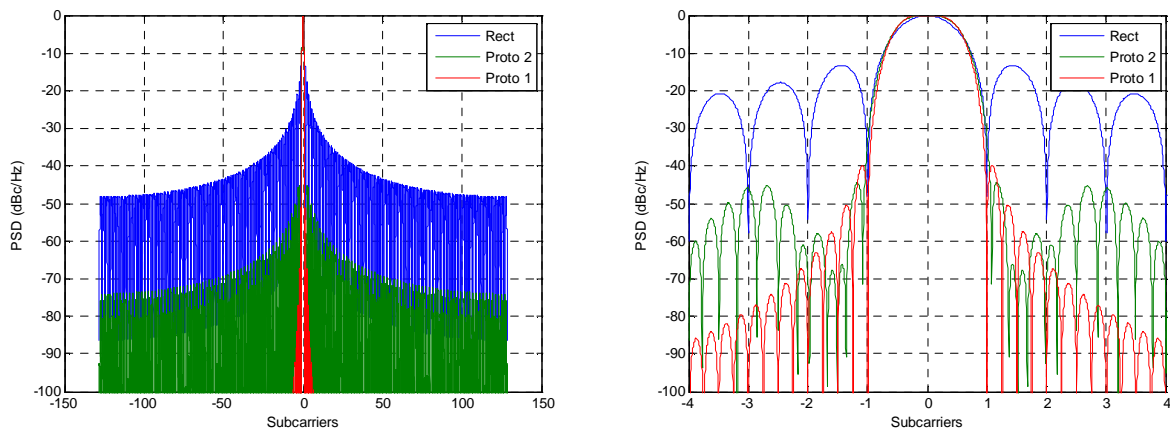


Figure 5.2. PSD of a single subcarrier for OFDM (rect function) and for two FBMC prototype filters designed in PHYDYAS. Left: Full spectrum with $M=256$. Right: Zoom on subcarriers -4 to 4.

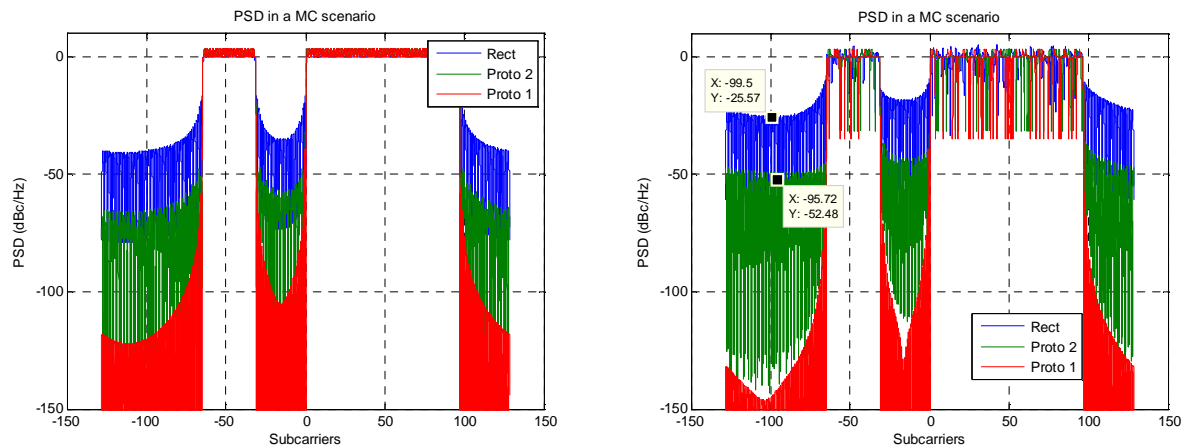


Figure 5.3. Theoretical PSD computed for the test scenario in the case of OFDM and for two types of FBMC filters designed in PHYDYAS. Left : with $dm=1$ for modulated subcarrier, $dm=0$ otherwise. Right : Random QPSK modulation

The level of SDR is evaluated in two locations of the in-band spectrum: in the smaller 32-subcarrier hole in the middle of the spectrum or in the 64-subcarrier hole on the left side of the band. Levels are measured at the deepest point of each spectrum portion. The SDR measured in Figure 5.3 are summarized in Table 5.4.

Table 5.4. Spectral Dynamic Range (SDR) computed in two different parts of the test signal spectrum.

	SDR (side)	SDR (hole)
OFDM	-25.6 dB	-18.4 dB
FBMC proto 1	-52.5 dB	-47.8 dB

These levels, computed from expressions (5.3), are used to validate the baseband simulation presented in the next section.

5.3 Baseband simulation parameters

Baseband simulations are performed using FBMC and OFDM test signals following the test scenario described above. The principle is presented in Figure 5.4. The baseband FBMC test signals are generated according to the polyphase implementation and Matlab code developed in the frame of PHYDYAS. The OFDM signal is generated based on the same parameters as FBMC and has basically the same properties except the OQAM processing and the filter bank.

For the sake of simplicity, no CP was included in the OFDM waveform. This assumption is considered to be acceptable in the following study because none of the imperfections studied hereafter produce time delays or have a memory effect. Also, it has to be noted that the implemented simulation scenario assumes a perfect synchronization between the two users. In reality, two different users are not perfectly synchronized. Due to its inherent properties of spectral selectivity, FBMC modulation scheme has the advantage over OFDM of being more robust to unsynchronization. This interesting feature of FBMC is not underlined hereafter but it is tackled in the frame of PHYDYAS in WP6 as well as in [Ra09].

RF impairments are then applied and finally the power spectral density of the received signal is estimated. The spectrum is computed using the Welch's periodogram method with an FFT size of 2^{16} points (256 times longer than the size of the 256-FFT block used in the modulation scheme) and with a Hamming apodization window. We ensure that the PSD estimation method is not the limiting factor in terms of spectral selectivity. The PSD is measured in dBc/Hz relatively to the power level in modulated subcarrier.

In parallel to the spectral estimation, the impaired waveform is also demodulated by an ideal OFDM/FBMC receiver (no equalization / assuming perfect synchronization). EVM is evaluated per subcarriers both on the modulated subcarriers and on the unmodulated holes (assuming that this corresponds to a 0-level symbol). Evaluation on modulated subcarriers allows estimating the quality of PU transmissions, while EVM evaluated on unmodulated subcarriers allows to bound the quality of a possible SU transmission that would be established in the hole (assuming a power level at the receiver equal or lower to the PU signal).

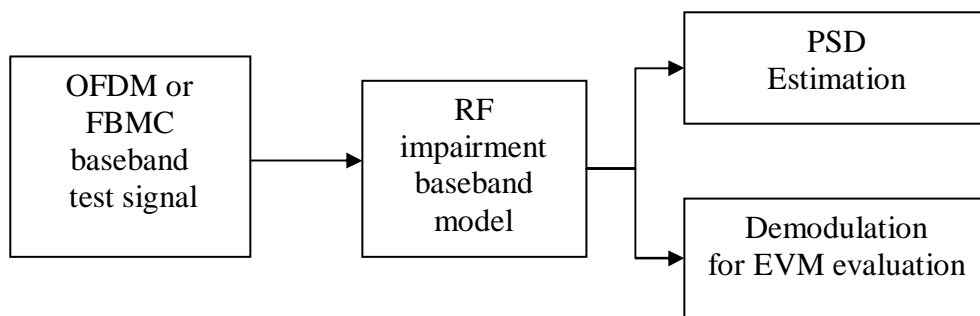


Figure 5.4. Schematic of the simulation

The main simulation parameters used to generate the baseband signal, common to both OFDM and FBMC, are given in Table 5.5.

Table 5.5. Common parameters for generation of OFDM and FBMC signal.

Parameter	OFDM	FBMC
# OFDM / FBMC Symbols	256	
# data bits	$4 \cdot 10^5$	
Sample Frequency FS	10 MHz	
Subcarrier modulation	QPSK	
FFT Size	256	
Bandwidth	9.76 MHz	
Sub-carrier spacing	39.06 KHz	

The filter bank implementation is based on the prototype filter and the polyphase implementation previously proposed in the PHYDYAS project. The parameters used are given in Table 5.6.

Table 5.6. Parameters of the prototype filter.

Parameter	Value
M	256
α	1
K	4
P_0	1
P_1	0.97195983
P_2	$1/\sqrt{2}$
P_3	0.23514695

Figure 5.5 shows the resulting spectrums for both modulation schemes when no imperfection is introduced and with an ideal channel. This will be used as a reference. As expected, it can be seen that the spectral selectivity of FBMC is better than the one of OFDM.

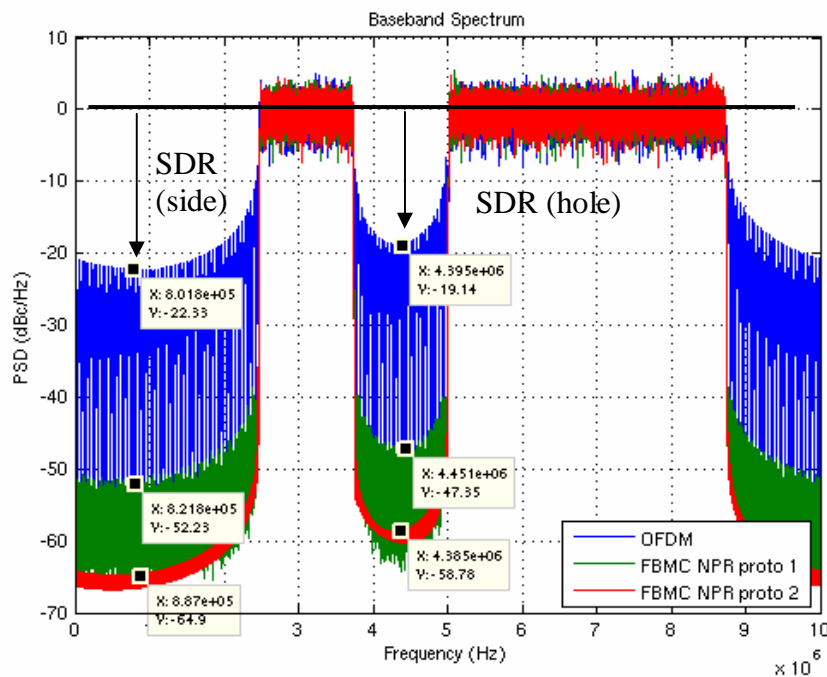


Figure 5.5. Simulation scenario for RF impairment study on spectral sensitivity.
Comparison between OFDM and FBMC.

It can be noted that the levels of SDR obtained from the PSD estimation on the baseband signal (see Table 5.7 below) are in very good agreement with PSD computed from analytical expressions presented in Figure 5.3 and Table 5.4.

Table 5.7. Spectral Dynamic Range computed in two different parts of the test signal spectrum.

	SDR (side)	SDR (hole)
OFDM	-22.2dB	-17.7 dB
FBMC proto 1	-51.6 dB	-46.9 dB

These levels of SDR correspond to in-band attenuations. They can be compared with the order of magnitude of the out-of-band spectral mask specified in the WIMAX standard (-25dB at 700 KHz offset and -50dB at 10 MHz offset) or with the signal-to-noise ratio reported in commercial WIMAX transmitter datasheet (60-70dB). Contrary to in-band attenuation, out-of-band attenuations are measured outside of the multicarrier spectrum at frequency offset equivalent to the channel bandwidth (i.e. 10MHz) and are not impacted by the sinc sidelobes of the OFDM waveform. Therefore such levels can be thought as lower bound for the in-band spectral selectivity achievable using current state-of-the art commercial transmitters, independently of the modulation scheme used.

5.4 Non linearity of a power amplifier

5.4.1 Model amplifier used

A power amplifier specified for WIMAX was measured and fitted to the parameters of a baseband model. The PA was delivered by Intracom Greece and its measurement was performed by LETI in the frame of the European project ROCKET. Details about the measurement are reported in the deliverable D9 of the IST FP7 ROCKET Project [Roc09]. It is composed from two cascaded amplifiers, pre-amplifier Hittite HMC327MS8G and amplifier Sirenza SZP-3026Z. The amplifier is a Class A GaAs InGaP HBT with 5V power supply.

5.4.2 Measurement and modeling of the power amplifier

Based on the performed measurements, four analytical models have been fitted to the data: Solid state high power amplifier (SSPA) model, Travelling Wave Tube (TWT) amplifier model, Idealized simple limiter amplifier model and spline fitted model.

The three first models are documented in [Rap91], the last one is based on a close fitting of the measured AMAM and AMPM characteristics using spline interpolation.

The normalized characteristics (i.e. $G=1$ in the small signal region and saturation power = 0dB) for the four models for AMAM and AMPM characteristics are plotted in Figure 5.6.

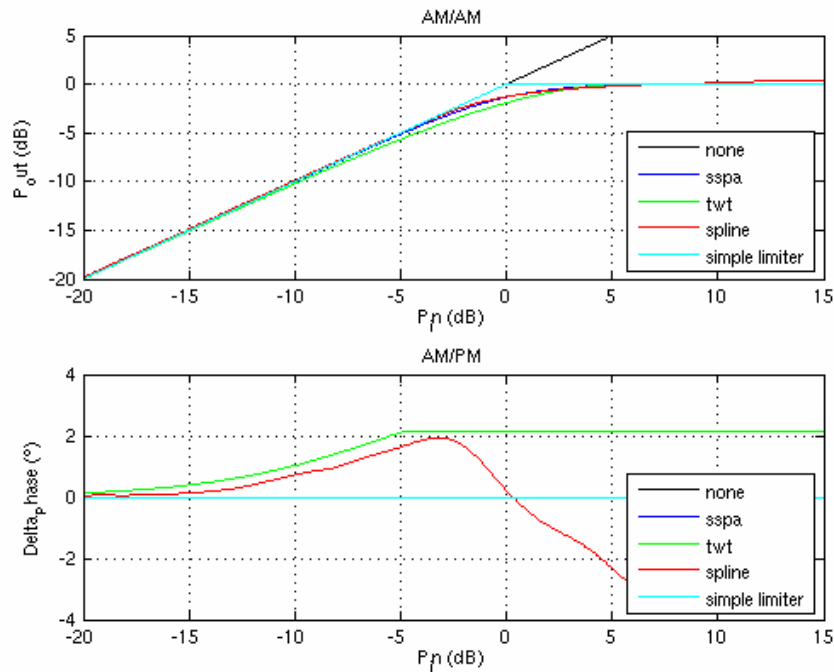


Figure 5.6. AM/AM and AM/PM characteristics for 4 models that have been fitted to the PA measurements.

Different PA models are compared for 5dB and 10dB of input power back-off (IBO) using the FBMC and OFDM baseband signals. The resulting spectrum is plotted in Figure 5.7.

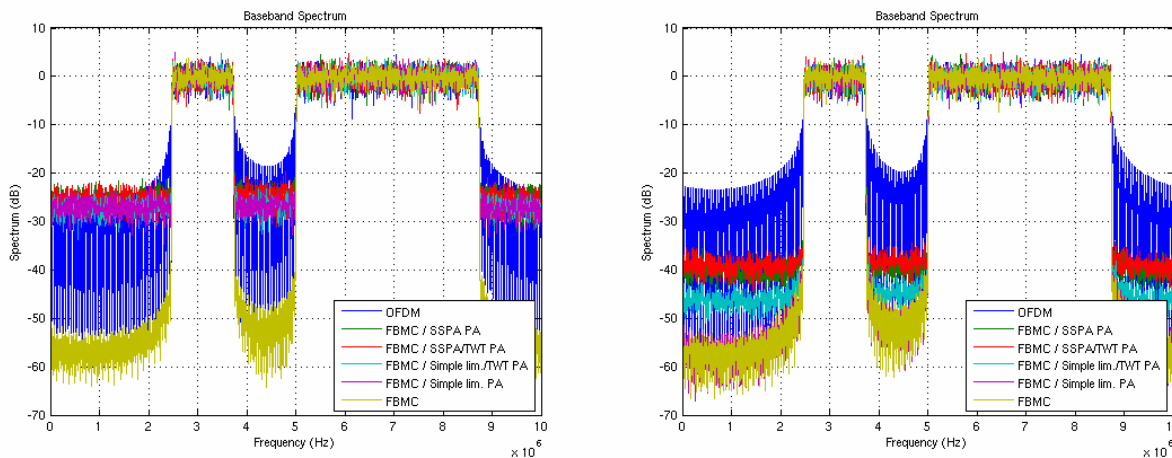


Figure 5.7. Comparison of several PA models. Left: IBO = 5dB. Right: IBO = 10 dB.

Four combinations are studied. The AMAM characteristic is modeled by simple limiter or SSPA model. The AMPM is either not modeled (if not specified in the legend) or is modeled by the TWT model.

For 10dB of IBO, the choice of the SSPA rather than the simple limiter model for the AMAM characteristic leads to a difference of nearly 10dB of SDR. Similarly, the effect of the AMPM characteristic leads to a 5dB difference on the SDR (when used jointly with the simple limiter model).

Consequently, the following study is carried out with the most realistic models among the ones being tested, that is to say:

- An SSPA AMAM characteristic with parameter $p = 2.25$.
- An TWT AMPM characteristic with parameters $\alpha_\varphi = 4.5$ and $\beta_\varphi = 1.1$.

5.4.3 Simulations

Figure 5.8 presents spectrum for four values of IBO. IBO is defined as the back-off of the mean baseband signal to the input saturation power.

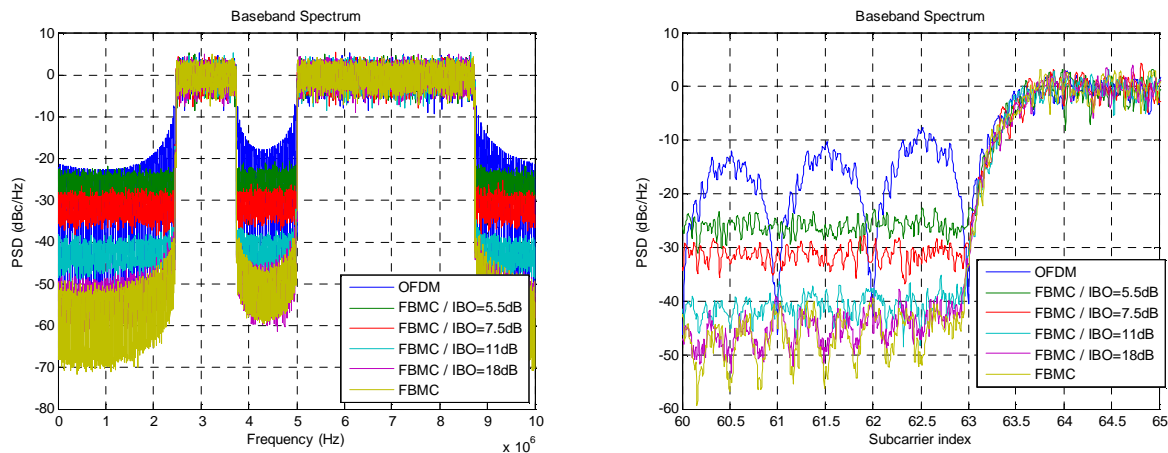


Figure 5.8 . Impact of the power amplifier non linearity on the transmitted spectrum for several values of the input back-off. Right: Full in-band spectrum. Left: Zoom on [60 65] subcarriers.

The conclusion of this simulation is that:

- For $\text{IBO} > 18 \text{ dB}$, the effect of the PA become nearly negligible and the full spectral sensitivity of theoretical FBMC can be reached.
- For $\text{IBO} = 11 \text{ dB}$, the criterion of an SDR of 40dB can be obtained on both side and hole.
- For $\text{IBO} = 5.5$, the same characteristics as OFDM are obtained.

The Figure 5.9 compares OFDM and FBMC waveform for 5 and 10 dB of IBO.

- For 5dB of IBO, the use of FBMC or OFDM leads to the same level of SDR making the advantage of FBMC insignificant.
- However, for higher IBO, there is a clear advantage to use FBMC rather than OFDM in term of SDR. For 10dB of IBO, the SDR is improved by 15dB with FBMC rather than OFDM.

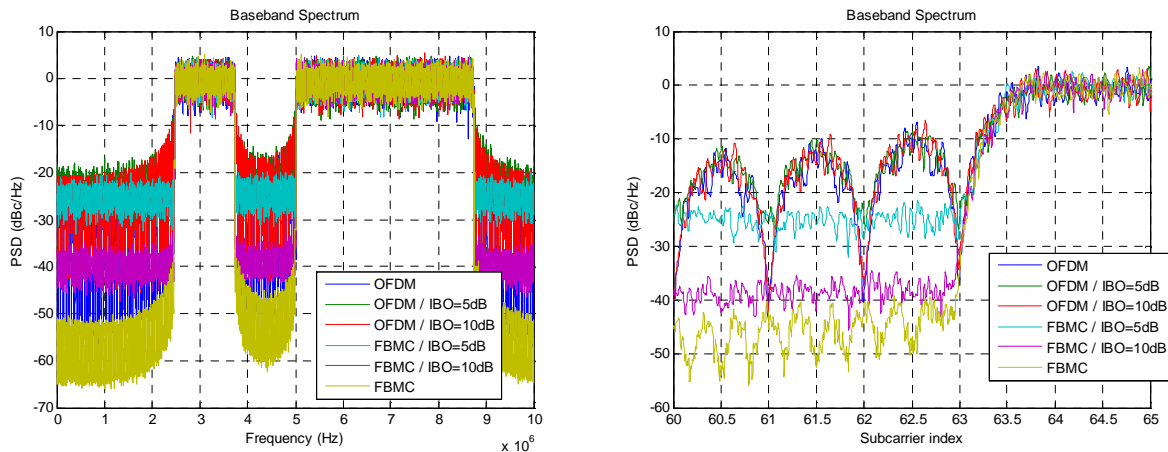


Figure 5.9. Impact of the power amplifier non linearity on the transmitted spectrum for several values of the input back-off.

Table 5.9 evaluates and compares degradation in term of EVM per subcarrier as a function of IBO. An IBO of 7.5dB allows reaching WIMAX specifications for 16-QAM. An IBO of 11dB is correct for 64-QAM. See Table 5.3 for EVM WIMAX specifications.

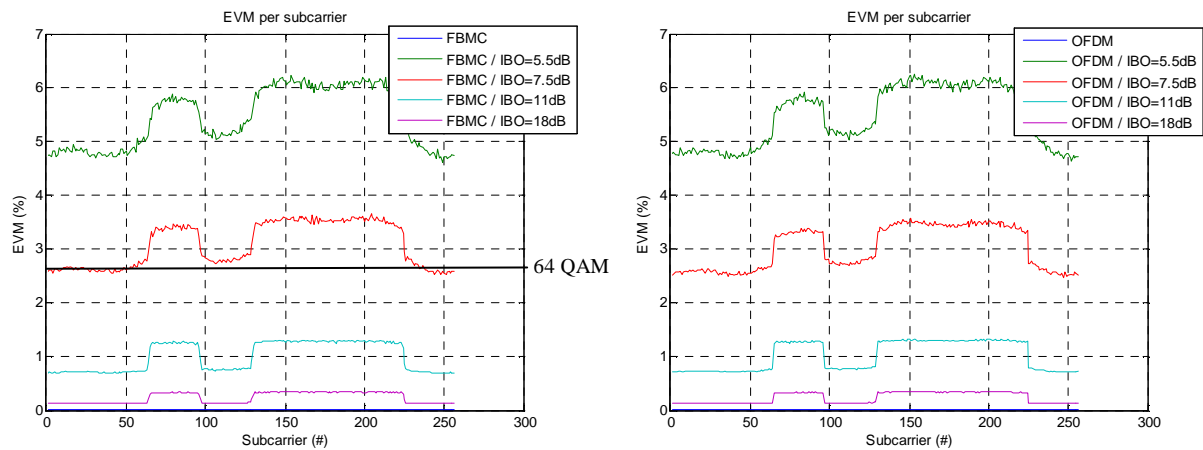


Figure 5.10. EVM per subcarrier as a function of IBO. Left side: FBMC, Right side: OFDM.

5.4.4 Power consumption

Operating the Power Amplifier (PA) at a high input back-off decreases its power efficiency. As the power amplifier is usually one of the most power demanding component in a radio transmitter, this has a direct impact on the overall consumption of the transmitter.

The power-added efficiency (PAE) characterizes the ratio of DC power consumed by the PA to its RF output power and is defined by:

$$PAE = \frac{\text{output signal power} - \text{input signal power}}{\text{DC power}} \quad (5.4)$$

Figure 5.11 shows the theoretical relationship between input back-off and power efficiency for different classes of power amplifiers.

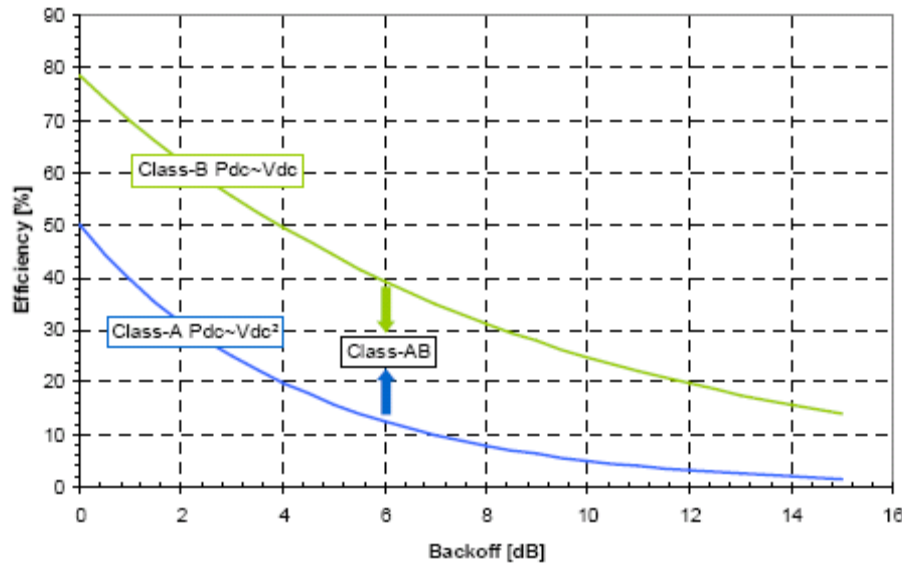


Figure 5.11. Backoff vs. efficiency in class A operation amplifier

Operating the PA at an IBO of 11dB rather than 5.5dB will increase the power consumption by a factor 3. This assumes the case of a class A amplifier. Class A amplifiers differ from class B in the sense that they are less efficient but demonstrate a far better linearity. Most power amplifiers designed for WIMAX application are class A as the linearity is a key point.

5.5 IQ imbalance

IQ mismatch occurs in transmitter's architectures where the signal is converted from digital to analog domain at the baseband level by two distinct analog branches for I and Q signals. Any differences between DAC, filters, mixers generate an imbalance between the two branches that will impact the transmitted signal.

5.5.1 Model

In most radio architectures, the RF signal is converted to or from baseband in the analog domain. Therefore, at some point in the circuit, I and Q components are transmitted by two separate paths which can be unbalanced in phase or in amplitude. This introduces a distortion in the signal which can be modeled by an amplitude mismatch ε and a phase mismatch $\Delta\phi$ as illustrated by the figure below [Tub05].

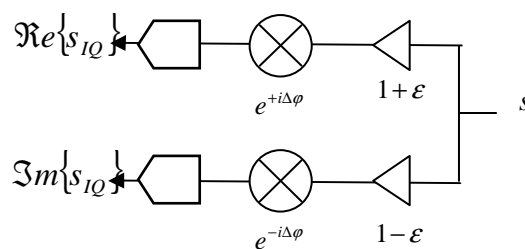


Figure 5.12. IQ gain and phase mismatches.

Figure 5.12 presents a model of the IQ mismatch impairments. The expressions of the real and imaginary parts (I and Q) of the baseband signal after impairment are given by:

$$\begin{aligned} \text{Re}\{s_{IQ}(t)\} &= (1 + \varepsilon) \cos \Delta\Phi \text{Re}\{s(t)\} - (1 + \varepsilon) \sin \Delta\Phi \text{Im}\{s(t)\} \\ \text{Im}\{s_{IQ}(t)\} &= (1 - \varepsilon) \cos \Delta\Phi \text{Im}\{s(t)\} - (1 - \varepsilon) \sin \Delta\Phi \text{Re}\{s(t)\} \end{aligned} \quad (5.5)$$

with ε and $\Delta\phi$ respectively the amplitude and phase imbalances.

We introduce two complex number α and β which are related to the imbalance parameters ε and $\Delta\phi$ by :

$$\begin{cases} \alpha = \cos(\Delta\phi) + j \cdot \varepsilon \cdot \sin(\Delta\phi) \\ \beta = \varepsilon \cdot \cos(\Delta\phi) - j \cdot \sin(\Delta\phi) \end{cases} \quad (5.6)$$

Based on (5.5) and (5.6), the impact of the IQ imbalance acts as a linear combination of the non impaired signal and the complex conjugate of itself :

$$s_{IQ}(t) = \alpha \cdot s(t) + \beta \cdot s^*(t) \quad (5.7)$$

Due the property of the Fourier Transform, the impaired signal is expressed in the frequency domain by:

$$S_{IQ}(f) = \alpha \cdot S(f) + \beta \cdot S^*(-f) \quad (5.8)$$

In the case of OFDM modulation scheme, the value of a given subcarrier i of a given OFDM symbol after impairment is thus a combination of the non impaired subcarrier i and of the complex conjugate of the mirror subcarrier $N-i$:

$$S_{IQ}(f_i) = \alpha \cdot S(f_i) + \beta \cdot S^*(f_{N-i}) \quad (5.9)$$

N being the length of the FFT. This is illustrated in Figure 5.13.

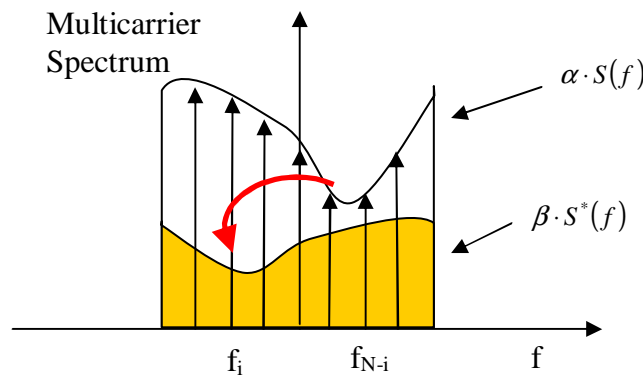


Figure 5.13. Impact of IQ mismatch on the spectrum.

5.5.2 Effect on the spectral selectivity

From (5.9), the ratio between the signal at subcarrier $N-i$ and interferences that this signal produce at subcarrier i (by subcarrier $N-i$) can be expressed by:

$$SIR_{IQ} = \frac{S^*(f_{N-i})}{S_{IQ}(f_i)} \Big|_{S(f_i)=0} = \frac{1}{\beta} \quad (5.10)$$

$$SIR_{IQ} = -10 \log_{10} \left[\left(10^{\frac{\Delta G db}{20}} - 1 \right) \cdot \cos(\Delta \phi) - j \cdot \sin(\Delta \phi) \right] \quad (5.11)$$

Curves are plotted in Figure 5.14 for some values of $\Delta \phi$ and ΔG . Even for relatively small imbalances, the interferences are above the targeted SDR of 40dB.

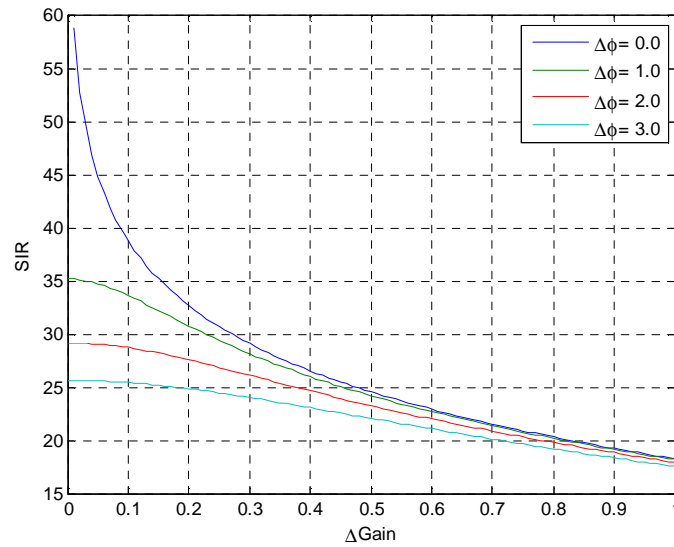


Figure 5.14. Theoretical signal-to-interference ratio produced by IQ mismatch as a function of ΔG and $\Delta \phi$.

5.5.3 Simulations

Figure 5.15 presents the spectrum of an FBMC signal impaired by IQ mismatch for several couples of amplitude/phase. Amplitudes and phases are defined as the amplitude and phase above/below the mean value of both branches.

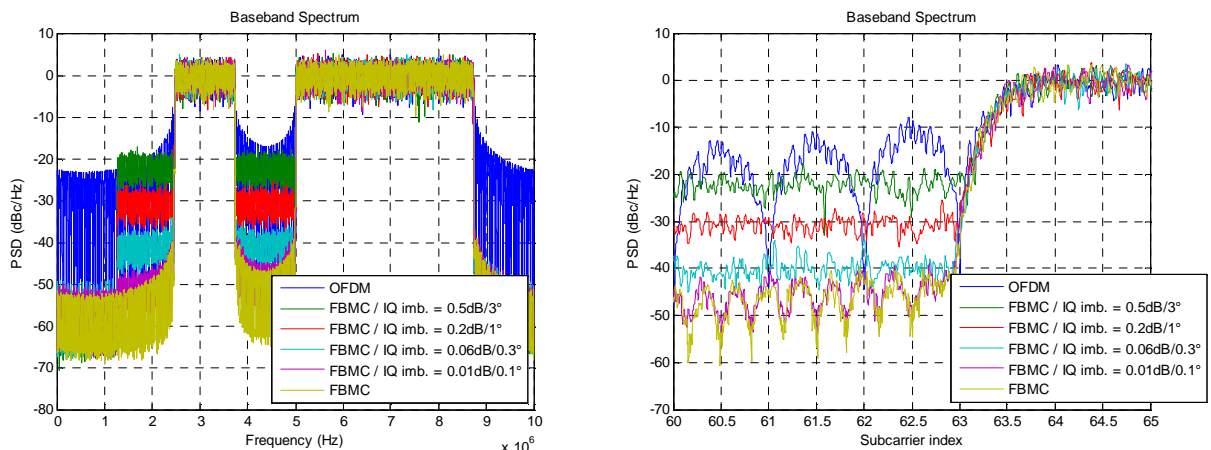


Figure 5.15. Impact of IQ mismatch on the transmitted spectrum

As can be seen on Figure 5.15:

- For $0.5\text{dB}/3^\circ$, the impaired FBMC gives the same SDR as a non impaired OFDM.
- For $0.06\text{dB}/0.3^\circ$, an SDR of 40dB is guaranteed in the whole in-band spectrum. Finally, values as low as $0.01\text{dB}/0.1^\circ$ are necessary in order to roughly meet the full possibilities of FBMC in terms of SDR.

Finally, in Figure 5.16, the impact of the studied IQ mismatch values are evaluated in term of EVM per subcarrier. Results are identical for FBMC and OFDM. An IQ imbalance of $0.06\text{dB}/0.3^\circ$ is sufficient in order to meet 64-QAM WIMAX specifications.

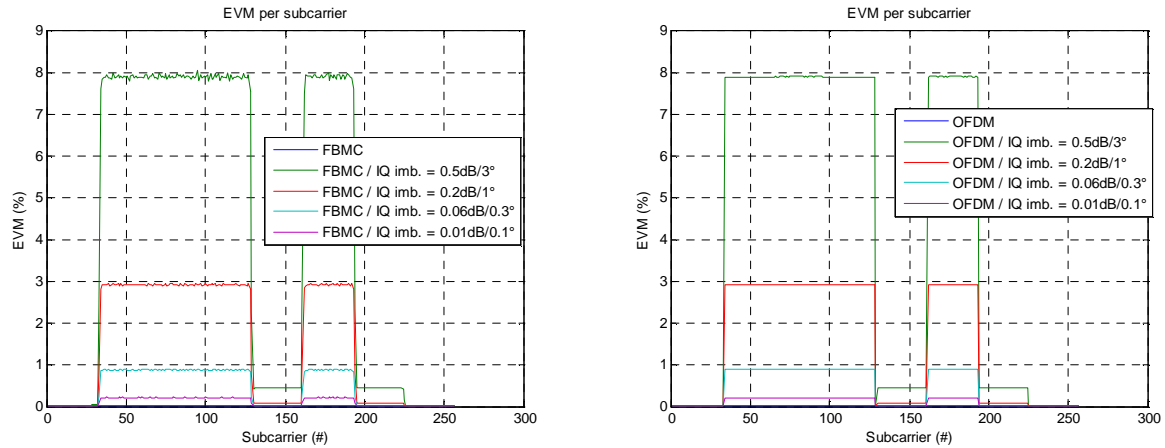


Figure 5.16. EVM per subcarrier as a function of the IQ mismatch. Left side: FBMC, Right side: OFDM.

It should be noted that efficient post-compensation techniques based on preamble-aided or adaptive approaches exist for OFDM and might be adapted in the frame of FBMC systems which allows relaxing significantly these constraints [Tub05, Deh05].

5.6 Phase noise

Two simulations are performed below in order to estimate impact of the phase noise on the spectral regrowth in an FBMC system.

5.6.1 Model

The phase noise is here modeled by the superposition of a Wiener random process whose spectrum is a Lorentzian distribution asymptotically decaying in $1/f^2$ and a white noise floor.

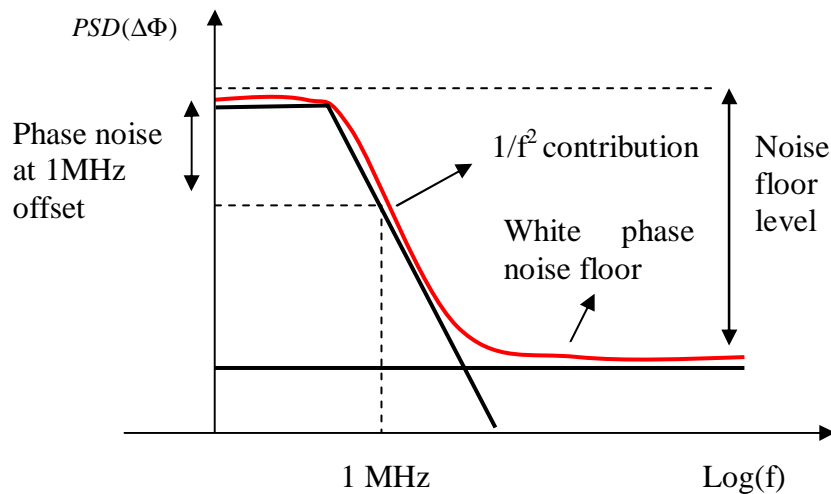


Figure 5.17. Typical power density spectrum (PSD) of a phase noise modeled as a Wiener process ($1/f^2$) and a noise floor.

5.6.2 Simulations

Simulations are run with different $1/f^2$ phase noise levels, from -140 to -85 dBc/Hz at 1 MHz offset frequency. The white noise floor is set to -140dBc/Hz in all three simulations but is not limiting in either cases. Resulting FBMC spectrums are plotted in Figure 5.18.

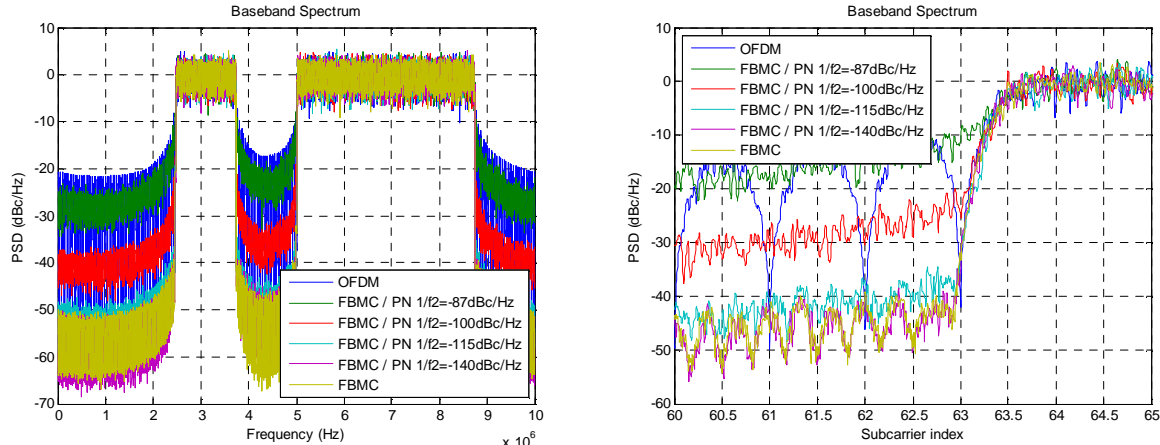


Figure 5.18. Impact of phase noise on the transmitted FBMC spectrum as a function of the phase noise

Conclusions are the following:

- A phase noise of -87dBc/Hz corresponds to the level of spectral regrowth obtained with ideal OFDM.
- Values between -100dBc/Hz and -115dBc/Hz allow to reach 40dB of SDR respectively on the side of the spectrum scenario and on the hole. -115dBc/Hz is required to make the specification in the whole spectrum.
- Finally values as low as -140dBc/Hz are required so that the phase noise effect become negligible compared to an ideal FBMC waveform.

Figure 5.19 shows the impact of the previous values of phase noise on EVM. The EVM profile inside the spectrum hole shows that subcarriers adjacent to the hole's edges are impacted by phase noise. This will impact a potential secondary user using this band.

The overall levels of EVM computed in the figure below are very high compared to the WIMAX requirements. It should be understood that the phase noise is not compensated at the reception because no equalizer or phase tracking is implemented in this ideal demodulator. As a consequence, the results presented here are just for theoretical study and should not be considered as representative of the performance of a real system.

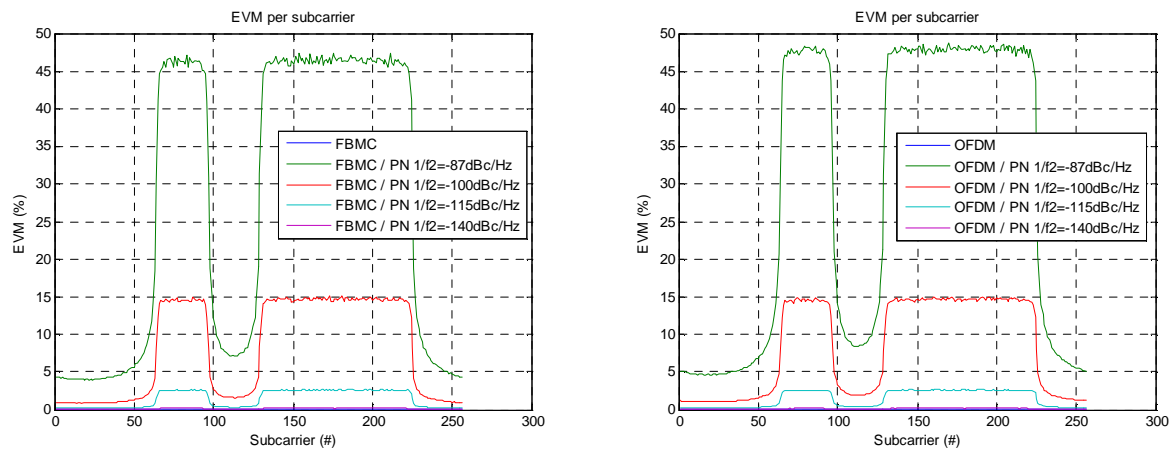


Figure 5.19. EVM per subcarriers as a function of the phase noise. Left side: OFDM, Right side: FBMC.

5.7 Joint effect of the three imperfections

In the previous sections, the effect of each impairment has been studied separately. However in a real system, all imperfections are present simultaneously. In order to set specifications, it is necessary to simulate the system with all the imperfections activated at the same time. The effects are non linear and alter different properties of the waveform. This is not straightforward to predict how imperfections will add up.

As decided in the introduction, we aim at defining three set of specifications: equivalent to ideal OFDM without impairment; SDR of 40dB; and no limiting effect on ideal FBMC.

Figure 5.20 presents the result of these three sets when values previously defined for each separate imperfections are simulated jointly. The imperfection adds up and the target conditions are not meet.

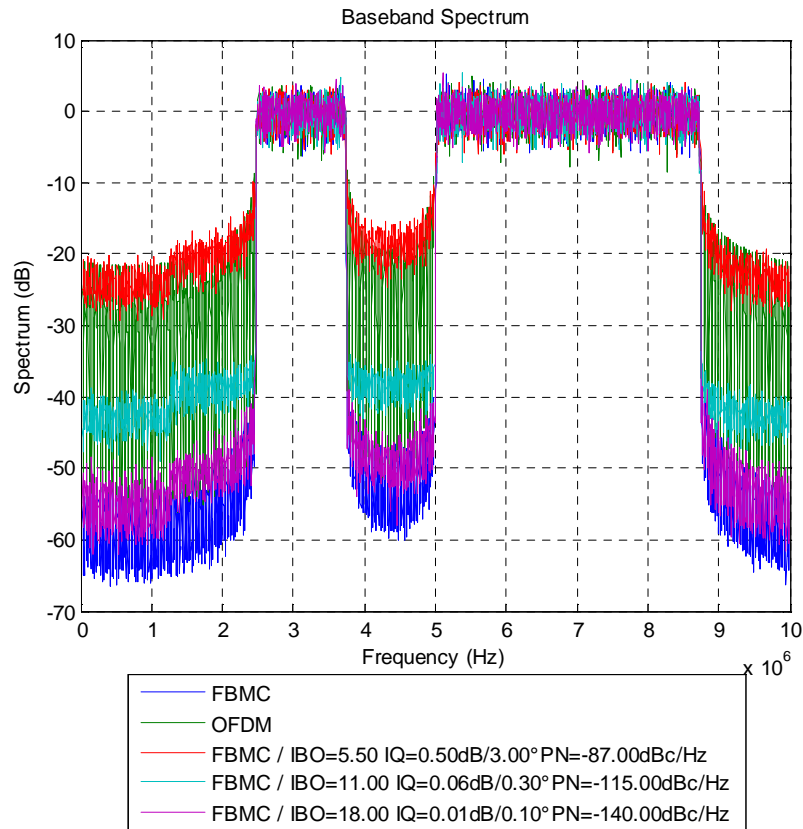


Figure 5.20. Impact of the joint imperfections (PA, IQ mismatch and Phase noise) on the FBMC spectrum for three set of conditions.

In a second step, each set of parameters is optimized by a given factor until the targeted conditions are met.

The results are:

- For the case “OFDM equivalent”, parameters need to be improved by 37% (or 2.0dB)
- For cases “SDR of 40dB”, and “no limiting effect on ideal FBMC”, parameters need to be improved by 40% (or 2.2 dB)

Finally, the resulting spectrum and corresponding parameters are shown in Figure 5.21.

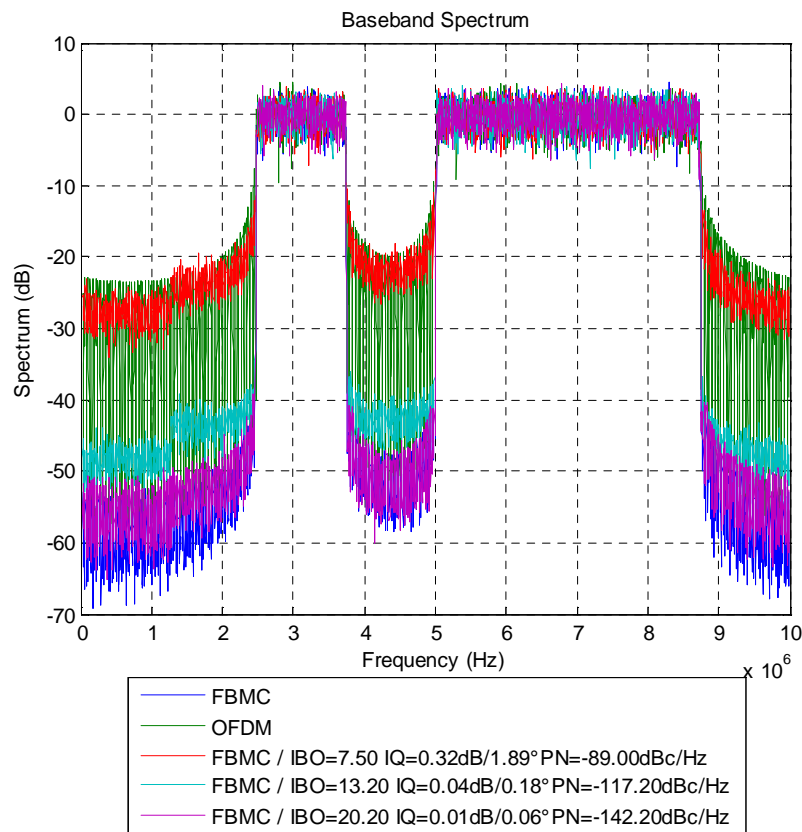
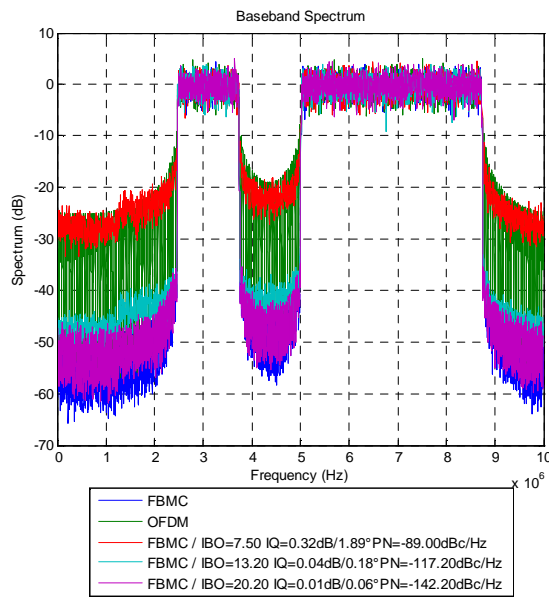
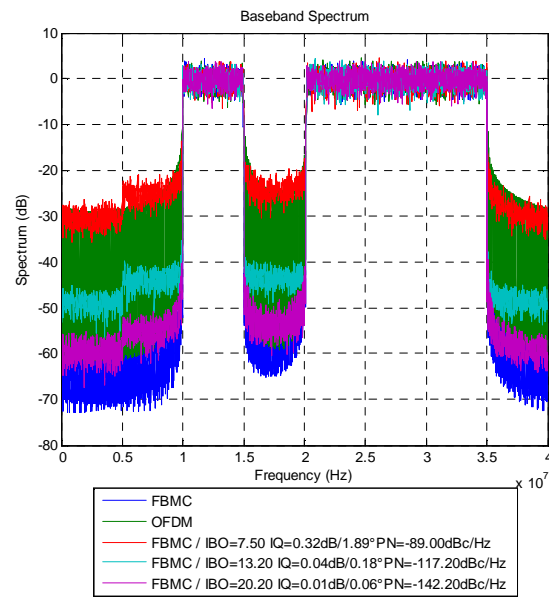
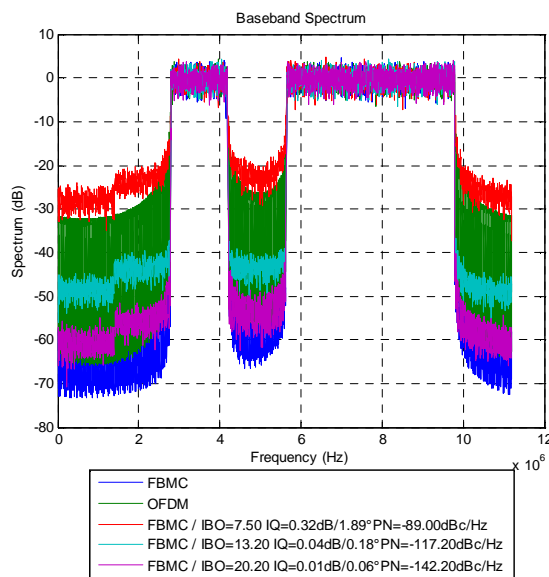
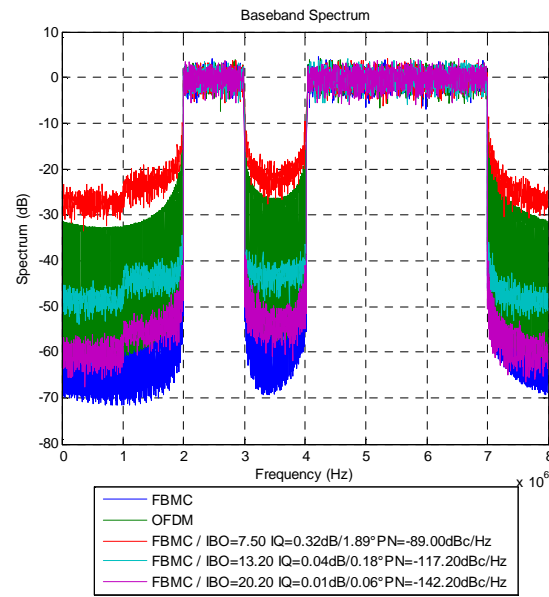


Figure 5.21. Impact of the joint imperfections (PA, IQ mismatch and Phase noise) on the FBMC spectrum for three set of conditions after optimization.

The three sets of parameters obtained after optimization are given in the legend below Figure 5.21. The first set of parameter allows obtaining a transmitted FBMC signal having the same SDR as if OFDM was used. The second set allows guarantying 40dB of SDR in the whole spectrum and the last one allows reaching the intrinsic spectral selectivity of FBMC.

5.8 Other values for K and M

The study has been carried out for an overlapping factor $K = 4$ and a number of subcarrier $M = 256$. Figure 5.22 presents the same simulation conditions as in Figure 5.22 but with different values of K and M.

(a) $K = 3$ and $M = 256$, $F_s = 10$ MHz(b) $K = 4$, $M = 1024$, $F_s = 40$ MHz(c) $K = 4$ and $M = 1024$, $F_s = 11.2$ MHz(d) $K = 4$, $M = 1024$, $F_s = 8$ MHzFigure 5.22. Same simulation as Figure 5.21 with different parameters for K and M .

In simulation (a), for $K = 3$ instead of 4, the SDR of the ideal FBMC waveform is decreased by 5 dB. The shorter length of FBMC symbol logically results in a lower spectral resolution. However this is not significant when imperfections limit the SDR. Simulations (b), (c) and (d) with $M = 1024$ shows that the SDR of the FBMC waveform does not depend strongly on the number of subcarriers. Simulations (c) and (d) correspond to M and F_s as recommended in the mobile WIMAX 802.16e-2005 specification and shows that SDR depends on the intercarrier spacing due to the effect of the phase noise.

5.9 Summary of the requirements

The purpose of this subsection is finally to summarize the results obtained for each impairment.

In Table 5.8, it is assumed that only one imperfection exists at a time. This is useful to evaluate the effect of each imperfection separately on the system.

Table 5.9 summarizes the specifications required when all imperfections are activated at the same time, which is representative of a real implementation and corresponds to the result of section 5.7.

Table 5.8. RF impairment specifications in the case of a single imperfection

	OFDM equivalent	40dB SDR	Not limiting factor
PA Non linearity	IBO = 5.5 dB	IBO = 11.0 dB	IBO = 18 dB
IQ imbalance	0.5dB / 3°	0.06 / 0.30°	0.01dB / 0.1°
Phase noise	-87 dBc/Hz	-115 dBc/Hz	-140 dBc/Hz

Table 5.9. RF impairment specifications in the case of all imperfections activated at the same time

	OFDM equivalent	40dB SDR	Not limiting factor
Non linearity	IBO = 7.5 dB	IBO = 13.2 dB	IBO = 20.2 dB
IQ imbalance	0.32dB / 1.9 °	0.04 dB / 0.18 °	0.01 dB / 0.06 °
Phase noise	-89.0 dBc/Hz	-117.2 dBc/Hz	-142.2 dBc/Hz

5.10 Conclusions

Three common impairments of transmitter RF front-ends have been studied in term of their impacts on the SDR of an FBMC signal and requirements have been derived.

Basically, in the hypothesis where a dynamic range of 40dB is targeted, requirements on IQ mismatch and phase noise are not so different that those required for 64-QAM WIMAX. However, the impact of the power amplifier might be more important. It could be necessary to operate at an IBO of 13 or 14dB, where an OFDM system typically target around 7-8dB. This would lead to an increase of the power consumption of the transmitter in a factor of 2 or 3. Possible solutions that could be investigated are pre-compensation techniques of the power amplifier non linearity's.

This study is focused on the effect of RF impairments on the SDR of the transmitted waveform. This is an important issue in order to set a cognitive radio system, but this is not the only aspect putting constraints of the transmitter front-end. The study was conducted assuming a particular scenario for the allocation of the subcarrier, for $M = 256$ subcarriers and for an overlapping factor $K = 4$. Moreover desynchronization of the multiple users is not taken into account here. However simulations suggest that results are not dependant on these parameters as long as the intercarrier spacing is kept constant. If the intercarrier spacing decreases, then the constraints of the RF front-end specification increase.

6 Interference-aware power allocation algorithm in multicarrier based cognitive radio networks: OFDM and FBMC systems

Rapid development of wireless communication makes the spectrum scarcity as a one of the serious problems. The Federal Communication Commission (FCC) has reported that the most of the licensed spectrum is currently underutilized [FCC02].

Cognitive radio (CR) [Mit99][Wei04-1][Hay05], which is an intelligent wireless communication system capable of learning from its radio environment and dynamically adjusting its transmission characteristics accordingly, is considered to be one of the possible solutions to solve the spectrum efficiency problem. By CR, a group of unlicensed users [referred to as secondary users (SU's)] can use the licensed frequency channels (spectrum holes) without causing a harmful interference to the licensed users [referred to as primary users (PU's)] and thus implement efficient reuse of the licensed channels.

Multicarrier communication systems have been suggested as a candidate for CR systems due to its flexibility to allocate resources between the different SU's. As the SU and PU bands may exist side by side and their access technologies may be different, the mutual interference between the two systems is considered as a limiting factor affects the performance of both networks. In [Wei04-2], the mutual interference between PU and SU was studied. The mutual interference depends on the transmitted power as well as the spectral distance between PU and SU. Orthogonal frequency division multiplexing (OFDM) based CR system suffers from high interference to the PU's due to large sidelobes of its filter frequency response. The insertion of the cyclic prefix (CP) in each OFDM symbol decreases the system capacity. The leakage among the frequency sub-bands has a serious impact on the performance of FFT-based spectrum sensing and in order to combat the leakage problem of OFDM, very tight and hard synchronization implementation have to be imposed among the network nodes [Far08-1].

The filter bank multicarrier system (FBMC) doesn't require any CP extension and can overcome the spectral leakage problem by minimizing the sidelobes of each subcarrier and therefore lead to high efficiency (in terms of spectrum and interference) [Far08-1][Zha09].

The problem of resource allocation for conventional (non-cognitive) multiuser multicarrier systems has been widely studied [Jan03][Kiv03][She03][Won99]. The maximum aggregated data rate in downlink can be obtained by assigning each subcarrier to the user with the highest signal to noise ratio (SNR) and then the optimal power allocation that maximizes the channel capacity is waterfilling on the subcarriers with a given total power constraint [Jan03]. In cognitive radio systems, two types of users (SU and PU) and the mutual interference between them should be considered. The use of the power allocation based on conventional waterfilling algorithm is not always efficient. An additional constraint should be introduced due to the interference caused by the sidelobes in different subcarriers. The transmit power of each subcarrier should be adjusted according to the channel status and the location of the subcarrier with respect to the PU spectrum.

P.Wang et al. in [Wan07] proposed an iterative partitioned single user waterfilling algorithm. The algorithm aims to maximize the capacity of the CR system under the total power constraint with the consideration of the per subcarrier power constraint caused by the PU's interference limit. The per

subcarrier power constraint is evaluated based on the pathloss factor between the CR transmitter and the PU protection area. The mutual interference between the SU and PU was not considered. In [Ban07][Ban08], the authors proposed an optimal and two suboptimal power loading schemes using the Lagrange formulation. These loading schemes maximize the downlink transmission capacity of the CR system while keeping the interference induced to only one PU below a pre-specified interference threshold without the consideration of the total power constraint. In [Qin07], an algorithm called *RC algorithm* was presented for multiuser resource allocation in OFDM based CR systems. This algorithm uses a greedy approach for subcarrier and power allocations by successively assign bits, one at time, based on minimum SU power and minimum interference to PU considerations. The algorithm has a high computational complexity and a limited performance with comparison to the optimal solution. In [Zha08-3], a low complexity suboptimal solution is proposed. The algorithm initially assumes that the maximum power that can be allocated to each subcarrier is equal to the power found by the conventional waterfilling and then modifies these values by applying a power reduction algorithm in order to satisfy the interference constraints. Experimental results like [Stu09] emphasize the need of low interference constraints where this algorithm has a limited performance. Moreover, the non transmission of the data over the subcarriers below the waterfilling level or the deactivated subcarriers due to the power reduction algorithm decreases the overall capacity of the CR system.

Throughout this work, a computationally efficient resource allocation algorithm in multicarrier based CR systems is proposed. The proposed algorithm maximizes the downlink capacity of the CR system under both total power and interference induced to the PU's constraints. The CR system can use the non active and active PU bands as long as the total power and the different interference constraints are satisfied. The simulation results demonstrate that the proposed solution is very close to the optimal solution with a good reduction in the computational complexity. Moreover, The proposed algorithm outperforms the previously presented algorithms in the literature. The efficiency of using FBMC in CR systems is investigated and compared to OFDM based CR systems. Section 6.2 gives the system model while Section 6.3 formulate the problem. The proposed algorithm is presented in Section 6.4. Selected numerical results are presented in Section 6.5. Finally, Section 6.6 concludes the paper.

6.1 System model

The downlink scenario will be considered. As shown in Fig. 6.1, the CR system coexist with the PU's radio in the same geographical location.

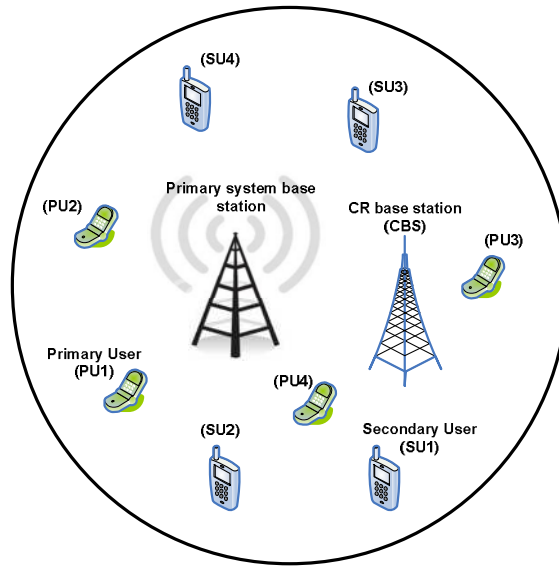


Figure 6.1. Cognitive Radio Network

The cognitive base station (CBS) transmits to its SU's and causes interference to the PU's. Moreover, the PU's base station interferes with the SU's. The CR system's frequency spectrum is divided into N subcarriers each having a Δf bandwidth. The side by side frequency distribution of the PU's and SU's will be assumed (see Fig. 6.2).

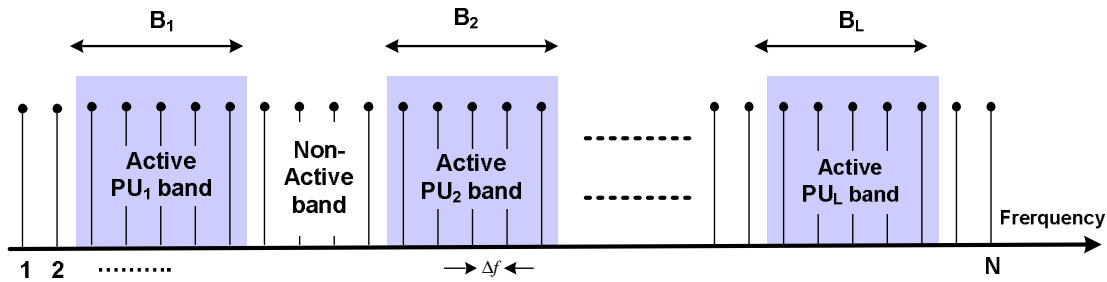


Figure 6.2. Frequency distribution of the active and non-active primary bands.

The frequency bands B_1, B_2, \dots, B_L has been occupied by the PU's (active PU bands) while the other bands represent the non-active PU bands. Its assumed that the CR system can use the non-active and active PU bands provided that the total interference introduced to the l^{th} PU band does not exceed I_l^{th} where $I_l^{th} = T_{th}^l B_l$ denotes the maximum interference power that can be tolerated by the PU_l and T_{th}^l is the interference temperature limit for PU_l .

6.1.1 Interference induced to/from the PU's

The interference introduced by the i^{th} subcarrier to l^{th} PU, $I_i^l(d_i, P_i)$, is the integration of the power spectrum density (PSD), Φ_i , of the i^{th} subcarrier across the l^{th} PU band, B_l , and can be expressed as [Wei04-2]

$$I_i^l(d_i, P_i) = \int_{d_i - B_l/2}^{d_i + B_l/2} |g_i|^2 \Phi_i(f) df = P_i \Omega_i \quad (6.1)$$

where P_i is the total transmit power emitted by the i^{th} subcarrier and d_i is the spectral distance between the i^{th} subcarrier and the l^{th} PU band. Ω_i denotes the interference factor of the i^{th} subcarrier.

The interference power introduced by the l^{th} PU signal into the band of the i^{th} subcarrier is [Wei04-2]

$$J_i^l(d_i, P_{PU_l}) = \int_{di-\Delta f/2}^{di+\Delta f/2} |y_i|^2 \psi_l(e^{j\omega}) d\omega \quad (6.2)$$

where $\psi_l(e^{j\omega})$ is the power spectrum density of the PU_l signal and y_i is the channel gain between the i^{th} subcarrier and l^{th} PU signal. The PSD expression, Φ_i , depends on the used multicarrier technique. The OFDM and FBMC PSD's are described in the following subsections

6.1.2 OFDM system and its PSD model

The OFDM symbol is formed by taking the inverse discrete Fourier transform (IDFT) to a set of complex input symbols $\{X_k\}$ and adding a cyclic prefix. The block diagram of the OFDM system is depicted in Fig. 6.3

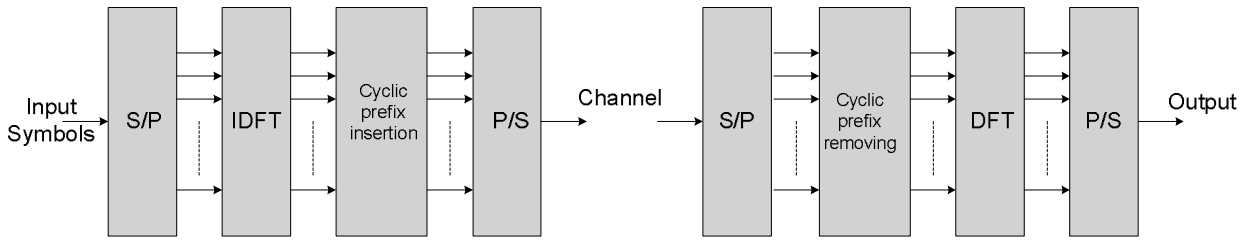


Figure 6.3. OFDM system block diagram.

This can be written mathematically as

$$x(n) = \sum_k \sum_{w \in \mathbb{Z}} X_{k,w} g_T(n - wT) e^{j2\pi(n-wT-C)k/N} \quad (6.3)$$

where $\{k\}$ is the set of data subcarrier indices and is a subset of the set $\{0, 1, \dots, N-1\}$, N is the IDFT size, C is the length of the cyclic prefix in number of samples, and $T = C + N$ is the length of the OFDM symbol in number of samples. w denoting the w^{th} OFDM symbol.

Following the derivation of the PSD for general baseband signal given in [Pro02], it can be shown that the OFDM PSD is :

$$\Phi_{OFDM}(f) = \frac{\sigma_x^2}{T} \sum_k \left| G_T \left(f - \frac{k}{N} \right) \right|^2 \quad (6.4)$$

where $G_T(f)$ is the Fourier transform of $g_T(n)$, and σ_x^2 is the variance of the zero mean (symmetrical constellation) and uncorrelated input symbols. The assumption of the uncorrelated input symbols can be justified because of coding and interleaving in practical symbols [Bal07-2].

$g_T(n)$ can be chosen as

$$g_T(n) = \begin{cases} 1 & n = 0, 1, \dots, T-1 \\ 0 & \text{otherwise} \end{cases} \quad (6.5)$$

and hence its Fourier transform is

$$|G_T(f)|^2 = T + 2 \sum_{r=1}^{T-1} (T-r) \cos(2\pi fr) \quad (6.6)$$

6.1.3 FBMC system and its PSD model

Each subcarrier in FBMC system is modulated with a staggered QAM (offset QAM) [Hir81]. The basic idea is to transmit real-valued symbols instead of transmitting complex valued ones. Due to this time staggering of the in-phase and quadrature components of the symbols, orthogonality is achieved between adjacent subcarriers. The modulator and the demodulator are implemented using the synthesis and analysis filter banks. The filters in the synthesis and analysis filter bank are obtained by frequency shifts of a single prototype filter. Fig. 6.4 depicts the structure of the synthesis and analysis filter bank at the transmitter and receiver in FBMC based multicarrier systems.

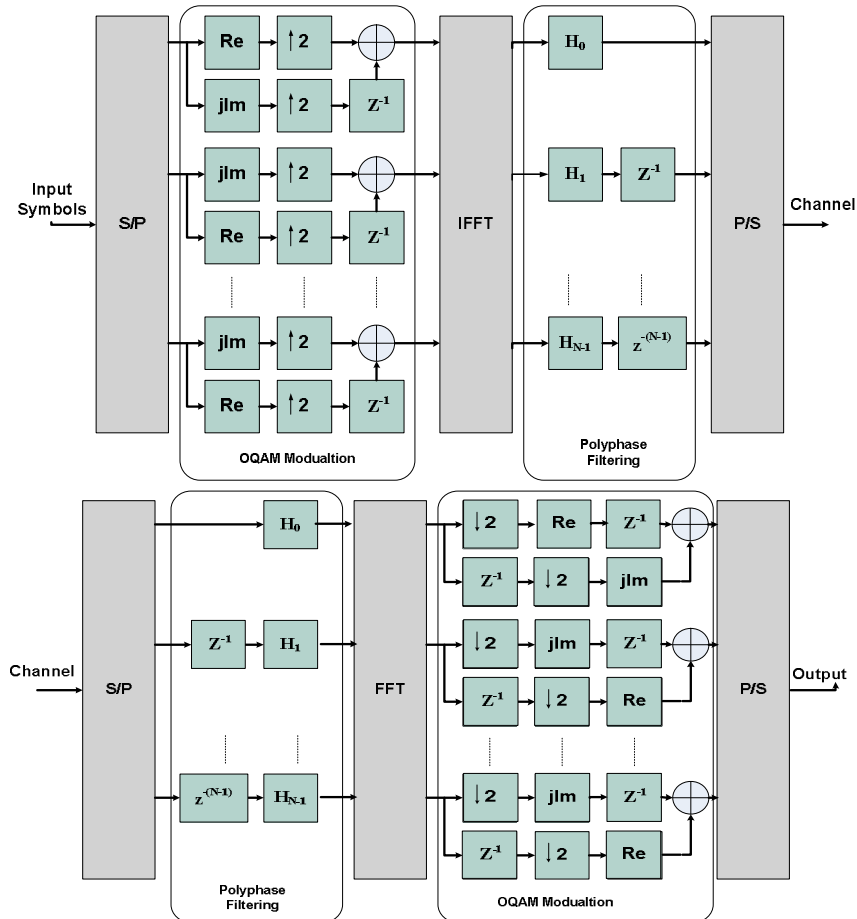


Figure 6.4. FBMC system's transmitter and receiver.

The FBMC signal can be written mathematically as [Skr06],

$$x(n) = \sum_k \sum_{w \in \mathbb{Z}} a_{k,w} h(n - w\tau_o) e^{j2\pi \frac{k}{N} n} e^{j\phi_{k,w}} \quad (6.7)$$

where $\{k\}$ is the set of subcarrier indices, h is the pulse shape, $\phi_{k,w}$ is an additional phase term and τ_o is FBMC symbol duration. $a_{k,w}$ are the real symbols obtained from the complex QAM symbols having a zero mean and variance σ_x^2 . Hence the symbols have a zero mean and finite variance $\sigma_r^2 = \frac{\sigma_x^2}{2}$. The PSD of the FBMC can be expressed by [Skr06]:

$$\Phi_{FBMC} = \frac{\sigma_r^2}{\tau_o} \sum_k \left| H\left(f - \frac{k}{N}\right) \right|^2 \quad (6.8)$$

where $H(f)$ is the frequency response of the prototype filter with coefficients $h[n]$ with $n = 0, \dots, W-1$, where $W = KN$ and K is the length of each polyphase components (overlapping factor). Assuming that the prototype coefficients have even symmetry around the $\left(\frac{KN}{2}\right)^{th}$ coefficient, and the first coefficient is zero [Bal07-2], we get

$$|H(f)| = h[W/2] + 2 \sum_{i=1}^{\frac{W}{2}-1} h\left[\left(\frac{W}{2}\right) - i\right] \cos(2\pi fi) \quad (6.9)$$

To make a parallel between OFDM and FBMC, we place ourselves in the situation where both systems transmit the same quantity of information. This is the case if they have the same number of subcarriers N together with duration of τ_o samples for FBMC real data and $T = 2\tau_o$ for the complex QAM ones [Bal07] [Skr06].

From the relations above we can notice that the PSDs of OFDM and FBMC are the summation of the spectra of the individual subcarriers. Using the PHYDYAS prototype filter [PHY08], Fig. 6.5 plots a single subcarrier power spectral densities of the OFDM and FBMC systems.

It can be noted that the FBMC system has very small side lobes with comparison to that of the OFDM system.

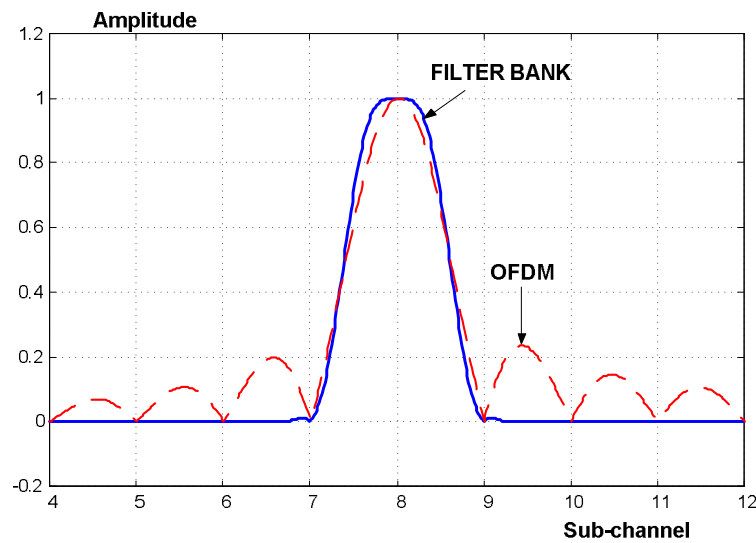


Figure 6.5. Single subcarrier PSD's of the OFDM and FBMC systems.

6.2 Problem formulation

The transmission rate of the i^{th} subcarrier, R_i , with the transmit power P_i can be evaluated using the Shannon capacity formula and is given by

$$R_i(P_i, h_{i,m}) = \Delta f \log_2 \left(1 + \frac{P_{i,m} |h_{i,m}|^2}{\sigma^2} \right) \quad (6.10)$$

where $h_{i,m}$ is the subcarrier fading gain from the CBS to the user m . $\sigma^2 = \sigma_{AWGN}^2 + J_i^l$ where σ_{AWGN}^2 is the mean variance of the additive white Gaussian noise (AWGN) and J_i^l is the interference introduced by the l^{th} PU's band into the i^{th} subcarrier.

It will be assumed that all the instantaneous fading gains are perfectly known at the CR system and there is no inter-carrier interference (ICI).

6.2.1 Optimization problem

Let $v_{i,m}$ to be a subcarrier allocation indicator, i.e. $v_{i,m} = 1$ if and only if the subcarrier is allocated to m^{th} user. It is assumed that each subcarrier can be used for transmission to at most one user at any given time. Our objective is to maximize the total capacity of the CR system subject to the instantaneous interference introduced to the PU's and total transmit power constraint. Therefore, the optimization problem can be formulated as follow

$$P1: \max_{P_i} \sum_{m=1}^M \sum_{i=1}^N v_{i,m} R_i(P_i, h_{i,m}) \quad (6.11)$$

subject to

$$v_{i,m} \in \{0, 1\}, \forall i, m \quad (6.12)$$

$$\sum_{m=1}^M v_{i,m} \leq 1, \forall i \quad (6.13)$$

$$\sum_{m=1}^M \sum_{i=1}^N v_{i,m} P_{i,m} \leq P_T \quad (6.14)$$

$$P_i \geq 0, \forall i \in \{1, 2, \dots, N\} \quad (6.15)$$

$$\sum_{m=1}^M \sum_{i=1}^N v_{i,m} P_i \Omega_i \leq I_{th}^l, \forall l \in \{1, 2, \dots, L\} \quad (6.16)$$

where N denotes the total number of subcarriers, M is the number of users, I_{th}^l denotes the interference threshold prescribed by the l^{th} PU and P_T is the total SU's power budget. Inequality (6.13) ensures that any given subcarrier can be allocated to at most one user.

6.2.2 Subcarriers to users allocation

The optimization problem $P1$ is a combinatorial optimization problem and its complexity grows exponentially with the input size. In order to reduce the computational complexity, the problem is solved in two steps by many of the suboptimal algorithms [Jan03][Kiv03][She03][Won99]. In the first step, the subcarriers are assigned to the users and then the power is allocated for these

subcarriers in the second step. Once the subcarriers are allocated to the users, the multiuser system can be viewed virtually as a single user multicarrier system. As proofed in [Jan03], the maximum data rate in downlink can be obtained if the subcarriers are assigned to the user who has the best channel gain for that subcarrier as described in Algorithm 1.

Algorithm 1 Subcarriers to User Allocation

Initialization:

Set $v_{i,m} = 0 \forall i, m$

Subcarrier Allocation:

for $i = 1$ to N **do**

$$m^* = \arg \max_m \{h_{i,m}\}; v_{i,m^*} = 1$$

end for

By applying the Algorithm 1, the values of the channel indicators $v_{i,m}$ are determined and hence for notation simplicity, single user notation can be used. The different channel gains can be determined from the subcarrier allocation step as follow

$$h_i = \sum_{m=1}^M \sum_{i=1}^N v_{i,m} h_{i,m} \quad (6.17)$$

and hence problem $P1$ can be reformulated as follow

$$P2: \max_{P_i} \sum_{i=1}^N \log_2 \left(1 + \frac{P_i |h_i|^2}{\sigma^2} \right) \quad (6.18)$$

subject to

$$\sum_{i=1}^N P_i \Omega_i \leq I_{th}^l \quad \forall l \in \{1, 2, \dots, L\} \quad (6.19)$$

$$\sum_{i=1}^N P_i \leq P_T \quad (6.20)$$

$$P_i \geq 0 \quad \forall i \in \{1, 2, \dots, N\} \quad (6.21)$$

6.2.3 Subcarriers power loading (optimal solution)

The problem $P2$ is a convex optimization problem. The Lagrangian can be written as

$$G = -\sum_{i=1}^N \log_2 \left(1 + \frac{P_i^* |h_i|^2}{\sigma^2} \right) + \sum_{l=1}^L \alpha_l \left(\sum_{i=1}^N P_i^* \Omega_i - I_{th}^l \right) + \beta \left(\sum_{i=1}^N P_i^* - P_T \right) - \sum_{i=1}^N P_i^* \mu_i \quad (6.22)$$

where $\alpha_l, l \in \{1, 2, \dots, L\}$, $\mu_i, i \in \{1, 2, \dots, N\}$, and β are the Lagrange multipliers. The Karush-Kuhn-Tucker (KKT) conditions can be written as follow

$$\begin{aligned}
P_i^* &\geq 0, \forall i \in \{1, 2, \dots, N\} \\
\alpha_l &\geq 0, \forall l \in \{1, 2, \dots, L\} \\
\beta &\geq 0 \\
\mu_i &\geq 0, \forall i \in \{1, 2, \dots, N\} \\
\alpha_l \left(\sum_{i=1}^N P_i^* \Omega_i - I_{th}^l \right) &= 0, \forall l \in \{1, 2, \dots, L\} \\
\beta \left(\sum_{i=1}^N P_i^* - P_T \right) &= 0 \\
\mu_i P_i^* &= 0, \forall i \in \{1, 2, \dots, N\} \\
\frac{\partial G}{\partial P_i^*} &= \frac{-1}{\frac{\sigma^2}{|h_i|^2} + P_i^*} + \sum_{l=1}^L \alpha_l \Omega_i + \beta - \mu_i = 0
\end{aligned} \tag{6.23}$$

and also the solution should satisfy the total power and interference constraints given by (6.19) and (6.20). Rearranging the last condition in (6.23) we get

$$P_i^* = \frac{1}{\sum_{l=1}^L \alpha_l \Omega_i + \beta - \mu_i} - \frac{\sigma^2}{|h_i|^2} \tag{6.24}$$

Since $P_i^* \geq 0$, we get

$$\frac{\sigma^2}{|h_i|^2} \leq \frac{1}{\sum_{l=1}^L \alpha_l \Omega_i + \beta - \mu_i} \tag{6.25}$$

If $\frac{\sigma^2}{|h_i|^2} < \frac{1}{\sum_{l=1}^L \alpha_l \Omega_i + \beta}$, then $\mu_i = 0$ and hence

$$P_i^* = \frac{1}{\sum_{l=1}^L \alpha_l \Omega_i + \beta} - \frac{\sigma^2}{|h_i|^2} \tag{6.26}$$

Moreover, if $\frac{\sigma^2}{|h_i|^2} > \frac{1}{\sum_{l=1}^L \alpha_l \Omega_i + \beta}$, from (6.24) we get

$$\frac{1}{\sum_{l=1}^L \alpha_l \Omega_i + \beta - \mu_i} \geq \frac{\sigma^2}{|h_i|^2} \geq \frac{1}{\sum_{l=1}^L \alpha_l \Omega_i + \beta} \tag{6.27}$$

and since $\mu_i P_i^* = 0$ and $\mu_i \geq 0$, we get that $P_i^* = 0$.

Therefore, the optimal solution can be written as follow

$$P_i^* = \begin{cases} \frac{1}{\sum_{l=1}^L \alpha_l \Omega_i + \beta} - \frac{\sigma^2}{|h_i|^2} & \text{if } \frac{\sigma^2}{|h_i|^2} < \frac{1}{\sum_{l=1}^L \alpha_l \Omega_i + \beta} \\ 0 & \text{if } \frac{\sigma^2}{|h_i|^2} \geq \frac{1}{\sum_{l=1}^L \alpha_l \Omega_i + \beta} \end{cases} \quad (6.28)$$

or more simply, (6.28) can be written as the following

$$P_i^* = \left[\frac{1}{\sum_{l=1}^L \alpha_l \Omega_i + \beta} - \frac{\sigma^2}{|h_i|^2} \right]^+ \quad (6.29)$$

where $[x]^+ = \max(0, x)$. Solving for $L+1$ Lagrangian multipliers is computational complex. These multipliers can be found numerically using ellipsoid or interior point method with a complexity $O(N^3)$ [Boy04]. In what follows we will propose an low complexity algorithm that achieve near optimal performance.

6.3 Proposed sub-optimal algorithm

The optimal solution for the optimization problem has a high computational complexity which make it unsuitable for the practical applications. A low complexity algorithm is proposed in [Zha08-3]. The subcarriers nulling and deactivating throughout this algorithm degrades the system capacity and causing the algorithm to have a limited performance in low interference constraints. To overcome the drawbacks of this algorithm, a low complexity power allocation algorithm will be presented.

As described in [Wei04-2], most of the interference introduced to the PU bands is induced by the cognitive transmission in the subcarriers where the PU is active as well as the subcarriers that are directly adjacent to the PU bands. Considering this fact, It can be assumed that each subcarrier is belonging to the closet PU band and only introducing interference to it, then the optimization problem $P2$ can be reformulated as follow

$$P3: \max_{P_i'} \sum_{i=1}^N \log_2 \left(1 + \frac{P_i' |h_i|^2}{\sigma^2} \right) \quad (6.30)$$

subject to

$$\sum_{i \in N_l} P_i' \Omega_i \leq I_{th}^l \quad \forall l \in \{1, 2, \dots, L\} \quad (6.31)$$

$$\sum_{i=1}^N P_i' \leq P_T \quad (6.32)$$

$$P_i' \geq 0 \quad \forall i \in \{1, 2, \dots, N\} \quad (6.33)$$

where N_l denotes the set of the subcarriers belong to the l^{th} PU band. Using the same derivation leading to (6.29), we get

$$P_i' = \left[\frac{1}{\alpha_i' \Omega_i + \beta'} - \frac{\sigma^2}{|h_i|^2} \right]^+ \quad (6.34)$$

where α_i' and β' are the non-negative dual variables corresponding to the interference and power constraints respectively. The solution of the problem is still has high computational complexity which encourage us to find a faster and efficient power allocation algorithm.

If the interference constraints are ignored in $P3$, the solution of the problem will follow the well known waterfilling interpretation [Lek97],

$$P_i^{(P_T)} = \left[\lambda - \frac{\sigma^2}{|h_i|^2} \right]^+ \quad (6.35)$$

where λ is the waterfilling level. On the other side, if the total power constraint is ignored, the Lagrangian of the problem can be written as

$$G^{(Int)} = -\sum_{i \in N_l} \log_2 \left(1 + \frac{P_i^{(Int)} |h_i|^2}{\sigma^2} \right) + \alpha_l'^{(Int)} \left(\sum_{i \in N_l} P_i^{(Int)} \Omega_i - I_{th}^l \right) \quad (6.36)$$

where α_l' is the Lagrange multiplier. Equating $\frac{\partial G^{(Int)}}{\partial P_i^{(Int)}}$ to zero, we get

$$P_i^{(Int)} = \left[\frac{1}{\alpha_l'^{(Int)} \Omega_i} - \frac{\sigma^2}{|h_i|^2} \right]^+ \quad (6.37)$$

where the value of α_l' can be calculated by substituting (6.37) into $\sum_{i \in N_l} P_i^{(Int)} \Omega_i = I_{th}^l$ to get

$$\alpha_l'^{(Int)} = \frac{|N_l|}{I_{th}^l + \sum_{i \in N_l} \frac{\Omega_i \sigma^2}{|h_i|^2}} \quad (6.38)$$

It is obvious that if the summation of the allocated power under only the interference constraints is lower than or equal the available total power budget, i.e. $\sum_{i=1}^N P_i^{(Int)} \leq P_T, \forall i \in \{1, 2, \dots, N\}$, then

(6.37)-(6.38) will be the optimal solution for the optimization problem $P3$. In most of the cases, the total power budget is quite lower than this summation and hence the **Power Interference (PI)** constrained algorithm, referred to as *PI-Algorithm*, is proposed to allocate the power under the both the total power and interference constraints.

In order to solve the optimization problem $P3$, we can start by assuming that the maximum power that can be allocated for a given subcarrier P_i^{Max} is determined according to the interference constraints only by using (6.37)-(6.38) for every set of subcarriers $N_l, \forall l \in \{1, 2, \dots, L\}$. By such an assumption, we can guarantee that the interference introduced to PU bands will be under the pre-specified thresholds. Once the maximum power P_i^{Max} , the total power constraint is tested. If the total power constraint is satisfied, then the solution has been found and equal to the maximum power that can be allocated to each subcarrier, i.e. $P_i' = P_i^{Max}$. Otherwise, the available power budget should be distributed among the subcarriers giving that the power allocated to each

subcarrier is lower than or equal to the maximum power that can be allocated to each subcarrier P_i^{Max} and hence the following problem should be solved

$$P4: \max_{P_i^{W.F}} \sum_{i=1}^N \log_2 \left(1 + \frac{P_i^{W.F} |h_i|^2}{\sigma^2} \right) \quad (6.39)$$

subject to

$$\sum_{i=1}^N P_i^{W.F} \leq P_T \quad (6.40)$$

$$0 \leq P_i^{W.F} \leq P_i^{Max} \quad (6.41)$$

The problem $P4$ is called "*cap-limited*" waterfilling [Pap08]. The problem can be solved efficiently using the concept of the conventional waterfilling. Given the initial waterfilling solution, the channels that violate the maximum power P_i^{Max} are determined and upper bounded with P_i^{Max} . The total power budget is reduced by subtracting the power assigned so far. At the next step, the algorithm proceeds to successive waterfilling over the subcarriers that not violated the maximum power P_i^{Max} in the last step. This procedure is repeated until the allocated power $P_i^{W.F}$ doesn't violate the maximum power P_i^{Max} in any of the subcarriers in the new iteration. The "*cap-limited*" waterfilling algorithm implementation is described in Algorithm 2.

Algorithm 2 Cap-Limited Waterfilling

1. **Initialize** $F = M = N = \{1, 2, \dots, N\}$, $\bar{P}_i = P_i^{Max}$, and $S = P_T$.
2. Sort $\left\{ T_i = \frac{\sigma^2}{|h_i|^2}, i \in N \right\}$ in decreasing order with J being the sorted index. Find the waterfilling λ as follows:
 - (a) $T_{sum} = \sum_{i \in N} T_i$, $\lambda = (T_{sum} + S) / |N|$, $n = 1$.
 - (b) **while** $T_{J(n)} > \lambda$ **do**

$$T_{sum} = T_{sum} - T_{J(n)}, N = N \setminus \{J(n)\}, \lambda = (T_{sum} + S) / |N|, n = n + 1$$
end while
 - (c) Set $P_i^{W.F} = [\lambda - T_i]^+, \forall i \in F$
3. **repeat**
 - if** $P_i^{W.F} \geq \bar{P}_i$
 - Let $P_i^{W.F} = \bar{P}_i$, $S = S - P_i^{W.F}$, $M = M \setminus \{i\}$, $N = M$, and go to step 2;
 - end if**
 - until** $P_i^{W.F} \leq \bar{P}_i, \forall i \in F$

The solution $P_i^{W.F}$ of the problem $P4$ is satisfying the total power constraint of the problem $P3$ with equality which is not the case for the different interference constraints I_{th}^l . Since it's assumed that $P_i^{W.F} \leq P_i^{Max}$, some of the powers allocated to subcarriers will not reach the maximum allowable values which will make the interference introduced to the PU bands below the thresholds I_{th}^l . In order to use all the allowable interference values, the values of the maximum power that can

be allocated to each subcarrier P_i^{Max} should be updated depending on the left available interference. The left available interference can be determined as follow

$$I_{Left}^l = I_{th}^l - \sum_{i \in N_l} P_i^{W.F} \Omega_i \quad (6.42)$$

Assuming that $A_l \subset N_l$ is the set of the subcarriers that reach its maximum, i.e. $P_i^{W.F} = P_i^{Max}, \forall i \in A_l$, then, $P_i^{Max}, \forall i \in A_l$ can be updated by applying the equations (6.37)-(6.38) on the subcarriers in the set A_l with the following interference constraints

$$I_{th}^l = I_{Left}^l + \sum_{i \in A_l} P_i^{W.F} \Omega_i \quad (6.43)$$

After determining the updated values of P_i^{Max} , the "cap-limited" waterfilling is performed again to find the final solution $P_i' = P_i^{W.F}$. Now, the solution P_i' is satisfying approximately the interference constraints with equality as well as guaranteeing that the total power used is equal to P_T . A graphical description of the *PI-Algorithm* is given in Fig. 6.6 while the implementation procedures is described in Algorithm 3.

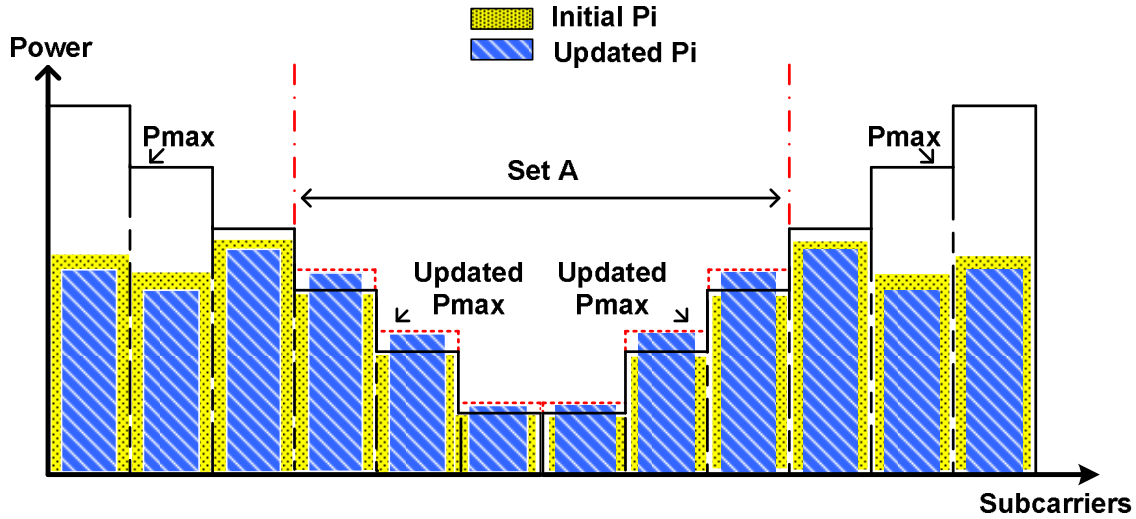


Figure 6.6. An Example of the SU's allocated power using PI-Algorithm.

Algorithm 3 PI-Algorithm

1. **Initialize** $N = \{1, 2, \dots, N\}$, $N_l = N_l$, $I_{Left}^l = 0$, $S = P_T$ and $A_l = \emptyset$.
2. $\forall l \in \{1, 2, \dots, L\}$, sort $\left\{ H_i = \frac{\sigma^2}{|h_i|^2} \Omega_i, i \in N_l \right\}$ in decreasing order with k being the sorted index. Find the P_i^{Max} as follows:
 - (a) $H_{sum} = \sum_{i \in N_l} H_i$, $\alpha_l^{(Int)} = |N_l| / (I_{th}^l + H_{sum})$, $n = 1$.
 - (b) **while** $\alpha_l^{(Int)} > H_{k(n)}^{-1}$ **do**

$$H_{sum} = H_{sum} - H_{k(n)}, N_l = N_l \setminus \{k(n)\}, \alpha_l^{(Int)} = |N_l| / (I_{th}^l + H_{sum}), n = n + 1$$
end while

$$(c) \text{ Set } P_i^{Max} = \left[\frac{1}{\alpha_i^{(Int)} \Omega_i} - \frac{\sigma^2}{|h_i|^2} \right]^+$$

$$3. \text{ if } \sum_{i \in N} P_i^{Max} \leq P_T$$

Let $P'_i = P_i^{Max}$ and stop the algorithm.

end if

4. Execute the "*cap-limited*" waterfilling (Algorithm 2) and find the set $A_l \subset N_l$ where $P_i^{W.F} = P_i^{Max}$.

5. Evaluate $I_{Left}^l = I_{th}^l - \sum_{i \in N_l} P_i^{W.F} \Omega_i$ and set $N_l = A_l$, $I_{th}^l = I_{Left}^l + \sum_{i \in A_l} P_i^{W.F} \Omega_i$ and apply again only step 2 to update P_i^{Max} .

6. Execute the "*cap-limited*" waterfilling (Algorithm 2) and set $P'_i = P_i^{W.F}$.

The computational complexity of Step 2 in the proposed PI-Algorithm (Algorithm 3) is $\sum_{l=1}^L O(|N_l| \log |N_l|) \leq O(N \log N)$. Steps 4 and 6 of the algorithm execute the "*cap-limited*" waterfilling which has a complexity of $O(N \log N + \eta N)$ where $\eta \leq N$ is the number of the iterations. Step 5 has a complexity of $\sum_{l=1}^L O(|A_l| \log |A_l|) + O(L) \leq O(N \log N) + O(L)$. Hence, The overall complexity of the algorithm is lower than $O(N \log N + \eta N) + O(L)$. The value of η is estimated via simulation to be lower than five, i.e. $\eta \in [0, 5]$. Comparing to the computational complexity of the optimal solution, $O(N^3)$, the proposed algorithm has much lower computational complexity specially when the number of the subcarriers N increased.

6.4 Simulation results

The simulation are performed under the scenario given in Fig. 6.2. A multicarrier system of $M = 3$ cognitive users and $N = 32$ subcarriers is assumed. The value of T_s , Δf and P_T are assumed to be 4μ second, 0.3125 MHz and 1 watt respectively. Additive white Gaussian noise (AWGN) of variance 10^{-6} is assumed. Without loss of generality, the interference induced by PU's to the SU's band is assumed to be negligible. The channel gains h and g are outcomes of independent, identically distributed (i.i.d) Rayleigh distributed random variables (rv's) with mean equal to "1" and assumed to be perfectly known at the (CBS). OFDM and FBMC based cognitive radio systems are evaluated. The OFDM system is assumed to have a 6.67% of its symbol time as cyclic prefix (CP). For FBMC system, the prototype coefficients are assumed to be equal to PHYDYAS coefficients with overlapping factor $K = 4$ [PHY08] [Bel08-2]. The optimal solution is implemented using the interior point method. We refer to the method proposed in [Zha08-3] by Zhang algorithm. All the results have been averaged over 1000 iterations.

6.4.1 Case 1: two active PU bands

Two interference constraints belonging to two active PU bands , i.e. $L = 2$, is assumed as given in Fig. 6.7.

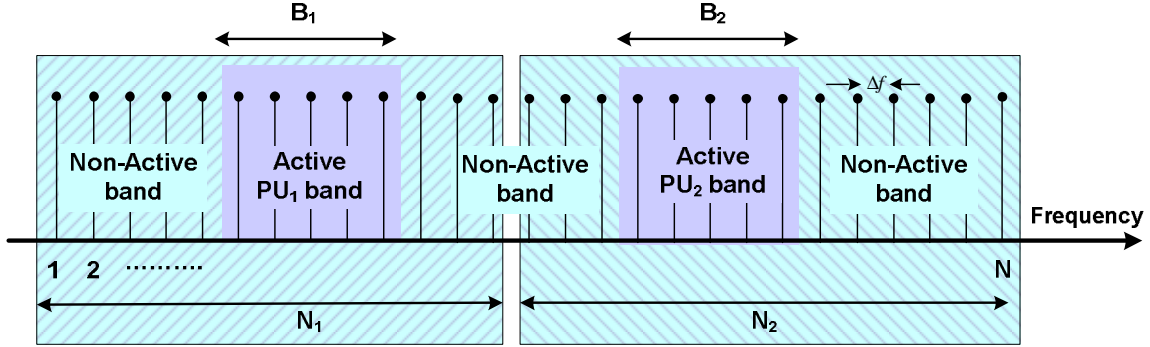


Figure 6.7. Frequency distribution with two active PU bands.

Each active PU band is assumed to have six subcarriers where $|N_1| = |N_2| = 16$. The achieved capacity using optimal, PI and Zhang algorithms for different interference constraints where $I_{th}^1 = I_{th}^2$ is plotted in Fig. 6.8.

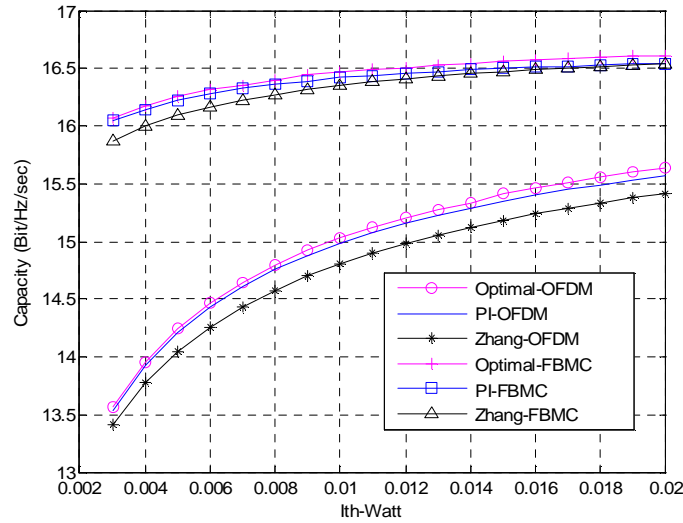


Figure 6.8 Achieved capacity vs allowed interference threshold for OFDM and FBMC based CR systems - Two active PU bands.

It can be noted that the proposed PI-algorithm approaches the optimal solution and outperforms Zhang algorithm. The effect of assuming that every subcarrier is belonging to the closest PU band and introducing interference to it only on the net interference introduced to the active PU bands is studied in Fig. 6.9 and Fig. 6.10 for PU_1 and PU_2 respectively.

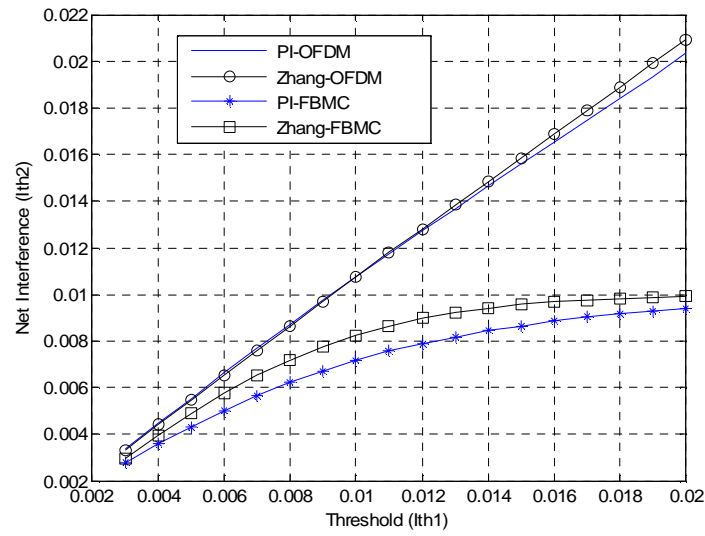


Figure 6.9. Total interference introduced to the PU_1 vs interference threshold.

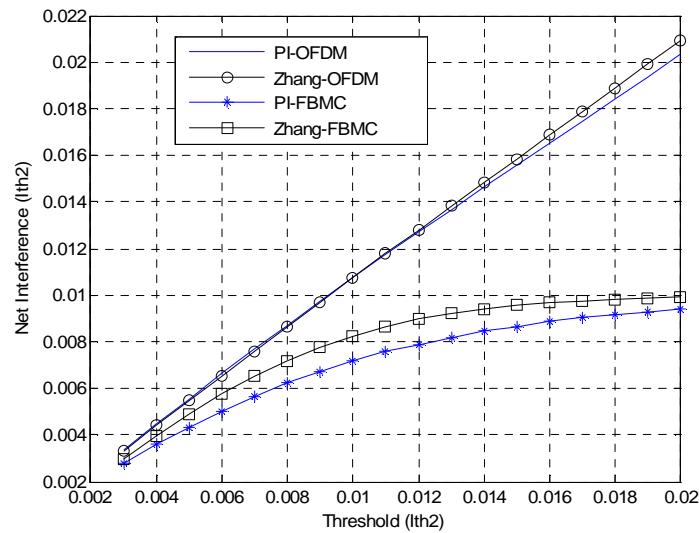


Figure 6.10. Total interference introduced to the PU_2 vs interference threshold.

It can be observed that the net interference induced using the PI-algorithm is approximately equal to the pre-specified thresholds which make the assumption reasonable. The achieved capacity of the different algorithms is plotted in Fig. 6.11 with lower values of the interference constraints.

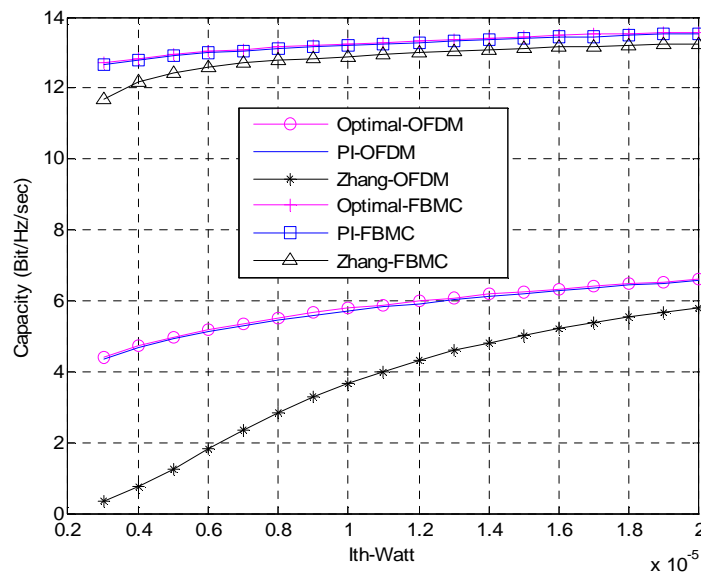


Figure 6.11. Achieved CR vs allowed interference threshold (low) for OFDM and FBMC based CR systems - Two active bands.

One can notice that Zhang algorithm has a limited performance with low interference constraints because the algorithm turns off the subcarriers that have a noise level more than the initial waterfilling level and never uses these subcarriers again even if the new waterfilling level exceeds its noise level. Moreover, the algorithm deactivates some subcarriers, i.e. transmit zero power, in order to ensure that the interference introduced to PU bands is below the pre-specified thresholds. The lower the interference constraints the more the deactivated subcarriers which justify the limited performance of this algorithm in low interference constraints.

To show the efficiency of transmitting over the active PU bands as well as the non-active bands, Fig. 6.12 and Fig. 6.13 plot the achieved capacity using the PI algorithm with and without allowing the SU's to transmit over the PU active bands.

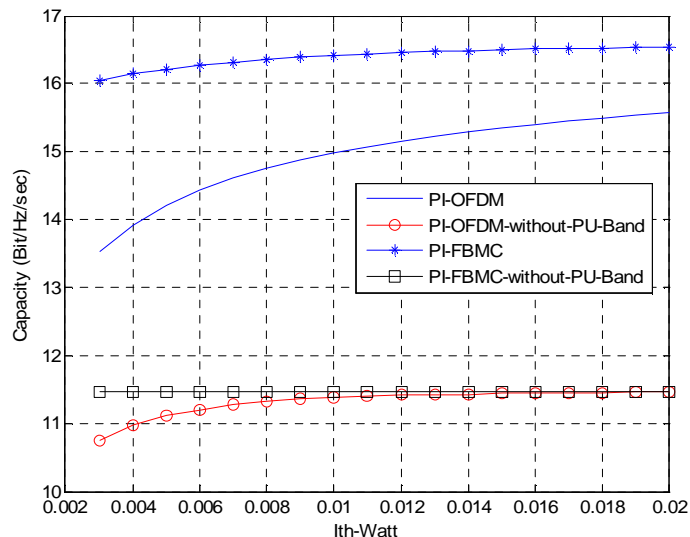


Figure 6.12. Achieved capacity vs allowed interference threshold with and without transmitting over active bands- Two active PU bands.

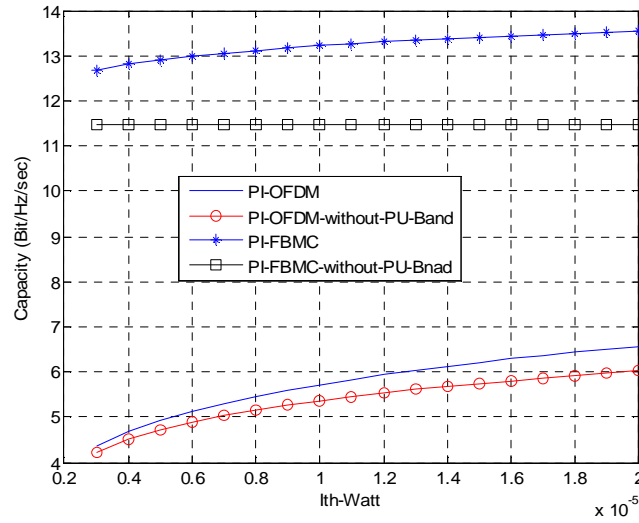


Figure 6.13. Achieved capacity vs allowed interference threshold (low) with and without transmitting over active bands - Two active PU bands.

The capacity of the CR system transmitting on both the active and non-active bands is more than that one transmitting only on the non-active band. Since the cognitive transmission in the active PU band introduces more interference to the PU's than the other subcarriers, low power levels can be used in these bands with low interferences constraints which justify why when the interference constraints decrease, the difference between the two systems decreases.

6.4.2 Case 2: one active PU band

RC algorithm can be used if there is only one active PU band, i.e. $L = 1$. The RC algorithm allocate the subcarriers and bits considering the relative importance between the power needed to transmit and the interference induced to the PU band. In order to compare the proposed PI-algorithm with RC algorithm, One active PU band with "12" subcarriers will be assumed as given in Fig. 6.14.

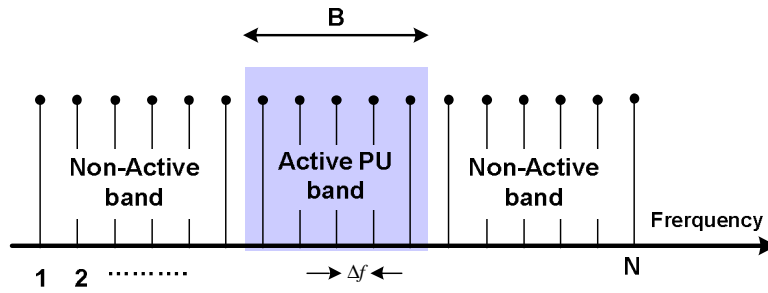


Figure 6.14. Frequency distribution with one active PU band.

For fair comparison, the same bit mapping used in [15] is considered as follow

$$b_i = \left\lfloor \log_2 \left(1 + \frac{P_i' |h_i|^2}{\sigma^2} \right) \right\rfloor \quad (6.44)$$

where b_i denotes the maximum number of bits in the symbol transmitted in the i^{th} subcarrier and $\lfloor \cdot \rfloor$ denoted the floor function. Fig. 6.15 and Fig. 6.16 show that the proposed algorithm performs better than the RC and Zhang algorithms.

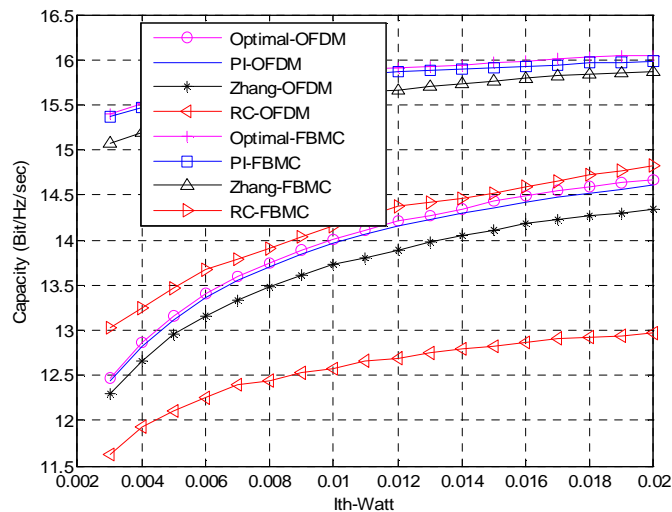


Figure 6.15. Achieved capacity vs allowed interference threshold for OFDM and FBMC based CR systems - One active PU band.

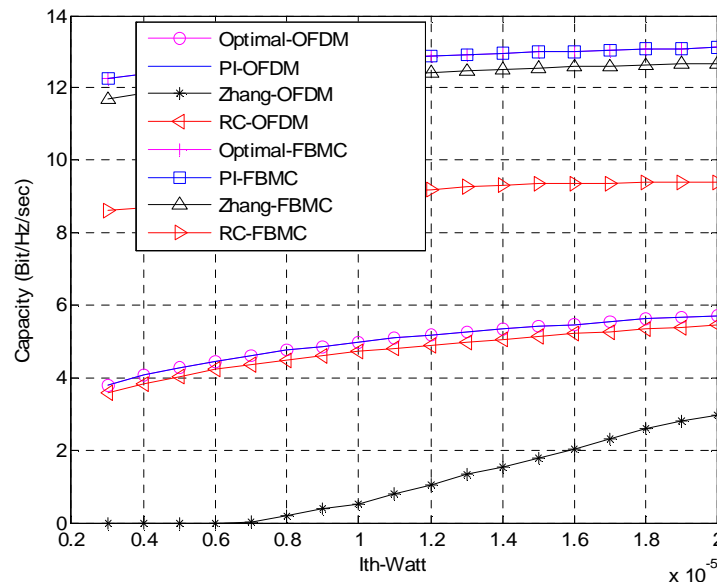


Figure 6.16. Achieved capacity vs allowed interference threshold (low) for OFDM and FBMC based CR systems - One active PU band.

In low interference constraints, RC algorithm performs better than Zhang algorithm because of the limited performance of Zhang algorithm with low interference constraints.

For all the so far presented results, the capacity of FBMC based CR system is higher than that of OFDM based one because the sidelobes in FBMC's PSD is smaller than that in OFDM which introduce less interference to the PU's. Moreover, the inserted CP in OFDM based CR systems reduces the total capacity of the system. It can be noticed also that the interference condition introduce a small restriction on the capacity of FBMC based CR systems which is not the case in OFDM based CR systems. The significant increase in the capacity of FBMC based CR systems over the OFDM based ones recommends the FBMC as a candidate for the CR network applications.

6.5 Conclusions

A low complexity sub-optimal resource allocation algorithm for multicarrier based CR networks has been proposed. Our objective was to maximize the total downlink capacity of the CR network while respecting the available power budget and guaranteeing that no excessive interference is caused to the PU's. With a significant reduction in the computational complexity from $O(N^3)$ to $O(N \log N + \eta N) + O(L)$, $\eta \in [0, 5]$, It's shown that the proposed PI-algorithm achieves a near optimal performance and outperforms the sub-optimal algorithms proposed so far. It's found that the net total interference introduced to the PU's band is relatively not affected by assuming that each subcarrier is belong to the closest PU band and only introducing interference to it. It's demonstrated also that capacity of the CR system uses the non-active as well as the active bands is more than that only use the non-active bands. Simulation results prove that the FBMC based CR systems have more capacity than OFDM based ones. FBMC offers more spectral efficiency and introduces small interference to the PU's. The obtained results contribute in recommending the use of FBMC physical layer in the future cognitive radio systems. Developing a resource allocation algorithm that consider the fairness among different users as well as their quality of service (QoS) will be the guideline of our future research work towards better radio resource management.

7 Resource allocation in cognitive radio networks with MAC layer cooperation

7.1 Problem definition and requirements

The proliferation of mobile devices, coupled with the ever increasing demand for higher data rates, constitutes static frequency allocation schemes suboptimal in various scenarios. Cognitive Radios supporting opportunistic spectrum access have emerged as a paradigm that offers an effective solution to this problem. However, at the same time a number of challenges need to be addressed. Specifically, for Cognitive Radio systems operating in licensed spectrum bands with co-existence of both primary and secondary users, spectrum sensing and spectrum mobility are of key importance. On the other hand, Cognitive Radio systems operating in license exempt spectrum bands (e.g. case of different operators in unlicensed spectrum bands), require efficient spectrum decision and spectrum sharing, as well as power control mechanisms for interference mitigation. For example, if all users transmit at the maximum valid power level then every user is causing significant interference to all other users, which can result in reduced total utility from the network perspective and poor QoS from the user perspective.

In this scope, algorithms that employ power control in order to maximize the overall utility are required. At the same time, these algorithms need to be distributed in order to be applied efficiently in ad-hoc networks operating in unlicensed spectrum bands (e.g. only users from the same operator are synchronized). Such algorithms should be able to utilize message exchange schemes between the users in order to maximize the overall utility (therefore the related systems are classified as cooperative CR systems); however, uncertainties in message exchange should also be considered. Furthermore, they should be able to converge in an optimal solution within a finite number of iterations in order to be applicable in real systems. Finally, the algorithms need to be flexible in order to take advantage of improvements in the physical layer (e.g. FBMC). The overall assumptions and definitions for the proposed algorithm are the following:

- Focus: DSA for horizontal cognitive systems with subsystems sharing license exempt spectrum, directly applicable to a case of different operators in unlicensed spectrum bands
- L pairs of users (one dedicated transmitter & one dedicated receiver). The terms user and transmitter/receiver pair are used interchangeably in the sequel
- M spectrum areas with same width
- Only users from the same operator are synchronized
- Every user selects his transmission power level trying to maximize a utility function. Utility function is selected such that the algorithm converges in a global maximum in a finite number of steps
- Message exchange (“interference prices” [Hua05]) between users is completely asynchronous
- PHY layer parameters are directly impacting the **final utility value for the network**. Reduced power level for a given bandwidth in FBMC compared to OFDM results in lower interference to other users

Various pricing mechanisms have been proposed for allocating resources in various types of networks, targeting both wired and wireless network topologies. However, the problem in distributed networks that operate in license exempt spectrum bands is different from most of the previous works, since the interference that each user is causing to the rest of the users implies that the users’ utility functions are coupled. This means that in the general case the overall network utility is not necessarily concave in regard to the transmission power of each user. We assume a scenario similar to [Hua05], in which the communication is not fixed-rate but the transmission rate can be adaptive (“elastic” data applications) and the goal is to maximize the total utility of the network without guaranteeing interference margins for each user.

7.2 Algorithm outline

The proposed algorithm is based in the algorithm of [Hua05] for distributed interference compensation, but it refines the utility function to improve the scalability in the case of a large number of user pairs and to take into account uncertainties (i.e. from user mobility and large delays in the update of the interference prices). Specifically, a fuzzy logic reasoner is utilized in order to take into account the effect of a large number of users in the impact of interference as well as to cope for uncertainties in the message exchange (e.g. from high mobility or a large time interval for the update of interference prices).

Fuzzy logic is based on fuzzy set theory in which every object has a grade of membership in various sets. Inputs are mapped to membership functions, or sets (fuzzification process). Knowledge of a restricted domain is captured in the form of linguistic rules. Relationships between two goals are defined using fuzzy inclusion and non-inclusion between the support and hindering sets of the corresponding goals [Fou96]. As a last step, the required output is defuzzified (to numerical) from the 'THEN' part of the rules in order to produce the consequent.

An important advantage of fuzzy logic is that it can be applied transparently in combination with other well known decision methods, such as multi-objective genetic algorithms [Bul08] and game theoretic approaches [Wei03]. Moreover, proper definition of the linguistic rules can be used to reduce signaling overhead by avoiding the ping-pong, i.e. when decisions or selections are made and the input variables are not constant but temporarily present regressive behavior. Finally, Fuzzy logic can handle vague requirements more efficiently than Boolean algebra. Network-related

decision making and resource allocation based on fuzzy logic approaches have been proposed in various works (e.g. [Mer08]) with promising results.

The main idea of the algorithm is that the users exchange information about their interference levels, using for this purpose explicit message exchange mechanisms at the MAC layer. A transmitter sets its power level by considering not only its own Signal to Interference Plus Noise Ratio (SINR) information but also the negative impact in utility for other users caused from the increased interference that will come as side effect of the increase in power of that particular transmitter. This functions as a counter-motive that prevents users from always setting their transmission power to the maximum valid level.

Assuming that there are a total of L users in a spectrum band with k available channels, the SINR of the i th user in channel k is given by the equation:

$$\gamma(p_i^k) = \frac{p_i^k \cdot h_{ii}}{n_0 + \sum_{j \neq i} p_j^k \cdot h_{ji}}$$

Where p_i^k is the transmission power for i user on channel k , h_{ii} is the link gain between i th receiver and i th transmitter, $n_0=10^{-2}$ is the noise level, p_j^k is the transmission power for all other users on channel k and h_{ji} is the link gain between i th receiver and j th transmitter. It should be noted that $h_{ij} \neq h_{ji}$, since the first expresses the gain between i th transmitter and j th receiver and the latter expresses the gain between j th transmitter and i th receiver.

In the general case, the carrier frequency of a signal is varied; therefore the magnitude of the change in amplitude will vary. The coherence bandwidth measures the separation in frequency after which two signals will experience uncorrelated fading. Specifically, in the case of frequency-selective fading, the coherence bandwidth of the channel is smaller than the bandwidth of the signal. Thus, different frequency components of the signal experience decorrelated fading. On the other hand, in the case of flat fading, the coherence bandwidth of the channel is larger than the bandwidth of the signal. Therefore, all frequency components of the signal will experience the same magnitude of fading. In the following analysis we assume a flat-faded channel without shadowing effects. For a flat-faded channel there is no delay spread and no frequency selectivity, as mentioned previously. This means that a single coefficient is used for channel attenuation. Since the described channel is static, i.e., the coefficient is fixed, the only attenuation present is the path loss. Therefore, in this particular case h is strictly the channel attenuation or channel gain. We assume that the environment causes average to high loss (path loss exponent is four, typical for urban environments), thus the channel gain $h_{ji} = d_{ji}^{-4}$, where d is the distance between the j th transmitter and i th receiver.

In order to model the impact in utility for user i caused by the transmission of all other users, we adopt from [Hua05] the notion of interference price. Interference price is defined as:

$$\pi_i^k = \frac{\partial u_i(\gamma(p_i^k))}{\partial \left(\sum_{j \neq i} p_j^k \cdot h_{ji} \right)}$$

It is clear that the interference price expresses the marginal loss in utility due to a marginal increase in sustained interference. Interference prices are exchanged between the users in a completely asynchronous fashion. Furthermore, not only the updates of interference price between users are asynchronous, but also every user is able to update its own price and power level at different times. Each user selects an appropriate level for its transmission power in order to maximize the difference between the increase in its own utility minus the reduction in utility incurred by the increased

interference as expressed by the interference price. Specifically, the mathematical formula that [Hua05] is trying to maximize is:

$$u_i(\gamma(p_i^k)) - p_i^k \sum_{j \neq i} \pi_j^k \cdot h_{ji} \quad (7.1)$$

The first part of this equation is closely **related to the Shannon capacity** for user i (the constant term is excluded in order to have a form that can be proved to converge in all cases). Increasing that part is directly related to an increase in the maximum bit rate. However, since the transmission of every user is seen as noise by the other users, the second term expresses what the other users will lose if user i increases its transmission power level.

The algorithm is comprised by the following steps:

1. **Initialization:** For every user $i \in L$ transmitting in channel k select a valid transmission power level p_i^k and a positive value for the interference price π_i^k
2. **Power Update:** For every user i at a time interval $t_{ai} \in T_i$, where T_i is a set of positive time instances in which the user i will update its transmission power level and $t_{a1} \neq t_{a2} \neq \dots \neq t_{ai}$, update its transmission power level p_i^k trying to maximize equation (7.1)
3. **Interference Price Update:** For every user i at a time interval $t_{bi} \in T'_i$, where T'_i is a set of positive time instances in which the user i will update its interference price and $t_{b1} \neq t_{b2} \neq \dots \neq t_{bi}$, calculate and announce the updated interference price π_i^k and notify the rest of the users for the updated value

Steps 2 and 3 are repeated asynchronously for all users until the algorithm reaches its final steady state. In order to perform the power update in step 2, users select p_i^k from the set TP of the allowable transmission power levels, so that the surplus of (7.1) is maximized. Provided that the allowable power levels are equidistant values that can be derived from the previous value by adding a constant increment, then it can be proved that the algorithm converges, as long as the increment is sufficiently small (for a normalized in $[0, 1]$ power level and a typical number of less than 100 users, an increment of 0.001 is sufficiently small). Moreover, if the problem is partitioned so that there is a single available spectrum area or if the algorithm is executed only for subgroups selecting the same spectrum area M , then it can be proved that the algorithm converges to a **global maximum** under arbitrary asynchronous updates [Hua05].

In order to execute the algorithm, every user in the network needs to know its own SINR and channel gain, as well as the channel gains and the interference prices announced by other users. The SINR and the channel gain between a user pair can be calculated at the receiver and forwarded back to the transmitter. The channel gains between users can be calculated if receivers periodically broadcast a beacon [Hua05] (h_{ji} message between Receiver i and Transmitter j in Figure 7.1). This information can also be provided on demand through a specially defined message sent from the receiver. Thus, in case the transmitter requires channel gain information before the reception of the next scheduled beacon, it can request this information from the receiver who will respond with the relative measurements. Finally, interference price values can be also conveyed in the same manner (message p_{ij} from Receiver i to Transmitter j in Figure 7.1). Every user announces a single interference price, therefore the delay that is introduced by the algorithm scales linearly with the number of users. In a “real” protocol implementation parameters such as the storage requirements and scalability of the message exchange mechanism should be addressed. Moreover, the overhead and delays introduced by message exchange should be taken into consideration together with parameters such as timeliness and path optimality (for increased reliability in message transmission). However, the algorithm is shown to operate relatively well even if message exchange

is imperfect and this property is further improved in our work, therefore an end to end reliability mechanism is probably not well justified for the cooperation of nodes in an ad-hoc manner. Moreover, since the MAC protocol itself is not the scope of our work, we assumed a typical range of delays for the transmission of signaling messages at the radio interface (this is included in the values of the interference price update time).

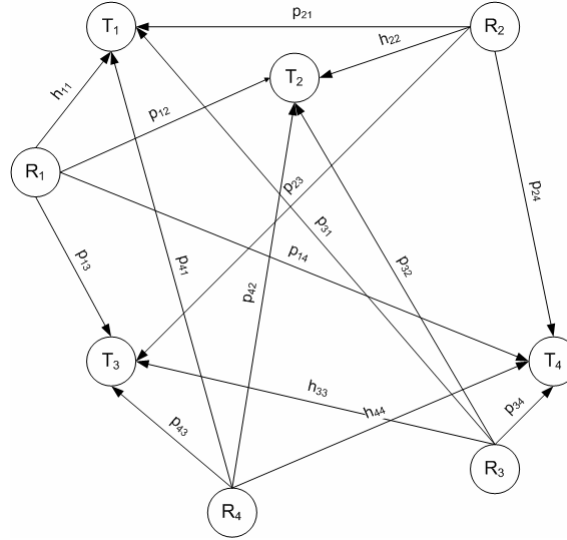


Figure 7.1. An example network topology with four transmitter-receiver pairs

However, in the original version of the algorithm from [Hua05], without coefficient α in (7.1), an underestimation of interference prices is likely in some cases (e.g. due to problems in message exchange or increased update time intervals for the interference prices) and the effect of the underestimation is the convergence of the algorithm in a non optimal solution. Moreover, as the number of users increases, they are more likely to choose the highest allowable transmission power level, which is not always desirable since it will often result in increased interference to a large number of neighboring users.

Therefore, coefficient α is introduced in our work in order to improve the scalability of the algorithm if a large number of users are sharing the same spectrum bands. In such cases the relative impact of the subtracted term should be enhanced, otherwise the first term usually dominates even for a relatively small number of users (e.g. more than 20) and this results to all users selecting the maximum valid power level. Furthermore, factor α also copes for uncertainties in the message exchange mechanism, such as large update time intervals from the previous interference price update (considering that updates are asynchronous for all users) and potential problems in message exchange due to high mobility. In both cases there is a danger that the impact of the interference to others due to the increase in transmission power will be underestimated as explained above, thus factor α needs to avert this scenario by increasing the weight of the second term. In such cases factor α compensates for the underestimation of interference and if it is defined appropriately it can result in a system that approximates the case of “perfect” message exchange. Fuzzy logic is well suited for this since it can handle vague and unclear requirements efficiently and the system can be easily fine-tuned to exhibit the desirable behavior. Therefore, if coefficient α is included as a weight that is multiplied with the subtracted interference term then we derive the following equation that is the objective we are trying to maximize:

$$u_i(\gamma(p_i^k)) - a \cdot p_i^k \sum_{j \neq i} \pi_j^k \cdot h_{ji} \quad (7.2)$$

7.3 Results

The algorithm has been implemented in MATLAB. The overall structure of the implementation is depicted in Figure 7.2 with each box corresponding to a separate m-file. Specifically:

- “Tournament” sets the initial values for the Transmission Power and Interference Price for every user pair, orchestrates the execution of the other m-files, generates and prints the final results,
- “IteratedCall” calls “Play” in order to generate the new values of Power and Interference Price for each user pair in a complete round of execution,
- “Play” implements the update of Power and Interference Price for one user in a round, trying to maximize equation (7.1).



Figure 7.2. Structure of the algorithm implementation in MATLAB

The coefficient α sets the weight of the subtracted interference-related term in equation (7.1) and is determined before the initiation of the optimization phase (in “Tournament”) by executing a Fuzzy Logic reasoner. Specifically, α is defined as 1/100 of the Interference Weight derived after defuzzification. The Fuzzy reasoner we have used is of type “Mamdani”, because this type of reasoner is intuitive, well suited for human input, flexible and widely accepted. It receives three inputs (number of users, mobility level and update time interval for the interference prices) and one output (the Interference Weight). The membership functions are triangular (selected mainly for simplicity in calculations) and we have defined three membership functions per input variable, therefore the number of fuzzy rules is $3^3=27$. The representations of the membership functions for two input variables of the system are depicted in Figure 7.3 and Figure 7.4:

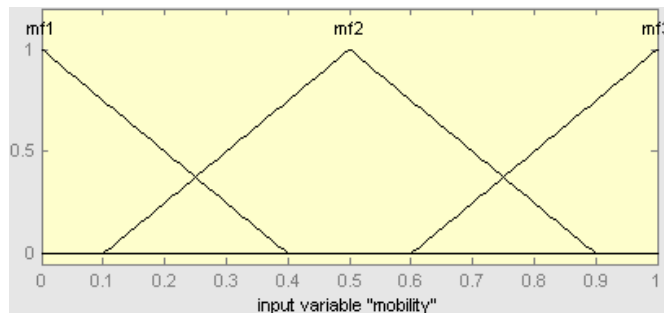


Figure 7.3. Membership functions for input variable “mobility level”

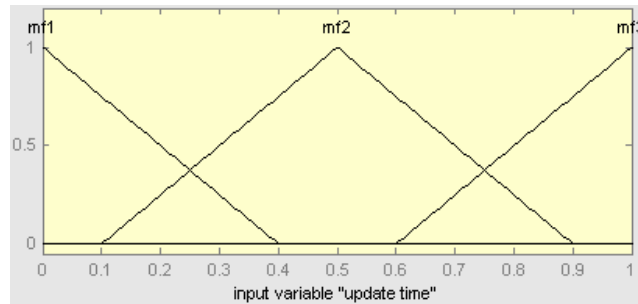


Figure 7.4. Membership functions for input variable “interference price update time interval”

The membership functions for the output variable “Interference Weight” are presented in Figure 7.5. In this case a number of five membership functions are defined and the output value is set in the range [0, 500], in order to achieve a greater degree of resolution and flexibility for the output of the fuzzy reasoner. The membership functions mf1-mf5 are given the labels “very low”, “low”, “moderate”, “high” and “very high respectively”.

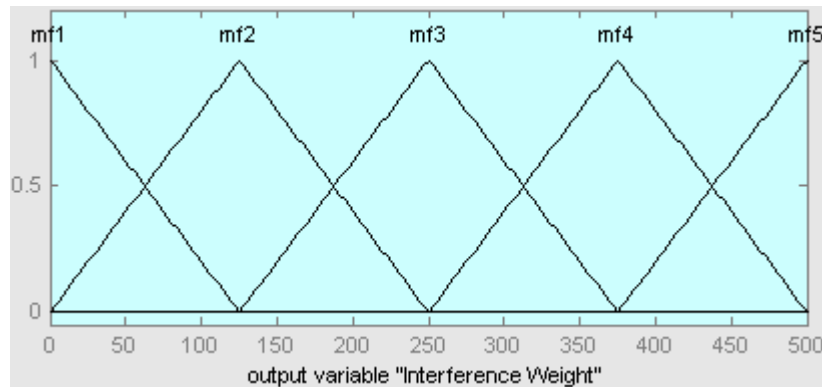


Figure 7.5. Membership functions for output variable “interference weight”

The rule base for the fuzzy reasoner is presented in the following table:

Table 7.1. Fuzzy Reasoner Rule Base

Rule Number	Users	Update Interval	Mobility Level	Consequent
1	Low	Low	Low	Very Low
2	Low	Low	Moderate	Very Low
3	Low	Low	High	Low
4	Low	Moderate	Low	Low
5	Low	Moderate	Moderate	Low
6	Low	Moderate	High	Low
7	Low	High	Low	Low
8	Low	High	Moderate	Low
9	Low	High	High	Moderate
10	Moderate	Low	Low	Low
11	Moderate	Low	Moderate	Low
12	Moderate	Low	High	Moderate
13	Moderate	Moderate	Low	Moderate
14	Moderate	Moderate	Moderate	Moderate
15	Moderate	Moderate	High	High
16	Moderate	High	Low	Moderate
17	Moderate	High	Moderate	High
18	Moderate	High	High	High
19	High	Low	Low	High

20	High	Low	Moderate	High
21	High	Low	High	High
22	High	Moderate	Low	High
23	High	Moderate	Moderate	High
24	High	Moderate	High	Very High
25	High	High	Low	High
26	High	High	Moderate	Very High
27	High	High	High	Very High

As can be seen we have selected the number of users to be the dominant factor, which has the greatest effect in the final outcome. This is because if the number of users is large even a small increase in the transmission power of a user has the potential to cause increased interference and reduce the QoS to a large number of users. The update time interval and the mobility level have similar weights but different behavior. The first has a uniform effect over the entire valid range of update times, while the latter starts to affect the outcome only after a relatively high level, but after that point it increases sharply, because only after a relatively high level of mobility users are likely to underestimate the interference they will cause to others (due to problems in message exchange, etc). It should be noted that the rule set of Table 7.1 is derived based on “common sense” and fine-tuned manually. Future work will include the development of a neuro-fuzzy controller able to learn and adapt dynamically the original set of rules based on the monitored behavior of the system.

The Defuzzification method we have used for generating the final crisp value is “Centroid”, also known as “Center of Gravity - COG”. This method determines the center of the area below the combined membership function; therefore the final output u_{COG} is given from equation (7.3), where u_i are the centers of the membership functions $\mu_F(u)$:

$$u_{COG} = \frac{\sum_1^{27} u_i \cdot \mu_F(u_i) \, du}{\sum_1^{27} \mu_F(u_i) \, du} \quad (7.3)$$

The defuzzification method takes into account the area as a whole, counting overlapping regions only once.

The 3D representation of the Interference Weight (crisp value in the range [0,500]) as a function of the interference price update time interval and the mobility level is presented in Figure 7.6. The coefficient increases if the update time interval is greater, because it is likely that transmitters do not have the updated interference price for other users and the increase is approximately uniform for the entire valid update time range. On the other hand, the coefficient also increases as the level of mobility increases. However, in this case the increase is not uniform but begins after a relatively high mobility level and quickly rises to high levels. The exhibited behavior is the outcome of the fuzzy rules defined in Table 7..

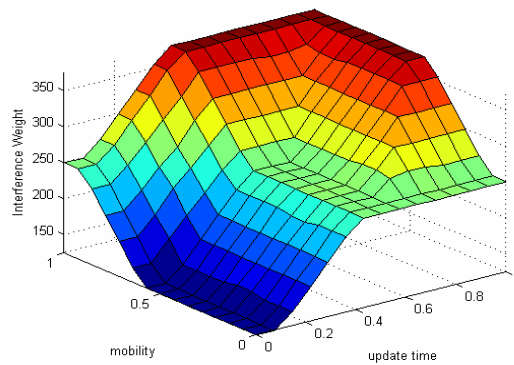


Figure 7.6. Interference coefficient as a function of the update interval and the mobility level

The 3D representation of the Interference Weight derived from the specified rule base and defuzzification method as a function of the interference price update time interval (defined as up to 100 seconds) and the number of users (up to 40 user pairs) is presented in Figure 7.7. For the update time interval we have the same behavior as in the previous case. On the other hand, the coefficient also increases with the number of users. The increase is rather sharp (as determined by the rules in Table 7.1) and the value of the coefficient is rising quickly even for a relatively small number of users. This is necessary in order to guarantee the scalability of the system, because as the number of users increases they are more likely to select the maximum allowable power level, since the first term is dominant in equation (7.1). Therefore a counter-motive is necessary in order to discourage such behavior and keep interference at an acceptable level.

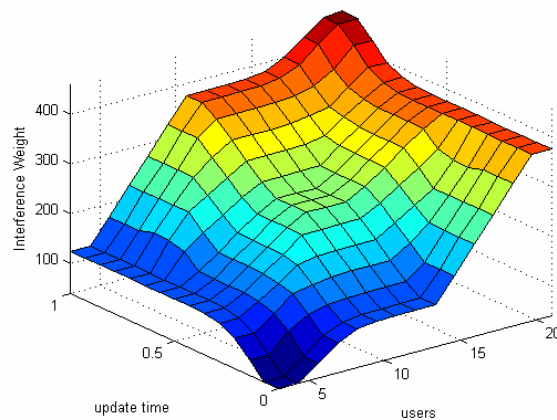


Figure 7.7. Interference coefficient as a function of the update interval and the number of users

The 3D representation of the Interference Weight as a function of the number of users and the mobility level is presented in Figure 7.8. For both parameters we have the behavior explained above. The overall form of the figure resembles the previous, however the mobility level is starting to affect the outcome only after a threshold is crossed, as expected according to the selected set of fuzzy rules.

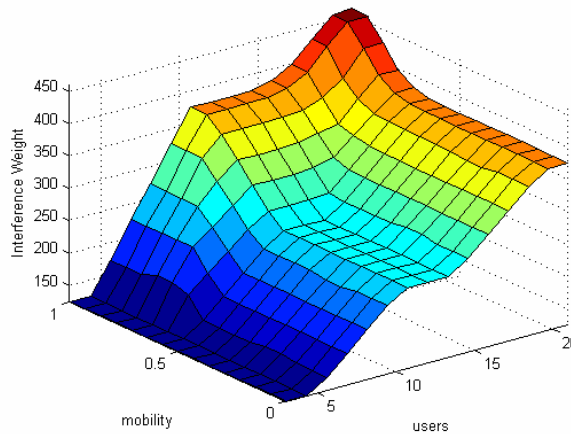


Figure 7.8: Interference coefficient as a function of the mobility level and the number of users

The transmission power levels derived from the proposed algorithm for a number of 20 and 10 user pairs i (transmitters and receivers) with random distance between the i th receiver and the i th transmitter is shown in Figure 7.9 and Figure 7.10. Users set their power level in order to maximize equation (7.1). The total “useful” utility for the network is the sum of the utilities for every user pair. The algorithm has converged (reached its final steady state) with a total of 24 iterations in the first example and 19 iterations in the second example. Convergence is guaranteed due to the form of the utility function [Hua05].

The final transmission power levels are selected from a range of values that provides enough bandwidth for users in distances typical for ad-hoc communication (up to a few hundred meters), therefore resulting in acceptable QoS. The effect is also captured in the total utility of the network, Figure 7.11, Figure 7.12 and Figure 7.13. Moreover, for these three figures perfect message exchange is assumed, therefore the value of the Interference Weight is only affected from the number of users.

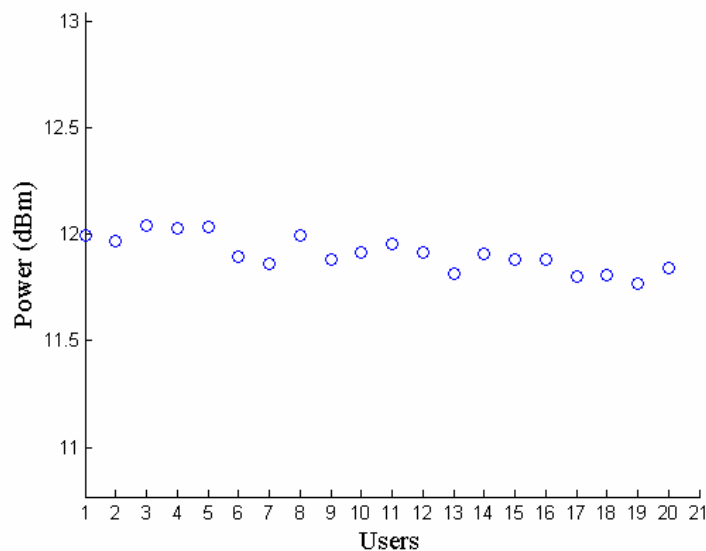


Figure 7.9. Transmission power levels for 20 user pairs with random transmitter and receiver distances

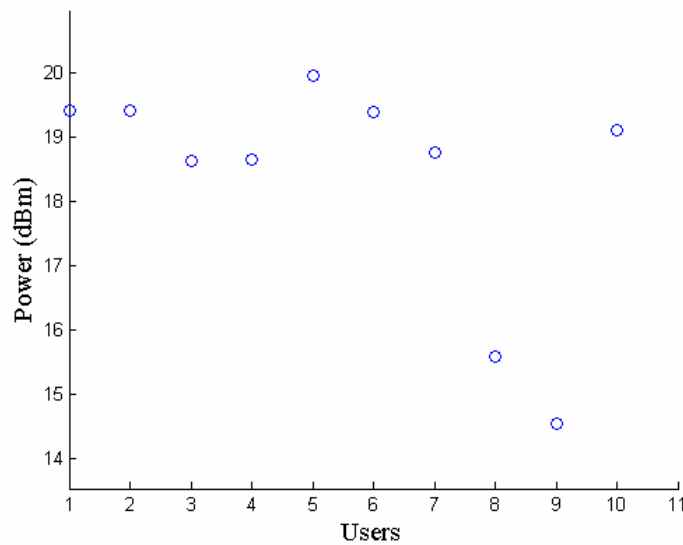


Figure 7.10. Transmission power levels for 10 user pairs with random transmitter and receiver distances

On the other hand, Figure 7.14 is explicitly showing the improvement in comparison with the original algorithm of [Hua05] if uncertainties that cause underestimation of the interference are present. If such uncertainties are not present then the algorithm behaves similarly to the algorithm of [Hua05]. It should be noted that all figures depict the “**useful**” **utility** of the system, the utility that is directly utilizable without resulting in poor QoS due to an increase in interference. The vertical axis in these figures is the achieved useful utility while the horizontal axis is the corresponding experiment number. Each experiment is calculated for a random distance between users, tens up to a few hundreds of meters (typical for the considered system model).

The improvement in the total utility of the network if we use the proposed algorithm over the scenario in which every user transmits using the maximum allowable power level is depicted in Figure 7.11 (calculated for 30 experiments). It is clear that the utility for the scenario in which the users transmit using always the maximum power level depends strongly from the (random) distance between the users and for this reasons fluctuations appear in the graph (the utility drops from 0.7 to 0.62 in some cases). This reduction is significant, since it is directly related to a reduction of SINR and therefore results in QoS degradation. On the other hand, in the case that the proposed algorithm is used, the utility function remains more or less stable near its highest value.

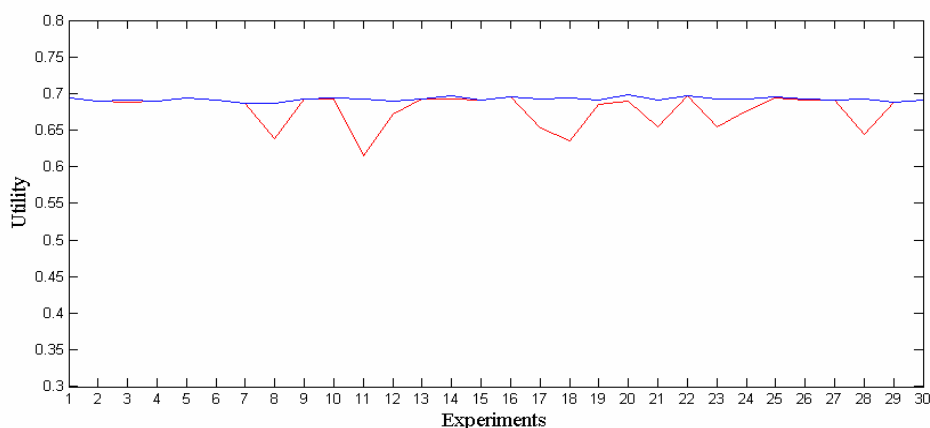


Figure 7.11. Utility function for the proposed algorithm (blue line) and for the always transmit with the maximum valid power scenario (red line)

The improvement in the total utility of the network if we use the proposed algorithm with FBMC over using the proposed algorithm with OFDM is depicted in Figure 7.12 and Figure 7.13 (both for 30 experiments). The improvement stems from the fact that FBMC uses lower transmission power for the same bandwidth compared to OFDM [Wal08] and therefore causes reduced interference. If we assume that 3dbm less power is required we derive the graph of Figure 7.12 while for 6dbm we get the graph shown in Figure 7.13.

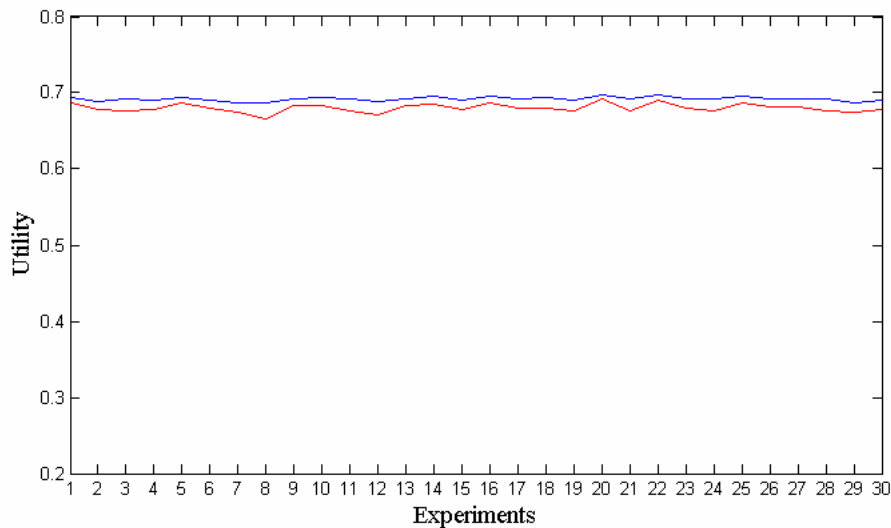


Figure 7.12. Utility function for the proposed algorithm with FBMC (blue line) and for OFDM requiring 3dbm more transmission power for the same bandwidth (red line)

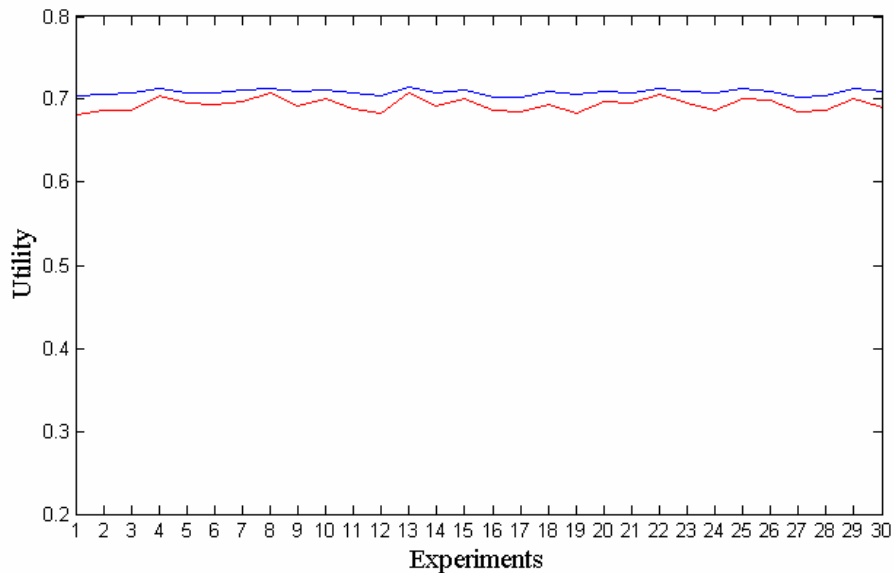


Figure 7.13. Utility function for the proposed algorithm with FBMC (blue line) and for OFDM requiring 6dbm more transmission power for the same bandwidth (red line)

The improvement in the total utility of the network if we use the proposed algorithm with FBMC over using the algorithm without the fuzzy logic parameter is depicted in Figure 7.14 (for 30 experiments). We assume that the interference is underestimated by 25% due to problems in the exchange of the interference prices caused from high mobility levels of some users, as well as from a large update time interval for the interference prices. The improvement in this case stems from the

fact that the introduced fuzzy logic parameter compensates for the underestimation by increasing the weight of the subtracted term.

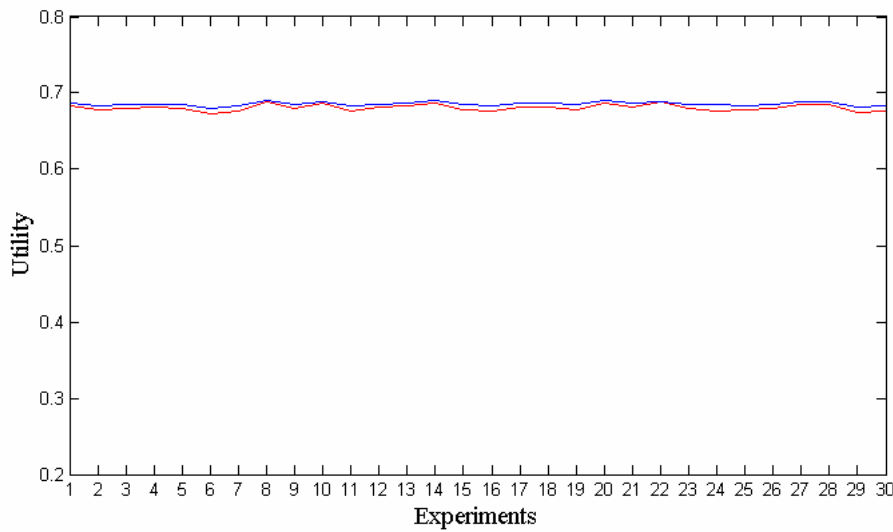


Figure 7.14. Utility function for the algorithm with (blue line) and without (red line) the proposed fuzzy logic parameter for expressing uncertainties

7.4 Conclusions

We have presented an improved algorithm, based on the algorithm of [Hua05], for cooperative DSA in unlicensed bands, utilizing MAC layer mechanisms for message exchange (“interference prices”) between the nodes, in order to achieve interference mitigation. The main improvement in our work compared to [Hua05] is the introduction of a coefficient that is serving as the weight of the interference term, increasing its impact in cases of imperfect message exchange, long update time intervals for interference prices, as well as increased number of users. In such cases the interference that caused to other users by an increase in the transmission power of a user is often underestimated, resulting in a convergence of the algorithm in a non-optimal solution. In the presence of such uncertainties, if this underestimation is compensated by a properly defined weight parameter, the system will approximate its optimal behavior as in the case of “perfect” message exchange.

The value of the weight parameter was derived from a fuzzy logic reasoner, because fuzzy logic is particularly effective at dealing with uncertainties and vague requirements. Moreover, the outcome of the proposed algorithm has been compared to the original algorithm in terms of the overall utility level (defined as the sum of the user utilities) under uncertainties that cause 25% underestimation of interference. Furthermore, comparison was also made between the proposed algorithm with FBMC and OFDM. In this case using FBMC increased the achieved utility and the improvement stems from the fact that FBMC uses lower transmission power for the same bandwidth compared to OFDM [Wal08] and therefore causes reduced interference.

Future work includes further study of the correlation between the utility value and typical network parameters such as the Bit Error Rate and Probability of Error, which define the end to end reliability of the system and determine QoS. Moreover, the rules of the fuzzy logic reasoner will be refined and methods for automatic update of the fuzzy rules will be proposed (e.g. utilizing a neuro-fuzzy controller). Finally, parameters such as fairness and scalability will also be investigated.

8 Decentralized dynamic spectrum allocation in uncoordinated cognitive radio networks based on adaptive antenna array interference mitigation diversity

Dynamic spectrum or channel allocation can be an effective way to increase spectral efficiency of wireless communications systems [Zha07], [Ges07], including cellular [Kat96], WLAN [Mal05], WIMAX [Ash07], and ad hoc [Sri05], [Nee06], [Zey07] networks. DSA may be implemented using explicit coordination between access nodes, which is mostly suitable for cellular systems [Kat96] in a licensed spectrum. In an unlicensed spectrum [Etk07] or in cognitive radio systems with primary and secondary users [Hay05], channel allocation has to be performed by each (secondary) provider in a decentralized autonomous way [Ash07], [Zha05].

A DSA strategy may be focused on maximal interference avoidance. For example, in [Ash07], a multichannel version of the carrier sense multiple access collision avoidance (CSMA/CA) algorithm operates by selectively activating or deactivating groups of OFDM sub-carriers separated by the guard bands in the WIMAX system [802.16-04]. In the most interesting scenario, where the total number of SSs that belong to different closely located but not explicitly cooperating subsystems exceeds the number of available bands, joint DSA and multiple-antenna interference suppression may be required.

A spectrum sharing problem in multiple input multiple output (MIMO) systems is addressed in [Ars07], [Scu08-1], [Scu08-2], [Scu08-3]. Based on game theory, it is shown in [Scu08-1], [Scu08-3] that local selection of the covariance matrices of the transmitted signals that maximize data rates of MIMO links subject to the power and interference to the primary users constraints, converges to Nash equilibrium (NE) from which every user is not willing to unilaterally move. Furthermore, the uniqueness of the NE is established in [Ars07], [Scu08-2] subject to some constraints on the interference level.

In the general case, local “selfish” (greedy) maximization of data rates cannot guarantee convergence to NE, for example, as demonstrated in [Men07]. Particularly, this is the case for joint iterative greedy DSA and beamforming in MIMO ad hoc networks. In [Zey07], simulations show good results for such a network based on the “selfish” DSA and MIMO beamforming [Itl06], but its convergence cannot be guaranteed. In [Zey08], it is pointed out that this makes such a solution “useless from a practical perspective”.

One way to overcome this difficulty could be some cooperation in channel allocation at the MAC layer supported by beamforming at the PHY layer. In [Zey08], channels are selected taking into account the interference seen at the receiver node, as well as the interference that this transmitter node causes to other nodes in the network. Then, the convergence is established by means of game theory. Generally, explicit MAC layer cooperation between nodes significantly limits applicability area of such networks.

Another approach to address this problem is explored in [Kuz09-1], [Kuz09-2], [Abr09] and summarized in this chapter. The main idea is that convergence with probability one to a certain

stationary (equilibrium) point or even existence of the unique NE, are not necessary for a particular algorithm if we are able to demonstrate:

- an overwhelming majority of stationary points with sufficiently high steady-state performance over few inappropriate ones;
- sufficiently high probability of the reasonably fast algorithm convergence compared with a tiny probability of non-convergence (so called ergodic behavior) or slow convergence.

Therefore, our approach is that if the probability of convergence to appropriate stationary points is high compared with the probability of convergence to inappropriate points or non-convergence to fixed points, then the suggested approach may still be treated as the one with a “practical perspective”.

To achieve the discussed above properties in the considered problem, we introduce new “good neighbor” strategies that can be viewed as some kind of rule-regulated cooperation [Cao08] between spectrum sharing nodes without explicit data exchange between them. Particularly, a “good neighbor” strategy at each iteration minimizes a number of changing channels subject to some quality of service (QoS) constraints. Minimization of the channel switches reduces non-stationary interference in the network leading to faster and more reliable convergence especially for a high number of users.

It is worth emphasizing that to demonstrate achievement of the required properties, we need an analytical tool additionally to conventional simulations. For example, fast convergence from some initial states cannot guarantee the same for other initial states or non-convergent and slow-convergent behaviors cannot be practically distinguished by means of simulations for the given propagation scenario. Theory of absorbing Markov chains, e.g., [Kem66], provides us with the required tool. For the given channel realization it allows classification of the network states in 3 groups: transient, absorbing and ergodic, and gives analytical expressions for probabilities and convergence rate to all the absorbing points (desirable convergent behavior in the considered system) and ergodic subchains (non-desirable non-convergent behavior) from all initial states.

Specifically, we consider DSA in the uplink interference-limited environment with a number of wireless systems consisting of multiple-antenna BSs and associated single-antenna SSs. These systems may belong to different providers, they are not synchronized, and do not explicitly cooperate in a centralized fashion. Frequency channels in this case can be formed in an OFDM-based, e.g., WIMAX [802.16-04], system by an appropriate sub-carrier allocation with guard bands for preventing energy leakage between channels allocated to unsynchronized users [Ash07] or in spectrally efficient FBMC systems by using frequency selective filters for adjacent channels, which is the main subject of the PHYDYAS project.

Since the number of available bands is less than the total number of SSs, some of these SSs belonging to different subsystems have to share the same frequency. For any given allocation made by all other BSs, a BS under its DSA adjustment can allocate its users to frequencies such that under adaptive receive beamforming, the required signal-to-interference-plus-noise ratio (SINR) is achieved. Note in this regard, that if all interference components arrive at an antenna array via propagation channels that are almost orthogonal to the desired signal, then even a powerful interference is not a problem, since it can be effectively suppressed at the receiver. In a free space environment, this means that interference directions of arrival are away from the adaptive antenna

main beam steered to the desired signal direction. On the contrary, even a weak interference in the main beam direction may cause significant performance degradation. Therefore, an IM-based DSA algorithm at each subsystem should allocate bands to its users, such that the propagation channels from the users to their BSs are as orthogonal as possible to the active interference propagation channels. We refer to such a variety of IM options as adaptive array interference mitigation diversity. The main problem here is that any decision made by a given BS regarding frequency allocation of its users may have an arbitrary impact on interference scenarios for other BSs, due to the non-reciprocal nature of propagation channels from the SSs of a given subsystem to other BSs.

To prove our approach viable, we first analyze the potential global performance of the considered IM-based DSA assuming Rayleigh fading with no pathloss and shadowing effects. Comparison of the global bounds for the extreme interference limited scenario with the global performance in the “no interference” case shows the overall IM diversity effect in the considered system. Global performance bounds can be used as the ultimate benchmark for different (not globally optimal) DSA algorithms including the ones with MAC layer cooperation between nodes as well as the decentralized algorithms introduced in this paper. Furthermore, the locally estimated “no interference” performance can be used for on-line selection of QoS thresholds for the proposed “good neighbor” strategies in the general propagation scenario with pathloss and shadowing.

For a relatively low dimension of the system (in terms of a number of BSs, SSs, and available bands), we analyze the performance of the introduced techniques by means of the theory of absorbing Markov chains. For higher dimensions, we rely upon direct statistical simulations, yet considering the trends established by the Markov chain theory.

The system model and problem formulation are given in Section 8.1. In Section 8.2, global performance bounds are derived. The rule-regulated “good neighbor” decentralized IM-based DSA technique is proposed in Section 8.3, while in Sections 8.4 we introduce its modified versions with additional power control. Our results on absorbing Markov chain modeling for a low-dimensional system are presented in Section 8.5. Behavior of mixed networks with a number of “selfish” subsystems that are not willing to follow the “good neighbor” rules is studied in Section 8.6. Simulation results for higher-dimension systems in different stationary and non-stationary propagation scenarios are given in Section 8.7. Section 8.8 summarizes the results of the chapter.

8.1 System model and problem formulation

The considered system consists of N independent subsystems containing base stations BS_n , $n=1, \dots, N$ and corresponding users SS_{nm} , $m=1, \dots, M$, where M is the number users per BS. A system model is illustrated in Fig. 8.1 for $N = M = 3$. Users transmit data to their BSs using one of the $F \geq M$ available frequency channels. BSs have full information and control of their own users. In particular, they can estimate propagation channels in all the available bands and assign the individual bands and transmit powers to their own users. Assuming for simplicity narrowband channels, the signal received by an antenna array of K elements for the n th subsystem can be expressed as follows:

$$\mathbf{x}_{nf}(t) = \sum_{l=1}^N \sum_{m=1}^M \delta_{fd_{lm}q_{lm}} \mathbf{h}_{d_{lm}m|n} s_{lm}(t) + \mathbf{z}_{nf}(t), n=1, \dots, N, f=1, \dots, F, \quad (8.1)$$

where $\mathbf{x}_{nf}(t)$ is the $K \times 1$ vector of the signal received at BS_n in the n th band at the t th time instant, \mathbf{h}_{fmln} is the $K \times 1$ vector of propagation channel to BS_n in the f th band from the m th user of the l th subsystem, $s_{nm}(t)$ is the SS_{nm} transmitted signal with $E\{|s_{nm}(t)|^2\} = 1$ and q_{nm}^2 is its power with constraint $\sum_{m=1}^M q_{nm}^2 = Q$, $n=1, \dots, N$, $\mathbf{z}_{nf}(t)$ is a $K \times 1$ vector of AWGN with $E\{\mathbf{z}_{nf}(t)\mathbf{z}_{nf}^*(t)\} = \sigma^2 \mathbf{I}_K$, d_{nm} is the nm th element of the $N \times M$ decision matrix \mathbf{D} denoting the frequency band assigned to SS_{nm} , $E\{\cdot\}$ is the averaging operator, $(\cdot)^*$ is the conjugate transpose operation, \mathbf{I}_K is the $K \times K$ unity matrix, and

$$\delta_{ij} = \begin{cases} 1 & \text{if } i = j \\ 0 & \text{if } i \neq j \end{cases} \quad (8.2)$$

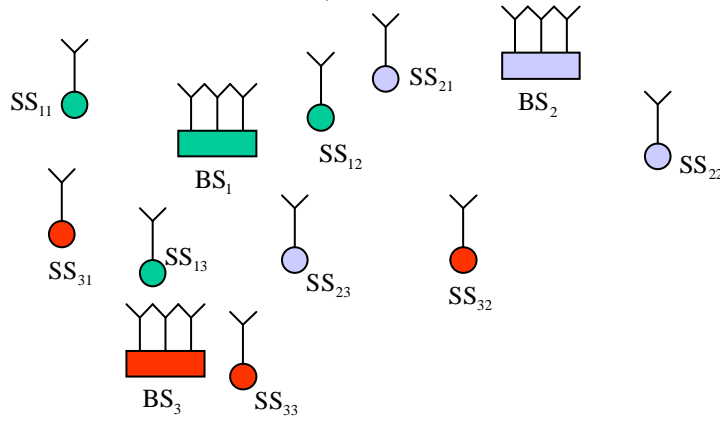


Figure 8.1. System model for horizontal CR scenario

A global performance metric, which cannot be estimated locally at each BS_n , is defined as the data rate for the weakest link in the system

$$\gamma = \min_{m=1, \dots, M, n=1, \dots, N} \log_2 [1 + \text{SINR}(\mathbf{D})], \quad (8.3)$$

where

$$\text{SINR}(\mathbf{D}) = \mathbf{h}_{d_{nm}mn}^* \mathbf{R}_{d_{nm}n}^{-1} \mathbf{h}_{d_{nm}mn} \quad (8.4)$$

is the SINR at the output of the optimal spatial filter for the nm th user and

$$\mathbf{R}_{d_{nm}n} = \sum_{\substack{i=1 \\ i \neq n}}^N \sum_{j=1}^M \delta_{d_{nm}d_{ij}} q_{ij}^2 \mathbf{h}_{d_{ij}jin} \mathbf{h}_{d_{ij}jin}^* + \sigma^2 \mathbf{I}_K \quad (8.5)$$

is the $K \times K$ interference covariance matrix at BS_n in the band occupied by SS_{nm} .

The main system assumptions are as follows:

- BSs allocate different bands for all users in their subsystems, i.e., all rows in matrix \mathbf{D} contain different elements.
- Rayleigh propagation channels \mathbf{h}_{fmln} are stationary independent random Gaussian vectors

$$\mathbf{h} \propto CN(0, \sigma_h^2 \mathbf{I}_K), \quad (8.6)$$

where $\sigma_h^2 = 1$ is assumed at the beginning to emphasize interference limited scenario and derive performance bounds. Then in Section 8.7.2, σ_h^2 is a random variable according to the pathloss and shadowing models for particular system geometry.

- BS_{*n*}, $n=1, \dots, N$ know \mathbf{R}_{fn} and \mathbf{h}_{fmm} for $m=1, \dots, M$, $f=1, \dots, F$, and have no information on \mathbf{R}_{jl} and \mathbf{h}_{fml} for $j \neq n$.
- Space-time spectrum sensing is required at each BS_{*n*} to obtain the interference covariance matrices (8.5) in all the available bands. To do this, we assume that all users can transmit data signals or stay silent during data and sensing intervals controlled by the BSs. (Generally, users can transmit training data during the sensing intervals for direct estimation of the antenna array weight vectors. This problem becomes important for analysis of finite amount of data effects, which will be studied in the next deliverable D8.2). Furthermore, focusing on the cognitive radio effects, we assume that the sensing intervals for different subsystems do not overlap and the interference covariance matrices are estimated accurately during corresponding sensing intervals. A low probability of overlapping of the sensing intervals can be achieved, for example, by means of random duration of the data intervals as illustrated in Fig. 8.2.
- At the beginning, constant power $q_{nm}^2 = Q/M$ for all users in the system is assumed, i.e., locally selected frequency bands are the only adjustable parameters. Power control is discussed in Section 8.4.

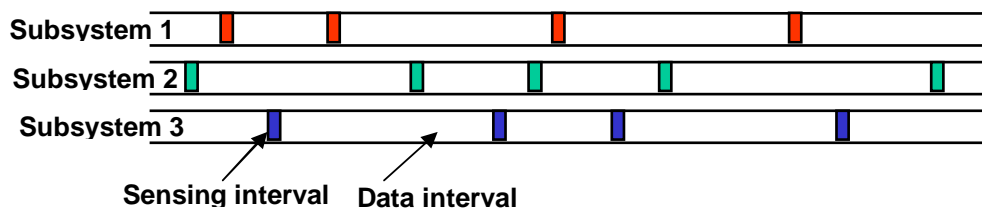


Figure 8.2. Illustration of space-time spectrum sensing with random duration of data intervals

The problem is to estimate the potential global performance of the IM-based DSA algorithms as well as to develop and analyze decentralized algorithms for selection of the decision matrix \mathbf{D} that with high probability achieve reasonably fast convergence to acceptable steady-state global performance (8.3).

It is worth emphasizing that the considered system configuration is relevant for both vertical (primary and secondary users) and horizontal (no primary users) CR spectrum sharing approaches.

Particularly, in the vertical CR case illustrated in Fig. 8.3 (Fig. 1.2 in Section 1), we can assume that a set of F bands available for secondary users is defined by a spectrum sensing system. If some primary users change their bands, then the sensing outcome for secondary users can be interpreted as random change of all propagation channels in some bands. Efficiency of the developed solutions in such a dynamic CR environment is illustrated in Section 8.7.3 for Poisson model of band changes.

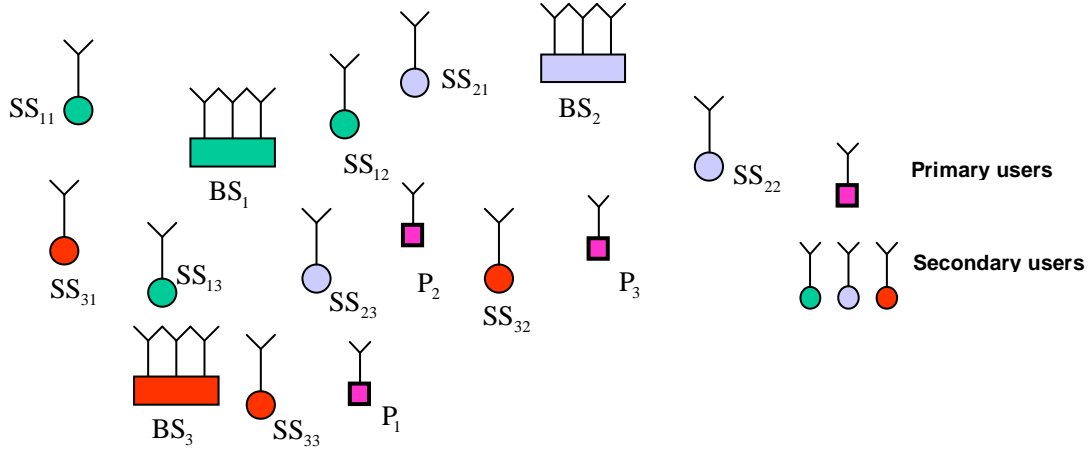


Figure 8.3. System model for vertical CR scenario

8.2 Potential performance of IM-based DSA

Potential global performance of the system defined in Section 8.1 is analyzed hereafter for interference limited scenario with Gaussian channels (8.6) and $\sigma_h^2 = 1$ [Abr09]. This assumption allows us to derive analytical bounds for the global performance that can be used for assessment of decentralized algorithms in the challenging scenario with strong interference that must be mitigated by an antenna array in order to enable reliable signal reception. Particular realistic propagation conditions with variable σ_h^2 for different users are analyzed in Section 8.7.2.

Let us recall that the performance of the best possible frequency allocation is specified as the potential global performance. With M users at each BS and F available bands, there are A_M^F different options how M users could be allocated over F bands at a given BS. Since there are N such BSs, the total number of all different allocations is $(A_M^F)^N$, where $A_M^F = \frac{F!}{(F-M)!}$. Strictly

speaking, we have to search the best allocation among all $(A_M^F)^N$ of them. We actually consider such an exhaustive search while conducting direct Monte-Carlo simulations to support our analytical derivations.

Now, our goal is to derive statistical characteristics of the best allocation. From statistical point of view, it is quit evident that this search may be performed over a limited subset of all options. Indeed, the set of all options includes even the ones where some frequencies are used by all BSs and some of them are free. Obviously, the probability of these allocations being the best ones in terms of criterion (8.3) is negligible. In fact, statistically, at least for channels described in (8.6), it is straightforward to demonstrate that SINR degrades with the increased number of interferences. Therefore, we have to consider search only among allocations, where the number of maximal users

per bound is minimal. To achieve this, we need to distribute all NM sources over F available bands in the most even way, so that the maximal number of SSs per band is equal to

$$N_0 = \left\lceil \frac{NM}{F} \right\rceil, \quad (8.7)$$

where $\lceil \cdot \rceil$ is the least integer ("ceiling") function.

Obviously, the total number of BSs that have to operate with N_0 users in one band is equal to

$$N_1 = MN - F(N_0 - 1). \quad (8.8)$$

The number of different allocations of N_0 users of different BSs among totally N BSs is equal to

$C_{N_0}^N$, where $C_{N_0}^N = \frac{A_{N_0}^N}{N_0!}$. For each such situation, particular users from each involved BS may be selected in M^{N_0} different ways, and then be allocated to one of F available bands. Therefore, the total number of all different allocations of N_0 users per band is equal to

$$L = FC_{N_0}^N M^{N_0}. \quad (8.9)$$

Generally, these L different allocations could not be treated as statistically independent since some subsets of them may be repeated. In the following statistical analysis, we ignore this dependence and treat (8.9) as the number of independent allocations leading to optimistic nature of our statistical bounds.

We estimate the performance of the best allocation over L independent options of N_1 simultaneously activated bands with N_0 signals per band, ignoring all other $NM - N_0N_1$ users that could be evenly distributed over remaining bands with at most $N_0 - 1$ users per band. By doing this, we ignore a tiny probability that the best allocation of $N_0 - 1$ sources could give lower SINR than the best allocation of N_0 sources per band.

To find the SINR pdf, we need to address two critically different situations, depending on the available number of antennas:

$$K \geq N_0, \quad (8.10)$$

$$K < N_0. \quad (8.11)$$

In the first case of $K \geq N_0$, an antenna array at any BS is capable of complete co-channel interference suppression and SINR maximization searches for such an option, where for the weakest user, the $N_0 - 1$ interferer propagation channels are most "orthogonal" to the propagation channel of the useful signal. Therefore, interference mitigation in this case is associated with the least possible signal-to-noise (SNR) degradation.

In the second situation of $K < N_0$, the SINR maximization is searching for the case where the $N_0 - 1$ interference channels span a smaller subspace that do not contain the channel of the useful signal, to make spatial processing efficient and leading to maximization of the lowest SINR over $N_0 N_1$ users.

It is clear that for $K \gg N_0$ and $K \ll N_0$ the situation is back to the best diversity and least total interference power selection respectively, while the most challenging scenario is with

$$K \approx N_0. \quad (8.12)$$

For this reason, let us address the two regimes (8.10) and (8.11) separately, focusing on scenario (8.12).

8.2.1 SINR pdf for $K \geq N_0$

Let us simplify the notations for the interference-plus-noise covariance matrix and SINR ν in the considered case of $N_0 - 1$ co-channel interferences with the propagation channels $\mathbf{H}_{N_0-1} = [\mathbf{h}_1, \dots, \mathbf{h}_{N_0-1}]$:

$$\mathbf{R} = \sigma_{\text{int}}^2 \sum_{j=1}^{N_0-1} \mathbf{h}_j \mathbf{h}_j^* + \sigma^2 \mathbf{I}_K, \quad (8.13)$$

$$\nu = \mu_s \mathbf{h}_0^* \left(\mathbf{I}_K + \mu_{\text{int}} \sum_{j=1}^{N_0-1} \mathbf{h}_j \mathbf{h}_j^* \right) \mathbf{h}_0, \quad (8.14)$$

where \mathbf{h}_0 is the propagation channel of the desired signal, $\mu_s = \sigma_s^2 / \sigma^2$ and $\mu_{\text{int}} = \sigma_{\text{int}}^2 / \sigma^2$ are the SNR and interference-to-noise (INR) ratios, and $\mathbf{h}_0, \mathbf{h}_1, \dots, \mathbf{h}_{N_0-1} \sim CN_{K, N_0}(0, \mathbf{I}_K)$ is a set of independent Gaussian vectors.

According to the matrix inversion lemma [Gol96], the SINR (8.14) can be expressed as

$$\begin{aligned} \nu &= \mu_s \mathbf{h}_0^* \left(\mathbf{I}_K + \mu_{\text{int}} \mathbf{H}_{N_0-1} \mathbf{H}_{N_0-1}^* \right)^{-1} \mathbf{h}_0 = \\ &= \mu_s \mathbf{h}_0^* [\mathbf{I}_K - \mathbf{H}_{N_0-1} (\mathbf{H}_{N_0-1}^* \mathbf{H}_{N_0-1} + \mu_{\text{int}}^{-1} \mathbf{I}_{N_0-1})^{-1} \mathbf{H}_{N_0-1}^*] \mathbf{h}_0 \approx \\ &\approx \mu_s \mathbf{h}_0^* [\mathbf{I}_K - \mathbf{H}_{N_0-1} (\mathbf{H}_{N_0-1}^* \mathbf{H}_{N_0-1})^{-1} \mathbf{H}_{N_0-1}^*] \mathbf{h}_0 \end{aligned} \quad (8.15)$$

for $\mu_{\text{int}} \gg 1$.

The normalized SINR $\nu_0 = \mu_s^{-1} \nu$ is distributed according to the X^2 law with $2(K - N_0 + 1)$ degrees of freedom [Fos98]. Taking into account that if $a_i > \alpha$ and $b_i < \alpha$ for all $i \in I$ then $\min_{i \in I} a_i > \alpha$ and

$\max_{i \in 1} b_i < \alpha$, the probability that maximum over L independent situations of the minimum SINR over $N_1 N_0$ users is below α , is equal to

$$\text{Prob}\left(\max_L \min_{N_0 N_1} \text{SINR} < \alpha\right) = \left[1 - P_1\left(\frac{\alpha}{\mu_s}, N_0\right)\right]^{N_0 N_1 L}. \quad (8.16)$$

According to [Gra94], we obtain

$$P_1\left(\frac{\alpha}{\mu_s}, N_0\right) = \frac{1}{\Gamma(K - N_0 + 1)} \int_{\frac{\alpha}{\mu_s}}^{\infty} y^{(K - N_0)} e^{-y} dy = e^{-\frac{\alpha}{\mu_s}} \sum_{j=0}^{K - N_0} \frac{1}{j!} \left(\frac{\alpha}{\mu_s}\right)^j, \quad (8.17)$$

where X^2 distribution $w(y) = \Gamma(K - N_0 - 1)^{-1} y^{K - N_0} e^{-y}$ is used, and $\Gamma(a)$ is the gamma function.

For $K = N_0$, we get

$$\text{Prob}\left(\max_L \min_{N_0 N_1} \text{SINR} < \alpha\right) = \left(1 - e^{-N_1 K \frac{\alpha}{\mu_s}}\right)^L. \quad (8.18)$$

Another “no interference” bound can be derived similarly to (8.16) assuming that subsystems do not interfere to each other. In this case, the global performance corresponds to the minimum over N subsystems of the maximum of the minimum SNR for each of them:

$$\text{Prob}\left(\min_N \max_{A_F^M} \min_M \text{SINR} < \alpha\right) = 1 - \left\{1 - \left[1 - P_1\left(\frac{\alpha}{\mu_s}, 1\right)^M\right]^{A_F^M}\right\}^N, \quad (8.19)$$

where $N_0 = 1$ active user in a band is taken into account in (8.17). Comparison of bounds (8.18) and (8.19) that correspond to the extreme interference levels in the system can be useful in the considered case of $K \geq N_0$. Furthermore, “no interference” performance can be especially important because it can be estimated locally for each subsystem for arbitrary σ_h^2 as exploited in Section 8.7.2 for on-line selection of the QoS thresholds.

8.2.2 SINR pdf for $K < N_0$

Here, the main difference compared to Section 8.2.1 is that the interference cannot be suppressed completely because of lack of degrees of freedom. Taking into account that $\mu_{\text{int}} \gg 1$, we assume that the noise effect is negligible in this case. So, (8.14) can be approximated as

$$\nu = \mu \mathbf{h}_0^* \left(\sum_{j=1}^{N_0-1} \mathbf{h}_j \mathbf{h}_j^* \right) \mathbf{h}_0, \quad (8.20)$$

where $\mu = \sigma_s^2 / \sigma_{\text{int}}^2$ is the input signal-to-interference ratio. Then, according to [Ree74], we get the following SINR distribution in the case of $\mathbf{h}_0, \mathbf{h}_1, \dots, \mathbf{h}_{N_0-1} \sim CN_{K, N_0}(0, \mathbf{I}_K)$:

$$w(y) = \frac{1}{B(K, N_0 - K)} y^{K-1} (1+y)^{-N_0}, \quad (8.21)$$

where $B(a, b)$ is the beta function [Gra94]. Therefore,

$$\begin{aligned} P_1\left(\frac{\alpha}{\mu}, N_0\right) &= \frac{1}{B(K, N_0 - K)} \int_{\frac{\alpha}{\mu}}^{\infty} y^{K-1} (1+y)^{-N_0} dy = \\ &= \frac{\left(\frac{\alpha}{\mu}\right)^{K-1}}{(N_0 - K)B(K, N_0 - K)} F\left(N_0, N_0 - K; N_0 - K + 1; -\frac{\mu}{\alpha}\right) = \\ &= \frac{\left(\frac{\alpha}{\mu}\right)^{K-1}}{(N_0 - K)B(K, N_0 - K) \left(1 + \frac{\alpha}{\mu}\right)^{N_0-1}} F\left(-K + 1, 1; N_0 - K + 1; -\frac{\mu}{\alpha}\right), \end{aligned} \quad (8.22)$$

where $F(a, b; c; z)$ is the hypergeometric function [Gra94].

Then, the global bounds can be found similar to (8.16), (8.18). Particularly, in the most interesting case $N_0 = K + 1$, we obtain

$$P_1\left(\frac{\alpha}{\mu}, K + 1\right) = \frac{\left(\frac{\alpha}{\mu}\right)^{K-1}}{B(K, N_0 - K) \left(1 + \frac{\alpha}{\mu}\right)^K} F\left(-K + 1, 1; 2 - \frac{\alpha}{\mu}\right) = 1 - \left(\frac{\frac{\alpha}{\mu}}{1 + \frac{\alpha}{\mu}}\right)^K,$$

and hence

$$\text{Prob}\left(\max_L \min_{N_0 N_1} \text{SINR} < \alpha\right) = \left\{ 1 - \left[1 - \left(\frac{\frac{\alpha}{\mu}}{1 + \frac{\alpha}{\mu}} \right)^K \right]^{N_1(K+1)} \right\}^L. \quad (8.23)$$

Now, the derived expressions together with the parameters defined in (8.7) - (8.9) can be used as the performance bounds for a given system configuration. Let us illustrate them in the following example of the system specified in Section 8.1: $N = 5$, $M = 2$, $F = 3$, $Q = M$, and $\sigma^2 = 0.01$. According to (8.7) - (8.9), we find $N_0 = 4$, $N_1 = 1$ and $L = 240$ in this case. The upper bounds together with the global performance found by means of exhaustive search among all $(A_M^F)^N = 7776$ solutions in this case are plotted in Fig. 8.4 for $K = 4$ and $K = 3$ using (8.18) and (8.23), respectively. The actual global performance is estimated over 200 trials for independent channel realizations. For comparison, performance for independent random allocations of the bands is presented in Fig. 8.4 as well. The bound for random allocation is calculated as follows:

$$\text{Prob}\left(\min \text{SINR} < \alpha\right) = (A_M^F)^{-N} \sum_{j=1}^J L_j \beta_j(\alpha), \quad (8.24)$$

where J is the number of variants of different band occupancy, e.g., in the considered case $J = 5$ for $[4,3,3]$, i.e., 1 band is occupied by 4 users and 3 users are active in each of 2 other bands, $[4,4,2]$, $[5,3,2]$, $[5,4,1]$, and $[5,5,1]$, L_j is the number of scenarios for the j th variant, which can be found similarly to (8.9), $\beta_j(\alpha)$ can be derived from (8.17) and (8.22) for $L = 1$ corresponding to each variant of band occupancy.

One can see that both bounds are close to the estimated performance in Fig. 8.4. As mentioned above, the main reason for some mismatch for the global bound is that not all of L different solutions with $N_0 = 4$ are independent and only a subset of all possible solutions corresponding to the bands with N_0 activated SSs, is taken into account.

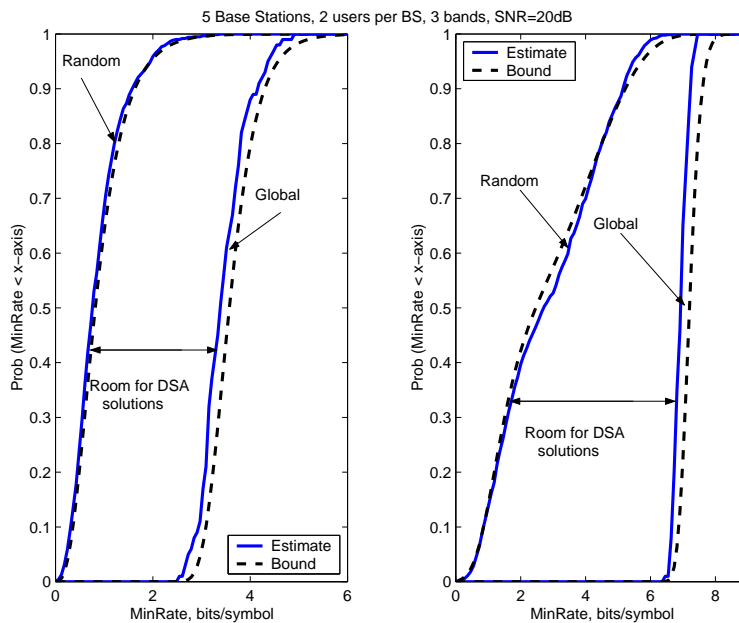


Figure 8.4. Global and random solutions for $N_0 = 4$: $K = 3$ (left) and $K = 4$ (right)

The global bounds for different system configurations and fixed $N_0 = 4$ are shown in Fig. 8.5 together with bounds (8.19) to compare with the virtual “no interference” case. One can see that all the bounds move to the right for higher-dimension systems because of the increased number of situations to select from. The difference between bounds (8.18) and (8.19) for $K = 4$ (approximately 2 times in SINR in Fig. 8.5) corresponds to the overall interference impact in the globally optimized system. Bounds (8.18), (8.19), and (8.23) represent the ultimate performance in the considered system that can be used for assessment of any practical coordinated as well as decentralized IM-based DSA algorithms.

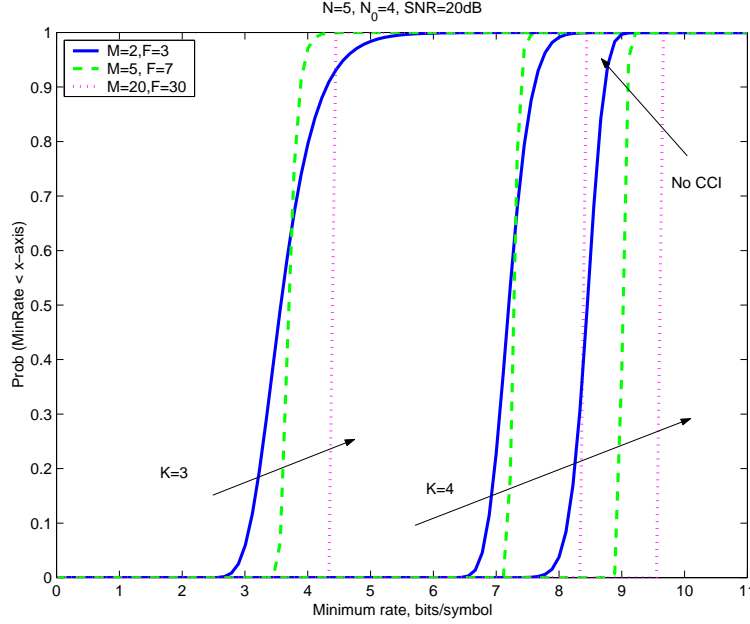


Figure 8.5. Global bounds for different system configurations and fixed $N_0 = 4$ for $K = 3$ and $K = 4$

8.3 IM-based DSA algorithms

8.3.1 “Selfish” IM-based DSA algorithm

A basic element of an IM-based DSA algorithm is a local search of the band assignment. In the considered system, a “selfish” search of \mathbf{d}_n can be based on local maximization of the minimum SINR independently for each BS_{*n*}:

$$\mathbf{d}_n = \arg \max_{m=1, \dots, M; f_m \in \Phi; f_m \neq f_q, q=1, \dots, M, q \neq m} \min_{f_m} \mathbf{h}_{f_m m n}^* \mathbf{R}_{f_m n}^{-1} \mathbf{h}_{f_m m n}, \quad (8.25)$$

where \mathbf{R}_{f_n} is defined in (8.5), $\mathbf{d}_n = [d_{n1}, \dots, d_{nM}]$ is the $1 \times M$ vector of different elements representing the n th row of the global allocation matrix \mathbf{D} , and $\Phi = 1, \dots, F$ is the set of all available bands. Local search (8.25) will be referred to as *maximum minimum* (MaxMin) search.

The exhaustive local search over A_M^F options required in (8.25) may be computationally very expensive even for moderate values of M and F . Simplified search algorithm can be applied at this stage to find suboptimal solutions, such as a maximum element search of d_{nm}

$$d_{nm} = \arg \max_{f \in \Phi; f \neq d_{n1}, \dots, d_{n(m-1)}} \min_{f \in \Phi; f \neq d_{n1}, \dots, d_{n(m-1)}} \mathbf{h}_{fmm}^* \mathbf{R}_{fn}^{-1} \mathbf{h}_{fmm} \quad (8.26)$$

for $m = 1, \dots, M$.

The “selfish” algorithm can be summarized for the n th subsystem as follows:

- Sensing interval

Step 1: Estimate \mathbf{R}_{fn} , $f = 1, \dots, F$;

Step 2: Find \mathbf{d}_n according to (8.25) or simplified search algorithms, e.g., (8.26), and assign bands \mathbf{d}_n to SS_{nm} , $m = 1, \dots, M$;

Step 3: Calculate the optimal Wiener spatial filters [Mon80] for interference suppression at the sensing BS

$$\mathbf{w}_{nm} = \frac{\mathbf{R}_{d_{nm}n}^{-1} \mathbf{h}_{d_{nm}n}}{\mathbf{h}_{d_{nm}n}^* \mathbf{R}_{d_{nm}n}^{-1} \mathbf{h}_{d_{nm}n}}, m = 1, \dots, M. \quad (8.27)$$

- Data interval

SS_{nm} , $m = 1, \dots, M$ transmit data in bands assigned in \mathbf{d}_n ;

BS_n receives data with the optimal weight vectors \mathbf{w}_{nm} , $m = 1, \dots, M$ for interference suppression.

Generally, convergence of decentralized algorithms to a stationary point can be guaranteed if some kind of “energy reciprocity” condition can be satisfied, which means that a local decision should improve not only local performance, but also not degrade performance of other nodes, as in the interference reducing network [Nee06]. This is not the case in the considered system, where activation of some band in one subsystem may significantly degrade performance of other subsystems, depending on propagation conditions. This means that, generally, there is no reason to expect good convergence properties or even convergence itself of the “selfish” algorithm in this case.

The main disadvantage of the “selfish” algorithm is that in pursuing the best results for its own BS, the interference environment of other BSs keeps changing, leading to poor convergence for the whole system. Furthermore, it does not allow any control of the convergence properties, such as a trade-off between convergence probability and convergence rate, and the global performance.

8.3.2 “Good Neighbor” threshold-regulated IM-based DSA algorithm

The main idea is to prevent selection of new bands at some BS if its SINR is already above some threshold γ_0 and minimize the number of new band allocations to achieve the given threshold [Kuz09-1]. This approach introduces two new features of IM-based DSA:

- Comparison with the performance threshold leading to threshold-regulated algorithms;
- Minimization of the number of new band allocations compared to the current ones.

Both these “good neighbor” features may reduce non-stationary interference in the network and improve convergence properties compared to the “selfish” algorithm. So, our objective is to introduce the “good neighbor” algorithms and study the effect of these features separately.

The search problem of \mathbf{d}_n can be formulated as follows:

$$\mathbf{d}_n = \arg \min_{m=1,\dots,M; f_m \in \Phi; f_m \neq f_q, q=1,\dots,M, q \neq m} \sum_{m=1}^M |\text{sign}(f_m - d_{nm}^{(0)})|, \quad (8.28)$$

subject to

$$\log_2(1 + \mathbf{h}_{f_n m n}^* \mathbf{R}_{f_n n}^{-1} \mathbf{h}_{f_n m n}) \geq \gamma_0, \quad (8.29)$$

where $d_{nm}^{(0)}$ is the m th element of the current band allocation vector $\mathbf{d}_n^{(0)}$ before the current sensing interval at BS _{n} and $\text{sign}(a) = \{-1, 0, 1\}$ is the sign function.

A search procedure in (8.28) will be referred to as *minimum switch* (MinSwitch) search.

Again, exhaustive search in (8.28), (8.29) may not be feasible. One possible simplification, based on a partial search over a subset of all possible allocations $[d_{nm}, m \in M_s]$ when the number of users with SINR below the threshold is low, is as follows [Kuz09-2]:

$$\mathbf{d}_n = \arg \min_{m \in M_s; f_m \in \Phi_s; f_m \neq f_q, q \in M_s, q \neq m} \sum_{m \in M_s} |\text{sign}(f_m - d_{nm}^{(0)})|, \quad (8.30)$$

subject to (8.29), where M_s is the set of users selected for search, which includes all users with SINR below the threshold, and Φ_s is the set of bands selected for search, which includes all the bands currently occupied by the users from M_s and, possibly, some of bands not currently occupied by the n th subsystem.

The “good neighbor” threshold-regulated algorithm can be specified by adding two more steps to the algorithm in Section 8.3.1 after Step 1 and modifying Step 2:

- Sensing interval

Step 1: Estimate \mathbf{R}_{f_n} , $f = 1, \dots, F$;

Step 1a: Calculate

$$\gamma_n = \log_2(1 + \min_{m=1, \dots, M} \mathbf{h}_{d_{nm}^{(0)} m m n}^* \mathbf{R}_{d_{nm}^{(0)} n}^{-1} \mathbf{h}_{d_{nm}^{(0)} m m n}); \quad (8.31)$$

Step 1b: If $\gamma_n \geq \gamma_0$, then go to the “Data interval” stage without updating \mathbf{d}_n and \mathbf{w}_{nm} ; otherwise, go to Step 2;

Step 2: Find \mathbf{d}_n according to (8.28), (8.29) or form sets \mathbf{M}_s and Φ_s , and apply simplified search according to (8.30), (8.29), then assign bands \mathbf{d}_n to \mathbf{SS}_{nm} ;

Step 3: Calculate the optimal weight vectors according to (8.27).

It is worth emphasizing that a threshold-regulated approach also can be implemented based on the MaxMin search, where the best local bands can be reallocated only if some of the user's SINRs fall below the threshold. However, even in this case, the MaxMin search may reallocate many or all the users even if only a few of them actually need that to satisfy the threshold. Thus, it is expected that the MinSwitch search may show better convergence, especially for high-dimension systems. The corresponding algorithm will be referred to as a “good neighbor” with MaxMin (GN-MaxMin) search.

It is clear that selection of the threshold γ_0 is critical for the “good neighbor” algorithms. The difficulty is that in the general propagation scenario with arbitrary σ_h^2 , one precalculated threshold may not be suitable for different subsystems. Our proposal is to use locally estimated “no interference” performance for on-line selection of the thresholds:

$$\gamma_{0n} = \alpha \max_{f_i \neq f_j \in \Phi} \min \sigma^{-2} \|\mathbf{h}_{f_m m m n}\|^2, \quad (8.32)$$

where $0 < \alpha < 1$ is a weight coefficient that controls convergence properties of the algorithm. This choice is based on expectation that for $K \geq N_0$ the interference limited and “no interference” performances are closely related as illustrated in Fig. 8.5.

8.4 Power control for IM-based DSA algorithms

Normally, in wireless systems, power control is required to reduce the overall interference. It is important to note that in the IM-based DSA case the situation may be very different for $K \geq N_0$. Indeed, if the interference can be cancelled by an antenna array ($K \geq N_0$), then the SINR at the output of the optimal spatial filter practically does not depend on the interference power in the interference-limited scenario as shown in (8.15). This means that power control can be performed at each \mathbf{BS}_n for its local users \mathbf{SS}_{nm} , $m=1, \dots, M$ practically without affecting other subsystems [Kuz09-2].

Some options for the local power control could be as follows:

- “Water filling” power control to improve the weakest local link for the given power constraint:

$$q_{nm}^2 = Q \frac{\frac{1}{\text{SINR}_{nm}}}{\sum_{l=1}^M \frac{1}{\text{SINR}_{nl}}}, m=1, \dots, M, \quad (8.33)$$

where $Q = \sum_{m=1}^M q_{nm}^2$ is the total constrained power and SINR_{nm} is defined in (8.2).

- Power saving control to increase battery life for SS_{nm} , e.g., for the threshold-regulated algorithms:

$$q_{nm}^2 = \frac{2^{\gamma_0-1}}{\text{SINR}_{nm}}, m=1, \dots, M. \quad (8.34)$$

- The required QoS based power control, for example, to provide some users, e.g., SS_{n1} with the target $\text{SINR}_{\text{targ}}$ if it is possible with $q_{n1}^2 \leq \varsigma Q$, $0 < \varsigma < 1$:

$$q_{n1}^2 = \begin{cases} \bar{q}_{n1}^2 & \text{if } \bar{q}_{n1}^2 < \varsigma Q \\ \varsigma Q & \text{if } \bar{q}_{n1}^2 \geq \varsigma Q \end{cases}, \quad (8.35)$$

$$q_{nm}^2 = (Q - q_{n1}^2) \frac{\frac{1}{\text{SINR}_{nm}}}{\sum_{l=1}^M \frac{1}{\text{SINR}_{nl}}}, m=2, \dots, M, \quad (8.36)$$

$$\text{where } \bar{q}_{n1}^2 = \frac{\text{SINR}_{\text{targ}}}{\text{SINR}_{n1}}.$$

Clearly, in (8.34)-(8.36) γ_0 can be replaced with γ_{0n} defined in (8.32) in the general case of arbitrary σ_h^2 .

It is worth emphasizing that the presented power control approach for IM-based DSA is not directly applicable in the $K < N_0$ case because interference power significantly affects SINR if interference cannot be effectively suppressed by an antenna array. Other power control techniques are required in this case, which could be a subject for future work.

8.5 Using absorbing Markov chains for analysis of the IM-based DSA algorithms

Qualitative reasoning presented in Section 8.4 suggests that the proposed “good neighbor” IM-based DSA algorithms should significantly outperform the “selfish” solution. Now, our goal is to verify that by means of analysis of the performance of the decentralized IM-based DSA algorithms for given stationary propagation channels. The theory of Markov chains, e.g., [Kem66], provides us with a tool to do this.

8.5.1 Markov chain model for IM-based DSA

To formulate a Markov model we assume that all possible $I = (A_M^F)^N$ different allocation matrices \mathbf{D}_i , $i = 1, \dots, I$ form states of the Markov chain. For a given state \mathbf{D}_i , sensing of the n th subsystem transfers the system to state \mathbf{D}_{j_n} depending on the given channel realization and DSA algorithm, where $j_n \in [1, I]$, including $j_n = i$. Repeating this procedure for $n = 1, \dots, N$, a set of \mathbf{D}_{j_n} can be found, where not all j_n may be different. It is worth emphasizing that for the stationary channels and known local second-order statistics as assumed in Section 8.1, each \mathbf{D}_i can be transformed to the unique state \mathbf{D}_{j_n} as the sensing outcome at the n th subsystem. This means that each \mathbf{D}_i cannot be transformed to more than N different states.

Assuming that, at each sensing interval, one randomly selected subsystem is sensed with probability $p_{\text{sens}} = N^{-1}$, the nonzero elements of the $I \times I$ transition probability matrix \mathbf{P} can be defined as follows:

$$p_{ij} = g_j p_{\text{sens}}, i = 1, \dots, I, j \in \Omega, \quad (8.37)$$

where $1 \leq g_j \leq N$ is the number of outcomes of sensing trials from the i th state at BS_n , $n = 1, \dots, N$, leading to $\mathbf{D}_{j_n} = \mathbf{D}_j$, Ω is a set of $J \leq N$ state indexes corresponding to the number of different sensing outcomes \mathbf{D}_j , and $\sum_{j \in \Omega} g_j = N$. If sensing at each of N subsystems leads to different states for the given initial state, then all the corresponding states get equal probabilities p_{sens} . If some of the sensing trials lead to the same outcome, then this state gets increased probability according to (8.37). For example, if for $N = 5$, sensing at BS_2 , BS_3 , and BS_5 leads to the same state for the i th initial state, e.g., $j_2 = j_3 = j_5$, and sensing at BS_1 and BS_4 gives other outcomes j_1 and j_4 , then $g_{j_1} = g_{j_4} = 1$ and $g_{j_2} = 3$ leading to $J = 3$ nonzero elements in the i th row: $p_{ij_1} = p_{ij_4} = 0.2$, and $p_{ij_2} = 0.6$.

The transition probability matrix \mathbf{P} is a sparse $I \times I$ stochastic matrix with maximum N nonzero elements in a row, such that $\sum_{j=1}^I p_{ij} = 1$ for $i = 1, \dots, I$, which completely defines the Markov model of the considered system.

Certainly, application of Markov analysis is possible only for reasonably small values of M , F , and N . Nevertheless, analytical study can give us useful information on the algorithm properties that could be further investigated by means of simulations in more complicated scenarios as in Section 8.7.

The Markov theory, e.g., [Kem66], provides us with analytical expressions for the convergence probabilities and rates for an absorbing Markov chain, which has at least one absorbing point with transition probability $p_{ii} = 1$, and all other states are transient with non-zero probabilities to transit to one of the absorbing points not necessarily in one step. One difficulty is that in the general case, the Markov chain may contain ergodic subchains with states that can transit only within corresponding subchains. Obviously, in the considered application of Markov theory, situations with no absorbing states and/or with ergodic subchains lead to a non-zero probability of undesirable non-convergent network behavior.

To apply the theory of absorbing Markov chains to our problem, we need the following:

- calculate a transition probability matrix;
- classify all the states into three groups: transient, absorbing, and ergodic;
- estimate the global performance for the absorbing states;
- if ergodic subchains are found, then transform the initial Markov chain to the reduced size absorbing Markov chain by means of replacing the ergodic subchains with the corresponding absorbing states;
- calculate probabilities of absorption by the absorbing states (desirable behavior) and ergodic subchains (undesirable non-convergent behavior), and calculate average convergence rate rates for all possible initial states.

Classification of the states can be based a Boolean representation $\tilde{\mathbf{P}}$ of the transition matrix \mathbf{P} with elements

$$\tilde{p}_{ij} = \begin{cases} 1 & \text{if } p_{ij} > 0 \\ 0 & \text{if } p_{ij} = 0 \end{cases}, \quad (8.38)$$

with iterative application of the following four rules [Fox68]:

- (a) State is absorbing if and only if $\tilde{p}_{ii} = 1$ and $\tilde{p}_{ij} = 0$ for all $i \neq j$;
- (b) If State j is absorbing and $\tilde{p}_{ij} = 1$, then State i is transient;
- (c) If State j is transient and $\tilde{p}_{kj} = 1$, then State k is also transient;
- (d) If State i communicates with State j and State j communicates with State k , then State i communicates with State k .

The classification algorithm [Fox68] searches for sets of communicating states and replaces them by their respective unions, reducing the dimension of the initial matrix $\tilde{\mathbf{P}}$. Ergodic subchains are identified when a set of communicating states collapses into an absorbing state.

When all the states are classified, then the absorbing Markov chain with the $(I_t + I_a) \times (I_t + I_a)$ transient probability matrix \mathbf{P}_a can be formed by means of replacing all the ergodic subchains, if

they exist, with absorbing states, where $I_a > 0$ is the number of absorbing states including the actual ones and the collapsed ergodic subchains if they exist, I_t is the number of transient states, and $I_t + I_a \leq I$.

For a given \mathbf{P}_a , the probabilities of convergence to the corresponding absorbing states can be found as follows [Kem66]:

$$\mathbf{E} = \mathbf{CB}, \quad (8.39)$$

where \mathbf{E} is the $I_t \times I_a$ matrix of convergence probabilities from each transient state to each absorbing point, \mathbf{A} and \mathbf{B} are the $I_t \times I_t$ and $I_t \times I_a$ components of the canonical form $\bar{\mathbf{P}}_a$ of the transition probability matrix

$$\bar{\mathbf{P}}_a = \begin{bmatrix} \mathbf{A} & \mathbf{B} \\ \mathbf{0} & \mathbf{I}_{I_a} \end{bmatrix}, \quad (8.40)$$

and $\mathbf{C} = (\mathbf{I}_{I_t} - \mathbf{A})^{-1}$ is the $I_t \times I_t$ fundamental matrix of $\bar{\mathbf{P}}_a$.

The average number of iterations (sensing intervals in our case) before absorption is

$$\mathbf{t} = \mathbf{C}\mathbf{1}, \quad (8.41)$$

where \mathbf{t} is the $I_t \times 1$ vector of the average number of iterations before absorption from each initial transient state, and $\mathbf{1}$ is a $I_t \times 1$ vector of all ones.

8.5.2 Analysis of low-dimensional DSA networks

Now, for the given system configuration and propagation channels, we can analyze the steady-state and convergence performance of the algorithms presented in Sections 8.3.1 and 8.3.2. Similarly to Section 8.2, we present the results for $N = 5$, $M = 2$, $F = 3$, $K = 4$, and $\sigma^2 = 0.01$.

Fig. 8.6 illustrates distribution of non-zero elements of the canonical forms of the transition matrices for the “selfish” and threshold-regulated algorithms based on exhaustive local search. No ergodic subchains were found in this example. One can see that introduction of the threshold dramatically increases the number of absorption points, as expected.

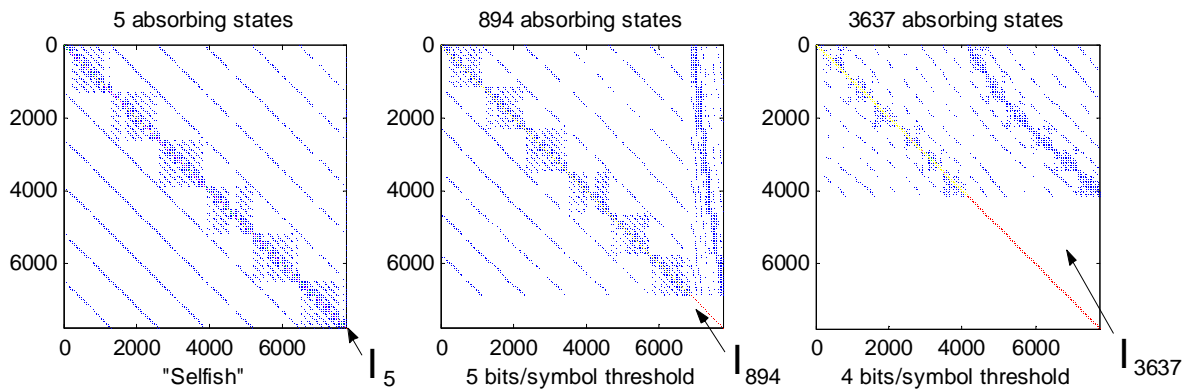


Figure 8.6. Examples of transition probability matrices
for $N = 5$, $M = 2$, $F = 3$, $K = 4$, and $\sigma^2 = 0.01$

The probabilities p_e of absorption by ergodic subchains (non-convergence) from all possible initial states averaged over 200 channel realizations are presented in Table 8.1 together with probabilities p_{na} to find a chain with no absorbing points for the “selfish” MaxMin-based algorithm and the “good neighbor” threshold-regulated MinSwitch solution.

Table 8.1. Probability of undesirable non-convergent behavior

Performance	“Selfish”	“Good neighbor” - MinSwitch	
		5 bits/symbol	4 bits/symbol
p_{na}	2.5%	0%	0%
p_e	4.1%	0.15%	0.002%

Tabl. 8.1 presents the overall results on the non-convergent network behavior. Particular parameters of the ergodic subchains found in 200 channel realizations are summarized in Tables 8.2 and 8.3.

Table 8.2. Percentage of channel realizations for the given number of found ergodic subchains

Number of ergodic subchains	0	1	2
“Selfish”	94.5%	5.5%	0%
“Good neighbor” – MinSwitch 5 bits/symbol threshold	82.5%	14%	3.5%

Table 8.3. Percentage of channel realizations for the given length of found ergodic subchains

Length of ergodic subchain	4	6	7	1229	1555	1989	2032	2061
“Selfish”	37%	9%	9%	9%	9%	9%	9%	9%
“Good neighbor” – MinSwitch 5 bits/symbol threshold	97.6%	2.4%	0%	0%	0%	0%	0%	0%

The cumulative distributed functions (CDF) of the number of absorption states, convergence rate, and global performance for the absorption states are presented in Fig. 8.7 – 8.9.

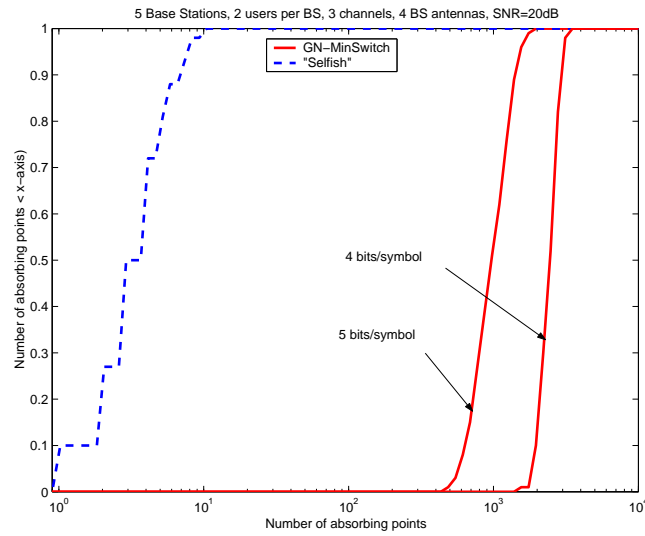


Figure 8.7. Number of absorbing states

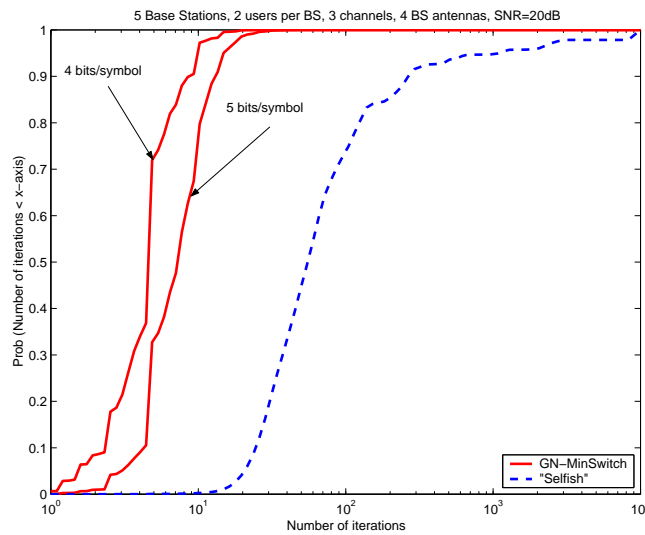


Figure 8.8. Average number of sensing intervals before absorption

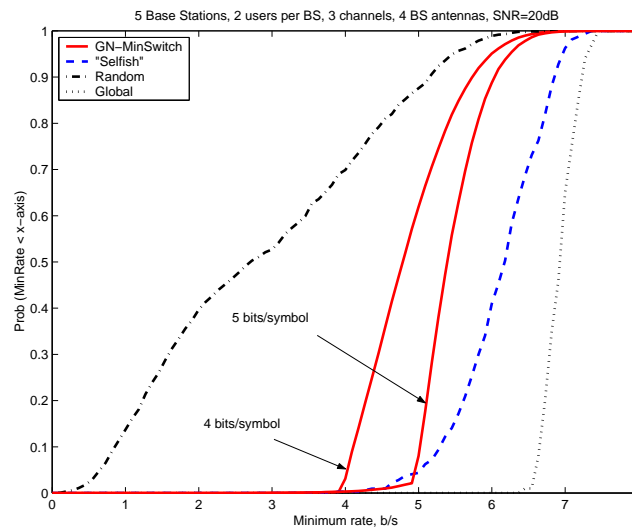


Figure 8.9. Global steady-state performance

The following observations can be made from the presented results:

- The probability of non-convergence can be controlled by selection of the threshold. Particularly, the results in Table 8.1 show that it can be reduced from 4% in the “selfish” case by more than 1000 times for the 4 bits/symbol threshold. The price is the controllable degradation of the steady-state performance by approximately 1.5 bits/symbol, as presented in Fig. 8.9.
- The results in Tables 8.2 and 8.3 show that although ergodic subchains may appear in both “selfish” and “good neighbor” networks, they are very different in terms of their length. Particularly, only short ergodic subchains of 4 and 6 states were found in the “good neighbor case”. On the contrary, almost 50% of chains detected in the “selfish” case were longer than 1000 states.
- The number of absorbing points grows significantly with introduction of the threshold, compared to the “selfish” solution. In Fig. 8.7, one can see that it grows from an average of 5 to 1000 points for the 5 bits/symbol threshold. Furthermore, in more than 2% of channel realizations, no absorbing points were found in the “selfish” case. That never happened for the threshold-regulated algorithms.
- The most important observation is that threshold selection allows significant improvement of the convergence rate. Particularly, in Fig. 8.8, one can see that the “selfish” solution required more than 100 iterations in 30% of trials. Some channel realizations demonstrated very slow convergence with 1000 or more required iterations. In the “good neighbor” threshold-regulated case, the average number of iterations was around 5 with a maximum of 30 iterations for the 5 bits/symbol threshold.

Similar results were obtained for the same system configuration with $K = 3$ for a lower level of global performance, as expected from the analysis in Section 8.2. The main difference is that a much lower number of absorbing points and slower convergence were observed in the $K = 3$ case compared with 4 BS antennas for thresholds selected at the same relative distance from the optimal

global performance. Fig. 8.10 presents a comparison of the number of absorbing points and convergence rates for 3 and 4 BS antennas for thresholds at 60% of the global performance shown in Fig. 8.4: 4 bits/symbol for $K = 4$ and 2 bits/symbol for $K = 3$. One can see that for a similar relative performance, the $K = 3$ case shows approximately 10 times fewer absorbing points and at least twice longer convergence compared with the case of 4 BS antennas. A possible explanation of this behavior is that if the number of antennas is not enough to cancel all interference components, then the number of good solutions should be much lower because they require a reduced dimension of the interference subspace additionally to avoiding colinearity between propagation channels of the desired signal and interference. This makes decentralized algorithms less efficient compared to the case of complete interference suppression. One can expect that this situation may be even more complicated for higher dimension systems.

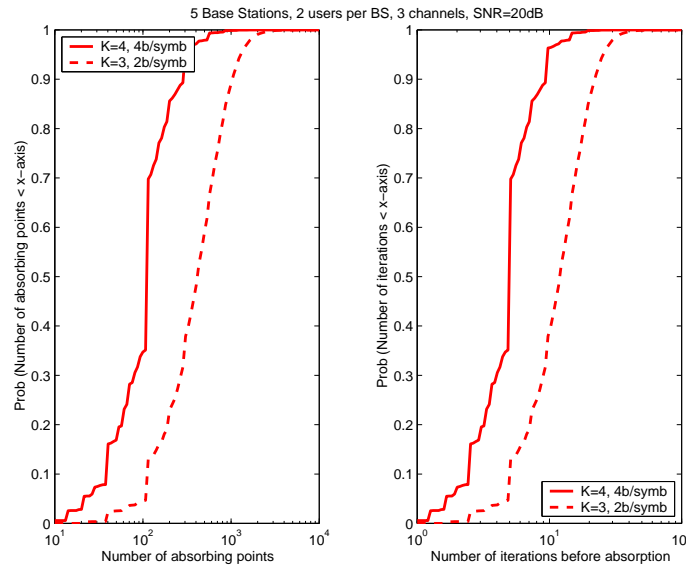


Figure 8.10. Comparison of the number of absorbing points (left) and convergence rate (right) for thresholds at 60% of the global performance: 4 bits/symbol for $K = 4$ and 2 bits/symbol for $K = 3$

Overall, the presented Markov chain analysis illustrates the desirable properties of the introduced “good neighbor” threshold-regulated IM-based DSA algorithms. More complicated system configurations will be studied in Section 8.7 by means of simulations.

It is worth emphasizing that the presented results are analytical for the given channel realizations. Particularly, the non-convergence results in Tables 8.1 - 8.3 practically cannot be obtained by means of simulations because of difficulty to distinguish between non-convergence and slow convergence behavior.

8.5.3 Possibilities to reduce non-convergence probability

The results in Section 8.5.2 demonstrate that the probability of undesirable non-convergent behavior can be reduced by means of reduction of the threshold in the “good neighbor” algorithm. Obviously, some degradation of the steady-state performance should be paid for that as shown in Fig. 8.9. Furthermore, the analysis in Section 8.5.2 shows that in the “good neighbor” networks we have a low probability to meet only a few very short ergodic subchains for a given channel realization with a high number of absorbing points. This situation suggests that modified “good

neighbor” algorithms that allow some variations of the regular operation during a transient stage could escape from such short ergodic subchains.

One interesting option for such a variation could be to allow rare MaxMin steps instead of the MinSwitch ones. Assuming that at each sensing interval the MaxMin search is applied with probability $p_r \ll 1$ and the MinSwitch search is selected with probability $1 - p_r$, the randomized GN-MinSwitch algorithm can be formulated as follows:

- Sensing interval

Step 1: Estimate \mathbf{R}_{f_n} , $f = 1, \dots, F$.

Step 1a: Calculate γ_n according to (8.31).

Step 1b: If $\gamma_n \geq \gamma_0$, then go to the “Data interval” stage without updating \mathbf{d}_n and \mathbf{w}_{nm} ; otherwise, go to Step 2.

Step 2a: Generate a random value a uniformly distributed in $[0,1]$.

Step 2b: If $a > p_r$, then find \mathbf{d}_n according to (8.28), (8.29) or form sets \mathbf{M}_s and Φ_s , and apply simplified search according to (8.30), (8.29), otherwise find \mathbf{d}_n according to (8.25) or simplified search algorithms, e.g., (8.26), then assign bands \mathbf{d}_n to \mathbf{SS}_{nm} .

Step 3: Calculate the optimal weight vectors according to (8.27).

- Data interval

\mathbf{SS}_{nm} , $m = 1, \dots, M$ transmit data in bands assigned in \mathbf{d}_n .

\mathbf{BS}_n receives data with the optimal weight vectors \mathbf{w}_{nm} , $m = 1, \dots, M$ for interference suppression.

The Markov chain analysis can be applied to the randomized GN-MinSwitch algorithm similarly to Section 8.5.2. Particularly, the nonzero elements of the transition probability matrix \mathbf{P} can be calculated similarly to (8.37) as follows:

$$p_{ij} = [g_j p_{\text{sens}} (1 - p_r), j \in \Omega_{\text{MinSwitch}}] + [\tilde{g}_j p_{\text{sens}} p_r, j \in \Omega_{\text{MaxMin}}], i = 1, \dots, I, j \in \Omega_{\text{MinSwitch}} \cup \Omega_{\text{MaxMin}}, \quad (8.42)$$

where $1 \leq g_j \leq N$ is the number of MinSwitch search outcomes from the i th state at \mathbf{BS}_n , $n = 1, \dots, N$, leading to $\mathbf{D}_{j_n} = \mathbf{D}_j$, $j \in \Omega_{\text{MinSwitch}}$, $\Omega_{\text{MinSwitch}}$ is a set of $J_{\text{MinSwitch}} \leq N$ state indexes corresponding to the number of different sensing outcomes \mathbf{D}_j , $1 \leq \tilde{g}_j \leq N$ is the number of MaxMin search outcomes from the i th state at \mathbf{BS}_n , $n = 1, \dots, N$, leading to $\mathbf{D}_{j_n} = \mathbf{D}_j$, $j \in \Omega_{\text{MaxMin}}$,

Ω_{MaxMin} is a set of $J_{\text{MaxMin}} \leq N$ state indexes corresponding to the number of different sensing outcomes \mathbf{D}_j , and $\sum_{j \in \Omega_{\text{MinSwitch}}} g_j = \sum_{j \in \Omega_{\text{MaxMin}}} \tilde{g}_j = N$.

The randomization consequence in this case is that some rows of the transition probability matrix \mathbf{P} may contain up to $2N$ nonzero elements depending on the sensing outcomes based on both MinSwitch and MaxMin search procedures compared to maximum N nonzero elements in a row in the basic GN-MinSwitch, GN-MaxMin, or “selfish” cases addressed in Section 8.5.2.

Two examples of matrix \mathbf{P} for both algorithms in different propagation conditions are shown in Figs. 8.11 and 8.12 where all nonzero elements are plotted in the same color. The example in Fig. 8.11 corresponds to the network with 1 ergodic subchain of 4 elements with high non-convergence probability of $p_e = 3\%$. The example in Fig. 8.12 corresponds to the simple case with no ergodic subchains. The observation is that the increased number of nonzero elements in \mathbf{P} allows removing the ergodic subchain in the first case and does not cause new undesirable subchains in both examples.

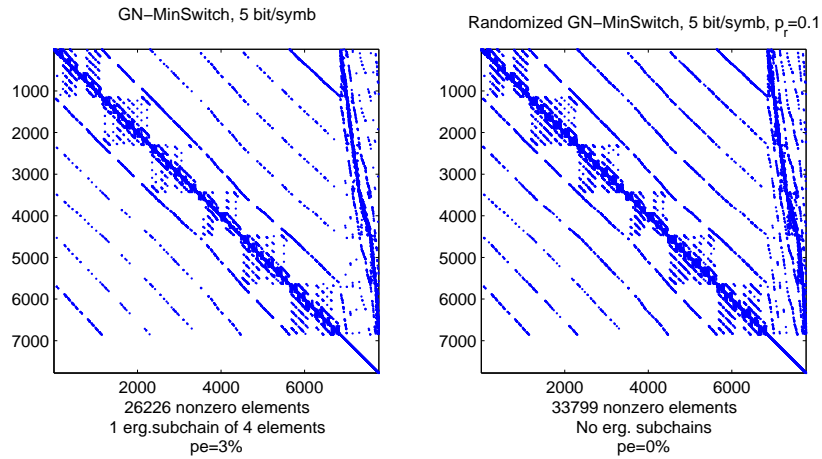


Figure 8.11. Transition probability matrices for the basic and randomized GN-MinSwitch algorithms for the network with 1 ergodic subchain of 4 elements

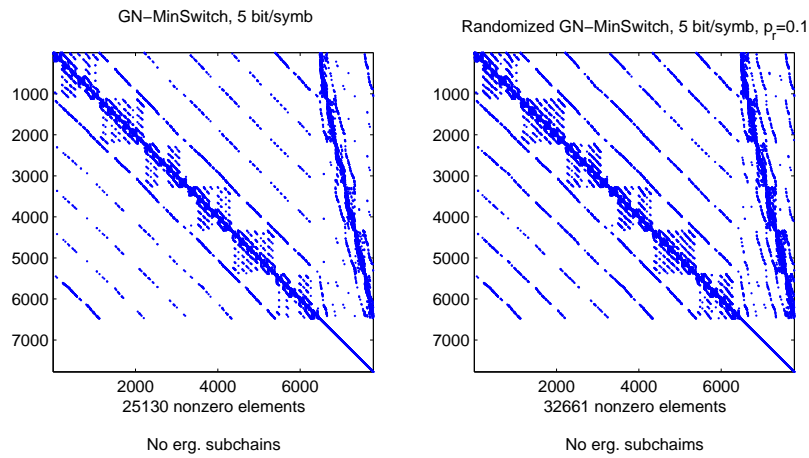


Figure 8.12. Transition probability matrices for the basic and randomized GN-MinSwitch algorithms for the network with no ergodic subchain

The results of the Markov chain analysis over 200 channel realization in the same scenario as in Table 8.1 for the 5 bits/symbol threshold are summarized in Table 8.4.

Table 8.4. GN-MinSwitch and randomized GN-MinSwitch comparison for $p_r = 0.1$ in the same scenario as in Table 8.1

Algorithm	Number of ergodic subchains found for 200 channel realizations	Non-convergence probability p_e
GN-MinSwitch	42	0.15%
Randomized GN-MinSwitch	7	0.04%

One can see from Table 8.4 that randomization significantly improves the convergence properties. Particularly, in the considered scenario, it reduces the number of ergodic subchains by 6 times and non-convergence probability by almost 4 times.

The price to be paid for this reduction of the non-convergence probability is some reduction of the convergence rate generally associated with the MaxMin search. Fig. 8.13 presents the convergence rates for all the initial states in the same scenario as in Fig. 8.11. One can see significant convergence rate degradation for some initial states in the case of randomized GN-MinSwitch. On the contrary, Fig. 8.14 shows that the convergence rates are practically the same for both solutions in the no ergodic subchain case corresponding to the scenario in Fig. 8.12.

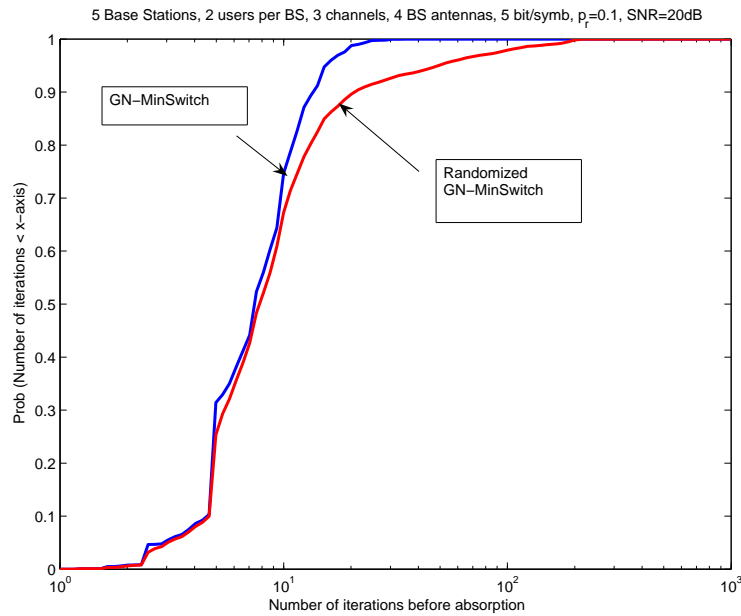


Figure 8.13. Convergence rate for different initial states in the same scenario as in Fig. 8.11

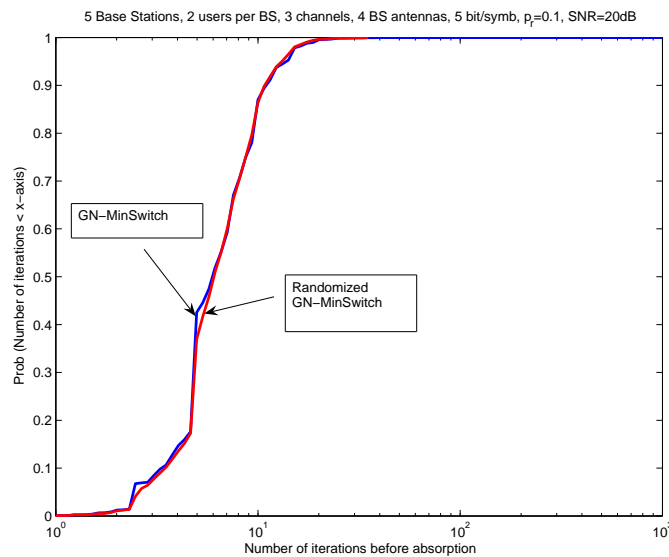


Figure 8.14. Convergence rate for different initial states in the same scenario as in Fig. 8.12

Fig. 8.15 shows the overall results of Markov chain analysis similar to the one in Fig. 8.8. Again, one can see that significant degradation of the convergence rate is found for a very small portion of the channel realization/initial states for the randomized “good neighbor” algorithm.

It is worth emphasizing that for higher number of users and available bands the proposed randomization procedure may be more effective because of the higher number of possible searching outcomes in that case. This supposition will be verified in Section 8.7.1 by means of simulations because the Markov chain analysis becomes too computationally expensive for higher dimension networks.

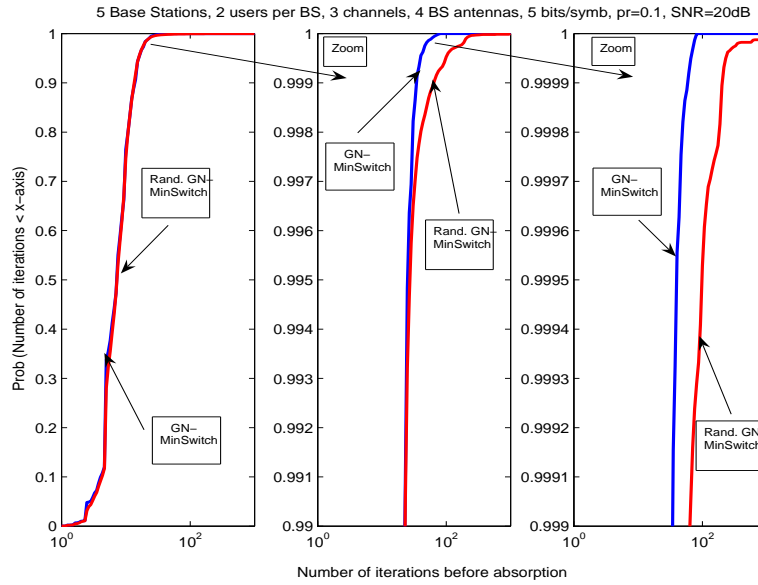


Figure 8.15. Convergence rates comparison for GN-MinSwitch and randomized GN-MinSwitch

It is important to note that although the proposed GN-MinSwitch randomization can reduce probability of the undesirable non-convergent behavior, it still cannot guarantee convergence to the fixed stationary points with probability one. Nevertheless, together with threshold selection it can help in keeping the non-convergence probability at the acceptable level.

8.6 Mixed “good neighbor”/”selfish” IM-based DSA networks

A very interesting and practically important question is the following:

- What can happen if some subsystems in the network are not willing to follow the “good neighbor” rules and demonstrate the “selfish” behavior?

Generally, a problem of incentives and regulations is currently under discussion in cognitive radio literature, e.g., [Sah09], [Woy08] (“crime and punishment in cognitive radios”). To introduce CR incentives and regulations it is critically important to understand consequences of possible undesirable/impolite behavior of some cognitive radios.

The analysis tool developed in Section 8.5 allows us to study such consequences in the considered IM-based DSA networks. Figs. 8.16 – 8.22 present generalization of the results in Section 8.5 for a mixed “good neighbor”/”selfish” system in the same scenario with 5 bits/symbol threshold. Particularly, similarly to Tables 8.1 – 8.3, Figs. 8.16 – 8.18 summarize the effect and parameters of the ergodic subchains in the mixed network. Figs. 8.19 – 8.21 show the steady-state performance and convergence rate. Eventually, Fig. 8.22 presents the steady-state data rate results separately for all $N = 5$ subsystems.

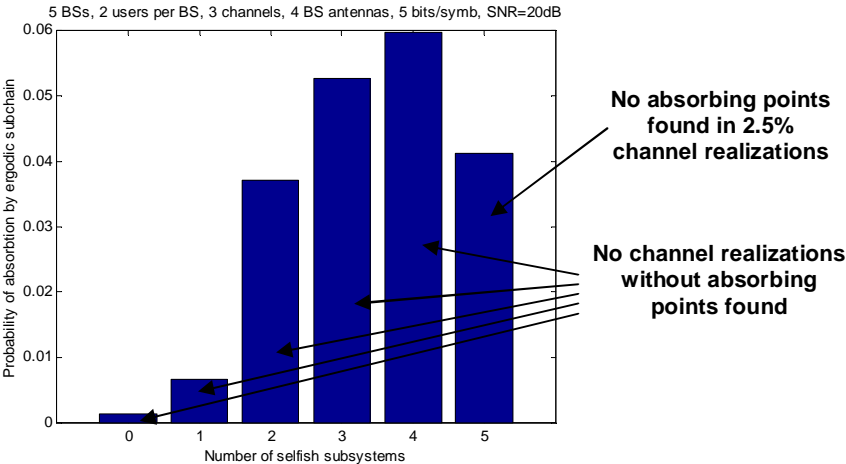


Figure 8.16. Probability of undesirable non-convergent behavior

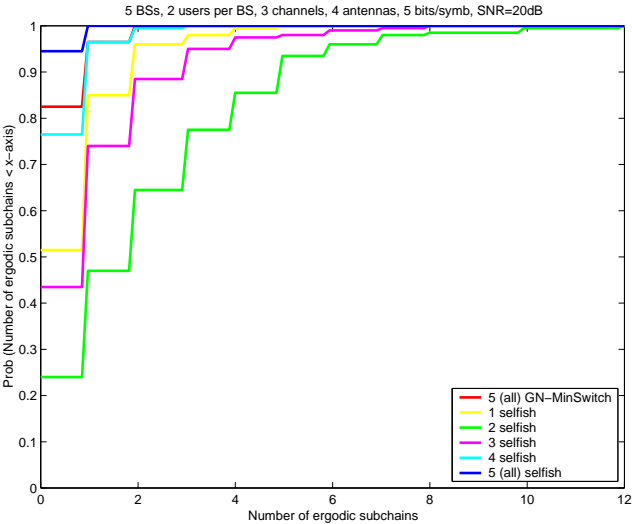


Figure 8.17. Number of ergodic subchains per channel realization

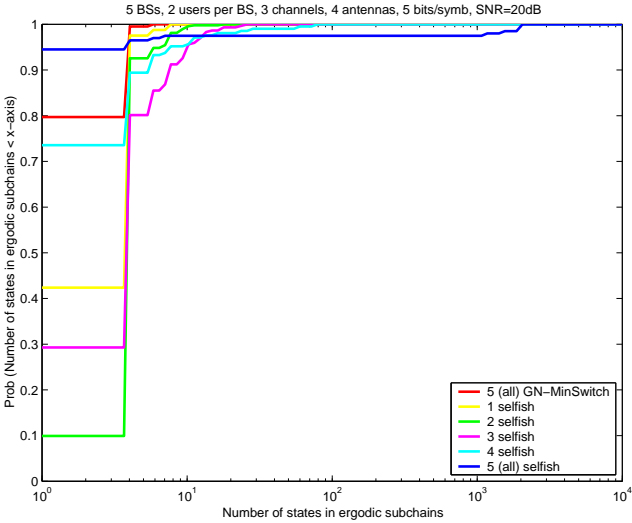


Figure 8.18. Number of states in an ergodic subchain

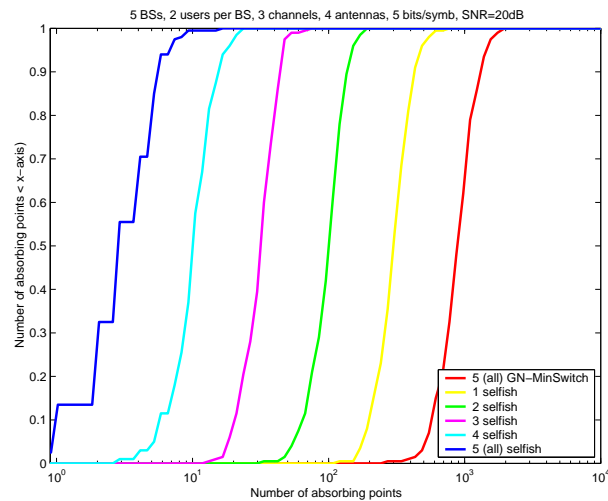


Figure 8.19. Number of absorbing points per channel realization

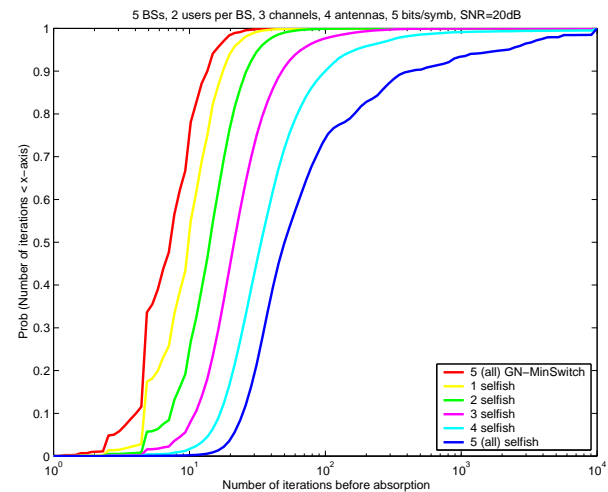


Figure 8.20. Average number of sensing intervals before absorption

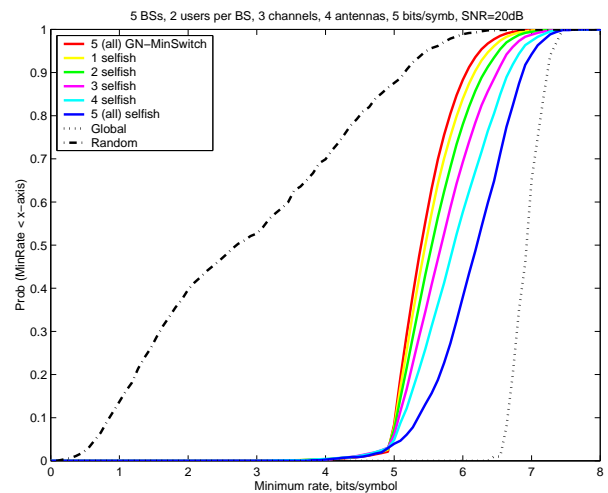


Figure 8.21. Steady-state performance

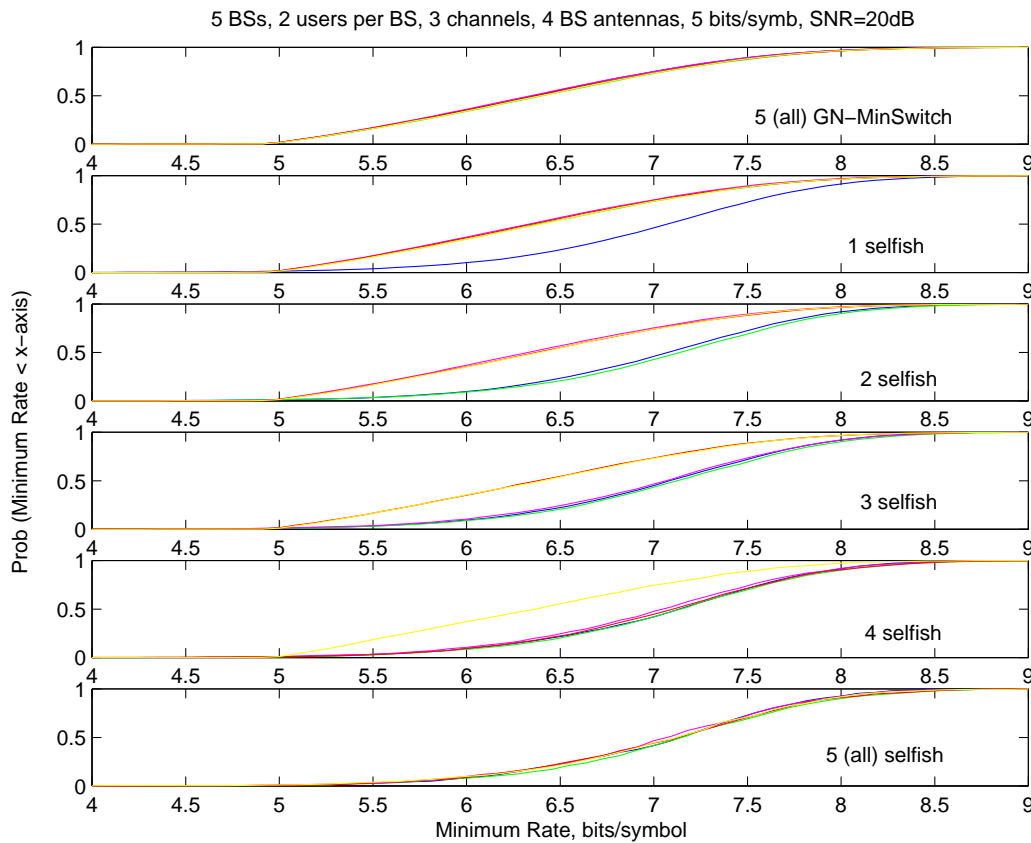


Figure 8.22. Steady-state data rate performance separately for each subsystem

The following observations can be made from the presented results:

- Although the “selfish” subsystems can slightly improve their steady-state performance as can be seen in Fig. 8.22, the overall network convergence gradually degrades with the growing number of “selfish” subsystems in terms of the increased non-convergence probability as shown in Fig. 8.16, decreased number of absorbing points for the given threshold as presented in Fig. 8.19, and decreased convergence rate as illustrated in Fig. 8.20.
- Degradation of the convergence properties affects all the players including the “selfish” ones trying to get advantage on polite users.
- The pure “selfish” and “good neighbor” systems have the lowest number of ergodic subchains for a given channel realization: maximum 1 or 2 if any as shown in Fig. 8.17. The main difference between these algorithms is that these subchains are short (4 - 6 states) in the “good neighbor” case and they may be very long (up to a few thousands states) as can be seen in Fig. 8.18.
- Comparison of the results presented in Figs. 8.17 and 8.18 suggests that the highest number of ergodic subchain can be found in mixed networks with similar numbers of the “selfish” and “good neighbor” subsystems.

- In overall, the mixed network results illustrate how Markov chain theory can be used for quantitative analysis of rule-regulated CR networks that may be important for development of incentives and regulations requirements for cognitive radio.

8.7 Simulation results

Taking into account that the main objective of this report is cognition and convergence effects for the system specified in Section 8.1, for simulations we assume that all base stations know the propagation channels for their own users and the corresponding interference-plus-noise covariance matrices (space-time sensing for estimation of the channel and interference environment will be addressed in the next deliverable D8.2) and adopt the simplified version of sensing timing shown in Fig. 8.2. We simulate T intervals, where even intervals contain information data transmitted from all the users and each odd interval corresponds to a sensing interval for one randomly selected subsystem and information intervals for all other subsystems. This simplification allows us to avoid situations with simultaneous sensing for a number of subsystems.

To verify the correspondence between our simulation and the Markov models, Fig. 8.23 shows the distribution of the number of sensing intervals before absorption, estimated in 1000 trials corresponding to different random sensing sequences for one particular channel realization and initial state for the GN-MinSwitch with $\gamma_0 = 5$ bits/symbol threshold. Comparison of the estimated mean value of the number of iterations with that calculated by (8.41) for the same channel and initial state demonstrates correspondence between the analytical Markov model developed in Section 8.5.1 to the simulation scenario, which can be applied for higher-dimension systems.

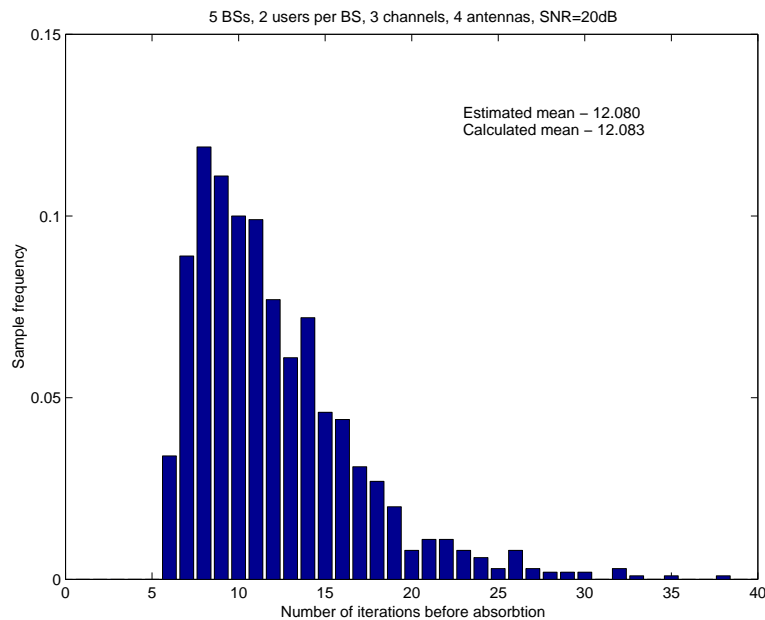


Figure 8.23. Estimated distribution of the number of iterations before absorption

8.7.1 Stationary horizontal CR scenarios without pathloss and shadowing

Typical examples of the adaptation process are illustrated in Fig. 8.24 – 8.26, where the minimum data rate is plotted for the $T/2$ even information intervals for all users in the system as well as the number of the allocated state. In Fig. 8.24, one can see a typical fast convergent situation, while Figs. 8.25 and 8.26 show the short (6 states) and long (1229 states) ergodic subchains correspondingly for the “good neighbor” and “selfish” algorithms. These subchains were found by means of Markov chain analysis presented in Section 8.5.

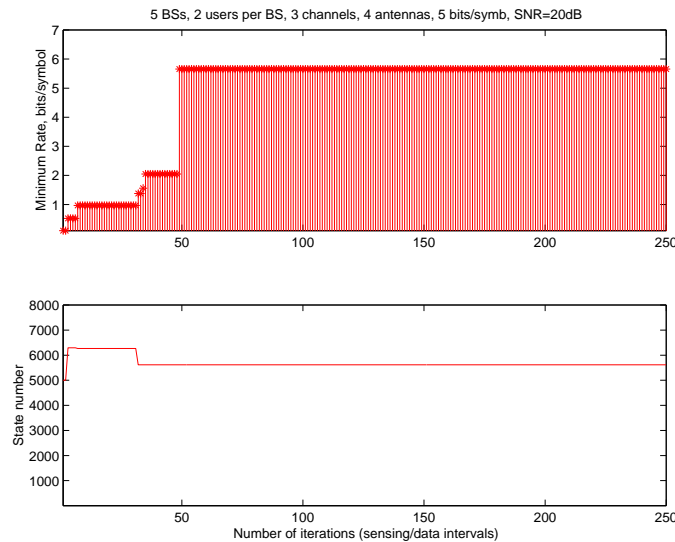


Figure 8.24. Typical example of fast convergence

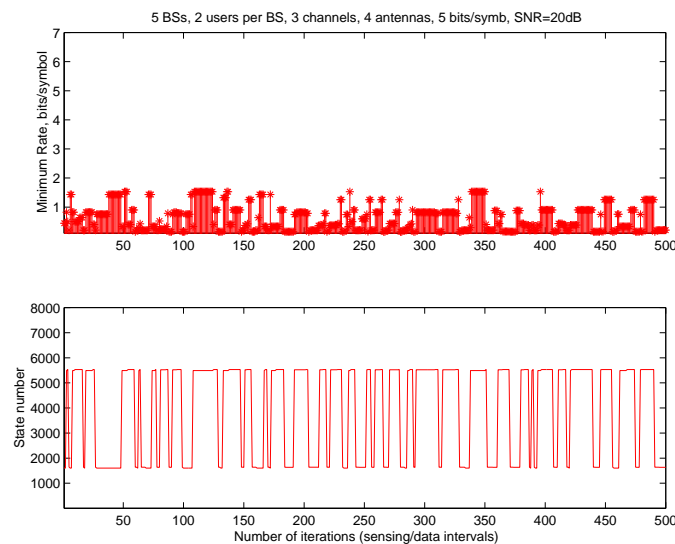


Figure 8.25. Typical example of short ergodic subchain

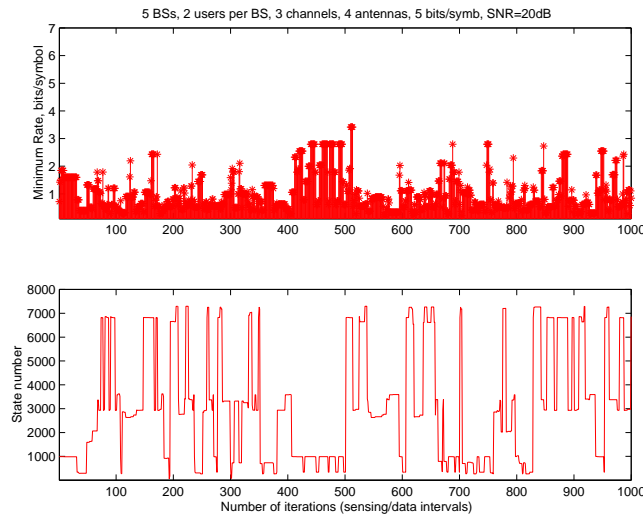


Figure 8.26. Typical example of long ergodic subchain

For higher-dimension system with $N=5$, $M=5$, $F=7$, $K=4$, and SNR=20 dB, 10 short ergodic subchains were found in 5000 trials with random channel realizations and initial states. All found subchains were successfully recovered by means of the randomized GN-MinSwitch algorithm introduced in Section 8.5.3. Three of them are shown in Fig. 8.27 for illustration. It is worth emphasizing that no ergodic subchains were found for the randomized GN-MinSwitch solution.

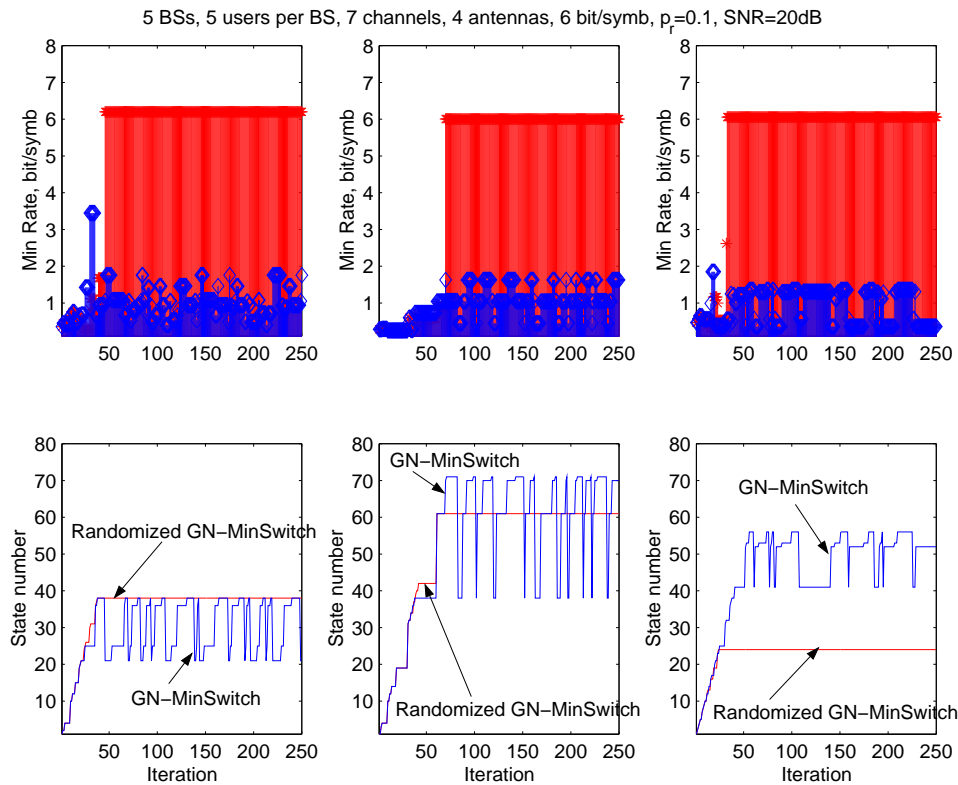


Figure 8.27. Ergodic subchains found by means of simulations for the higher-dimension system and their “recovery” by means of the randomized GN-MinSwitch algorithm with $p_r = 0.1$

Comparison of the convergence rates (without the ergodic subchains in the case of GN-MinSwitch) in this simulation is presented in Fig. 8.28 for GN-MinSwitch and its randomized version with $p_r = 0.1$. One can see that similarly to the low-dimensional case in Figs. 8.13 and 8.15, some degradation of the convergence rate is found in a few trials. Particularly, the slowest trials for the randomized GN-MinSwitch algorithm have about 50% longer convergence compared to the slowest trials in the basic GN-MinSwitch case. This difference is much lower compared with the order of magnitude degradation in Figs. 8.13 and 8.15 for the low-dimension network, which is in agreement with our supposition in Section 8.5.3 on higher randomization efficiency for higher dimension systems.

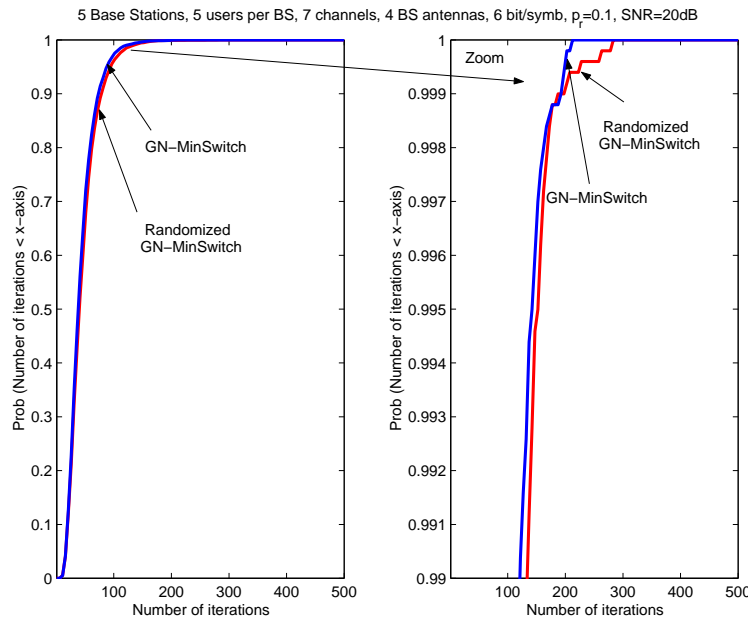


Figure 8.28. Convergence rates comparison for the basic and randomized GN-MinSwitch algorithms

Generally, the presented results suggest that modified “good neighbor” algorithms may be introduced for more efficient control of the convergence properties additionally to selection of the threshold. This problem requires further investigation, which is out of the scope of this report.

Figs. 8.29 – 8.31 summarize the simulation results for different system configurations and algorithms over 200 independent channel realizations for each scenario, with $\sigma_h^2 = 1$, $Q = M$, $N = 5$, and SNR=20 dB. In each case, the thresholds were selected as close to the global bound as possible to observe convergence of all trials for the GN-MinSwitch algorithm within the selected time window of 500 sensing intervals. Fig. 29 (left) presents the minimum data rate results after 500 sensing trials for the threshold-regulated algorithms based on MaxMin and MinSwitch exhaustive local search with and without PC, according to (8.33) for $K = N_0 = 4$, $M = 5$, and $F = 7$. The corresponding estimated convergence rate is plotted in Fig. 8.29 (right).

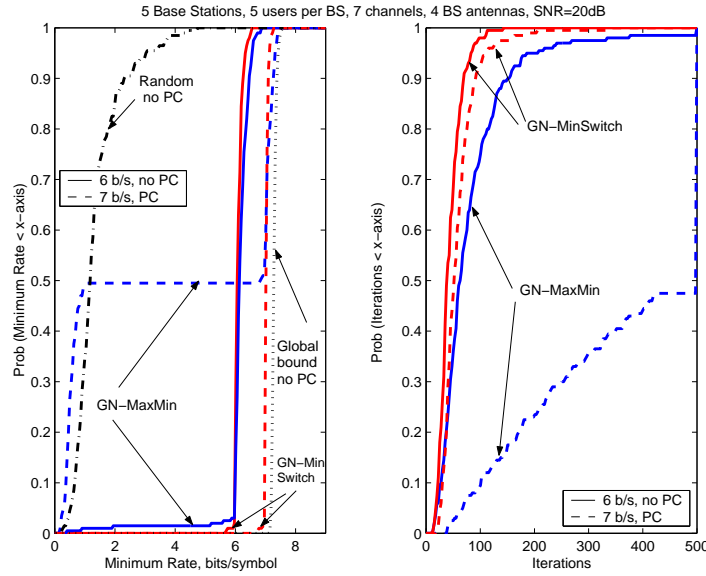


Figure 8.29. CDF of the global performance (left) and convergence rate (right) for $K = N_0 = 4$

The following observation can be made from Fig. 8.29:

- Fig. 8.29 (left) shows that steady state results close to the global bound in the no-PC case are observed for the decentralized IM-based DSA algorithms, which are much better than for random band allocation.
- For the 6 bits/symbol threshold, GN-MaxMin and GN-MinSwitch demonstrate similar steady-state results after 500 sensing intervals, but GN-MinSwitch shows better convergence speed. One can see in Fig. 8.29 (right) that in 50% of channel realizations, GN-MinSwitch is at least twice as fast as GN-MaxMin. This is expected because the MinSwitch search minimizes the number of band reallocations and reduces non-stationary interference.
- The local “water filling” PC (8.33) allows significant improvement for GN-MinSwitch. GN-MaxMin converges much slower in this case, as shown in Fig. 8.29 (right). Furthermore, in 50% of the channel realizations, absorbing states were not achieved after 500 sensing trials for this algorithm.

Fig. 8.30 presents the results in the same scenario as in Fig. 8.29, but for $K = N_0 - 1 = 3$ BS antennas:

- The steady-state performance for the IM-based DSA algorithms is still much better than in the random allocation case, but the distance from the global bound is higher compared with the previous case. A possible reason is that a number of good solutions may be much lower in this case because they require a reduced dimension of the interference subspace additionally to avoiding colinearity between propagation channels of the desired signal and interference, which makes decentralized algorithms less efficient compared to the complete interference suppression case.

- Although, the local PC based on (8.33) still improves the GN-MinSwitch performance, its efficiency is much lower compared to the case in Fig. 8.29. This is expected behavior for $K < N_0$ as explained in Section 8.8.

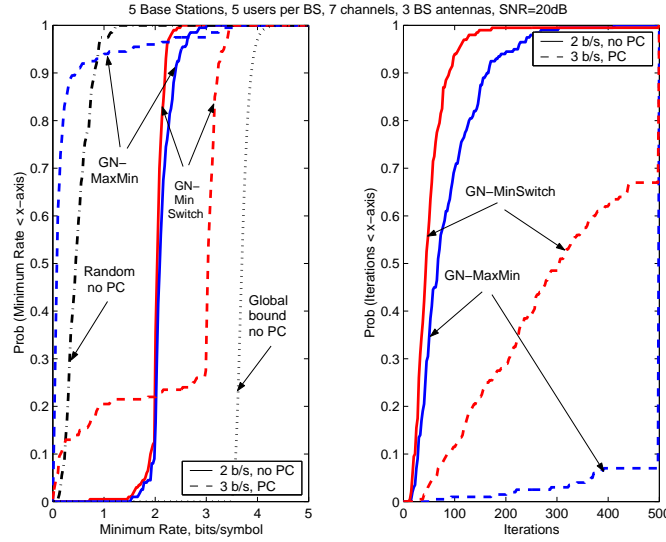


Figure 8.30. CDF of the global performance (left) and convergence rate (right) for $K = N_0 - 1 = 3$

A higher dimension system is addressed in Fig. 8.31 for $K = N_0 = 4$, $M = 20$, and $F = 30$. Obviously, exhaustive local search is not possible in this case. The maximum element search (8.26) and simplified MinSwitch search (8.30) are applied. In this last case, we select 3 users with the lowest SINR in the set M_s and 5 bands in the set Φ_s : 3 bands currently occupied by the users from M_s and 2 arbitrary bands not currently occupied at the BS_n . If $\gamma_{nm} > \gamma_0$ for more than 3 users, then we apply the maximum element search (8.26). In Fig. 8.31 this algorithm is referred to as “GN-MinSwitch, 3(5)-restricted”. The main observation in Fig. 8.31 is that GN-MinSwitch significantly outperforms GN-MaxMin in both cases with and without “water filling” PC. This illustrates the expected growing efficiency of the MinSwitch search for higher-dimension systems.

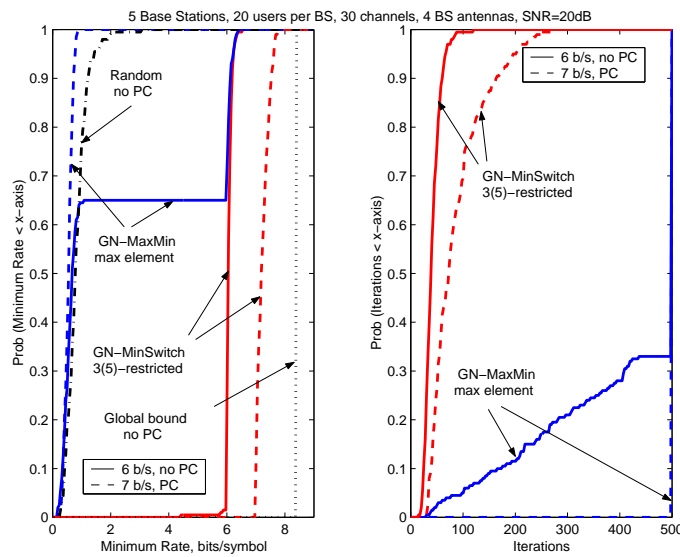


Figure 8.31. CDF of the global performance (left) and convergence rate (right) for $K = N_0 = 4$

It is worth emphasizing that in all scenarios in Figs. 8.29 – 8.31, the “selfish” solution (unconstrained MaxMin local search) demonstrates significantly worse results (not shown) even compared with the GN-MaxMin performance. Comparison of the GN-MinSwitch “no PC” results with the global bounds (8.18) in Figs. 8.29 and 8.31, and (8.23) in Fig. 8.30, shows the potential room for improvements for IM-based DSA algorithms, for example, by means of explicit coordination between subsystems: approximately 2 times in SINR in Fig. 8.29, and up to 5 times in Figs. 8.30 and 8.31.

8.7.2 Stationary horizontal CR scenarios with pathloss and shadowing

Pathloss and shadowing propagation models leading to variable σ_h^2 are used similarly to [Tri08] in Figs. 8.32 - 8.35 that present the GN-MinSwitch simulation results with on-line threshold selection according to (8.32). Particularly, we assume:

- $N = 5$ BSs, each with $M = 5$ users deployed in the 100×100 m area sharing $F = 7$ bands;
- the reference SNR=20 dB at the reference distance of 50 m with the pathloss coefficient of 3, and standard deviation of 6 dB for the lognormal shadowing;
- the same pathloss and shadowing for all bands.

Two examples of system geometry are shown in Figs. 8.32 and 8.34 (left) corresponding to the regular and random BSs positions in the area with random positions of all users. The corresponding local minimum data rate results for each subsystem are given in Figs. 8.32 and 8.34 (right) for GN-MinSwitch with $\alpha = 0.25$ in (8.32) in 200 trials with independent Rayleigh fading. The estimated global performance in the scenario in Fig. 8.32 is given in Fig. 33. The estimated global performance for random system geometries similar to the one in Fig. 34 (left), is presented in Fig. 8.35 for GN-MinSwitch with $\alpha = [0.1, 0.25]$. The estimated performance of random band allocation and “no interference” bounds are plotted in Figs. 8.32 - 8.35 as well.

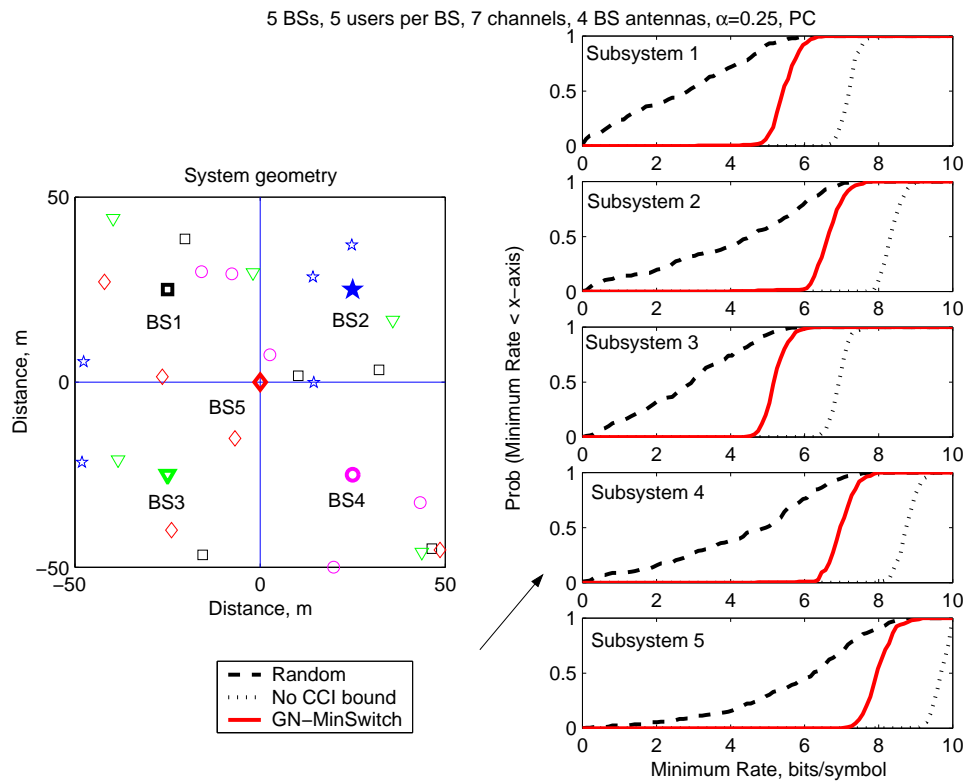


Figure 8.32. Example of system geometry (left) with bolt signs indicating the corresponding BSs, and CDF for the local performance for all 5 subsystems (right)

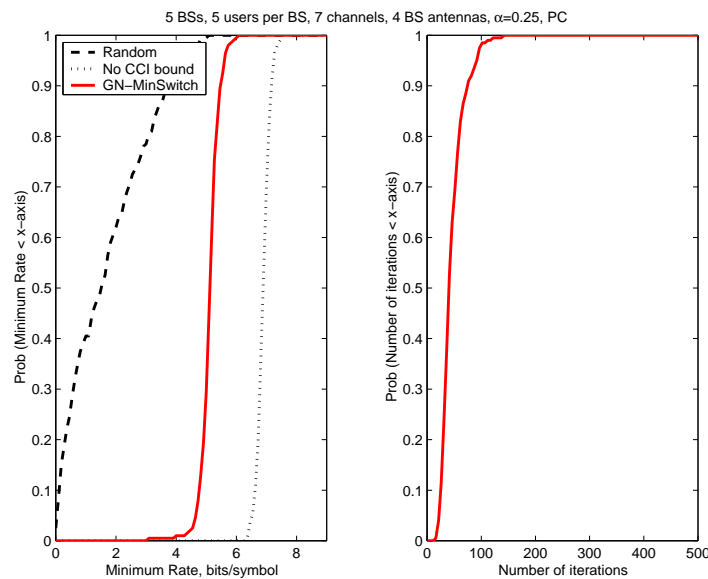


Figure 8.33. CDF of the global performance (left) and convergence rate (right) in 200 independent Rayleigh fading realizations in the scenario shown in Fig. 8.32 (left)

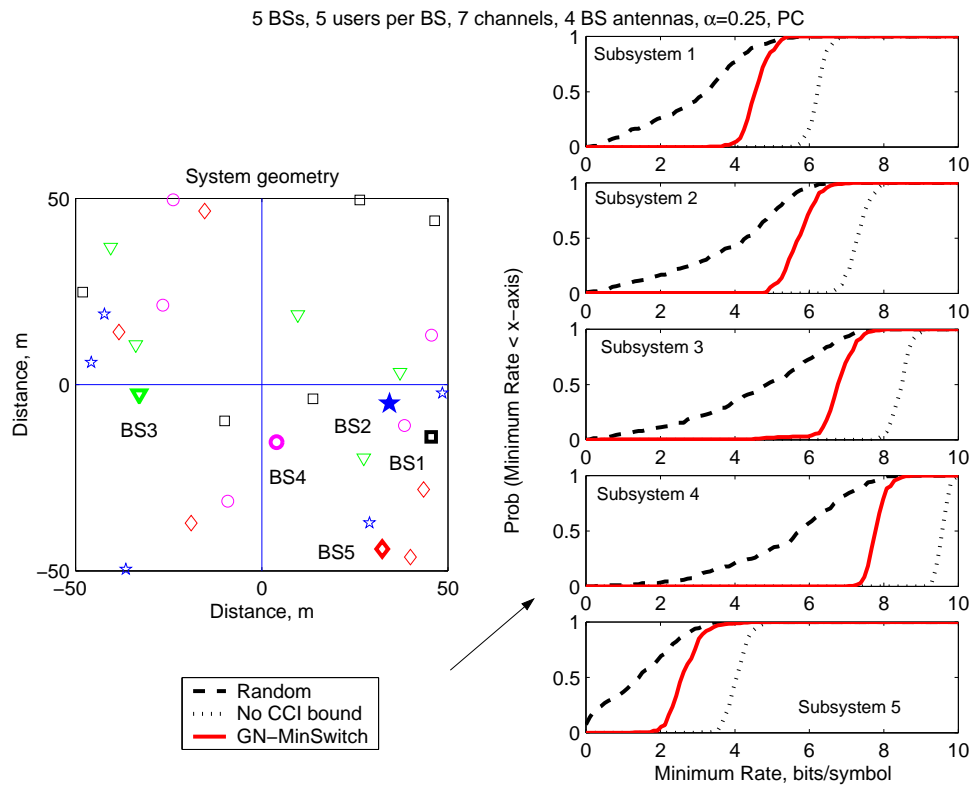


Figure 8.34. Example of system geometry (left) with bolt signs indicating the corresponding BSs, and CDF for the local performance for all 5 subsystems (right)

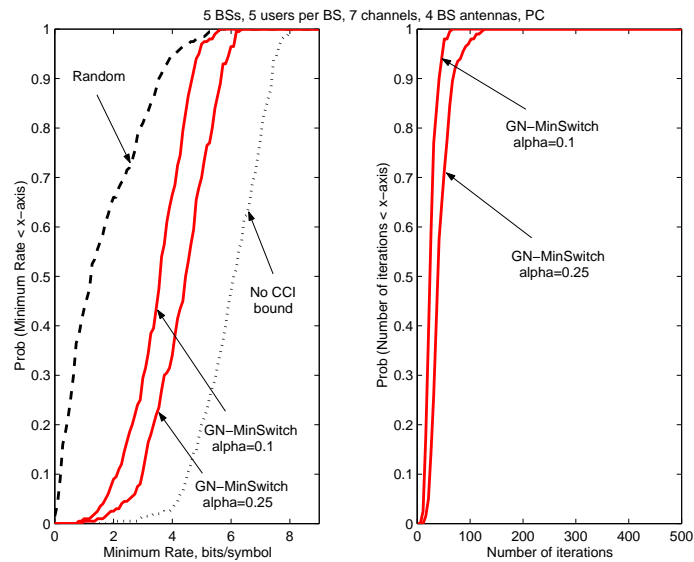


Figure 8.35. CDF of the global performance (left) and convergence rate (right) in 200 random system geometries similar to shown in Fig. 8.32 (left)

The presented simulation results show the following:

- The proposed on-line threshold selection allows control of the steady-state performance and convergence rate by means of a single parameter α in (8.32) even if different subsystems experience very different propagation and interference conditions.
- In the particular scenarios in Figs. 8.32 and 8.34, the relative positions of the GN-MinSwitch and “no interference” curves are similar for all subsystems, although the actual performance is very different, e.g., by approximately 2^5 times in terms of SINR for subsystems 4 and 5 in Fig. 8.34 (right). One can see in Fig. 8.34 (left) that the geometrical reason for this difference between subsystems 4 and 5 is that BS_4 is the closest to the center and BS_5 is the closest to the corner of the area with randomly located users. Similarly, the best results can be seen in Fig. 8.32 for Subsystem 5 with the BS located in the center of the deployment area.
- The relative DSA improvement compared with random band allocation is generally lower in the case of variable σ_h^2 than in the extreme interference limited scenario with $\sigma_h^2 = 1$ for all users for the same system dimension. This is because performance degradation for some subsystems may come from difficult propagation conditions for their own users rather than from interference environment, e.g., as in subsystem 5 in Fig. 8.34. The IM-based DSA efficiency may be compromised in this situation. Nevertheless, in the particular scenarios as in Fig. 8.34, up to 8 times SINR gain compared to random band allocation still can be observed. Generally, other criteria, e.g., based on proportional fairness [Tri08], could be considered in this case, which is beyond on the scope of this report.

8.7.3 Nonstationary vertical CR scenarios

Dynamic properties of the considered algorithms are illustrated in Figs. 8.36 and 8.37 in the nonstationary vertical CR scenario illustrated in Fig. 8.3, where primary users change their band according to Poisson law with parameter $\lambda = [0.001, 0.003]$ correspondingly (1 and 3 changes per 1000 sensing intervals on average). It is assumed that the spectrum sensing outcome for the secondary users is that all the propagation channels are randomly change in some bands, which means that the secondary subsystem leaves some bands and occupies the same number of others that become free from the primary system. The “selfish”, GN-MaxMin, and GN-MinSwitch algorithms are shown in Figs. 8.36 and 8.37 in the same scenario parameters as in Fig. 8.29 using the visualization format as in Figs. 8.24 – 8.27.

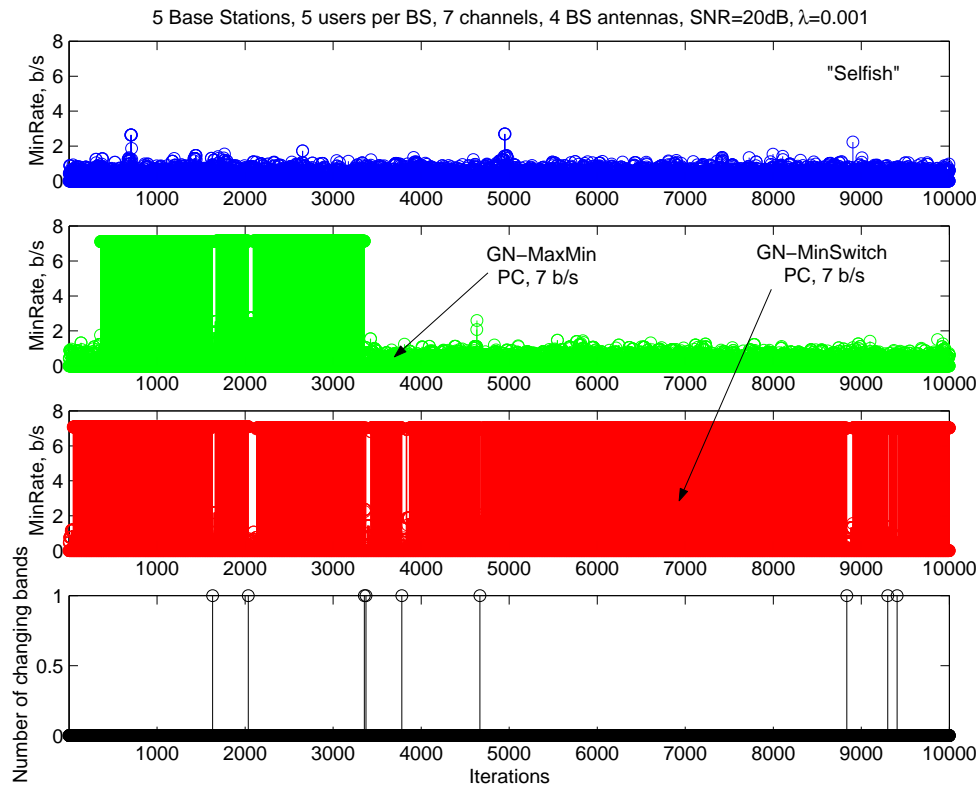


Figure 36. IM-based DSA algorithms in the nonstationary vertical CR scenario with $\lambda = 0.001$

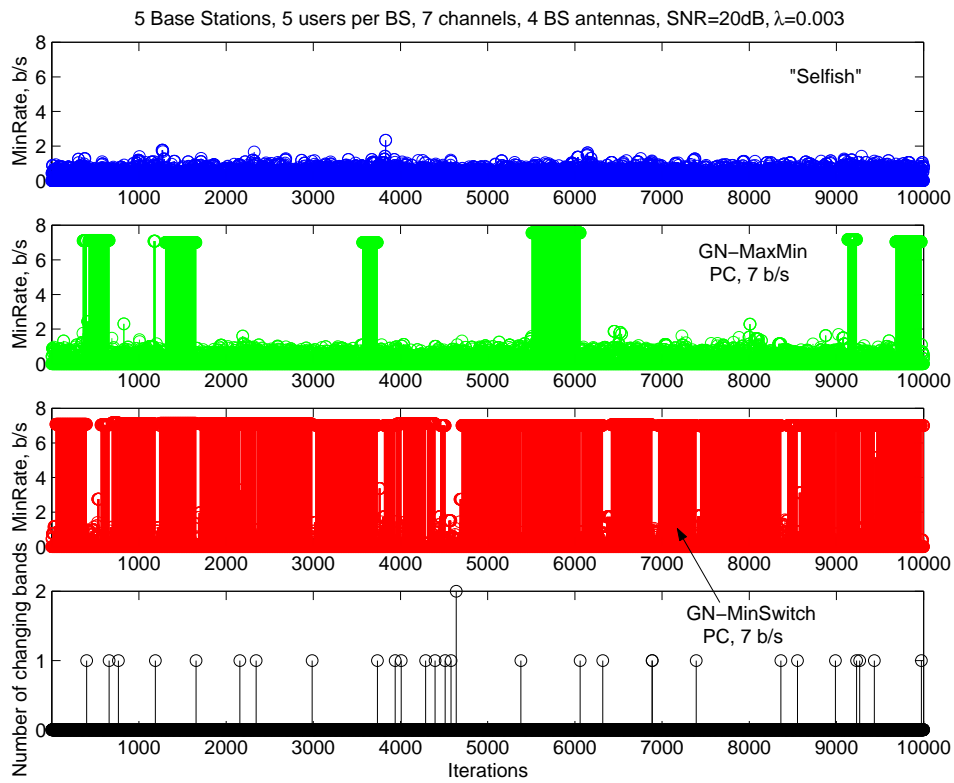


Fig. 37. IM-based DSA algorithms in the nonstationary vertical CR scenario with $\lambda = 0.003$

One can see that the “selfish” algorithm, indeed, has no practical perspective in both scenarios because it never converges during the observed time interval. GN-MaxMin demonstrates better results because it can track some of changes, especially for $\lambda = 0.001$, but it is still too slow to track most of the changes for $\lambda = 0.003$. Eventually, GN-MinSwitch demonstrates the acceptable performance in the considered non-stationary environment for both $\lambda = 0.001$ and $\lambda = 0.003$.

It is important to note that convergence to stationary points (NE) cannot be guaranteed for all the algorithms shown in Figs. 8.36 and 8.37. Actually, it is not required in such a non-stationary environment, where non-convergence cannot be practically distinguished from slow convergence. The overall conclusion from the presented simulation results is that the introduced controllable convergence behavior gives a practical perspective for the “good neighbor” solution in a dynamic CR environment even if its global convergence with probability one still cannot be guaranteed.

8.8 Conclusions

In this chapter we have considered a new class of DSA techniques that operate in a non-reciprocal environment, where any changes in frequency allocation of a certain subsystem introduces a non-stationary interference scenario for other subsystems in the network. Statistical bounds of the global performance have been derived under the Rayleigh propagation model that can be used for assessment of IM-based DSA algorithms.

Two types of decentralized IM-based DSA strategies have been introduced. One is the usual “selfish” approach, where each BS tries to find the best possible frequency allocation for each of its SSs, regardless their actual current performance on the already allocated bands. The problem with this approach is that a complete frequency re-assignment in pursuit of possibly negligible improvement, creates a new interference scenario for all other subsystems, and forces them to do the same.

As a result, the entire system has very slow convergence, or in some cases, may not converge at all.

Another strategy, “good neighbor”, is when each subsystem tries to achieve a certain QoS by means of minimization of a number of re-allocations. This approach tends to minimize changes introduced by the DSA algorithm at a given subsystem upon the interference environment for the rest of the network.

Analysis of the two techniques has been conducted both analytically and by statistical simulations. For a relatively simple example with a reasonable (7776, in fact) number of different allocations, we found it feasible to analyze both the algorithms using the absorbing Markov chain model, which specifies all absorbing points (Nash equilibriums in game theory terminology), all ergodic subchains (undesirable non-convergent behavior), and also the average number of sensing intervals before absorption (convergence rate). These analytical estimates, derived for a large number of random propagation channels as well as the results of direct statistical simulations, demonstrated much better global performance of the “good neighbor” strategy. In all these cases where the targeted QoS was established at a high performance level of (60 – 70) % with respect to the global bound, all the considered systems reached their target performance reasonably fast.

The “selfish” algorithm can indeed provide better steady-state performance, but at a cost of a high probability of non-convergence or a number of iterations that is several orders of magnitude higher than that for the “good neighbor” strategy.

It has been shown that modified “good neighbor” algorithms may be introduced for more efficient control of the convergence properties additionally to selection of the threshold. Particularly, the randomized “good neighbor” algorithm has been proposed that allows significant reduction of the non-convergence probability with some degradation of the convergence rate, which has been demonstrated by means of the Markov chain analysis and simulations for higher dimension networks.

The Markov chain analysis has been applied in mixed scenarios, where some of subsystems are not willing to follow the “good neighbor” rules and demonstrate the “selfish” behavior. The main conclusion is that although “selfish” subsystems can slightly improve their steady-state performance, the overall network convergence gradually degrades with the growing number of “selfish” subsystems. Furthermore, degradation of the convergence properties affects all the players including the “selfish” ones trying to get advantage on polite users. In overall, the mixed network results illustrate how Markov chain theory can be used for quantitative analysis of rule-regulated CR networks that may be important for development of incentives and regulations requirements for cognitive radio.

In the scenario where the number of antenna elements is large enough for efficient interference suppression, power control can be used for performance improvement almost like in a noise-limited scenario. The overall performance of the proposed IM-based DSA in such systems has been proven to be reasonably high including non-stationary cognitive radio scenario and general propagation conditions with pathloss and shadowing effects.

In this chapter we have focused on the issues associated with cognition and allocation potentials of the different decentralized strategies, and did not consider effects associated with finite training sample support, involved in estimation of the propagation channels and interference covariance matrices. This and a number of other second-order phenomena will be addressed in the next PHYDYAS deliverable D8.2.

9 Summary

The FBMC PHY has been studied and compared with OFDM as a potential physical layer for CR networks. Spectral efficiency, impact of the RF impairments, and resource allocation techniques have been investigated. It has been shown that FBMC can be considered as a perspective physical layer for future CR networks.

The main results are as follows.

Section 3:

- FBMC and OFDM receivers were compared in terms of spectral selectivity when signals with high dynamic range were assumed on the frequency band under investigation. The FBMC receiver was found to provide a clear advantage over OFDM due to its significantly enhanced spectral rejection properties.
 - As for the secondary data multiplexing, FBMC technique shows potential to facilitate flexible and spectrally efficient asynchronous multi-user access. Therefore, FBMC modulation is considered to be particularly well suited for the secondary transceivers.
-

- A concept of a time-frequency sensing window, which allows for two-dimensional integration of the energy observations, was introduced and found to match well with the multicarrier receiver model. The basic tradeoff between the spectral resolution and the sensing latency, influenced by the dimensions of this window, was clarified. The sensing time can be shortened at the cost of the reduced spectral resolution and vice versa. Further, the presented concept is found to improve the flexibility of the system dimensioning and to provide adaptability to different primary signal scenarios and SNR conditions.
- For spectrum monitoring during secondary transmission an idea of a silent sensing window (a spectrum sensing block within secondary data) was introduced. The overheads, resulting from multiplexing of these sensing blocks, were discussed both in case of OFDM and FBMC. Moreover, an optimal shape for the sensing window in FBMC case was presented.
- Two different sensing window structures were proposed. They were found to provide different tradeoffs between the spectral efficiency of the secondary transmission (due to overheads in multiplexing silent sensing windows), the synchronization requirements, and the reaction time in case of a reappearing primary transmission. The optimally-shaped windows (located in the beginning or end of a frame at the edge of a subcarrier group) provide higher efficiency. On the other hand, the structure based on continuous sensing subbands both relaxes the time synchronization requirements among different SUs and sensing devices, and improves the ability to detect collisions due to reappearing PUs.
- The future spectrum sensing studies are planned to focus on the following topics: More detailed studies of energy detection methods with FBMC, including the evaluation of the feasibility of residual interference and zero-pilot based methods. Combining cyclostationary detection with FBMC. Evaluation of the feasibility of the other mentioned sensing methods in the FBMC context. Developing practical sensing methods for PHYDYAS dynamic spectrum access scheme.

Section 4:

- Available time-frequency resource exploitation and corresponding interference power of OFDM/OQAM based systems were compared to OFDM in the Cognitive Radio context. According to the out-of-band radiation analysis of different multicarrier systems and the throughput definitions of RU, we demonstrated that when as a CR data communication technique, filter bank multicarrier modulation offers higher spectral efficiency than OFDM. As a result, OFDM/OQAM is a natural candidate for physical layer data communication in cognitive radio systems. Conventional OFDM and raised cosine windowed OFDM have to compromise between two important performance parameters: maximum throughput for secondary user and minimum interference on primary user. Although there is a little additional complexity for OFDM/OQAM system structure due to prototype pulse shaping, it is profitable for achieving better spectral efficiency.

Section 5:

- Three common impairments of a transmitter's RF front-end were studied in terms of their impacts on the spectral selectivity of an FBMC waveform in the context of a cognitive radio application. These impairments are the non linearity of the power amplifier, the IQ mismatch and the phase noise.
 - The objectives were to relate the level of each RF imperfection to a level of spectral dynamic range (SDR), to evaluate the effect on the transmission performance in terms of EVM per subcarrier, and to compare with an equivalent system based on OFDM. Finally,
-

we formulated requirements that should be met by the RF front-end in order not to degrade excessively the spectral selectivity of the transmitted FBMC signal.

- Simulation studies show that in the hypothesis where a dynamic range of 40dB is targeted, requirements on IQ mismatch and phase noise are not so different that those required for 64-QAM WIMAX. However, the impact of the power amplifier is more significant. It could be necessary to operate at an input power back-off of 13 or 14dB, where an OFDM system typically target around 7-8dB. This would lead to an increase of the power consumption of the power amplifier in a factor of 2 or 3.
- Possible solutions that could be investigated are pre-compensation techniques of the power amplifier non linearity's.

Section 6:

- A computationally efficient sub-optimal resource allocation algorithm for multicarrier based CR networks has been proposed. The algorithm aims to maximize the downlink capacity of the cognitive system without causing excessive interference to the licensed users. The proposed algorithm has a near optimal performance with a significant reduction in the computational complexity. The proposed algorithm outperforms the performance of Zhang's algorithm and overcome its limited performance in the low interference constraints. The efficiency of using FBMC instead of OFDM in cognitive radio systems is proved throughout the simulation. The high spectral efficiency and the low interference introduced to the primary users make the FBMC more suitable for future cognitive radio systems. We are extending the algorithm to maintain the quality of service of the different cognitive users. Moreover, an algorithm that considers the resource allocation problem in the uplink scenario will be developed.

Section 7:

- An improved algorithm has been presented for cooperative DSA in unlicensed bands, utilizing MAC layer mechanisms for message exchange ("interference prices") between the nodes, in order to achieve interference mitigation. The main improvement is the introduction of an uncertainty coefficient that sets the weight of the interference term, increasing its impact in cases of imperfect message exchange, long time intervals for interference price update, as well as increased number of users. In such cases the interference caused to other users by an increase in the transmission power of a user is often underestimated, resulting in a convergence of the algorithm in a non-optimal solution. In the presence of such uncertainties, if this underestimation is compensated by a properly defined weight parameter, the system approximates its optimal behavior as in the case of "perfect" message exchange.
 - The value of the weight parameter was derived from a fuzzy logic reasoner, because fuzzy logic is particularly effective at dealing with uncertainties and vague requirements. Moreover, the effect of the proposed algorithm has been compared to the original algorithm in terms of the overall utility level (defined as the sum of the user utilities) under uncertainties that cause 25% underestimation of interference. Furthermore, comparison was also made between the proposed algorithm with FBMC and OFDM. In this case using FBMC increased the achieved utility and the improvement stems from the fact that FBMC uses lower transmission power for the same bandwidth compared to OFDM and therefore causes reduced interference.
-

- Future work includes further study of the correlation between the utility value and typical network parameters such as the Bit Error Rate and Probability of Error, which define the end to end reliability of the system and determine QoS. Moreover, the rules of the fuzzy logic reasoner will be refined and methods for automatic update of the fuzzy rules will be proposed (e.g. utilizing a neuro-fuzzy controller). Finally, parameters such as fairness and scalability will also be investigated.

Section 8:

- A new class of DSA techniques has been introduced that operate in a non-reciprocal environment, where any changes in frequency allocation of a certain subsystem introduces a non-stationary interference scenario for other subsystems in the network. Statistical bounds of the global performance have been derived under the Rayleigh propagation model that can be used for assessment of IM-based DSA algorithms.
 - Two types of decentralized IM-based DSA strategies have been introduced. One is the usual “selfish” approach, where each BS tries to find the best possible frequency allocation for each of its SSSs, regardless their actual current performance on the already allocated bands. The problem with this approach is that a complete frequency re-assignment in pursuit of possibly negligible improvement, creates a new interference scenario for all other subsystems, and forces them to do the same. As a result, the entire system has very slow convergence, or in some cases, may not converge at all.
 - A new strategy, “good neighbor”, is when each subsystem tries to achieve a certain QoS by means of minimization of a number of re-allocations. This approach tends to minimize changes introduced by the DSA algorithm at a given subsystem upon the interference environment for the rest of the network.
 - Analysis of the two techniques has been conducted both analytically and by statistical simulations. For a relatively simple example with a reasonable (7776, in fact) number of different allocations, we found it feasible to analyze both the algorithms using the absorbing Markov chain model, which specifies all absorbing points (Nash equilibriums in game theory terminology), all ergodic subchains (undesirable non-convergent behavior), and also the average number of sensing intervals before absorption (convergence rate). These analytical estimates, derived for a large number of random propagation channels as well as the results of direct statistical simulations, demonstrated much better global performance of the “good neighbor” strategy. In all these cases where the targeted QoS was established at a high performance level of (60 – 70) % with respect to the global bound, all the considered systems reached their target performance reasonably fast.
 - The “selfish” algorithm can provide better steady-state performance, but at a cost of a high probability of non-convergence or a number of iterations that is several orders of magnitude higher than that for the “good neighbor” strategy.
 - It has been shown that modified “good neighbor” algorithms may be introduced for more efficient control of the convergence properties additionally to selection of the threshold. Particularly, the randomized “good neighbor” algorithm has been proposed that allows significant reduction of the non-convergence probability with some degradation of the
-

convergence rate, which has been demonstrated by means of the Markov chain analysis and simulations for higher dimension networks.

- The Markov chain analysis has been applied in mixed scenarios, where some of subsystems are not willing to follow the “good neighbor” rules and demonstrate the “selfish” behavior. The main conclusion is that although “selfish” subsystems can slightly improve their steady-state performance, the overall network convergence gradually degrades with the growing number of “selfish” subsystems. Furthermore, degradation of the convergence properties affects all the players including the “selfish” ones trying to get advantage on polite users. In overall, the mixed network results illustrate how Markov chain theory can be used for quantitative analysis of rule-regulated CR networks that may be important for development of incentives and regulations requirements for cognitive radio.
- In the scenario where the number of antenna elements is large enough for efficient interference suppression, power control can be used for performance improvement almost like in a noise-limited scenario. The overall performance of the proposed IM-based DSA in such systems has been proven to be reasonably high including non-stationary cognitive radio scenario and general propagation conditions with pathloss and shadowing effects.
- Effects associated with finite training sample support, involved in space-time sensing for estimation of the propagation channels and interference covariance matrices at the IM-based DSA CR system and a number of other second-order phenomena will be addressed in the next PHYDYAS deliverable D8.2.

References

- [Abr09] Y. I. Abramovich, A. M. Kuzminskiy, “Performance bounds for dynamic spectrum allocation based on adaptive antenna array interference mitigation diversity,” in Proc. SSP, Sept. 2009.
- [Ars07] G. Arslan, M. F. Demirkol, Y. Song, “Equilibrium efficiency improvement in MIMO interference systems: a decentralized stream control approach,” IEEE Trans. Wireless Commun, vol. 6, no. 8, Aug. 2007.
- [Ash07] O. Ashagi, S. Murphy, L. Murphy, “A distributed approach to interference mitigation between OFDM-based 802.16 systems operating in license-exempt spectrum,” in Proc. ICC, pp.4855-4860, June 2007.
- [Bak08] O. Bakr, M. O. Johnson, B. Wild and K. Ramchandran, “A Multi-Antenna Framework for Spectrum Reuse Based on Primary-Secondary Cooperation”, in Proc. 3rd IEEE International Symposium on New Frontiers in Dynamic Spectrum Access Networks 2008 (DySPAN '08), pp. 1-5, Oct. 2008.
- [Bal07-1] L. G. Baltar, D. S. Waldhauser, “Out-Of-Band Radiation in Multicarrier Systems: A Comparison”, Lecture Notes in Electrical Engineering, vol. 1, pp. 107-116, 2007.
- [Bal07-2] L. G. Baltar, D. S. Waldhauser, and J. Nosssek, “Out-of-band radiation in multicarrier system: a comparison,” in Proc. MC-SS Workshop. Springer, pp. 107–116, May 2007.
-

- [Ban07] G. Bansal, M. J. Hossain, and V. K. Bhargava, "Adaptive power loading for OFDM-Based cognitive radio systems," in Proc. IEEE International Conference on Communication (ICC), pp. 5137–5142, 2007.
- [Ban08] G. Bansal, M. J. Hossain, and V. K. Bhargava, "Optimal and suboptimal power allocation schemes for OFDM-based cognitive radio systems," IEEE Transactions on Wireless Communications, vol. 7, no. 11, pp. 4710–4718, Nov. 2008.
- [Bel01] M. Bellanger, "Specification and design of a prototype filter for filter bank based multicarrier transmission", in Proc. ICCASP, Vol. 1, pp. 2417-2420, 2001.
- [Bel08-1] M. Bellanger, "Future radio systems: Impact of the air interface," Keynote Talk at International Conference on Advanced Technologies for Communications, Oct. 2008.
- [Bel08-2] M. Bellanger, "Filter banks and OFDM-OQAM for high throughput wireless LAN," in Proc. 3rd International Symposium on Communications, Control and Signal Processing (ISCCSP'08), pp. 758–761, March 2008.
- [Bel08-3] M. Bellanger, "A note on FBMC for multi-user and dynamic access," (PHYDYAS-D002.doc).
- [Boy04] S. Boyd and L. Vandenberghe, Convex optimization, Cambridge Univ. Press., Cambridge, U.K., 2004.
- [Bri05] V. Brik, E. Rozner, S. Banarjee and P. Bahl, "DSAP: a protocol for coordinated spectrum access", in Proc. 1st IEEE International Symposium on New Frontiers in Dynamic Spectrum Access Networks 2005 (DySPAN '05), pp. 611–614, Nov. 2005.
- [Bul08] S. Buljore et al. "Introduction to IEEE P1900.4 Activities", IEICE Transactions on Communications, Special Section on Cognitive Radio and Spectrum Sharing Technology (Invited Paper), vol. E91-B, pp 2-9, Jan. 2008.
- [Cab05] D. Cabric and R.W. Brodersen, "Physical layer issues unique to cognitive radio systems," in Proc. of the IEEE 16th Int. Symposium on Personal, Indoor and Mobile Radio Communications (PIMRC), Berlin, Germany, pp. 759-763, Sept. 2005.
- [Cha08] S. Chaudhari, V. Koivunen, and H.V. Poor, "Distributed autocorrelation-based sequential detection of OFDM signals in cognitive radios," in Proc. of the IEEE 3rd Int. Conference on Cognitive Radio Oriented Wireless Networks and Communications (CROWNCOM), pp. 1-6, Singapore, May. 2008.
- [Cao05] L. Cao and H. Zheng, "Distributed spectrum allocation via local bargaining", in Proc. IEEE Sensor and Ad Hoc Communications and Networks (SECON) 2005, pp. 475–486, Sept. 2005.
- [Cao08] L. Cao, H. Zheng, "Distributed rule-regulated spectrum sharing," IEEE J. Sel. Areas in Commun., vol. 26, no. 1, pp. 130-145, Jan. 2008.
- [Cog07] "Cognitive networks," Q. H. Mahmoud, Ed., Wiley, 2007.
-

- [Cog08] "Cognitive radio communications and networks," A. Wyglinski, Ed., IEEE Communications Magazine, Apr. 2008.
- [Cog09] "Cognitive radio part 1: practical perspective," S. Haykin, J. H. Reed, G. Y. Li, and M. Shafi, Ed., Proc. of the IEEE, vol. 97, no. 4, Apr. 2009.
- [Cor05] C. Cordeiro, K. Challapali, D. Birru, and S. Shankar, "IEEE 802.22: The First Worldwide Wireless Standard based on Cognitive Radios", in IEEE DySPAN, pp. 328-337. Nov, 2005.
- [Deh05] Dehos C., Morche D., "Method and Device for Compensating a Receiver Imbalances," Patent WO/2006/090033, 2005.
- [Du07] J. Du, S. Signell, "Comparison of CP-OFDM and OFDM/OQAM in Doubly Dispersive Channels", Future generation communication and networking, vol. 2, pp. 207- 211, Dec 2007.
- [Dur04] R. Durrett, Probability: Theory and Examples, 3rd ed., Duxbury, Belmont, CA 2004.
- [Etk07] R. Etkin, A. Parekh, D. Tse, "Spectrum sharing for unlicensed bands," IEEE J. Sel. Areas in Commun., vol. 25, no. 3, pp. 517-528, Apr. 2007.
- [Far08-1] B. Farhang-Boroujeny and R. Kempter, "Multicarrier communication techniques for spectrum sensing and communication in cognitive radios," IEEE Commun. Mag. (Special Issue on Cognitive Radios for Dynamic Spectrum Access), vol. 48, no. 4, Apr. 2008.
- [Far08-2] B. Farhang-Boroujeny, "Filter bank spectrum sensing for cognitive radio," IEEE Trans. on Signal Processing, vol. 56, pp. 1801-1811, May 2008.
- [FCC02] Federal Communication Commission, "Spectrum Policy Task Force," Report of ET Docket 02-135, Nov. 2002.
- [Flo95] B. Le Floch, M. Alard, C. Berrou, "Coded orthogonal frequency division multiplex", Proceedings of the IEEE, vol. 83, pp. 982-996, June 1995.
- [Fos98] G. J. Foschini, M. J. Gans, "On limits of wireless communications in fading environment when using multiple antennas," Wireless Personal Commun., vol. 6, pp. 311-335, no. 3, Mar. 1998.
- [Fox68] B. L. Fox, D. M. Landi, "An algorithm for identifying the ergodic subchains and transient states of a stochastic matrix," Communications of the ACM, vol. 11, no. 9, pp. 619-621, Sept. 1968.
- [Fou96] R. Foulter, C. Carlsson, "Fuzzy multiple criteria decision making: Recent developments" Fuzzy Sets and Systems, vol. 78, pp. 139-153, 1996.
- [Fu08] F. Fu and M. van der Schaar, "Stochastic Game Formulation for Cognitive Radio Networks," in Proc. 3rd IEEE International Symposium on New Frontiers in Dynamic Spectrum Access Networks 2008 (DySPAN '08), pp. 1-5, Oct. 2008.
- [Gar86-1] W. A. Gardner, "The spectral correlation theory of cyclostationary time-series", Signal Processing, vol. 11, pp. 13-36, July 1986.
-

- [Gar86-2] W. A. Gardner, "Introduction to Random Processes with Applications to Signals and Systems", Macmillan, New York, 1986.
- [Gar87-1] W. A. Gardner, "Spectral correlation of modulated signal, Part I-Analog modulation", Communications, IEEE Transactions, vol. COM-35, pp. 584-594, June 1987.
- [Gar87-2] W. A. Gardner, W. A. Brown, and C. K. Chen, "Spectral correlation of modulated signals, Part II-Digital modulation", Communications, IEEE Transactions, vol. COM-35, pp. 595-601, June 1987.
- [Gar92] W. A. Gardner and C. M. Spooner, "Signal interception: Performance advantages of cyclic-feature detectors," IEEE Trans. Communications, vol. 40, pp. 149-159, Jan. 1992.
- [Gar99] K. G. Gard, H. M. Gutierrez, M. B. Steer, "Characterization of spectral regrowth in microwave amplifiers based on the nonlinear transformation of a complex Gaussian process," IEEE Transactions on Microwave Theory and Techniques, vol.47, no.7, pp.1059-1069, July 1999.
- [Ges07] D. Gesbert, S. G. Kiani, A. Gjendemsjo, G. E. Oien, "Adaptation, coordination, and distributed resource allocation in interference-limited wireless networks," Proceedings of the IEEE, vol. 95, no. 12, pp. 2393-2409, Dec. 2007.
- [Gha08] A. Ghasemi and E.S. Sousa, "Spectrum sensing in cognitive radio networks: requirements, challenges and design trade-offs," IEEE Commun. Mag., vol. 46, pp. 32-39, Apr. 2008.
- [Gho09] M. Ghoszi, B. Zayen and A. Hayar, "Experimental study of spectrum sensing based on distribution analysis," in Proc. ICT Mobile Summit 2009, Santander, Spain, June 2009.
- [Gol96] G. H. Golub, C. F. Van Loan, "Matrix computations," 3rd ed., Johns Hopkins University Press, 1996.
- [Gra94] L. S. Gradshteyn, I. M. Ryzhik, "Tables of integrals, series, and products," Academic Press, 1994.
- [Haa97] R. Haas, J. Belfiore, "A Time-Frequency Well-localized Pulse for Multiple Carrier Transmission", Wireless Personal Communications: An International Journal, vol. 5, pp. 1-18, July 1997.
- [Hay05] S. Haykin, "Cognitive radio: Brain-empowered wireless communications," IEEE J. Select. Areas Commun., vol. 23, no. 2, pp.201-220, Feb. 2005.
- [Hil04] T. Weiss and J. Hillenbrand, "Mutual interference in OFDM-based spectrum pooling systems," in Vehicular Technology Conference (VTC), vol. 4, May 2004.
- [Hir81] B. Hirosaki, "An orthogonally multiplexed QAM system using the discrete fourier transform," IEEE Transactions on Communication Technology, vol. 29, pp. 982 – 989, July 1981.
- [Höy07] M. Höyhty, A. Hekkala, M. Katz, and A. Mämmelä, "Spectrum awareness: Techniques and challenges for active spectrum sensing," in Cognitive Wireless Networks, F. H. Fitzek and M. D. Katz Eds., chapter 18, pp. 353-372, Springer, Dordrecht, The Netherlands, 2007.
-

- [Hua05] J. Huang, R. A. Berry and M. L. Honig, "Spectrum sharing with distributed interference compensation", in Proc. 1st IEEE International Symposium on New Frontiers in Dynamic Spectrum Access Networks 2005 (DySPAN '05), pp. 88–93, Nov. 2005.
- [Iha08] T. Ihalainen, A. Viholainen, and M. Renfors, "On spectrally efficient multiplexing in cognitive radio systems," in Proc. of the IEEE Int. Symposium on Wireless Pervasive Computing (ISWPC, pp. 675-679), Santorini, Greece, May 2008.
- [Ilt06] R. A. Iltis, S-J. Kim, D. A. Hoang, "Noncooperative iterative MMSE beamforming algorithms for ad hoc networks," IEEE Trans. Commun., vol. 54, no. 4, pp. 748-759, Apr. 2006.
- [Jan03] J. Jang and K. Lee, "Transmit power adaptation for multiuser OFDM systems," IEEE Journal on Selected Areas in Communications, vol. 21, no. 2, pp. 171–178, Feb. 2003.
- [Kat96] I. Katzela, M. Naghshineh, "Channel assignment schemes for cellular mobile telecommunication systems: a comprehensive survey," IEEE Personal Communications, vol. 3, no. 3, pp. 10-31, June 1996.
- [Kem66] J. G. Kemeny, G. L. Thompson, Introduction to finite mathematics, Prentice-Hall, N. J., 1966.
- [Kiv03] D. Kivanc, G. Li, and H. Liu, "Computationally efficient bandwidth allocation and power control for OFDMA," IEEE Transactions on Wireless Communications, vol. 2, no. 6, pp. 1150–1158, 2003.
- [Kuz09-1] A. M. Kuzminskiy, Y. I. Abramovich, "Decentralized dynamic spectrum allocation based on adaptive antenna array interference mitigation diversity: Algorithms and Markov chain analysis," in Proc. ICASSP, Apr. 2009.
- [Kuz09-2] A. M. Kuzminskiy, Y. I. Abramovich, "Adaptive antenna array interference mitigation diversity for decentralized dynamic spectrum allocation in license-exempt spectrum," in Proc. ICC, June 2009.
- [Lac01] D. Lacroix, N. Goudard, M. Alard, "OFDM with Guard Interval versus OFDM/offsetQAM for High Data Rate UMTS Downlink Transmission", in Proc. Vehicular Technology Conference (VTC), vol. 4, pp. 2682- 2684, fall 2001.
- [Lee04] C. S. Lee, K. Y. Yoo, "Polyphase Filter-based OFDM Transmission System," in Proc. Vehicular Technology Conference (VTC), vol. 1, pp. 525- 528, Sept 2004.
- [Les06] T. Lestable, E. Zimmerman, M.-H. Hamon, and S. Stiglmayr, "iBlock-LDPC codes vs. Duo-Binary Turbo-Codes for european next generation wireless systems," in Proc. 64th IEEE Vehicular Technology Conference (VTC), Montreal, Canada, 2006.
- [Lee08] W. Y. Lee and I. F. Akyildiz, "Joint Spectrum and Power Allocation for Inter-Cell Spectrum Sharing in Cognitive Radio Networks," in Proc. 3rd IEEE International Symposium on New Frontiers in Dynamic Spectrum Access Networks 2008 (DySPAN '08), pp. 1-12, Oct. 2008.
-

- [Lek97] A. Leke and J. Cioffi, "A maximum rate loading algorithm for discrete multitone modulation systems," in Proc. IEEE Global Telecommunications Conference (GLOBECOM'97), vol. 3, pp. 1514–1518, 1997.
- [Ma05] L. Ma, X. Han and C.-C. Shen, "Dynamic open spectrum sharing MAC protocol for wireless ad hoc network," in Proc. 1st IEEE International Symposium on New Frontiers in Dynamic Spectrum Access Networks 2005 (DySPAN '05), pp. 203–213, Nov. 2005.
- [Mac09] A. B. MacKenzie, J. H. Reed, P. Athanas, C. W. Bostian, R. M. Buehrer, L. A. DaSilva, A. W. Ellingson, Y. T. Hou, M. Hsiao, J.-M. Park, C. Patterson, S. Raman, C. R. C. M. Da Silva, "Cognitive radio and networking research at Virginia Tech," Proc. of the IEEE, vol. 97, no. 4, pp. 660-688, Apr. 2009.
- [Mal05] D. Maldonado, B. Lie, A. Hugine, T. W. Rondeau, C. W. Bostian, "Cognitive radio applications to dynamic spectrum allocation. A discussion and illustrative example," in Proc. DySPAN, pp. 597-600, Nov. 2005.
- [Mar98] K. W. Martin, "Small Side-Lobe Filter Design for Multitone Data-Communication Applications," IEEE Trans. Circuits and Systems II: Analog and Digital Signal Processing, vol. 45, no. 8, pp. 1155-1161, Aug. 1998.
- [Mas07] Masse, C. & Luu, Q. A 2.4 GHz WiMAX Direct Conversion Transmitter, AN-826 Application Note Rev. B., Analog Device, 2007.
- [Men07] R. Menon, A. B. MacKenzie, R. M. Buehrer, J. H. Reed, "A game-theoretic framework for interference avoidance in ad hoc networks," in Proc. GLOBECOM, pp. 694-699, Nov. 2007.
- [Mer08] A. Merentitis, E. Patouni, N. Alonistioti, M. Doubrava, "To Reconfigure or Not to Reconfigure: Cognitive Mechanisms for Mobile Devices Decision Making" in Proc. 68th IEEE Vehicular Technology Conference (VTC), Calgary, Canada, Sept. 2008.
- [Mit99] J. Mitola, "Cognitive radio for flexible mobile multimedia communications," in Proc. IEEE International workshop on Mobile multimedia communications (MoMuC'99), pp. 3–10, Nov. 1999.
- [Mit06] J. Mitola. III, "Cognitive radio architecture," Wiley, 2006.
- [Mol09] A. F. Molish, L. J. Greenstein, M. Shafi, "Propagation issues for cognitive radio," Proc. of the IEEE, vol. 97, no. 4, pp. 787-804, Apr. 2009.
- [Mon80] R. A. Monzingo and T. W. Miller, "Introduction to Adaptive Arravs," Wiley, 1980.
- [Nee06] J. O. Neel, J. H. Reed, "Performance of distributed dynamic frequency selection schemes for interference reducing networks," in Proc. in proc. MILCOM, Oct. 2006.
- [Nie05] N. Nie, C. Comaniciu, "Adaptive channel allocation spectrum etiquette for cognitive radio networks," in Proc. 1st IEEE International Symposium on New Frontiers in Dynamic Spectrum Access Networks 2005 (DySPAN '05), pp. 269–278, Nov. 2005.
-

- [Nie06] N. Nie and C. Comaniciu, "Adaptive Channel Allocation Spectrum Etiquette for Cognitive Radio Networks," Springer's. Mobile Networks and Applications, vol. 11, no. 6, pp. 779–797, Dec. 2006.
- [One07] M. Oner, F. Jondral, "On the Extraction of the Channel Allocation Information in Spectrum Pooling Systems," IEEE Journal on Selected Areas in Communications, vol. 25, no 3, pp. 558-565, April 2007.
- [Pap08] N. Papandreou and T. Antonakopoulos, "Bit and power allocation in constrained multicarrier systems: The single-user case," EURASIP Journal on Advances in Signal Processing, vol. 2008, Article ID 643081, 4 pages, doi:10.1155/2008/43081, 2008.
- [Pro02] J. G. Proakis and M. Salehi, Communication Systems Engineering, 2nd ed. Upper Saddle River, NJ Prentice-Hall, 2002.
- [PHY08] "PHYDYAS-Physical layer for dynamic spectrum access and cognitive radio," Project website: www.ict-phydyas.org.
- [Pen05] C. Peng, H. Zheng and B. Y. Zhao, "Utilization and fairness in spectrum assignment for opportunistic spectrum access," Springer's. Mobile Networks and Applications, vol. 11, no. 4, pp. 555-546, Aug. 2005.
- [Pen06] C. Peng, H. Zheng and B. Y. Zhao, "Utilization and fairness in spectrum assignment for opportunistic spectrum access," in: ACM Mobile Networks and Applications (MONET), 2006.
- [Qin07] T. Qin and C. Leung, "Fair adaptive resource allocation for multiuser OFDM cognitive radio systems," in Second International Conference on Communications and Networking in China (CHINACOM '07), Aug. 2007
- [Ra09] M. U. Rahim, T. Stitz Hidalgo, M. Renfors, "Analysis of Clipping-Based PAPR-Reduction in Multicarrier Systems," in Vehicular Technology Conference (VTC Spring 2009), 2009.
- [Rap91] C. Rapp, "Effects of HPA non linearity on a 4-DPSK/OFDM-Signal for a digital sound broadcasting system," in Proc. 2nd European Conference on Satellite Communications, Oct., 1991.
- [Ree74] I. S. Reed, J. D. Mallett, L. E. Brennan, "Rapid convergence rate in adaptive arrays," IEEE Trans. Aerospace and Electronic Systems, vol. AES-10, no. 6, pp. 853-863, Nov. 1974.
- [Rhe98] W. Rhee, J.C. Chuang, C.L.J. Jr, "Performance Comparison of OFDM and Multitone with Polyphase Filterbank for Wireless Communications," in Proc. Vehicular Technology Conference (VTC), vol. 2, pp. 768- 772, May 1998.
- [Roc09] IST FP7 Rocket project, D9, "6d2 - Compensation techniques for large constellations", 2009.
- [Sah09] A. Sahai, S. M. Mishra, R. Tandra, K. A. Woyach, "Cognitive radios for spectrum sharing," IEEE Signal Proc. Magazine, no.1, pp. 140-145, Jan. 2009.
-

- [Scu08-1] G. Scutari, D. Palomar, S. Barbarossa, "Cognitive MIMO radio," IEEE Signal Proc. Magazine, pp. 46-59, Nov. 2008.
- [Scu08-2] G. Scutari, D. Palomar, S. Barbarossa, "Competitive design of multiuser MIMO systems based on game theory: a unified view," IEEE J. Select. Areas Commun., vol 26, no. 7, pp. 1089-1103, Spt. 2008.
- [Scu08-3] G. Scutari, D. Palomar, S. Barbarossa, "MIMO cognitive radio: a game theoretic approach," in Proc. SPAWC, pp. 426-430, 2008.
- [Sen08] 7th framework programme: SENDORA, Deliverable D2.1, "Scenario descriptions and system requirements", www.sendora.eu.
- [She03] Z. Shen, J. Andrews, and B. Evans, "Optimal power allocation in multiuser OFDM systems," in Proc. IEEE Global Telecommunications Conference (GLOBECOM'03), vol. 1, 2003.
- [Shi07] Q. Shi, D. Taubenheim, S. Kyperountas, P. Gorday and N. Correal, "Link Maintenance Protocol for Cognitive Radio System with OFDM PHY," in Proc. 2nd IEEE International Symposium on New Frontiers in Dynamic Spectrum Access Networks 2007 (DySPAN '07), pp. 440-443, April 2007.
- [Shi08] H. P. Shiang and M. van der Schaar, "Delay-Sensitive Resource Management in Multi-Hop Cognitive Radio Networks," in Proc. 3rd IEEE International Symposium on New Frontiers in Dynamic Spectrum Access Networks 2008 (DySPAN '08), pp. 1-12, Oct. 2008.
- [Sio00] P. Siohan, C. Roche, "Cosine-Modulated Filterbanks Based on Extended Gaussian Gunctions," IEEE Transactions on Signal Processing, vol. 48, pp. 3052-3061, 2000.
- [Skr06] A. Skrzypczak, P. Siohan, and J. Javaudin, "Power spectral density and cubic metric for the OFDM/OQAM modulation," in Proc. IEEE ISSPIT, Vancouver-Canada, August 2006.
- [Sri05] V. Srivastava, J. Neel, A. B. MacKenzie, R. Menon, L. A. DaSilva, J. E. Hicks, J. H. Reed, R. P. Gilles, "Using game theory to analyze wireless ad hoc networks," IEEE Communications Surveys and Tutorials, vol. 7, no. 4, pp. 46-56, 2005.
- [Sti07] S. Stiglmayr, M. Bossert, E. Costa, "Adaptive Coding and Modulation in OFDM Systems using BICM and Rate-compatible Punctured Codes," in Proc. European Wireless Conf, Paris, 2007.
- [Stu09] G. Stuber, S. Almalfouh, and D. Sale, "Interference analysis of TV-band whitespace," Proceedings of the IEEE, vol. 97, no. 4, pp. 741-754, April 2009.
- [Sub08] S. Subramani, T. Basar, S. Armour, D. Kaleshi and Z. Fan, "Noncooperative Equilibrium Solutions for Spectrum Access in Distributed Cognitive Radio Networks," in Proc. 3rd IEEE International Symposium on New Frontiers in Dynamic Spectrum Access Networks 2008 (DySPAN '08), pp. 1-5, Oct. 2008.
- [Tan05] H. Tang, "Some physical layer issues of wide-band cognitive radio systems," in Proc. IEEE Int. Symposium on New Frontiers in Dynamic Spectrum Access Networks (DYSPAN), pp. 619-625, Baltimore, Maryland, USA, Nov. 2005.
-

- [Tan08] R. Tandra and A. Sahai, "SNR walls for signal detection," *IEEE J. Select. Topics Signal Processing*, vol. 2, pp. 4-17, Feb. 2008.
- [Tri08] M. Trivellato, F. Boccardi, H. Huang, "Zero-forcing vs unitary beamforming in multiuser MIMO systems with limited feedback," in *Proc. PIMRC*, Sept. 2008.
- [Tub05] J. Tubbax, B. Come, L. Van der Perre, S. Donnay, M. Engels, Hugo De Man, M. Moonen, "Compensation of IQ imbalance and phase noise in OFDM systems," *Wireless Communications, IEEE Transactions on*, vol.4, no.3, pp. 872-877, May 2005.
- [Wal06] D.S. Waldhauser, L.G. Baltar, J.A. Nossek, "Comparison of Filter Bank Based Multicarrier Systems with OFDM", in *Proc. Circuits and Systems, IEEE Asia Pacific Conference*, pp. 976- 979, Dec 2006.
- [Wal08] D. S. Waldhauser, L. G. Baltar, J. A. Nossek, "Filter Bank Based Multicarrier systems" *Techniken, Algorithmen und Konzepte für zukünftige COFDM Systeme (TakeOFDM)*.
- [Wan07] P. Wang, M. Zhao, L. Xiao, S. Zhou, and J. Wang, "Power allocation in OFDM-Based cognitive radio systems," in *Proc. IEEE Global Telecommunications Conference (GLOBECOM)*, pp. 4061–4065, 2007.
- [Wan08] C-X. Wang, H-H. Chen, X. Hong, and M. Guizani, "Cognitive radio network management," *IEEE Veh. Tech. Mag.*, vol. 3, pp. 28-35, Mar. 2008.
- [WINN] "WINNER, EU FP6 Integrated Project", Available: <http://www.ist-winner.org>
- [Wei03] W. Wei and M. J. Wang, "Fuzzy-MOGA-based Traffic Signal Control at Intersection," in *Proc. International Conference on Machine Learning and Cybernetics*, Nov. 2003.
- [Wei04-1] T. Weiss, F. Jondral, "Spectrum Pooling: An Innovative Strategy for the Enhancement of Spectrum Efficiency," *IEEE Communications Magazine*, vol. 42, no. 3, pp. 8-14, March 2004.
- [Wei04-2] T. Weiss, J. Hillenbrand, "Mutual interference in OFDM-based spectrum pooling systems," in *Proc. Vehicular Technology Conference (VTC)*, vol. 4, pp. 1873- 1877, May 2004.
- [Woy08] K. A. Woyach, "Crime and punishment for cognitive radios," M.S. thesis, Dept. Elect. Eng. Comput. Sci., Univ. CA Berkeley, 2008.
- [Won99] C. Wong, R. Cheng, K. Lataief, and R. Murch, "Multiuser OFDM with adaptive subcarrier, bit, and power allocation," *IEEE Journal on Selected Areas in Communications*, vol. 17, no. 10, pp. 1747–1758, 1999.
- [Xu08] D. Xu, E. Jung and X. Liu, "Optimal Bandwidth Selection in Multi-Channel Cognitive Radio Networks: How Much is Too Much?" in *Proc. 3rd IEEE International Symposium on New Frontiers in Dynamic Spectrum Access Networks 2008 (DySPAN '08)*, pp. 1-11, Oct. 2008.
- [Zay08] B. Zayen, A. M. Hayar, and D. Nussbaum, "Blind spectrum sensing for cognitive radio based on model selection," in *Proc. of the IEEE 3rd Int. Conference on Cognitive Radio Oriented Wireless Networks and Communications (CROWNCOM)*, pp. 1-4, Singapore, May. 2008.
-

- [Zey07] E. Zeydan, D. Kivanc-Tureli, U. Tureli, "Joint iterative channel allocation and beamforming algorithm for interference avoidance in multiple-antenna ad hoc networks," in proc. MILCOM, Oct. 2007.
- [Zey08] E. Zeydan, D. Kivanc, U. Tureli, "Cross layer interference mitigation using a convergent two-stage game for ad hoc networks," in Proc. CISS, pp. 671-675, Mar. 2008.
- [Zha05] Q. Zhao, L. Tong, A. Swami, "Decentralized cognitive MAC for dynamic spectrum access," in Proc. DySpan, pp. 224-232, Nov. 2005.
- [Zha07] Q. Zhao, B. M. Sadler, "A survey of dynamic spectrum access," IEEE Signal Processing Magazine, vol. 24, no. 3, pp. 79-89, May 2007.
- [Zha08-1] W. Zhang and U. Mitra, "A Spectrum-Shaping Perspective on Cognitive Radio," in Proc. 3rd IEEE International Symposium on New Frontiers in Dynamic Spectrum Access Networks 2008 (DySPAN '08), pp. 1-12, Oct. 2008.
- [Zha08-2] H. Zhang D. Le Ruyet, M. Terré, "Signal Detection for OFDM/OQAM System Using Cyclostationary Signatures," in Proc. IEEE International Symposium on Personal Indoor and Mobile Radio Communications (PIMRC), pp. 1-5, Sept. 2008.
- [Zha08-3] Y. Zhang, "Resource allocation for OFDM-Based cognitive radio systems," Ph.D. dissertation, Univ. of British Columbia, Vancouver, December 2008.
- [Zha09] H. Zhang, D. Le Ruyet, and M. Terre, "Spectral efficiency analysis in OFDM and OFDM/OQAM based cognitive radio networks," in Proc. of the IEEE 69th Vehicular Technology Conference (VTC), pp. 1-5, Barcelona, Spain, April 2009.
- [Zhe05] H. Zheng and L. Cao, "Device-centric spectrum management," in Proc. 1st IEEE International Symposium on New Frontiers in Dynamic Spectrum Access Networks 2005 (DySPAN '05), pp. 56-65, Nov. 2005.
- [Zhe05] H. Zheng and C. Peng, "Collaboration and fairness in opportunistic spectrum access," in Proc. IEEE International Conference on Communications 2005 (ICC '05), vol. 5, pp. 3132-3136, May 2005.
- [Zho08] X. Zhou, J. Ma, Y. Li, Y. H. Kwon, A. Soong and G. Zhao, "Probability-Based Transmit Power Control for Dynamic Spectrum Access," in Proc. 3rd IEEE International Symposium on New Frontiers in Dynamic Spectrum Access Networks 2008 (DySPAN '08), pp. 1-5, Oct. 2008.
- [3GPP] "3GPP-Long-Term-Evolution", Available:<http://www.3gpp.org/Highlights/LTE/LTE.htm>.
- [802.16-04] IEEE 802.16-2004, "IEEE standard for metropolitan area network," Air interface for fixed wireless access.
-